Geochemical Characterization

of

Geologically Complex Mountain Front Aquifers:

Placitas, New Mexico

William J. LeFevre

Submitted In Partial Fulfillment Of The Requirements For The Degree Of

Master Of Science In Geochemistry

Earth and Environmental Science

New Mexico Institute of Mining and Technology

Socorro, NM 87801

June 2, 1999

ABSTRACT

Characterization of ground-water flow across geologically complex mountain-front recharge areas can be confounded by an intricate network of structural and stratigraphic controls. Standard exploration methods are inadequate because the hydrologic nature of geologic discontinuities may be difficult to discern and the collection of representative data may be prohibitively expensive. The use of geochemical techniques as a primary tool for characterizing ground-water flow and recharge in geologically complex terrain is demonstrated on the eastern margin of the Albuquerque Basin at the north end of the Sandia Mountains in New Mexico, where structural and stratigraphic controls produce hydrologic discontinuities and aquifer compartmentalization. The regional distribution of geochemical parameters such as radioisotopic dating, stable isotope analyses, major ion analyses, ground-water temperature, and dissolved oxygen concentration, differs significantly from the distribution predicted by a standard basin model and illustrates the heterogeneity and complexity of ground-water flow in the study area.

Local scale analysis of the geochemical results from ground-water, surface-water, and precipitation sampling permits the identification of recharge areas, discharge areas, preferential ground-water flow pathways, and barriers to ground-water flow. Comparison of stable isotope analyses on ground water and precipitation suggests that most ground water is recharged in the Sandia Mountains by infiltration of precipitation and runoff that is produced by winter-type storms originating over the northern Pacific Ocean. The Madera Limestone that caps the Sandia Mountains produces ground water that is typical of recharge areas and has a low temperature, low TDS concentration, and high dissolved oxygen concentration (*Madera type water*). Madera type water is also produced by isolated Mesozoic aquifers between the mountains and the Albuquerque Basin, and down-gradient of basin bounding faults, suggesting that some faulted and compartmentalized aquifers have a good hydraulic connection to the Madera Limestone, and also that local infiltration of surface water is a significant source of recharge to the basin-fill aquifer. An evaporation-altered stable isotope composition and a high tritium concentration in Madera type ground water near Las Huertas Creek and other arroyos suggests that ground water from the mountains is redistributed across the study area, and to the Albuquerque Basin, by ephemeral arroyos and Las Huertas Creek, and that infiltration from Las Huertas Creek is the single most important source of ground-water recharge within the study area. Mesozoic aquifers between the Sandia Mountains and the Albuquerque Basin generally produce ground water with higher temperatures, higher TDS concentrations, and higher dissolved oxygen concentrations than the Madera Formation, suggesting that ground-water flow from the Sandia Mountains to the Albuquerque Basin is generally blocked by basin-margin faults and by tilted and rotated fault blocks that orient the bedding planes of sedimentary units normal to ground-water flow. Several instances of Madera type water produced by Mesozoic aquifers suggest that ground-water flow across basin margin faults is permitted where permeable sandstone formations are in fault contact with the Madera Limestone and at the highly faulted junction of the Placitas fault zone and the San Francisco fault. Anomalous ground-water ages and temperatures, stable isotope compositions, and dissolved oxygen concentrations along the San Francisco fault suggest that this fault, and other faults in the Madera Limestone, may act as discrete ground-water flow paths.

The results of this thesis illustrate that geochemical techniques can be a valuable primary tool for characterizing ground-water flow through geologically complex mountain front aquifers. Measurements of the stable isotope and major ion composition, temperature, and dissolved oxygen concentrations were the most useful parameters measured during this study and prior knowledge of the geology was critical to the hydrogeologic investigation.

ACKNOWLEDGMENTS

Thanks are given to the faculty and staff of New Mexico Institute of Mining and Technology and the New Mexico Bureau of Mines, particularly my research advisor Peggy Johnson for her perseverance in requiring technical writing of the highest standard and developing skilled hydrogeologic judgment. Andrew Campbell piqued my interest in isotope geochemistry, served as my academic advisor, and supervised my stable isotope laboratory work, Fred Phillips answered more than his fair share of questions about isotope hydrology, and Brian McPherson contributed a critical review of this thesis. This project would not have been possible without the cooperation and motivation of citizens of Placitas, who volunteered use of their personal water supply systems for water level monitoring and sample collection, and shared existing ground-water analyses. This thesis is part of Phase II of a water resources assessment of the Placitas development area that was initiated and funded by Sandoval county.

This thesis is dedicated the PSP. Thanks to St. Joseph for encouragement, St. Bernard for keeping me alive, and my wife, Rhonda, for her faith and patience, and for reminding me of the purpose of my work.

TABLE OF CONTENTS

LIST OF FIGURES

LIST OF TABLES

INTRODUCTION

Characterization of ground-water flow across geologically complex mountain-front recharge areas can be confounded by an intricate network of structural and stratigraphic controls. Typical ground-water exploration methods such as geologic mapping, core logging, ground-water level measurement, and aquifer pumping tests, are inadequate because the hydrologic nature of geologic discontinuities may be difficult to discern and the collection of representative data may be prohibitively expensive. Geochemical techniques such as radioisotopic dating, stable isotope analyses, and major ion analyses, provide an independent means of testing hydrogeologic models developed from more conventional methods. However, geochemical techniques are generally applied after the flow system has been well constrained, and are typically used in areas with few geologic complexities (e.g. Lopez and Hoffmann, 1997; Classen, 1985; Hoonton and Lundy, 1979; and Awad and et al., 1997).

In this thesis, I demonstrate that geochemical techniques can be used as a primary tool for the characterization of ground-water flow in geologically complex terrain where structural and stratigraphic controls produce hydrologic discontinuities and aquifer compartmentalization. This geochemical method is illustrated by characterizing ground-water flow between the north slope of the Sandia Mountains and the Albuquerque basin in central New Mexico. Within the 90 km^2 ($\approx$35 mi^2) study area more than 20 geologic formations, 16 major faults, and numerous smaller subsidiary faults produce hydrologic discontinuities and aquifer compartmentalization to such a degree that standard hydrogeologic methods are inadequate to fully characterize the ground-water flow system. Water samples are readily available from existing wells, springs, and surface water. The objectives of this thesis are to use geochemical techniques to identify and qualitatively characterize: (a) geologic controls on the occurrence and movement of ground water; (b) recharge and discharge areas; (c) ground-water flow pathways, including preferential flow paths and hydrologic discontinuities; and (d) ground-water recharge rates and residence times within this ground-water system.

In a practical sense, these results will be a valuable tool to water resource managers, land owners, developers, consultants, drillers, and regulatory personnel. The results will be a useful asset for identifying

parts of the study area that either can, or should not, be developed, predicting the effects of development within the study area, evaluating the potential impairment of existing water rights, and choosing a well location or target aquifer within local areas. This thesis contributes to Phase II of the Placitas area water resources assessment. The geochemical data collected for this thesis can be used to predict the quality of water produced from a target aquifer and as a baseline for future work. In a more academic context, the method is a valuable tool for regional ground-water resource investigations, particularly in geologically complex areas and when budget constraints are severe.

HYDROLOGIC FRAMEWORK

This section describes potential geologic controls on the occurrence and movement of ground water, and summarizes the geography, surface-water hydrology, and climate of the study area. The geology and hydrology of Placitas and the surrounding area have been described in several reports. The main contributors are Menne (1989), Picha (1982), and Connell et al. (1995), who examined the structure and stratigraphy of the area in detail. Kelly and Northrop (1975) and Kelly (1977) summarized the geology of the Sandia Mountains and the Albuquerque Basin respectively. In a hydrologic report about the Sandia Mountains, Titus (1980) included Placitas as a distinctive terrain. Several wells in the Albuquerque basin near Placitas have been sampled by the United States Geological Survey (USGS) as part of the ongoing Middle Rio Grande Basin Study (Plummer et al., 1998). Phase I of the water resources assessment for the Placitas development area compiled existing data and developed a preliminary site conceptual model (Groffman et al., 1996).

Location, Geography, and Climate

The study area is located in the southeast corner of Sandoval County New Mexico, approximately 30 km (19 mi) northeast of Albuquerque and just east of Bernalillo (Figure 1). The study encompasses the Placitas development area as defined by Sandoval County land subdivision regulations. The development area is bounded on the south by the Cibola National Forest, on the east by the Town of Tejon Grant, on the north by the San Felipe Pueblo, on the northwest by the Santa Ana Pueblo Grant, and on the west by the Town of Bernalillo. The Village of Placitas is in the eastern part of the study area, but residential development covers much of the area.

The study area is a region of diverse topography, landforms, vegetation, and climate. Diverse topography, typical of the Basin and Range physiographic province, ranges from the rugged 3255-m (10,850-ft) Sandia Mountains (Sandias) to the Rio Grande floodplain at 1600 m (≈5100 ft). The topography is mountainous in the southern and eastern parts of the study area, with up to 1500 m (≈5000 ft) of relief

between Placitas and Sandia Crest. The north-trending limestone salients of Cuchilla Lupe* and Crest of Montezuma are separated by Las Huertas Creek and its canyon which drains much of the northern and eastern part of the Sandia Mountains. Cuchilla de San Francisco is a northern, lower elevation, extension of the Crest of Montezuma. The central portion of the study area is characterized by 60-m (200-ft) hills and a piedmont slope cut by several major arroyos. The northern and western portions of the study area are in the Albuquerque Basin proper and are characterized by dissected piedmont slopes at the base of the Sandia Mountains and the Rio Grande floodplain. Vegetation is sparse except near springs and along perennial reaches of streams where cottonwood, salt cedar, and dense wetland vegetation are found. Grasses dominate at lower altitudes; piñon, juniper, and scrub oak are found at middle altitudes; and mixed conifer and aspen forests cover the highest portions of the Sandias (Williams and McAllister, 1979).

The study area has a warm, arid to semi-arid climate with notable contrasts between seasons and different elevations. Mean annual temperature ranges from 14°C (57 °F) in the lowest regions, to 4°C (40 °F) at Sandia Crest. Average annual precipitation ranges from 210 mm (8.4 in) in Albuquerque to 760 mm (30 in) at Sandia Crest (Tuan et al., 1969). Most of the area's precipitation (65-70%) is produced between April and September by convective storms originating from tropical Gulf of Mexico air masses (Figure 2). Winter precipitation is principally caused by orographic uplift of cool, moist polar-Pacific air masses. Precipitation during spring and autumn can be from either source (Dorroh, 1964). Annual potential evapotranspiration (PE) based on the Thornthwaite formula ranges from 442 mm (17.4 in) at Sandia Crest to 772 mm (30.4 in) in the basin and is several times greater in the summer than in the winter. Precipitation exceeds PE only from November to February by 20 mm (0.79 in) in the basin (Figure 3) and 290 mm (11.4 in) at Sandia Crest. The extremely high PE during the summer results in annual moisture deficits ranging from 140 mm (5.4 in) at Sandia Crest to 564 mm (22.2 in) in the basin. (Tuan et al., 1969).

---

* Cuchilla is Spanish for "knife" and properly refers to long narrow ridges near the study area.

Geologic Setting

Placitas is located on the eastern margin of the Albuquerque Basin of the Rio Grande rift and at the northern termination of the east tilted Sandia uplift (Figure 4). The northern termination of the Sandias contains a transition zone where the Sandia uplift ramps down into the Albuquerque basin between two major basin-bounding, north-trending, normal faults: the Rincon fault and the San Francisco fault. The east-trending Placitas fault zone accommodates the offset between the Rincon and San Francisco faults (Kelly and Northrop, 1975). Almost all geologic formations of the region are exposed in the study area. The sedimentary units are extensively dissected by the Placitas fault zone and numerous north-trending subsidiary faults crossing the study area (Figure 5).

Stratigraphy

Proterozoic to Holocene age rocks are exposed in and around the study area (Table 1). Extensive faulting exposes only small portions of the stratigraphic section at any one location. The following descriptions of stratigraphy are condensed from Kelly and Northrop (1975), Connell et al. (1995), Hawley et al. (1995), Cather (1997), Menne (1989) and Picha (1982). Basic hydrogeologic interpretations are derived from Titus (1980).

Proterozoic and Paleozoic

Exposures of Proterozoic crystalline rocks are found in the southwest corner of the study area on Rincon Ridge, south of the Placitas fault zone and at the base of the Crest of Montezuma. The core of the Sandia Mountains consists of mixed metamorphic rocks and the Sandia Granite. These crystalline rocks have no primary porosity or permeability but locally permeable zones are created by faults, fractures, and a weathered zone at the unconformity between the Sandia Granite and the overlying sedimentary rocks.

Mississippian and Pennsylvanian limestones and sandstones form the highest cliffs and salients of the northern Sandias. The Arroyo Peñasco, Sandia and Madera Formations cover the Sandias south of the Placitas fault zone. The Mississippian Arroyo Peñasco (0 to 23 m, 0 to 75 ft) is a discontinuous formation

of sandstone and limestone. Minor conglomerate, fine-grained sediments and a 1- to 2-m (3- to 6-ft) thick layer of quartzite in the upper part are locally present.

The Pennsylvanian Sandia Formation (59 m, 190 ft) is a sequence of interbedded, well-cemented sandstone, limestone, and shale. Fractures provide moderate permeability in the sandstone and high permeability in the limestone units. The transitional contact between the Sandia and the Madera Formations may allow the two formations to be hydraulically connected and act as one aquifer. This connection is further supported by results of Titus (1980) results showing that water from these formations is chemically indistinguishable.

The Pennsylvanian Madera Limestone (380 to 470 m, 1250 to 1550 ft) is the dominant unit and aquifer of the Sandias, and forms the eastern and northern dip slope of the Sandia Mountains, Cuchilla Lupe, Crest of Montezuma, and Cuchilla de San Francisco. The formation consists of a lower member of limestone, and an upper member of arkosic sandstone, limestone, and shale. The lower member of the formation has limestone beds 3 to 20 m (10 to 65 ft) thick separated by black shale, micaceous siltstone, or shaley limestone up to 3 m (10 ft) thick. The lower member comprises 40 to 45 percent of the total section. The upper member is vertically and laterally much more heterogeneous than the lower member and less than half is limestone. The limestone alternates or intertongues with thick (10 to 13 m, 30 to 36 ft) units of shale, siltstone, and poorly sorted arkosic sandstone. Permeability is provided by solution-enlarged fractures and bedding planes in the limestone and sandstone, and the majority of aquifer storage is in pore space in the rock matrix (Johnson, 1999). Thick units of shale in the upper member may hydraulically isolate permeable limestone units. Sandstone units are not believed to yield consequential amounts of water. In the transition zone between the Madera Limestone and the overlying Abo Formation, the number of sandstone and mudstone beds gradually increases as the number of limestone beds decreases, making a stratigraphic distinction between the Upper Madera Limestone and lower Abo Formation difficult. Faulting in the Placitas fault zone and upper Las Huertas canyon has juxtaposed Madera Limestone against the Abo Formation.

The Permian Abo Formation (230 to 330 m, 760 to 1100 ft) is a series of equally abundant mudstone and sandstone beds that outcrop in the Placitas fault zone, the bottom of Las Huertas Canyon, and the broad

valleys east of the Crest of Montezuma and Cuchilla de San Francisco. Due to faulting, the entire section is never exposed at one place in the study area. The lower 30 m of this formation consists of thin limestone beds (less than 2 m, 6 ft) interbedded with thin (2 to 8 m, 6 to 30 ft) beds of shale. The upper part of the Abo formation has thick (up to 30 m, 100 ft) sequences of fluvial sandstone interbedded with thick (20 to 70 m, 65 to 230 ft) sequences of shale. Fractured sandstone and limestone beds provide ample permeability throughout the section. The conformable contact between Abo Formation and the overlying Yeso Formation is difficult to discern because the sandstone units of the Upper Abo formation are similar to the Yeso sandstones.

The Permian Yeso, Glorieta and San Andres Formations outcrop as fault-bounded slivers and blocks in the Placitas fault zone and in stratigraphic sequence east of Cuchilla de San Francisco. The Yeso formation (165 to 210 m, 540 to 690 ft) consists primarily of friable sandstone. Thin limestone beds (1 to 2.5 m, 3 to 8 ft) are present in the middle of the section, and siltstone and gypsum occur locally near the top of the formation. Sandstone beds are porous enough to produce ground water, and solution channels in the limestone contribute to permeability. The contact between the Yeso and the overlying Glorieta formations is distinct, with no intertonguing or transition zone, but fine grained units likely limit hydraulic connectivity with the Glorieta.

The Glorieta and San Andres Formations probably function as one aquifer. The Glorieta Formation is a 10 m (33 ft) thick sandstone. The San Andres Formation is 20 to 25 m (66 to 82 ft) thick and consists primarily of fine grained limestone. Permeability in these well-indurated and massive formations is highly variable and depends on the density of fractures and solution-channels. There is a distinct contact between the San Andres Formation and the overlying Triassic Moenkopi Formation.

Mesozoic

Excellent exposures of the following Mesozoic formations are found as tilted stratigraphic sequences north of the Placitas fault zone and as fault bounded slivers and blocks in the fault zone. The formation of the rift and uplift of the Sandias has caused considerable faulting and fracturing that locally contributes to the permeability of otherwise low permeability formations.

The Triassic Moenkopi (20 to 25 m, 66 to 82 ft) and Agua Zarca (25 to 130 m, 82 to 430 ft) Formations consist primarily of sandstone. The Agua Zarca Formation is coarse grained and more conglomeratic near the base, with mudstone units becoming more common near the top. The contact with the overlying Petrified Forest Formation is gradational as mudstone becomes more common and sandstone less common. The Triassic Petrified Forest Formation (400 to 500 m, 1310 to 1640 ft) is primarily mudstone. Local thin sandstone and conglomerate lenses are present and there is a 10-m (33-ft) thick sandstone unit at the top of the section.

The Jurassic Entrada is a (35 m, 115 ft) thick formation of massively bedded and well-sorted eolian sandstone. The Jurassic Todilto Formation (15 to 60 m, 50 to 189 ft) consists of a lower unit of very thinly laminated fetid limestone and, locally, a thin upper unit of gypsum. The Jurassic Morrison Formation (about 260 m, 850 ft) and Cretaceous Dakota Sandstone (22 m, 72 ft) may function as a single hydrologic unit with similar hydraulic and chemical properties. The Morrison Formation consists primarily of friable sandstone, with mudstone and siltstone common in the lower and upper portions. The Dakota Sandstone consists of thin- to massive-bedded well-cemented sandstone with smaller beds of black shale near the top of the formation.

The Cretaceous Mancos Shale has minor thin sandstone and siltstone beds and is divided into upper and lower units by the intervening Hosta-Dalton Sandstone (65 to 115 m, 210 to 380 ft). The total thickness of all three units is 440 to 490 m (1440 to 1600 ft). The Hosta-Dalton Sandstone is weakly cemented. Permeability in the Mancos shale is provided by thin sandstone beds and sandy zones. The top of the Mancos Shale inter-tongues with the Point Lookout Sandstone.

The Cretaceous Point Lookout Sandstone (75 m, 250 ft) is fine-grained, and thin- to thick-bedded with limonitic sandstone lenses and minor shale that underlies the bottom coal bearing shale of the Cretaceous Menefee Formation. The Cretaceous Menefee Formation (250 to 560 m, 820 to 1840 ft) is an alternating sequence of sandstone and fine-grained rocks. In addition to sandstone, there are siltstone, shale, coal and ironstone lenses found in this formation. The top of the Menefee Formation in the study area is an angular unconformity with Lower Santa Fe Formation.

A northeast-striking, near-vertical mafic to intermediate dike (the "black dike") is located north of the village of Placitas. The dike cuts and is nearly perpendicular to the Mancos, Point Lookout and Menefee Formations, and the northeast end of the dike is covered by Lower Santa Fe Formation. The dike probably acts as a barrier to ground-water flowing in the sedimentary rocks.

Cenozoic

The Tertiary-Quaternary basin fill alluvium was produced by erosion of Paleozoic and Mesozoic rocks from the Sandia uplift and deposited beyond the basin-margin faults. The basin fill sediments are generally coarse near the mountains and become finer towards the Rio Grande. A strong correlation between permeability and grain size in poorly cemented units of the Santa Fe was found by Detmer (1995) but even moderate cementation obscured the relationship. Cather (1997) and Connell et al. (1995) have mapped individual units based on textural lithofacies that are defined by grain size.

Lower Santa Fe Group piedmont deposits consisting of clast-supported conglomerate outcrop on Lomas Altos and the ridges west of the San Francisco Fault. The conglomerate to sandstone ratio is 2:1 with no mudstone. Low permeability lacustrine mudstone and evaporites are common in parts of the Lower Santa Fe, but are found further basin-ward and only at depth outside the study area. Cementation reduces permeability in coarse-grained units. Lower Santa Fe deposits are in contact with Upper Santa Fe piedmont deposits across the Escala, Lomas and Ranchos faults.

The Upper Santa Fe Group (<300 m, 1000 ft) consists of deposits of piedmont and axial river sediments. Piedmont deposits are found basin-ward of the Escala, Lomas and Ranchos faults and consist of nearly equal portions of clast supported conglomerate and poorly sorted pebbly sandstone. Axial river deposits are found in the west end and northwest corner of the study area and consist of medium- to coarse-grained braided river channel sands and rare fine-grained floodplain deposits of the ancestral Rio Grande. There is a transition zone between the piedmont and axial river deposits where they interfinger. The axial river deposits have excellent aquifer properties and are often the target of well drilling activities.

Quaternary deposits of valley-fill, piedmont-slope and pediment alluvium and colluvium are present in the study area. Stream and terrace deposits (<6 m, <20 ft) of loam and gravel are found in the valleys of Las

Huertas Creek, Arroyo de Ojo del Orno and Arroyo Agua Sarca. Piedmont fan complexes and alluvium deposits form a thin veneer of conglomerate and sandy gravel over much of the Mesozoic strata between NM-165 and the Placitas fault zone and over the Upper Santa Fe Formation. Travertine deposits (15 m, 50 ft) are found at the northern end of Cuchilla de San Francisco and record the discharge area of paleosprings. Most of these deposits are located well above the regional potentiometric surface but valley-fill alluvium may locally contain ground water depending on recent recharge from streams.

Structure

The Sandia uplift is an eastward tilted fault block that forms the eastern margin of the Albuquerque Basin. The uplift ramps northward and down with a slope of about 1:5 into the northern Albuquerque basin between two major west dipping normal faults of the Rio Grande Rift: the Rincon fault on the west and the San Francisco fault on the east (Figure 5). Splays of these basin-margin faults extend into the basin. The Placitas fault zone accommodates offset between the Rincon and San Francisco faults and contributes to the northward down-ramping of the Sandia uplift. The following description of structure is from Woodward and Menne (1995) and Kelly and Northrop (1975).

Faults

The Rincon fault forms the boundary between the Albuquerque Basin and the west face of the Sandias. The Rincon is a northeast trending normal fault, with moderate to shallow dip and down to the west movement, that results in juxtaposition of Santa Fe sediments on the west with Proterozoic crystalline rocks on the east. Stratigraphic separation is up to 2400 m (7900 ft) near the junction with the Placitas fault zone, but decreases northward as the Rincon fault splays into the Ranchos and Valley View faults.

The San Francisco fault forms the eastern boundary of the Albuquerque Basin from Tecolote north along Cuchilla de San Francisco in the northeastern part of the study area. There is about 1800 to 2100 m (5900 to 6900 ft) of stratigraphic separation along this moderate-angle normal fault. Lower Santa Fe sediments are downthrown to the west against Madera limestone and the Abo Formation. Permian to Cretaceous formations are found wedged between several branches of the San Francisco fault at Tecolote.

The southern end of the San Francisco fault forks into the Placitas fault zone and the Las Huertas fault system south of Tecolote.

The Placitas fault zone is a complex system of at least two subparallel segments of steeply dipping normal faults stretching between the San Francisco and Rincon faults. As the fault zone trends northeast along the base of the Sandias individual faults are usually down to the northwest with less than 100 m (330 ft) of stratigraphic separation. Total offset is 850 to 1700 m (2800 to 5600 ft) at the northeast end where the fault zone is reduced to a single trace. Jumbled fault blocks juxtapose Proterozoic through Pennsylvanian rocks on the south against Proterozoic through Mesozoic rocks on the north. The Placitas fault zone abuts or merges with the Rincon fault under basin-fill sediments. Just north of this junction there are numerous low-angle (<30°) bedding-plane faults that have up to 50 m (160 ft) of stratigraphic separation and recemented fault breccia up to 5 m (16 ft) thick.

The north-trending Suela fault and Las Huertas fault system form horst and graben structures that produce Las Huertas canyon. The West Las Huertas fault, which separates Las Huertas canyon and Cuchilla Lupe, is a steeply dipping normal fault with down to the east motion. The East Las Huertas fault, which separates the canyon and Crest of Montezuma, is a north-trending, moderately (≈45°) dipping, normal fault that is offset down to the west. Up to 1000 m (3300 ft) of stratigraphic separation juxtaposes Permian Abo Formation in the graben against Proterozoic and Paleozoic rocks to the east and Madera Limestone to the west (Figure 6). The Cuchilla Lupe horst is bounded on the west by the Suela fault which is a steeply dipping, north-trending, normal fault that juxtaposes Abo sandstone on the west against Madera limestone. At the north end where it merges with the Placitas fault zone the Suela fault has up to 600 m (1970 ft) of offset. The South Montezuma fault is an east-trending steeply dipping reverse fault that forms the northern boundary of the Crest of Montezuma. The Abo Formation is dropped 100 to 300 m (330 to 980 ft) down to the north against Madera Limestone on the south. The western end of the South Montezuma fault abuts the East Las Huertas fault at Tecolote.

The Caballo, Agua Sarca and Pomecerro faults are a set of north-trending faults that offset two major blocks in the central part of the study area. All of these faults cross the Placitas fault zone and extend into the Sandias. North of the Placitas fault zone the Agua Sarca and Pomecerro faults abut the Caballo fault,

which then continues northward into the basin. All three are normal faults downthrown to the west, and steeply dipping with left separation. Stratigraphic separation across the Caballo fault is about 20 m (66 ft) south of the Placitas fault zone, and up to 700 m (2300 ft) north of highway 165. Stratigraphic separation across the Agua Sarca fault is probably 200 m (660 ft) south of the Placitas fault zone and 36 to 200 m (120 to 660 ft) between the Placitas fault zone and the Caballo fault. Stratigraphic separation across the Pomecerro fault is 100 to 200 m (330 to 660 ft) south of the Placitas fault zone. The Pomecerro fault has two splays in the Placitas fault zone. The western splay has 300 to 600 m (980 to 1970 ft) of stratigraphic separation while the eastern splay has up to 150 m (500 ft) of stratigraphic separation which increases north of the Placitas fault zone to about 500 to 600 m (1640 to 1970 ft) at the junction with the Caballo fault. Where these faults cross the Placitas fault zone, they juxtapose Paleozoic and Mesozoic rocks. Northward, they juxtapose Mesozoic rocks through Lower Santa Fe sediments on the west against Mesozoic rocks on the east.

Several moderate angle normal faults cut the basin-fill sediments. The north-trending Ranchos and Valley View faults are northern splays of the Rincon fault. The Ranchos fault juxtaposes Triassic formations through Lower Santa Fe alluvium on the east against Upper Santa Fe alluvium on the west. The Valley View fault offsets Upper Santa Fe piedmont deposits and at the northern end forms the boundary between transitional and axial facies of the Upper Santa Fe. Lower Santa Fe piedmont deposits are juxtaposed against Upper Santa Fe piedmont deposits across the Lomos and Escala faults. The Lomos fault is oriented east to west between the northern ends of the Ranchos and the Caballo faults. The Escala fault trends north from the east end of the Lomos fault along an escarpment in the northeast part of the study area.

Hydraulic Effects of Faults

Faults can act as either barriers or conduits to ground-water flow depending on fault displacement, lithology, three dimensional fault geometry, subsidiary structures, and fluid-rock interactions (Caine et al., 1996). Faults with large offset often contain a core of fine-grained fault gouge bordered by a highly fractured damage zone. Gouge is an effective barrier to flow across faults while a damage zone, with

permeability up to six orders of magnitude higher, transmits water parallel to faults (Smith et al., 1990). The Las Huertas fault system, the Suela fault, and the faults associated with the Placitas fault zone cut through well indurated sandstone and limestone. Faults in these kinds of rock typically have damage zones with enhanced permeability (Huntoon and Lundy, 1979) and cross-fault permeability drops of up to four orders of magnitude (Anatonellini and Aydin, 1995). Faults with significant offset can also affect cross-fault permeability by truncating or locally reducing the thickness of permeable units, or juxtaposing formations with different permeabilities. Ground water in crystalline rocks, like the Sandia granite, is limited to fracture zones which exhibit varying degrees of connectivity and transmissivity. These faults and fracture zones could be considered discrete hydrologic units (Levens et al., 1994). "Holes" in an otherwise impermeable fault may occur in areas of minimal displacement, or where little damage was done to the protolith resulting in minimal gauge development. It is also possible that conductivity windows exist at fault intersections and splays where damage to the protolith is maximized, and the development of fault gouge is minor compared to the amount of fracturing (Smith et al., 1990).

Large-displacement faults in unconsolidated sediments, like the Valley View and Escala faults, generally act as barriers to ground-water flow. An example is provided by the Sand Hill fault, which juxtaposes Upper and Lower Santa Fe Group sediments on the west side of the Albuquerque Basin (Heynekamp et al., 1999). The Sand Hill fault is characterized by a nearly continuous, well foliated, very low permeability core zone, that is bounded by heterogeneous mixed zones where a dramatic reduction in permeability is caused by mixing of clay and silt-rich sediments with sand, and cataclasis of lithic-rich sands. The thickness of the fault zone increases with increasing grain size. The orientation of preferentially cemented coarse-grained material in the hanging wall mixed zone indicates that ground-water flow was subhorizontal in the undisturbed footwall block and subvertical in the hanging wall mixed zone. The cross-fault permeability is controlled by the fault core and footwall mixed zone which are estimated to have shale-like permeabilities.

Faults and fracture zones are expected to play an very important role in directing ground-water flow throughout the study area. Faults through the Madera Formation are expected to provide preferential ground-water flow pathways parallel to the fault trace, and to suppress ground-water flow in a direction

normal to the fault. Individual faults through Mesozoic formations are also expected to provide preferential ground-water flow pathways parallel to the fault trace, but less continuously and on a much more localized scale than in the Madera Formation. The combined effect of the complex fault network that cuts the Mesozoic formations is uncertain. Intrabasin faults such as the Escala and Lomos faults, and basin margin faults such as the Ranchos and San Francisco faults, are expected to restrict cross-fault ground-water flow. Throughout the study area, contrasting lithologies are juxtaposed by rotated fault blocks and individual permeable layers are split into discontinuous and widely separated aquifers.

Hydrogeology

Portions of the study area have distinct hydrogeologic characteristics caused by similar stratigraphic and structural characteristics. By grouping aquifers with similar hydrogeologic characteristics, the study area can be divided into three hydrogeologic zones (Figure 7). The mountain zone encompasses the upland areas east of the San Francisco fault and south of the Placitas fault zone where Proterozoic crystalline rocks and the Madera and Sandia Formations form fractured aquifers with high transmissivity, low storativity, and localized areas of fault-controlled ground-water flow. The Mesozoic ramp encompasses the central portion of the study area, north of the Placitas fault zone, south of Las Huertas Creek and Lomos Altos, and east of the Ranchos Fault. Aquifers in the Mesozoic ramp have highly variable ground-water quality, ground-water supply, and hydraulic characteristics that area caused by the heterogeneous lithology, hydraulically isolated and small-scale aquifers, and faults that act as barriers and preferential pathways. The northern and western two thirds of the study area are situated in the Albuquerque basin where ground-water quality and supply are more predictable in a relatively homogeneous aquifer of Tertiary and Quaternary basin fill sediments. Spring-fed streams cross all three zones and redistribute ground water discharging from the mountain hydrogeologic zone, potentially recharging aquifers in the Mesozoic ramp and the basin.

Surface Water & Springs

Three major drainage basins drain the study area (Figure 8), Las Huertas Creek, Arroyo Agua Sarca, and Arroyo San Francisco. Springs discharge at many locations throughout the study area (Appendix A and

Figure 8) and sustain surface flow through limited stream reaches in all drainage basins. The largest drainage basin is Las Huertas Creek, which is presented here in terms of its three sub basins, drains most of the northeastern part of the Sandias and the Crest of Montezuma. The upper Las Huertas Creek sub-basin (49 km^2, 19 mi^2) is underlain by Madera limestone in the mountains and primarily the Abo Formation in the Las Huertas graben. Flow in upper Las Huertas Creek is highly variable throughout the year reflecting the spring snow-melt and monsoon thunderstorms. Base flow in the upper canyon is provided by several springs issuing from the Madera formation high in the side canyons of Las Huertas Canyon. Down stream of these springs Las Huertas creek recharges the aquifer where it crosses Madera limestone (Flemming, 1986). Spring PS-07 flows from limestone beds of the lower Abo Formation where the Tecolote fault intersects an arroyo. Water from this spring is diverted for residential use and irrigation, and excess flows through Tecolote and across the San Francisco fault where it infiltrates into basin-fill sediments. Small springs and seeps are found in the stream bed of Las Huertas Creek just above Tecolote where the creek crosses the San Francisco fault zone. Spring runoff in upper Las Huertas creek usually flows all the way through lower Las Huertas Creek.

Lower Las Huertas Creek traverses the basin from Tecolote to the Rio Grande and has an area of about 18 km^2 (7 mi^2). This reach of Las Huertas Creek is underlain by Tertiary and Quaternary basin-fill alluvium. Numerous small ground-water seeps are found in the creek bed between Tecolote and Rosa de Costilla spring (PS-08) which discharges up to seven liters per second (100 gpm) (Titus, 1980). Perennial flow in this reach of lower Las Huertas Creek infiltrates the basin-fill alluvium downstream from where the creek crosses the Escala fault. Downstream of the fault, flow is dependent on spring runoff and input from Arroyo de Ojo del Orno.

The Arroyo de Ojo del Orno sub-basin is a tributary to Las Huertas Creek and drains the north face of the Sandias including Cuchilla Lupe and most of the Mesozoic ramp from the village to west of Tunnel spring, a total area of 11 km^2 (4 mi^2). Tributaries cross all geologic formations present in the study area, as well as the Placitas, Caballo, Agua Sarca, Pomecerro, and Lomos faults. The arroyo crosses lower Santa Fe piedmont facies and the Caballo and Lomos faults before its confluence with lower Las Huertas Creek in the basin. Base flow is provided by several springs (the Placitas springs) discharging along the Placitas fault

zone. El Oso (PS-04), Ciruela (PS-01), and the smaller Placitas springs (PS-02, PS-03and PS-20) discharge from the Madera Limestone of Cuchilla Lupe and adjacent Abo formation into acequia systems that distribute the water throughout the village before draining into Arroyo del Oso and Arroyo Tierra Blanca. A series of springs, including Tunnel Spring (PS-05), discharge along the western splay of the Pomecerro fault as it enters the Placitas fault zone. Flow from these springs is diverted into the western-most arroyo in the drainage area. Two other small springs are also located along faults in the Placitas fault zone (PS-06 and PS-24). A spring in the arroyo northwest of the village (PS-19) discharges from Mancos shale where the Caballo fault crosses Arroyo de Ojo del Orno. Flow in Arroyo de Ojo del Orno contributes to flows in Lower Las Huertas Creek primarily in the winter, when the water discharged from the Placitas springs is not diverted for irrigation. During low flows, water infiltrates the Upper Santa Fe alluvium within a few meters of crossing the Lomos fault.

Arroyo Agua Sarca drains 16 km^2 (6 mi^2) on the northwest corner of the Sandia Mountains and the west end of the Mesozoic ramp. The upper part of the basin is underlain by Sandia granite and Madera limestone. The arroyo zigzags across the Placitas fault zone, onto the Mesozoic ramp, and enters the basin at the Ranchos fault. The main source is a spring which flows from the Madera limestone, high in Cañon Agua Sarca, for a short time after the spring snow-pack melts. The arroyo is dry the rest of the year except for ephemeral flows after local summer storms. Titus (1980) reports a spring in the arroyo where Agua Sarca crosses the Ranchos fault (PS-23).

Arroyo de San Francisco drains 9.5 km^2 (4 mi^2) east and north of Cuchilla de San Francisco. The Abo, Madera and Yeso Formations constitute the bedrock in the upper part of the drainage. The arroyo enters the basin hydrogeologic zone where it crosses the San Francisco fault north of Cuchilla de San Francisco. The upper part of the drainage flows only after thunderstorms but there are seeps in the arroyo where it cuts Abo sandstone beds just east of the San Francisco fault. At least nine distinct springs and numerous arroyo seeps contribute to flow in Arroyo San Francisco in the vicinity of the San Francisco fault. Springs PS-14 to PS-18, PS-21, and PS-22 discharge at low points in the Madera Limestone, along the San Francisco Fault, and where the Madera Limestone is juxtaposed against Lower Santa Fe piedmont deposits. Springs PS-10, PS-11, and PS-12 discharge from a thick deposit of travertine in the Lower Santa Fe Group, attesting to a long

history of ground-water discharge in this area. These springs maintain a perennial flow in the lower reach of San Francisco Creek to beyond the northern border of the study area.

A significant component of mountain front recharge is infiltration of surface water flowing across basin-bounding faults from the mountains. Surface flows can be effective in moving water into the basin even when low permeability faults and geologic units restrict ground-water flow into the basin. In Placitas, the springs and streams contribute to the complexity of the ground-water system by discharging ground water from one aquifer and redistributing it across faults and relatively impermeable formations to recharge otherwise isolated aquifers.

Ground Water

A generalized potentiometric surface was developed by the NMBMMR from direct measurements at 59 domestic wells and supplemented by 27 springs and artesian wells, 61 well records from the New Mexico Office of the State Engineer (NMOSE), and 20 water level records from the USGS database (Figure 9, Johnson, 1999). Ground water flows north and west from the mountains to the Rio Grande floodplain, northward along Cuchilla de San Francisco, and generally follows the topography. This regional ground-water gradient is consistent with the map of Titus (1980). A higher density of ground-water level measurements results in higher resolution than Titus' map and shows a much more complex system than previously described. The interaction of topography and hydraulic conductivity contrasts across faults and between adjoining stratigraphic units produces complex inflections, ridges, troughs, and changes of gradient in the potentiometric surface.

In the upland areas south of Placitas, the potentiometric surface follows the steep regional north and northeastward dip of the land surface and the Madera Limestone. Topographic highs along Cuchilla Lupe, Crest of Montezuma and Cuchilla de San Francisco also contribute to a high potentiometric surface. East of the East Las Huertas fault, ground water recharged in the Sandias flows north through the Madera Formation until the South Montezuma fault deflects a portion of the flow into the basin through Tecolote, with the remainder continuing north and parallel to the San Francisco fault through the Madera Formation of Cuchilla de San Francisco. High water levels in deeper wells east of the San Francisco fault indicate

strong vertical upward gradients consistent with a ground-water discharge area. A potentiometric surface drop of 52 m (170 ft) across the San Francisco fault is the result of permeability contrasts associated with the fault and/or the transition from fractured Madera limestone to Lower Santa Fe piedmont deposits. Head drop across the Placitas fault zone varies from 30 to 60 m (100-200 ft) depending on the permeability of the adjoining sediments. The highest gradient (≈0.5) occurs near the village, where the Placitas fault zone and the Suela fault merge, and fractured Madera limestone is placed next to fine-grained Mesozoic sediments. Ground water is clearly being diverted along the small unnamed fault between the West Las Huertas Fault and the Suela fault to discharge from El Oso spring where the fault abuts the Abo formation.

In the Mesozoic ramp, the potentiometric surface generally has a moderate gradient (0.04) that is distorted by numerous ridges, troughs, and inflections in the potentiometric surface. Ground water flowing across the Placitas fault zone encounters steeply dipping, low-conductivity layered sedimentary rocks, and is forced to flow across bedding planes. The wide range in hydraulic conductivity (an estimated six orders of magnitude) and high anisotropy in the Mesozoic rocks causes inflections in the potentiometric surface as ground-water flow is focused along higher conductivity formations and faults. This pattern of troughs and ridges suggests that ground water is compartmentalized in this area and is moving throughout the region along preferential flow paths, and at vastly different flow rates.

The potentiometric surface in the basin has a relatively low gradient (0.07 to 0.004), generally slopes westward, and shows the effects of stream infiltration and basin-bounding faults. A potentiometric surface drop of up to 100 m (320 ft) across the Ranchos fault suggests that ground-water flow is attenuated by a reduction in permeability associated with the fault. A ground-water mound located along Arroyo Agua Sarca indicates that this arroyo is a source of recharge to the basin. Depressions in the potentiometric surface between the Ranchos and Valley view faults suggest that recharge and interaquifer flow into this area are significantly less than ground-water withdrawal. The potentiometric surface along Lower Las Huertas Creek also shows the effect of ground-water recharge and discharge at springs. There is a ground-water mound along the creek between PS-08 and PW-202 caused by infiltration of surface water.

METHODS

In this study, the isotopic and geochemical composition of ground water from the various aquifers are evaluated as a complement to the geologic and hydrologic data. A brief discussion of the geochemical framework, collection of samples and analytical methods is presented in the following sections.

Geochemical framework

The stable isotope ratios $^{18}O/^{16}O$ and $^{2}H/H$ (reported as $\delta^{18}O$ and $\delta^{2}H$) are ideal hydrologic tracers because they are measured directly on the water molecule. Meteoric processes affect the stable isotope values of precipitation and impart systematic variations in $\delta^{18}O$ and $\delta^{2}H$ that are described by a meteoric water line (Figure 10). The global average relationship is (Craig, 1961):

$$\delta^{2}H = 8\,\delta^{18}O + 10‰ \qquad (1)$$

The humidity at the oceanic source of the precipitation affects the deuterium excess. The deuterium excess (d) is similar to the intercept of a meteoric water line but is rigorously defined as (Dansgaard, 1964):

$$d = \delta^{2}H - 8\,\delta^{18}O \qquad (2)$$

Atmospheric water vapor forms at a global average humidity of 85%, resulting in $d = 10‰$ in Equation (1). Increased humidity results in a lower d, and decreased humidity results in a higher d. These variations are reflected in local meteoric water lines which may vary significantly from the global average line. The mean annual sea surface temperature and humidity at the oceanic source, and transcontinental and mountain-front rainfall processes cause significant local variations in $^{18}O/^{16}O$ and $^{2}H/H$ that must be considered when examining precipitation at annual and regional scales. Water vapor produced over a warmer ocean results in precipitation that is more enriched and cooler ocean temperatures result in precipitation that is more depleted. Rainfall from frontal storm systems progressively depletes the moisture remaining in the storm. Thus, as a moist air mass moves inland from the ocean, or up a mountain slope, precipitation that falls farther inland or at higher altitude is more depleted than coastal or low altitude

precipitation. Latitude, local average annual temperature, and the amount of precipitation falling during a single storm have also been correlated to the $^{18}O/^{16}O$ and $^{2}H/H$ of meteoric waters. Individual weather patterns, storm tracks, and air mass mixing are so chaotic that at least a year of precipitation data is needed to use these relationships in ground water studies.

The distribution of $^{18}O/^{16}O$ and $^{2}H/H$ in ground water can be correlated with the spatial and temporal distribution of $^{18}O/^{16}O$ and $^{2}H/H$ in precipitation to characterize recharge events and the provenance of ground water (Clark and Fritz, 1997). The distribution of $^{18}O/^{16}O$ and $^{2}H/H$ in ground water yields information about the spatial extent and order of flow systems, and the mixing properties of a flow system. Interactions between ground water and surface water can also be identified (Wallick and Toth, 1976). Large deviations of $\delta^{18}O$ and $\delta^{2}H$ in ground water from the meteoric water line can indicate recharge from open bodies of water that are altered by evaporation, or isotope exchange reactions with the aquifer materials or dissolved gasses. Ground water with an unusually low deuterium excess and/or a disproportionately large depletion along the local meteoric water line compared to current precipitation has been recharged during a time when the climate was more humid and/or colder than the present climate (Figure 10). Ground water with depletions of 25‰ in $\delta^{2}H$ and 3‰ in $\delta^{18}O$ has been correlated with Pleistocene age ground water by carbon-14 dating (e.g., Phillips et al., 1986).

The activity of tritium and ^{14}C in ground water may be used to estimate ground-water recharge rates, mean residence times, flow velocities, confirm ground-water mixing, and identify stagnant zones. Tritium, ^{3}H, is part of the water molecule, has a short half-life (12.43 years) and is introduced to the ground water during recharge of precipitation. Atmospheric testing of nuclear weapons in the 1960's increased the tritium content of precipitation by three orders of magnitude. Decay and dilution into the oceans have reduced the concentration of tritium in recent precipitation to near background levels. A 31-year record (1962 to 1993) of the concentration in precipitation is available for Albuquerque (IAEA/WMO, 1998). Tritium is useful for examining local ground-water flow systems with short residence times (<40 years) and identifying the mixing of young and old ground water. Carbon-14 has a long half-life (5730 years) and is useful for examining regional ground-water systems with residence times of 1000 to 40,000 years. Carbon-14 is introduced to ground water as dissolved inorganic carbon by the dissolution of soil gas during recharge.

Variations in cosmic radiation over the past 40,000 years, dilution by carbon-14 free CO_2 from the combustion of fossil fuels, soil chemistry, and the type of vegetation in the recharge area affect the initial carbon-14 activity in ground-water recharge. Dissolution of carbonate aquifer material and diffusion into the aquifer matrix reduce the carbon-14 activity along the ground-water flow path. Carbon-14 age determinations can be corrected by accounting for these processes in an isotope evolution model.

The temperature of shallow ground water can indicate recharge and discharge areas. Recharge infiltrates the aquifer at the ambient air temperature. As ground water travels through deep aquifers it is warmed by the natural geothermal gradient. In discharge areas the upward flow of ground water facilitates the upward flow of heat by advection. Seasonal and longer-term climate variations, and potential variations in the geothermal gradient across the study area, add complications to the temperature field. The temperature of ground water discharged by an actively pumping well, however, is a depth-integrated measurement that reduces some of the variation. Therefore, ground water is generally cooler in recharge areas and warmer in discharge areas.

The dissolved oxygen concentration in ground water is higher in recharge areas and decreases along the flow path. The dissolved oxygen concentration in recently infiltrated ground-water is expected to be similar to water in contact with air. The concentration of dissolved oxygen in water in contact with air is controlled by the water temperature and the partial pressure of oxygen in the atmosphere. The saturated dissolved oxygen concentration in water ranges from 8.26 ppm at 25°C to 12.8 ppm at 5°C and one atmosphere. Dissolved oxygen concentrations would be lower at higher altitudes where the partial pressure of oxygen is lower. Dissolved oxygen is removed from ground water and soil moisture by bacterially catalyzed reactions that oxidize organic material and may deplete dissolved oxygen to below detection limits. The oxidation of ferrous iron, ammonia, manganese, and sulfide also lowers the dissolved oxygen concentration. Once all dissolved oxygen is consumed, organic matter is oxidized by NO_3^-, MnO_2, $Fe(OH)_3$ and SO_4^{2-}. As ground water becomes more reduced, organic compounds may undergo anaerobic degradation to produce methane and carbon dioxide. The presence of methane, carbon dioxide, and hydrogen sulfide, high dissolved manganese and iron, and lack of dissolved oxygen can indicate long residence times and isolation from active ground water recharge.

Major ion ratios and trace element compositions can also be used to trace ground-water flow paths and residence times based on a standard basin model of geochemical evolution (Chebotarev, 1955). As ground water flows from recharge area to discharge area and increases in age, the dominant anion normally changes from bicarbonate to sulfate and finally to chloride, while the dominant cations change from calcium and magnesium to sodium and potassium. This ionic evolution is normally accompanied by an increase in total dissolved solids. The geochemical evolution may be incomplete if sources for the ions are not present, or if processes such as biochemical sulfate reduction occur.

Anomalous concentrations of dissolved nonmetallic compounds and metal ions are caused by unusual geochemical conditions found in unique geologic settings and can also point to anthropogenic impacts on ground water. Fluoride in ground water is derived from the weathering of fluorite and apatite. Arsenic is common in sedimentary deposits derived from volcanic rocks and can be mobilized by increases in the dissolved oxygen concentration from irrigation and ground-water level fluctuations induced by pumping (Korte and Fernando, 1991). Typical sources of nitrate in ground water are fertilizer contaminated recharge, defective septic systems, and the oxidation of organic matter. Zinc and copper can be leached from plumbing systems or produced by the oxidation of sulfide minerals. Possible sources of dissolved iron in the study area are the oxidation of pyrite and iron well casings, and the exposure of limonite (ironstone lenses are common in the Menefee Formation) to reducing conditions (Hem, 1967). Manganese is contained in many igneous and metamorphic minerals, and is also a minor substitute for calcium in limestone and dolomite. High concentrations of manganese and iron can be an caused by the reduction of manganese and iron oxides by organic matter in ground water with low dissolved oxygen concentrations, and can be an indication of long residence times or a high concentration of organic material in the aquifer (Hem, 1985). High silica concentrations are usually a result of chemical breakdown of silicate minerals in the process of weathering and may be an indication of ground water that has experienced elevated temperatures at depth.

Sample Collection

Sampling procedures for precipitation, ground water and surface water are discussed in the following sections. The locations of precipitation stations, wells, springs and surface water sampling sites (Table 2

and Appendix A) were measured using a Trimble Pathfinder mobile GPS unit with a fixed base station at NMIMT. Differential correction and a 100-point data set allowed measurement of the locations to within approximately 2 m horizontally and 15 m vertically.

Precipitation

Precipitation amounts were measured and samples collected from seven locations in, and around, the study area (Figure 11) between April 1997 and September 1998. Quarterly integrated samples were collected each season to measure the summer and winter precipitation peaks and to collect stable isotope samples representative of these peaks. A precipitation collection schedule is presented in Table 3. Precipitation monitoring locations were selected to represent the full range of elevation, climate, and storm types throughout the study area and in potential recharge areas.

Precipitation collectors (Figure 12) were based on a design from Freidman et al. (1992) and built to preserve the isotopic composition of the seasonally integrated precipitation. Both rain and snow collectors were used at higher elevation (sites PPT-01 and PPT-02) and only rain collectors were used at the five lower elevation sites where minor amounts of snowfall were expected. Rain collectors consisted of a 10-cm (4-in) diameter funnel fixed about 1 m (3 ft) above ground, with a straight walled extension to increase the amount of snow they could hold before melting occurred. Copper tubing connected the funnel to a four-liter HDPE bottle that was insulated below ground and contained a 5-cm (2 in) layer of mineral oil to prevent evaporation. Snow collectors consisted of a 1-m (3 ft) length of 10-cm (4 in) diameter black Schedule-40 ABS pipe sealed at the bottom and supported on a 2-m (6-ft) post above the snow-pack. The snow collectors also had a layer of mineral oil to prevent evaporation.

At the end of a sampling period the collection bottle was replaced with a clean bottle and returned to the laboratory. The oil and water were separated with a separatory funnel and the volume of the aqueous phase was measured in a graduated cylinder. Duplicate water samples were filtered to remove any remaining oil and/or particulate matter, collected in 40-milliliter glass bottles with poly-seal™ caps and analyzed for $^{18}O/^{16}O$ and $^{2}H/H$ ratios. Laboratory equipment was washed and thoroughly dried between extraction of samples from different collectors.

Ground and Surface Water

Ground-water sampling sites were selected to provide spatial and stratigraphic coverage, with more samples collected in the highly faulted areas of the Mesozoic ramp. Fewer samples were collected from the more homogeneous basin and Madera Limestone aquifers (Figure 13). The use of existing domestic wells results in clustered data and data gaps in areas that are undeveloped or in large subdivisions supplied by community wells. Ground-water samples were collected from 74 residential, two industrial and ten community ground-water supply wells and analyzed for field parameters, major ions, trace elements, and oxygen and hydrogen isotope ratios. Private well owners and the USGS (N. Plummer, unpubl., 1997) provided geochemical analyses from 20 sites which have also been included. Samples were collected from 11 wells and one spring for tritium and carbon-14 age determination (Figure 14). To ensure that samples were representative of ground water, samples were collected from pumping wells after electrical conductivity, temperature, dissolved oxygen, and pH (field parameters) stabilized or three well-casing volumes of water were purged, whichever took longer.

Surface-water samples were collected at seven locations in perennial, ephemeral, and intermittent streams where interaction between ground water and surface water was expected to be significant, and from 13 springs in each of the five major drainage basins and sub-basins (Figure 15). Grab samples were collected after monitoring field parameters. Field parameters were measured using Orion field instruments and all surface-water and spring samples were analyzed for major ions, trace elements, and $^{18}O/^{16}O$ and $^{2}H/H$ ratios.

Ionic and trace metal samples were collected in Nalgene™ bottles. Trace metal and nitrate samples were preserved with nitric and sulfuric acid respectively. Samples were chilled in a cooler, promptly transported to the laboratory, and chain of custody was recorded. Stable isotope samples were collected in 40 ml glass bottles with no head space and poly-seal™ caps. Samples for tritium analysis were collected outdoors in one-liter HDPE bottles. Samples for radiocarbon analysis were collected by precipitating dissolved inorganic carbon (DIC) with barium chloride, decanting the supernatant fluid and transferring the precipitate to a one-liter HDPE bottle.

Five duplicate samples were collected for major ion, trace constituent, and stable isotope analyses, and nine analyses were available from other sources for wells sampled by this study. Additional stable isotope samples were collected along with the radiocarbon and tritium samples.

Analyses

The following section describes the analytical methods used to determine the isotopic, ionic and trace element composition of the water samples collected for this study.

Stable Isotopes

Samples were prepared for $^{2}H/H$ analysis by zinc reduction (Coleman et al., 1982). A sample was introduced into a reaction vessel containing 300 mg of optimally contaminated zinc turnings from the Indiana University Biogeochemical Laboratories using a 3 µl glass capillary tube. The sample was frozen and atmosphere was removed by vacuum. The reaction vessel was heated to 450 °C for 30 minutes then allowed to cool to room temperature before mass-spectrometric analysis of the resulting hydrogen gas.

Samples were prepared for $^{18}O/^{16}O$ analysis by CO_2-H_2O equilibration (Socki et al., 1992). Pre-evacuated 10 ml Vacutainer™ vials were filled with 250 µmol of cryogenically purified CO_2 before 1 ml of sample water was injected into the vials. Vials were agitated at 4.17 hertz and 25°C for a minimum of 3 hrs to ensure complete isotopic equilibration before CO_2 extraction. Equilibrated CO_2 was cryogenically extracted, purified and transferred to gas collection vessels for mass spectrometric analysis.

The $^{2}H/H$ and $^{18}O/^{16}O$ composition of the prepared hydrogen and carbon dioxide was measured on a Finnigan-MAT Delta-E model dual-inlet, gas-source ion-ratio mass spectrometer at the NMIMT stable isotope laboratory. Isotopic ratios are reported in per mil (‰) relative to VSMOW (0‰) using Oztec™ standard gases. The standard deviation (1σ) of $\delta^{2}H$ analyses (including sample preparation) calculated from between 19 and 29 analyses each of three international standards, one laboratory standard, and two field samples, is 2.7‰. Standard deviations (1σ) for $\delta^{18}O$ analyses (including sample preparation) calculated from triplicate analyses of 17 field samples is 0.15‰.

Radioisotope, Major Ion and Trace Element Chemistry

Radiocarbon samples were analyzed by Geochron Laboratories in Cambridge, Massachusetts. Barium-carbonate precipitate was converted to methane on which radiocarbon activity was measured by gas proportional counting. Standard deviations for radiocarbon analyses ranged from 0.63 to 1.14 percent modern carbon (PMC) and averaged 0.85 PMC. Minimum detectable radiocarbon was 0.80 PMC. Tritium samples were analyzed by low-level gas proportional counting without enrichment at the University of Miami's Tritium Laboratory. Standard deviation for tritium analyses is two to three tritium units (TU).

Major ion and trace metal analyses were completed by the NMBMMR Chemistry Laboratory. Samples were analyzed for eight major ions (Ca^{2+}, Mg^{2+}, Na^{+}, K^{+}, HCO_3^{2-}, SO_4^{2-}, Cl^{-}, and NO_3^{2-}) and seven trace elements (As, Cu, F, Fe, Mn, SiO_2, and Zn). Survey samples collected by NMBMMR in 1996 were analyzed for a broad suite of trace elements to determine which would be most significant. The concentration of anions was measured by ion-chromatography. Trace element and cation concentrations were measured by atomic adsorption spectroscopy and alkalinity was determined by titration. Detection limits for As were usually 3 ppb, Cu 2 ppb, F 0.2 ppm, Fe 30 ppb, Mn 2 ppb, and Zn 10 ppb. Chain of custody was monitored and holding time limitations were met.

RESULTS

The following section presents the precipitation measurements and stable isotope analyses, and the results of the stable isotope, major ion, trace element, and radioisotope analyses completed on the ground- and surface-water samples.

Precipitation

Precipitation measurements and stable isotope results are presented in Table 3 and Table 4 respectively. The amount of precipitation measured at mountain stations (PPT-01 and PPT-02) is very similar, and considerably greater than at the five lowland stations (PPT-03 to PPT-07) (Figure 16 and Figure 17). Annual precipitation ranged from 1170 mm (46.2 in) in the mountains (PPT-02) to only 500 mm (19 in) in Bernalillo (PPT-07). The amount of precipitation measured each season from the spring 1997 through spring 1998 at lowland and mountain stations is greater than the average amount measured at regional NOAA stations in the past (Appendix B), but followed a typical seasonal pattern. At mountain stations 40% of the total annual precipitation fell during the summer and 23% fell during a minor peak in the winter, at lowland stations about 35% of the total annual precipitation fell during the summer and 7% fell during the winter.

The $\delta^{18}O$ composition of precipitation samples ranges from -17.6 ‰ for winter precipitation to -3.7 ‰ for summer precipitation (Figure 18). The volume-weighted annual average stable isotope composition is -10.1 ‰ $\delta^{18}O$ and -74.2 ‰ $\delta^{2}H$. The local meteoric water line is described by Equation 3, and its slope is only slightly less than that of Craig's (1961) global meteoric water line. The deuterium excess is also less than Craig's global value but the same as the deuterium excess for Flagstaff Arizona (3.5 ‰) as reported by Rozanski et al. (1993). The slope may be reduced by summer precipitation that has been fractionated by secondary (virgis) evaporation as raindrops fall through a dry air column (Dansgaard, 1964). Nearly all precipitation should have a stable isotope composition within 15 ‰ $\delta^{2}H$ and 1.9 ‰ $\delta^{18}O$ (the 99% population confidence interval) of the local meteoric water line. For purposes of interpreting ground water, the meteoric water line is defined as the space within the 99% regression confidence interval.

$$\delta^2H = 7.7 \times \delta^{18}O + 3.4 \quad (3)$$

There is only a weak correlation between the stable isotope composition of precipitation and the altitude at which the sample is collected. The altitude effect calculated from the volume-weighted isotope composition at each station (-0.12 ‰ $\delta^{18}O$ per 100 m) has a large uncertainty, but is the same as the altitude effect (which also has a large uncertainty) calculated from precipitation in the Los Alamos region 80 km (50 mi) north of Placitas (Adams et al., 1995). The altitude effect exhibited by summer precipitation (-0.23 ‰ $\delta^{18}O$ per 100 m, Figure 19) is intermediate compared to eight global sites reported in Clark and Fritz (1997) and quite common according to Payne (1988). Autumn and winter precipitation show no altitude effect or in the case of Autumn 1997, a negative effect. A poorly constrained altitude effect is supported by Coplen (1993) and Winograd et al. (1998), who noted that the altitude effect is often not observed in snow fall or on mountains interior to a continent.

Seasonal variations in the stable isotope composition of precipitation reflect the oceanic source of the precipitation. Winter precipitation from frontal systems originating in the northern Pacific Ocean (the average δ^2H and $\delta^{18}O$ for samples collected 2 Feb, 1997 is -120 ‰ and -15.9 ‰ respectively) is about 10 ‰ depleted in ^{18}O and 80 ‰ depleted in ^2H compared with summer monsoon precipitation from the Gulf of Mexico (the average δ^2H and $\delta^{18}O$ for samples collected 2 Sept, 1997 and 4 Aug, 1998 is -43 ‰ and -6.0 ‰ respectively). Winter precipitation is more depleted because of cooler temperatures over the north Pacific and rainout along a thousand-mile continental storm track that crosses many mountain ranges. Summer precipitation is less depleted because the storm track from the Gulf of Mexico across Texas is shorter and less interrupted by mountain ranges. A similar pattern has been identified in southern Arizona (Simpson et al., 1972). The isotopic compositions of spring and fall samples are intermediate reflecting contributions from both sources (Figure 18).

One of the largest El Niño/Southern Oscillation (ENSO) events on record affected the study area from April 1997 to May 1998 (NOAA/OGP, 1998) and is reflected in the stable isotope composition and amount of precipitation. The stable isotope composition of precipitation from the summer of 1997 is more enriched than that of the summer of 1998 (Figure 18) suggesting that the sea surface temperature in the source area

was warmer during the summer of 1997. This is consistent with the ENSO, which is a spreading of warm equatorial Pacific waters north to and beyond California that occurs at two to five-year intervals. The above normal precipitation amounts measured by this study are also consistent with typical El Niño effects. Woolhiser et al. (1993) have shown that 90 to 120 days after ENSO there is an increase in the number of wet days and the mean daily precipitation at stations in New Mexico. Molles et al. (1992) observed strong correspondences between ENSO and high spring (April - June) runoff in the Gila and Pecos Rivers. Because high intensity, long duration precipitation events are more effective at recharging ground water, the stable isotope composition of El Niño precipitation (between May 26, 1997, and February 12, 1998, volume weighted average $\delta^{18}O$ = -8.7 ‰ and $\delta^{2}H$ = -64 ‰, Table 4) may be more representative of ground-water recharge than the stable isotope composition of non-ENSO precipitation.

The stable isotope composition of ground water is expected to reflect seasonal and long-term climatic variations in recharge but not the altitude of recharge. This is because seasonal and short term climatic variations are greater than altitudinal variations. Ground water recharged principally by infiltration of winter snow melt will be more depleted compared to ground water recharged by infiltration of summer rains.

Ground and Surface Water

This section presents the stable isotope, radioisotope age, major ion, and trace element determinations on ground and surface water. The major ion analytical results are presented in Appendix C. Stable isotope and field parameter determinations are presented in Appendix D. Trace metals analyzed for this study are presented in Appendix E.

Temperature, Dissolved Oxygen, and Total Dissolved Solids

The temperature of ground water and the distribution of dissolved oxygen and total dissolved solids (TDS) are presented in Figure 20, Figure 21, and Figure 22. Ground-water temperatures are lowest (<16 °C) along upper Las Huertas Creek, and two areas along lower Las Huertas Creek. The Mesozoic ramp has areas of low-, intermediate- (16 to 21 °C), and high- (>21 °C) temperature ground water. Ground water is warmest in the Albuquerque basin in the western part of the study area and at the northern end of Cuchilla

de San Francisco. The dissolved oxygen concentration (Figure 21) is highest (5.6 to 12 ppm) along Las Huertas Creek and west of the San Francisco fault. The dissolved oxygen concentration is low (0 to 2.87 ppm) in the Mesozoic ramp, in the basin west of the Valley View Fault, and east of the San Francisco fault. The concentration of total dissolved solids (TDS) ranges from 220 ppm to 7540 ppm (Figure 22). Ground water throughout most of the study area has TDS concentrations less than 400 ppm. Three clusters of ground water with very high TDS concentrations (> 1000 ppm) are located in the Mesozoic ramp, and at one well in the Abo Formation east of Cuchilla de San Francisco. The distribution of these parameters in the study area generally follows that predicted by the standard basin model of ground-water flow: low-temperature, high-dissolved oxygen, and low TDS ground water is found in the recharge areas at the basin margin, and ground water with high temperature and TDS concentrations are found at discharge areas in the lowest part of the basin. There are significant bodies of ground water, particularly in the Mesozoic ramp, that contradict the standard basin model. These inconsistencies illustrate the compartmentalization of aquifers, the existence of preferential pathways, and the variety of recharge areas.

Major Ions

Ground-water quality in the Placitas study area is highly variable (Figure 23, Figure 24, and Figure 25). In the mountain hydrogeologic zone, three groups of water are evident (Figure 23). Water from the Madera and Abo Formations on Cuchilla Lupe and Las Huertas Canyon (group A) is low-TDS (<260 ppm) calcium-bicarbonate type water. Water from the Madera Formation on Cuchilla de San Francisco (group B) has slightly higher TDS (<490 ppm) and sodium and magnesium concentrations that are consistent with geochemical evolution along a lengthy ground-water flow path. Ground water from the Abo Formation east of Cuchilla de San Francisco (group C) has the highest sodium, magnesium, and sulfate concentrations and even higher TDS concentrations (<1100 ppm) than ground water from Cuchilla de San Francisco. The increased magnesium concentration is most likely caused by incongruent dissolution of limestone where magnesium and calcium ions are added to the ground water from the dissolution of limestone in the Madera Formation and nearly pure calcite is reprecipitated. Magnesium concentrations and magnesium-calcium ratios thus tend to increase along the flow path of water undergoing such reactions (Hem, 1985). In the

vicinity of Cuchilla de San Francisco, this probably reflects a relatively long travel time from the recharge area.

In the Mesozoic ramp, samples from the same geologic formation, but at different locations, have very different chemical compositions as well as a wide range of TDS concentrations (Figure 24). In general, samples collected from the central part of the Mesozoic ramp near the Caballo, Agua Sarca, and Pomecerro faults, and along the Placitas fault zone (group A) have lower TDS (<810 ppm) and are calcium-magnesium bicarbonate-sulfate type waters. Samples collected from the Mesozoic ramp away from these faults have high TDS concentrations (up to 5950 ppm) caused by high sulfate concentrations. Sodium-bicarbonate type water (group B) was collected from the Petrified Forest Formation.

Ground water in the basin zone also has a wide range of compositions and generally has low TDS concentrations (Figure 25). There are two geochemical trends apparent in Figure 25. Trend A, increasing magnesium and sulfate concentrations, is produced by samples from the north end of the Caballo fault. Trend B, increasing sodium, sulfate, and chloride concentrations, is typical of the geochemical evolution of ground water from tectonic basins and produced by samples from the basin west of the Ranchos fault.

Surface water samples PSW-02, PSW-03, PSW-04 and PSW-07 (Figure 15) are low-TDS calcium bicarbonate type water typical of surface water (Figure 26). Sample PSW-06, from Arroyo de San Francisco, has elevated magnesium and sodium similar to the springs that discharge into the arroyo. Sample PSW-01, from lower Arroyo de Ojo del Orno, has higher TDS and sulfate concentrations suggesting that a significant portion of the stream flow is from spring PS-19 and/or dissolves sulfate minerals as it flows over the Mancos and Menefee Formations. The elevated sodium and chloride in PSW-05, which was collected from Lower Las Huertas Creek just before the creek dried up, may have been concentrated by evaporation. PSW-07 was collected where water was seeping out of the ground into the dry stream bed and is representative of shallow ground water.

Trace Elements

Only SiO_2 analyses are usable as tracers and contribute to the understanding of the ground-water flow systems in the study area. Elevated silica concentrations are indicative of long ground-water residence

times. The concentration of silica ranges from 0.96 to 110 ppm and is generally less than 40 ppm (Figure 27). Higher concentrations of silica were measured in samples from the Upper Santa Fe formation in the basin west of the Valley View fault, and in samples from the Menefee formation in the northern part of the Mesozoic ramp (Figure 28). There are no state or federal drinking water standards for silica.

The occurrence and concentration of As, Cu, F, Fe, Mn, NO_3, and Zn affect drinking water quality within the study area. The concentration of arsenic ranges from 0 to 64 ppb and is generally less than 20 ppb (Figure 29). All samples from the Upper Santa Fe axial and transitional facies, and some of the samples from the Upper and Lower Santa Fe Piedmont facies contained detectable arsenic. Arsenic was also detected in the Abo, Agua Sarca, Petrified Forest, Morrison and Point Lookout formations. The highest concentrations (36 to 64 ppm) are found in the Upper Santa Fe axial and transitional facies west of the Valley View fault (Figure 30). Arsenic concentrations between 10 ppm and 20 ppm are found in ground water from the Santa Fe group sediments west of the Ranchos Fault and at the northern part of the Escala fault. Arsenic concentrations between 10 ppm and 20 ppm are also found in ground water from the Agua Sarca and Petrified Forest Formations and the Morrison Formation where it is in contact with the Agua Sarca and Petrified Forest Formations. The Abo Formation east of Cuchilla de San Francisco has ground water with low concentrations of arsenic. No samples exceeded the New Mexico domestic water standard (100 ppb) and only the one sample (PW-205) exceeded the USEPA drinking water standard (50 ppb). These standards are currently under review and are expected to be lowered to, or below, 20 ppb. If standards are lowered to 10 ppb several community and commercial water supply systems will be affected.

The concentration of copper ranges from 0 to 270 ppb and is generally less than 20 ppb (Figure 31). The highest concentration was found in a sample from the Harmon sandstone member of the Menefee Formation in the northern part of the Mesozoic ramp. Copper in excess of 40 ppb is found in two isolated samples from the Upper Santa Fe and one sample from the Mancos shale in the village. New Mexico and USEPA standards for copper in drinking water (1000 and 1300 ppb respectively) were not exceeded in any samples.

The concentration of fluoride ranges from 0 to 1.6 ppm, and is usually less than one ppm. Fluoride was detected in nearly all samples and in samples from every geologic formation tested (Figure 32). The Agua

Sarca, Morrison, Dakota, and Upper Santa Fe Formations consistently have low concentrations (<0.75 ppm). The Abo, Petrified Forest, Mancos, and Lower Santa Fe formations can yield fluoride concentrations higher than 1 ppm. New Mexico and USEPA standards for fluoride in drinking water (1.8 and 4.0 ppm respectively) were not exceeded in any samples.

The concentration of iron ranges from 0 to 6.6 ppm and is generally less than 1 ppm (Figure 33). Iron was detected in all but one formation tested. Iron concentrations in excess of 2 ppm were found in samples from the Santa Fe, Menefee, Point Lookout, Dakota, and Morrison Formations. New Mexico standards for iron in drinking water (1 ppm) were exceeded by 11 samples and USEPA standards (0.3 ppm) were exceeded by an additional 13 samples. Three of these samples were collected from community water systems for which the standards are enforceable.

The concentration of manganese ranges from 0 to 580 ppb and is generally less than 100 ppb (Figure 34). Manganese was detected in all geologic formations except the Upper Santa Fe axial facies. The Petrified Forest, Morrison, and Point Lookout Formations consistently produce ground water with manganese concentrations in excess of 50 ppb. New Mexico standards for iron in drinking water (200 ppb) were exceeded by 3 samples and USEPA aesthetic standards (50 ppb) were exceeded by an additional 13 samples. One of these samples was collected from a community water system for which the standards are enforceable.

The concentration of nitrate ranges from 0 to 15 ppm, and is generally less than 5 ppm (Figure 35). Nitrate was detected in nearly all samples and in samples from all but one geologic formation. Nitrate concentrations greater than 5 ppm are found in ground water from the Lower Santa Fe piedmont deposits at isolated sites along the Escala fault and in ground water from the Lower Mancos, Dakota, and Petrified Forest Formations at one site each in the Mesozoic ramp. There is a cluster of three sites in upper Las Huertas Canyon where ground water from the Abo Formation has nitrate concentrations ranging from 3.6 ppm to 12 ppm (Figure 36). Elevated nitrate concentrations typically have an upgradient anthropogenic source. State and federal drinking water standards for nitrate are not exceeded by any samples collected for this study.

The concentration of zinc ranges from 0 to 1300 ppb (Figure 37). Samples from the Upper and Lower Santa Fe Formations generally contained less than 600 ppb, and samples from the Paleozoic and Mesozoic formations generally contained less than 200 ppb. New Mexico standards for zinc in drinking water (1000 ppb) were exceeded by 4 samples and USEPA standards (500 ppb) were exceeded by an additional 13 samples. Two of these samples were collected from community water systems for which the standards are enforceable.

Ground-Water Dating

The results of ^{14}C and tritium analyses, and ground water age interpretations are listed in Table 5. Qualitative ground water ages were first estimated from tritium results using criteria from Clark and Fritz (1997) for continental regions (Table 6). *Submodern ground water,* which was recharged prior to 1952 has a tritium concentration less than 0.8 tritium units (TU). *Modern ground water* has detectable tritium concentrations. Modern ground water that has been recharged since less than five to ten years ago has 5 TU to 15 TU. Ground water with a tritium concentration from 0.8 TU to about 4 TU is a mixture of submodern and modern water. Ground water dominantly recharged, or mixed with recharge from the 1960's through 1980's (>15 TU) is not present or has been significantly diluted by submodern or modern ground water.

Carbon-14 results were then used to further segregate *fossil ground water* from submodern ground water. Carbon-14 activities are normalized to 95% of the NBS oxalic acid (modern carbon) standard (Stuvier and Polach, 1977). The mean residence time of ground water has been calculated from uncorrected ^{14}C activities using the standard decay equation with modifications to account for (1) ^{14}C half-life of 5730 years (Godwin, 1962), (2) variations in the atmospheric ^{14}C levels in the past (Bard et al., 1990, and Pearson et al., 1986), (3) changes in the initial ^{14}C activity during open system conditions, (4) carbonate dissolution during closed conditions, and (5) a base year of 1997 (Equation 4).

$$t = -8267 \times \ln \frac{a^{14}C}{q \times a_0{}^{14}C} \qquad (4)$$

where t = time since recharge (years).

$a^{14}C$ = radiocarbon activity measured in dissolved inorganic carbon (DIC) in ground water (Table 5).

$a_0{}^{14}C$ = initial radiocarbon activity in soil (calculated in Equation 8).

q = dilution factor (calculated in Equation 5).

The dilution factor was determined using the $\delta^{13}C$ mixing model summarized in Clark and Fritz (1997) and accounts for closed system dilution of carbon-14 by carbonate dissolution between the time of recharge and sampling (Equation 5).

$$q_{\delta^{13}C} = \frac{\delta^{13}C_{DIC} - \delta^{13}C_{Carb}}{\delta^{13}C_{rech} - \delta^{13}C_{Carb}} \tag{5}$$

where $\delta^{13}C_{DIC}$ = $\delta^{13}C$ of DIC in ground water sample to be dated (Table 5).

$\delta^{13}C_{Carb}$ = composition of marine limestone, assumed to be 0 ‰ PDB.

$\delta^{13}C_{rech}$ = $\delta^{13}C$ composition of DIC in the infiltrating ground water (calculated in Equation 6).

Changes to carbon-14 during recharge are accounted for by estimating the $\delta^{13}C$ of recharge based on the $\delta^{13}C$ of the soil and the enrichment factor between soil gas and DIC in the infiltrating ground water.

$$\delta^{13}C_{rech} = \delta^{13}C_{soil} - \varepsilon^{13}C_{DIC-CO_2(soil)} \tag{6}$$

where $\delta^{13}C_{Soil}$ = estimated $\delta^{13}C$ composition of soil gas in the recharge area (-23 ‰ PDB, Clark and Fritz, 1997).

$\varepsilon^{13}C_{DIC\text{-}CO2(soil)}$ = enrichment factor between DIC and soil gas (9.0 ‰).

The plants which dominate at higher elevations in the Sandias, and at lower elevations in a more temperate and humid climate of 10,000 years or more ago, produce soil-respired gas with average $\delta^{13}C$ = -27 ‰ by the Calvin (C_3) pathway (Vogel, 1993). Outgassing of high CO_2-concentration soil gas to the atmosphere imparts an additional fractionation (Cerling et al., 1991) so $\delta^{13}C_{(soil)}$ = -23 ‰ was used.

The enrichment factor, $\varepsilon^{13}C_{DIC\text{-}CO2(soil)}$, is based on the pH of the soil, which determines the relative concentrations of carbonate species dissolved in the infiltrating ground water, and the fractionation factors between dissolved carbonate species and soil gas. In neutral soils (pH = 6.4 to 10.3) such as the well buffered soils overlying the Madera Formation, virtually all dissolved carbonate is in the bicarbonate form and the choice of pH is not as critical as in acidic or basic soils. The fractionation factor between DIC and soil CO_2 is thus equal to the fractionation factor between dissolved carbonate species and soil CO_2 ($\varepsilon^{13}C_{DIC\text{-}CO2(soil)}$). The fractionation factor was calculated from the following equation by Mook et al. (1974) to be 9.2 ‰ PDB:

$$\varepsilon^{13}C_{HCO_3\text{-}CO_2(g)} = 9.552\ (10^3T^{-1}) - 24.10 \qquad (7)$$

where T = the temperature at which equilibration occurs in the recharge area. The temperature used (13.9 °C) was the temperature of the surface water in the area presumed to be the most significant recharge area, upper Las Huertas Creek (PSW-03).

The initial ^{14}C in soil ($a_o{}^{14}C$ in Equation 4) was modeled from data from Bard et al. (1990) and Pearson et al. (1986) to account for changes in the carbon-14 composition of the atmosphere since 40,000 years before present according to the following:

$$a_0{}^{14}C = 98.44 + \frac{60.25}{1 + e^{-\left(\frac{t-14619}{3761}\right)}} \qquad (8)$$

where t = the calculated age of the sample.

The initial ^{14}C activity must be calculated from an estimate of the mean residence time, which is then refined using the calculated initial ^{14}C activity. Multiple iterations of these calculations yield the best estimate of the mean residence time of the ground water.

The ground water ages estimated from carbon-14 activities should be used with caution. Geochemical processes not accounted for (including dolomite dissolution, matrix diffusion, sulfate reduction, geogenetic CO_2, and methanogenesis) can cause overestimation of the ground-water age. The uncertainties in the

particular geochemical systems affecting the ground water sampled and the available data make the carbon-14 less useful for determining precise ages of ground water younger than about 2000 yrs than for older ground water. Despite these limitations, the ages estimated by the foregoing method are useful for identifying water that is isolated from currently active ground-water flow systems.

The analysis of carbon-14 and tritium ages and $^{2}H/H$ ratios permits ground water to be divided into three end-member age groups (*modern, submodern,* and *fossil ground water*) and the identification of mixing between these groups (Table 5 and Figure 38). The presence of modern ground water is identified by detectable tritium (e.g. PW-073 and PW-163). Fossil ground water, which was recharged in a climate different from the current climate, has a carbon-14 age greater than 10,000 yrs and/or a $^{2}H/H$ ratio less than -100‰ (PW-103, PW-149, and PW-143). Submodern ground water, which has been recharged during the Holocene more than 50 yrs ago, has a carbon-14 age less then 10,000 yrs, a tritium concentration less then 4 TU, and a $^{2}H/H$ ratio greater than -100‰ (PS-010).

Discordant tritium and carbon-14 ages, and $^{2}H/H$ ratios are an indication of mixed waters (Mazor et al., 1986). Ground water that has a carbon-14 age younger than 10,000 yrs, has detectable tritium concentration less than 4 TU, and a $^{2}H/H$ ratio greater than -100‰ is a mixture of modern and submodern recharge (PW-005, PW-089, and PW-109). Ground water that contains tritium, and has a $^{2}H/H$ ratio less than -100‰ is a mixture of modern and fossil water (PW-039). Ground water that has a carbon-14 age greater than 10,000 yrs and a $^{2}H/H$ ratio greater than -100‰ is a mixture of submodern and fossil water (PW-071 and PW-041).

The analysis of chlorofluorocarbon (CFC) determinations (N. Plummer, written comm., 1997) permits ground water to be divided into two age groups (*modern* and *submodern ground water*, Table 7). Discrimination between submodern and fossil ground water is not possible from CFC data alone. The mean residence time of ground water has been modeled from atmospheric concentrations and water solubility curves from Szabo et al. (1996) and Ekwurzel et al. (1994). Samples with detectable CFC concentrations were probably recharged within the past 56 years and are considered to be modern ground water. Samples containing CFC concentrations greater than historical atmospheric concentrations were considered to be contaminated and ages were not calculated.

Stable Isotopes

Ground-water samples can be divided into six groups based on their $\delta^{18}O$ and $\delta^{2}H$ compositions and major processes affecting the $\delta^{18}O$ and $\delta^{2}H$ compositions (Figure 39). Ground water that plots within the 99% confidence interval for the local meteoric water line is interpreted as being recharged by direct infiltration of precipitation or infiltration of surface water that has not been affected by evaporation (*unfractionated water*). Ground water that has a depleted composition along the local meteoric water line has been recharged by a greater proportion of winter snow melt and ground water with an enriched composition along the local meteoric water line has been recharged by a greater proportion of summer thunderstorms. Five of the 44 unfractionated samples have been ^{14}C dated and have mean residence times from recent to 8610 yrs.

Ground water with an unusually low deuterium excess, and/or a disproportionately large depletion along the local meteoric water line compared to unfractionated water, was probably recharged during a time when the climate was significantly different from the present climate (*fossil water*). Three of the five fossil ground water samples in this group have been ^{14}C dated and have mean residence times from 27,400 yrs to greater than 35,250 yrs. There is a group of 11 samples that have $\delta^{18}O$ and $\delta^{2}H$ compositions intermediate between the fossil water and the unfractionated recent recharge that may be caused by mixing (*mixed-age water*). The stable isotope composition of mixed-age ground water is defined by the ground water at PW-039 ($\delta^{2}H$=-100‰, $\delta^{18}O$=-12.5‰) and PW-071 ($\delta^{2}H$=-97‰, $\delta^{18}O$=-12.3‰). Ground-water dating methods previously discussed have shown that the ground water at PW-039 is a mixture of fossil and modern water and the ground water at PW-071 is a mixture of fossil and submodern water.

The remaining 30 ground-water samples that plot below the meteoric water line have been fractionated by evaporation (*evaporation-altered water*). Evaporation from an open body of water before infiltration imparts a characteristic fractionation (slope of 3 to 5) that is preserved during ground-water recharge. Evaporation from Las Huertas Creek is enhanced by low stream flows, low humidity, and high temperature typical of the streams in the study area during the summer. Two samples of evaporation-altered ground water have been age dated. The most depleted is PW-041 ($\delta^{2}H$=-96‰, $\delta^{18}O$=-12.0‰) which is a mixture of fossil and submodern water. The ground water at PW-073, which is more enriched than most evaporation-

altered water (δ^2H=-90‰, $\delta^{18}O$=-11.4‰), is modern water. The two ground-water samples that are most enriched in $\delta^{18}O$ (*^{18}O-enriched water*, PW-119 and PW186) may have been affected by water-rock interactions or by evaporation of soil moisture during the direct infiltration of precipitation. Evaporation and repeated cyclic movement of soil water within 1 m of the surface may be causing the ^{18}O enrichment. Over time, the cycling and infiltration processes tend to produce a consistent soil water stable isotope composition below the active zone (Liu, 1995). Soil water displaced by subsequent recharge events by piston flow should preserve the ^{18}O enrichment in the recharge (Allison, 1982). Although water-rock exchange is typical of ground water from deep sedimentary basins and hydrothermal systems, isotope exchange between cool (10°C to 20°C) ground water and limestone has also been observed (Clayton et al.,1966). The rate of exchange depends on aquifer properties not measured by this study (water-rock mass ratio, grain size of the rocks, the fraction of exchange completed, and the dominant exchange mechanism) and temperature. Isotope exchange rates are slower at low temperatures and faster at smaller water-rock ratios. Complete equilibration can take from a few months to 10^6 yrs (Cole et al., 1983). Determination of which process is causing the enrichment in the two ^{18}O-enriched samples is unnecessary because both processes (evaporation of soil water and water-rock exchange) indicate that the aquifers represented by these samples receive only very limited ground-water recharge.

There are six ground-water samples with $\delta^{18}O$ and δ^2H compositions that plot above the local meteoric water line (*deuterium enriched water*). This ground water may have been enriched in δ^2H by exchange with hydrocarbons, hydrogen sulfide, and/or hydrated minerals, or possibly by hyperfiltration.

The $\delta^{18}O$ and δ^2H composition of surface water is presented in Figure 40. Sample PSW-05 was collected downstream of sample PSW-04 and just above the point where Lower Las Huertas Creek completely dried up (Figure 15). The line connecting these two samples in $\delta^{18}O$ - δ^2H space has a slope of 4.4 which would be caused by evaporation from an open surface at about 50% humidity (Gonfiantini, 1986). Enrichment by evaporation is supported by the increased sodium and chloride concentrations in PSW-05 compared to PSW-04. Evaporation from the creek is enhanced by the turbulent low flow and high temperatures in the summer. Samples PSW-03 and PSW-01 are also evaporation-altered. Sample PSW-03 may have been fractionated by evaporation from upper Las Huertas Creek in August, and PSW-01, which

was collected from Arroyo de Ojo del Orno in March, may have been fractionated by partial evaporation from the acequias and arroyos that are fed by the Placitas springs. An evaporation line with a slope of 4.4 (the same slope as the line connecting PSW-05 and PSW-04, Figure 40), extrapolated from PSW-01 to the meteoric water line, intercepts PSW-03 and points to a hypothetical stable isotope composition of an unfractionated ground-water source for these surface waters ($\delta^{18}O \approx -13.2$ ‰ and $\delta^{2}H \approx -99$ ‰). Infiltration of surface water from the streams and arroyos at locations near PSW-02, PSW-04 and PSW-06 would recharge unfractionated water. Sample PSW-07 was collected from Lower Las Huertas Creek where water was seeping out of the ground in the bed of the creek and is directly representative of ground water.

As expected, the isotopic composition of ground and surface water is more homogenous than the composition of precipitation (Figure 41). Ground-water samples have $\delta^{2}H$ values that range from -80 to -117 ‰ and $\delta^{18}O$ values that range from -10.5 to -14.3 ‰ (Figure 39). Surface-water samples have $\delta^{2}H$ values that range from -83 to -93 ‰ and $\delta^{18}O$ values that range from -10.4 to -11.7 ‰ (Figure 40). The median isotope composition of unfractionated ground water ($\delta^{18}O = -12$ ‰, $\delta^{2}H = -91$ ‰) is more depleted than the volume-weighted annual average stable isotope composition of precipitation ($\delta^{18}O = -10.1$ ‰, $\delta^{2}H = -74$ ‰) suggesting that most ground-water recharge comes from winter frontal systems originating over the northern Pacific Ocean.

A rough estimate of the seasonality of ground-water recharge can be made by comparing the stable isotope composition of ground water to that of precipitation. Recharge in semi-arid environments occurs only when a precipitation event exceeds a threshold intensity and duration. Below this threshold, infiltrated water is lost to evapotranspiration or replenishment of the soil moisture deficit. The more frequent and intense precipitation generated by El Niño is thus more effective at recharging ground water and probably controls the stable isotope composition of ground water. Using only the enriched stable isotope composition of El Niño precipitation ($\delta^{18}O = -4.0$ ‰, $\delta^{2}H = -30$ ‰ collected September 2, 1997 and $\delta^{18}O = -15.6$ ‰, $\delta^{2}H = -115$ ‰ collected February 12, 1998), it is estimated that about 83% of ground-water recharge is from winter frontal systems originating over the northern Pacific Ocean.

Limitations of Data

The regional distribution of geochemical parameters illustrates the heterogeneity and complexity of ground-water flow in the study area but does not clearly define the compartmentalization of aquifers in the study area or allow differentiation between individual aquifers or ground-water flow systems. The distribution of TDS, dissolved oxygen, and the ground-water temperature all deviate somewhat from the standard basin model. The concentration of specific ions in ground water is often unique to a particular zone in addition to the geologic formation the water is from. The distribution of trace constituents is primarily a function of which geologic formation produced the ground water. Dating methods reveal that modern ground water is often down gradient of fossil water. Ground water with each of the six stable isotope signature compositions is found in nearly every part of the study area. Ground waters with very different stable isotope compositions are found in close proximity to each other and in the same geologic formation, and ground waters with nearly identical stable isotope compositions are found at isolated locations and in different formations throughout the study area.

The complexity of the structure and stratigraphy in the Placitas area requires that interpretations be made by examining the geochemistry at a smaller scale and within the hydrogeologic framework. To facilitate this evaluation, the three hydrogeologic zones are further divided into eight sub-zones. These sub-zones are divided primarily along structural and stratigraphic boundaries and group aquifers with similar hydraulic characteristics (Figure 42). The geochemistry of the ground water in these areas is illustrated in Figure 43 through Figure 66. Within each of the eight sub-zones, there is still a wide distribution of ground-water geochemistry caused by compartmentalized aquifers and preferential ground-water flow pathways, but the major ion and stable isotope analyses are much more clustered. These local clusters make it easier to identify ground-water flow pathways and to distinguish the effects of individual structures and stratigraphic units.

DISCUSSION

This section presents an interpretation of the spatial distribution of geochemical parameters to qualitatively describe regional ground-water flow. Ground-water flow in the hydrogeologic sub-zones is first discussed, then a quantitative analysis of recharge rates is presented.

Hydrogeologic Zones and Sub-zones

The three hydrogeologic zones are divided into eight sub-zones (Figure 42). The mountain hydrogeologic zone is divided into the upper Las Huertas Canyon and Cuchilla de San Francisco sub-zones. The upper Las Huertas Canyon sub-zone includes the northeast part of the Sandia Mountains south of the Placitas fault zone and the Tecolote Fault, and west of the Crest of Montezuma. The Cuchilla de San Francisco area includes the Crest of Montezuma and stretches from the San Francisco Fault on the west to the study area boundary on the east and north. Ground water in these sub-zones is produced from the laterally extensive and fractured Madera Limestone.

The Mesozoic ramp hydrogeologic zone is divided into the central, eastern, and western sub-zones. The limited extent, relatively thin bedding of permeable units, and heterogeneity of the Mesozoic formations compartmentalizes aquifers and requires that the geochemical data be evaluated on a smaller scale. The central Mesozoic ramp sub-zone extends from the unnamed fault east of the Pomecerro Fault westward to the Caballo Fault and north of the Placitas fault zone to the Todilto-Morrison contact. Ground water in this part of the Mesozoic ramp is contained in a complex set of discontinuous sandstone and limestone aquifers that are interbedded with shale aquitards, and compartmentalized by faults. The eastern Mesozoic ramp sub-zone is bounded on the south and southeast by the Placitas fault zone, on the north by the contact between the Menefee and Santa Fe Formations, and the Lomos Fault, on the west by the Caballo Fault, and on the southwest by the Todilto-Morrison contact. The ground-water flow system in this sub-zone is a system of interbedded sandstone aquifers and shale aquitards. The west part of the Mesozoic ramp is bounded on the south and east by the Caballo Fault, on the southwest by the Placitas fault zone, on the west by the Ranchos

Fault, and on the north by the contact between the Menefee and Santa Fe Formations. The ground-water flow system in this sub-zone is also a system of interbedded sandstone aquifers and shale aquitards.

The basin hydrogeologic zone is divided into the northeast, north-central, and western basin sub-zones. Ground water in these sub-zones is produced from the Santa Fe group sediments. The northeast basin sub-zone stretches from the San Francisco Fault on the east and southeast, to the Escala Fault on the west, and from the contact between the Menefee and Santa Fe formations on the southwest to the study area boundary on the north. The north-central basin sub-zone is bounded on the south by the contact between the Lower Santa Fe Formation and the Menefee Formation, on the southeast by the Caballo Fault, on the east by the Escala Fault, and on the north and west by the study area boundary. The western basin sub-zone includes the study area west of the Ranchos Fault to the study area boundary. The sub-zones are discussed in generally down-gradient order.

Las Huertas Canyon

The principle water bearing geologic formations in the Las Huertas Canyon sub-zone are the Madera Formation in upland areas and the Abo Formation in the floor of the Las Huertas graben. Ground water from the Madera Formation (*Madera type water*) has a high dissolved oxygen concentration, low temperature (<14°C), and low TDS concentration (<400 ppm, Figure 43), that is dominated by calcium and bicarbonate ions (Figure 44). The Abo Formation in Las Huertas Canyon usually produces water nearly identical to Madera type water. Two samples (PW-154 and PW-164) from the Abo Formation have slightly higher magnesium concentrations relative to Madera type water. The stable isotope compositions of ground water from both formations are tightly grouped into unfractionated, evaporation-altered, and mixed-age waters (Figure 45). There are two sources for ground-water recharge to the Madera Limestone aquifer in this sub-zone: direct infiltration of precipitation and/or snow melt and infiltration of surface water from Las Huertas Creek.

The ground water at PS-01 and PW-004 west of Cuchilla Lupe, and PW-003, PW-100, and PW-101 in Las Huertas Canyon was recharged primarily by infiltration of surface water from Las Huertas Creek. The strongest evidence for recharge from the creek is the isotopic match between these ground water samples

and a surface-water sample from Las Huertas Creek, PSW-03 (Figure 45). PSW-03 was collected from Las Huertas Creek just down stream of the Suela Fault (Figure 15). The ground water discharging from PS-01 has an evaporation-altered stable isotope composition that is consistent with ground water recharged from a surface water source. It is unlikely that this spring discharges ground water from a deep, regional flow system that originates high in the Sandia Mountains. The most likely recharge area is the stretch of Las Huertas Creek that crosses the Madera Limestone between the Suela and West Las Huertas faults.

Springs PS-02, PS-03, and PS-04 on Cuchilla Lupe discharge ground water with similar unfractionated stable isotope compositions (Figure 45) that suggest that these springs are recharged in a different manner than PS-01. Two possible sources of recharge that could produce ground water with an unfractionated stable isotope composition are infiltration of unfractionated surface water or direct infiltration of precipitation. Infiltration of surface water from Las Huertas Creek is consistent with the rapid increase in discharge from PS-04 (Johnson, 1999). Recharge from Las Huertas Creek to PS-02, PS-03 and PS-04 would have to occur at a different time of year than the recharge that supplies PS-01 because the water discharging from these springs has a different stable isotope composition than the water discharging from PS-01. Alternately, ground-water flow paths and travel times from Las Huertas Creek to PS-02, PS-03 and PS-04 could be significantly different than flow paths and travel times to PS-01. The unfractionated stable isotope composition is more consistent with direct infiltration of precipitation or snowmelt. Time-series data are not available to distinguish between these alternatives.

The ground waters at PW-051, PW-154, and PW-164 from the Abo Formation in Las Huertas Canyon, are loosely related by elevated nitrate (Figure 36) and magnesium concentrations, and depleted stable isotope compositions. Nitrate concentrations are highest at PW-164 (12 ppm) and decrease towards the northwest (7.5 ppm at PW-154 and 5.5 ppm at PW-051). The ground water at PW-051 and PW-164 are also related by similar stable isotope compositions. The stable isotope composition of the ground water at PW-154, which is not as depleted as that of the water at PW-164 and PW-051, suggests the aquifer at this location receives recharge from an unfractionated source. The ground water at PW-154 and PW-164 both have elevated magnesium concentrations, possibly from the incongruent dissolution of limestone. The

ground water represented by these samples may enter the Abo Formation from a lengthy, slow, or minimally recharged ground-water flow path through the Madera Limestone southeast of the canyon.

Ground-water flow in the Madera Formation is characterized by localized and discrete flow paths, along high-permeability faults and fractures, that are superimposed upon a regional flow system. The localized flow paths in the Madera Limestone permit both direct infiltration of precipitation and infiltration of surface water to contribute recharge to discrete parts of the aquifer.

Cuchilla de San Francisco

The principle water bearing geologic formations in the Cuchilla de San Francisco sub-zone are the Upper Madera Limestone along Cuchilla de San Francisco, the Abo Formation east of Cuchilla de San Francisco, and the Lower Santa Fe piedmont deposits west of the San Francisco Fault. Ground-water temperatures are higher in this sub-zone than in upper Las Huertas Canyon and the highest temperatures are found at the north end of Cuchilla de San Francisco (Figure 46). Ground water east of the San Francisco fault has consistently lower dissolved oxygen concentrations than ground water west of the fault. The quality of water from the Madera Formation is excellent, with a slightly increased sodium concentration and higher TDS compared to Madera type water (group , Figure 47). The Lower Santa Fe Formation west of the San Francisco fault produces water similar to the Madera Formation, but with less variation in anion concentrations (group B). The Abo Formation yields water with higher TDS, sodium, magnesium, and sulfate concentrations (group C) than water from the Abo Formation in Las Huertas Canyon. Ground water can be divided into two groups based on stable isotope data: a group of five samples from the Madera Formation and Santa Fe Group in the central part of this sub-zone around PW-089 (Figure 46), and a second group of samples from the springs that discharge at the northern end of the sub-zone. There are several outliers of fossil and ^{18}O-enriched ground water, mostly from east of the San Francisco fault (Figure 48). Tritium, CFC, and ^{14}C age dating results show that modern, submodern, and fossil water is present in this sub-zone (Table 6, Table 7, and Figure 38).

Chemical and isotopic data suggest that ground water from the Madera Formation of Cuchilla de San Francisco has a similar origin as that from Upper Las Huertas Canyon, but a much longer residence time. A

similar origin is supported by the low TDS ground water in both areas, and by the similar stable isotope composition of the two main groups of water in each area. The higher temperatures, higher sodium concentrations, and lower dissolved oxygen concentration in ground water from the Madera Formation of Cuchilla de San Francisco compared to Upper Las Huertas Canyon are indicative of a longer residence time. The most likely flow path connecting these areas is through the Madera Limestone east of Las Huertas Canyon.

Ground water from wells on both sides of the San Francisco fault (PW-082, PW-089, PW-090, PW-110, and PW-161 in Figure 46) have similar stable isotope compositions that suggest a common origin. However, ground water west of the fault has a significantly higher dissolved oxygen concentrations (4.38 to 7.98 ppm) than ground water east of the fault (1.53 to 2.04 ppm) which indicates that a hydraulic discontinuity is associated with the fault. This discontinuity is also supported by a dramatic drop in ground-water levels from Cuchilla de San Francisco westward across the San Francisco fault. Furthermore, ground water in the Madera Formation at PW-089 has a mean residence time of 8610 years, while ground water down gradient and west of the San Francisco fault at PW-216 has a much younger CFC age of 44 years (N. Plummer, unpubl., 1997). The high dissolved oxygen concentration and irregular ground-water ages across the San Francisco fault require a preferential pathway for ground-water flow to this part of the Santa Fe aquifer, other than through the Madera Formation and across the fault.

All springs along the San Francisco fault (PS-07 in Tecolote, and PS-17, PS-10 and PS-11 at the north end of Cuchilla de San Francisco, Figure 46) discharge water with a similar geochemical composition. These springs all discharge low TDS (285 to 360 ppm) calcium-sodium-bicarbonate type ground water with low dissolved oxygen (1.8 to 2.85 ppm), and have similarly unique stable isotope compositions. This suggests that a continuous, fault-controlled, and fault-parallel preferential flow path transmits ground water from the Upper Las Huertas Canyon area through the Madera Formation to its truncation at the north end of Cuchilla de San Francisco.

Ground water discharges from the Madera Formation to Santa Fe Group piedmont deposits at the northern end of Cuchilla de San Francisco. This flow path is demonstrated by the geochemistry of ground water discharging from the travertine deposits overlying basin-fill sediments at springs PS-10 and PS-11

(Figure 46). The low-dissolved oxygen, high-temperature, and tritium-free water discharging from these springs is indicative of distal recharge, and the low TDS, sodium-calcium-bicarbonate water type is characteristic of water from the Madera Formation in this sub-zone. Surface flow across the San Francisco fault is illustrated by the geochemistry of water from Arroyo de San Francisco (PSW-06) which is very similar to the water discharged by PS-10 and PS-11. The ground water from PW-077, which is screened in Santa Fe piedmont deposits, has major ion concentrations that are similar to those of PSW-06, a dissolved oxygen concentration and ground-water temperature that are intermediate to those at PSW-06 and the springs, and contains measurable amounts of CFC's (N. Plummer, unpubl., 1997). This combination of geochemical characteristics is most likely caused by mixing of subsurface flow from the Madera Formation with infiltration from Arroyo de San Francisco, and shows that ground water moves into this region of the Santa Fe Group aquifer via both subsurface and surface pathways.

Permeable units in the Abo Formation east of the San Francisco fault are isolated from ground-water flow originating in Las Huertas Creek. The isolation from recent recharge is shown by the higher temperatures and higher TDS, sulfate, magnesium, and sodium concentrations in ground water from the Abo Formation northeast of the San Francisco fault (PW-118, PW-119, and PW-120) than in ground water from the Abo Formation in Las Huertas Canyon. Northward flow of ground water from Las Huertas Creek is probably impeded by the South Montezuma fault which down-drops the Abo Formation against the Madera Formation. Slow ground-water flow to PW-095 is shown by the low dissolved oxygen, fossil stable isotope composition, and the concentration of sulfate and sodium in the ground water produced by this well. Ground water must either flow across bedding planes of the Abo Formation to reach PW-095 from the Madera Formation, or flow from the South Montezuma fault along strike through isolated permeable beds of Abo sandstone.

Ground water along south-to-north transect in this sub-zone yields both mixed and variable ages. For example, the ground water at PS-10 has the youngest ^{14}C age in this sub-zone (4340 yrs), whereas ground water from an up-gradient well (PW-089) yields a significantly older ^{14}C age of 8610 years. The oldest ground water in this sub-zone occurs to the north and east in the upper Madera and Abo Formations at PW-071, which has a fossil ^{14}C age and submodern stable isotope composition, and at PW-095, which has a

fossil stable isotope composition. The tritium content of ground water at PS-10, PW-089, and PW-071 is 1TU or less indicating that the Madera aquifer at these locations does not receive significant modern recharge. The fossil ages and stable isotope compositions of water from the Abo Formation northeast of Cuchilla de San Francisco are consistent with hydraulic and geochemical isolation of this formation and the variable ages of water from the Madera formation are consistent with the existence of a multiple preferential flow paths transmitting water through the Madera Formation.

This sub-zone constitutes a large and dynamic system characterized by south to north ground-water pathways and barriers to ground-water flow to the east and west. The Madera Formation is the major water transmitting geologic unit in this sub-zone. The San Francisco fault appears to be a hydrologic barrier that attenuates ground water movement between the Madera and Santa Fe Group aquifers along much of its trace north of Tecolote. In addition, the San Francisco fault appears to facilitate the movement of water through the Madera Formation in a continuous path parallel to the fault. The combination of impermeable boundaries, extreme topographic gradients, increased transmissivity in a fault parallel direction, and the progressive thinning and eventual truncation of the Madera aquifer with consequent ground-water discharge, are all consistent with a three-dimensional flow system that is dominated by south to north horizontal hydraulic gradients, vertically upward hydraulic gradients, and a discharge area at the northern termination of the Madera Formation.

Northeast basin

The principle water bearing geologic formation in the northeast basin sub-zone is the piedmont facies of the Lower Santa Fe Group. TDS concentrations are between 280 and 500 ppm, dissolved oxygen concentrations are between 0.49 and 7.98 ppm, and ground-water temperatures range from 14.6°C to 20.3°C (Figure 49). Major ion analyses fall into three distinct groups (Figure 50): calcium bicarbonate type water with only slightly more sodium and sulfate than Madera type water (group A) from along Las Huertas Creek, calcium-sodium bicarbonate type water (group B) from the basin northwest of Cuchilla de San Francisco, and sodium-calcium bicarbonate-sulfate type water (group C) from along the Escala fault. There is a cluster of samples with stable isotope compositions along the meteoric water line, a group of three

evaporation-altered water samples, and one each fossil, deuterium enriched, and ^{18}O-enriched water (Figure 51). One sample from this sub-zone (PW-143) has been ^{14}C and tritium dated as fossil water.

Geochemical analyses of ground- and surface-water samples from along lower Las Huertas Creek in this sub-zone suggest that there are two types of shallow ground water along the creek related to different gaining and losing reaches, and deep ground water that is geochemically unique from shallow ground water. The shallow Santa Fe Group aquifer along the losing reach of the creek just below Tecolote (PW-097) could be recharged by interaquifer flow across the San Francisco fault, reinfiltration of ground water discharged by PS-07, and/or infiltration of surface water from upper Las Huertas Creek. The ground water at PW-097 has an evaporation-altered stable isotope composition that is more fractionated than the water discharging from PS-07, and is calcium-bicarbonate type water with a slightly higher sodium concentration than Madera type water. The additional isotopic fractionation beyond that of PS-07 could be caused by evaporation from the arroyo carrying the overflow from the spring and from small irrigation ditches in a nearby orchard before the excess water crosses the San Francisco fault and infiltrates the into basin-fill sediments. The degree of evaporative fractionation in the ground water at PW-097 suggests that near Tecolote overland flow of water from the Crest of Montezuma (PS-07) is more significant than interaquifer flow across the San Francisco fault. There is also little evidence that infiltration of late-season surface water represented by PSW-04 (which has an unfractionated stable isotope composition) is a significant source of recharge.

Along the gaining reach of the creek at PS-08 and PSW-07, the stable isotope composition of shallow ground water plots between the composition of local surface water (PSW-04) and fossil ground water, and the stable isotope composition of PSW-07 is the same as PW-154 (Figure 45) in upper Las Huertas Canyon. The stable isotope compositions of PS-08 and PSW-07 may be caused by mixing of modern unfractionated water with fossil ground water. The higher temperatures, slightly higher TDS, sodium, and sulfate concentrations, and lower dissolved oxygen concentration in ground water discharged at PSW-07 and PS-08, compared to Madera type water, are indicative of a longer residence time compared to upper Las Huertas Canyon. This suggests that this part of the Santa Fe Group aquifer is recharged by interaquifer flow from the Las Huertas Canyon area, possibly at a discrete location near the highly faulted junction of the

Placitas fault zone, the San Francisco fault, the Las Huertas Canyon fault system, and the South Montezuma fault at Tecolote.

Deep ground water from PW-186 has a stable isotope composition that is more ^{18}O-enriched than any other ground water in the study area, and has TDS, sodium, and sulfate concentrations that are higher than any other water from the Santa Fe Group aquifer. The unique geochemical composition of the ground water at PW-186 suggests that the aquifer represented by this sample is isolated from the interaquifer flow that supplies PS-08 and PSW-07. The ^{18}O-enriched stable isotope composition could be caused by evaporation from Las Huertas Creek, and the moderate dissolved oxygen concentration suggests that recharge to this aquifer compartment occurs locally. The major ion and stable isotope composition of the ground water at PW-186 is also quite different from all samples from the Menefee formation, suggesting that water from the Menefee formation does not enter the basin-fill aquifer. The Menefee Formation and the black dike may be hydraulic boundaries that contribute to the compartmentalization of the Santa Fe Group aquifer at this location. The stable isotope and major ion compositions of the ground water at PW-094 are also different from all others along Las Huertas Creek and suggest that the aquifer supplying this well is also isolated from the Madera Formation.

There are two types of ground water along the Escala fault north of Las Huertas Creek: fossil ground water at PW-143 and relatively younger ground water at PW-142 and PW-150. The ground water at PW-142 and PW-150 has dissolved oxygen concentrations, TDS concentrations, and temperatures that are similar to ground water directly west of the San Francisco fault, but different from ground water in the Madera Formation of Cuchilla de San Francisco (Figure 49). The unfractionated stable isotope composition of the water at PW-142 and PW-150 is similar to the unfractionated water from Las Huertas Canyon and suggests that the water at these wells has been recharged within the Holocene and is part of an active ground-water flow system. There is no geochemical evidence of recently recharged ground water at PW-143. The dissolved oxygen concentration at PW-143 is lower, the temperature is higher, and sodium and sulfate concentrations are higher than those of ground water along Las Huertas Creek and from the Santa Fe Group aquifer just west of the San Francisco fault. The carbon-14 age of older than 35,250 yrs is a further indication that this water is not part of an active ground-water flow system. The presence of stagnant ground

water in the basin east of the Escala fault could be caused by hydrodynamic isolation between to two active flow paths. The two largest sources of recharge to the basin aquifer between the San Francisco and Escala faults are: (1) interaquifer flow across the highly faulted junction of the San Francisco fault and the Placitas fault zone near Tecolote, and (2) ground water discharged from the Madera Formation to the Santa Fe Group aquifer by subsurface (PW-077) and surface flow (PSW-06) at the north end of Cuchilla de San Francisco (previously discussed on page 46). Recharge from ephemeral flows in arroyos between the San Francisco and Escala faults is expected to be minimal. The paleo-flow direction in the Lower Santa Fe Formation in this part of the basin is from northeast to southwest (Connell et. al., 1995) and channel sands could facilitate flow of water recharged from Arroyo de San Francisco towards PW-142 and PW-150.

In summary, the dramatic change in the stable isotope and major ion composition of ground water along Las Huertas Creek, and the location of the gaining reach of the creek, illustrate the compartmentalization of aquifers, separation of ground-water flow paths, and further suggest that ground-water flow across the San Francisco fault is limited to discrete locations: the highly fractured junction of the San Francisco fault and the Placitas fault zone, and the termination of the Madera Formation north of Cuchilla de San Francisco. Between these two recharge windows, the San Francisco fault appears to be a hydrologic barrier between the Madera Formation of Cuchilla de San Francisco and the Santa Fe Group aquifer. A stagnant zone of fossil water exists between the two ground-water flow paths from the recharge windows.

Central Mesozoic ramp

The most exploited aquifers of the central Mesozoic ramp sub-zone are in the Agua Sarca, middle Petrified Forest, Entrada, Morrison, Dakota, and Mancos Formations. Ground water in this area has TDS less than 810 ppm, temperatures from 12.9°C to 20.1°C, and dissolved oxygen concentrations from 1.35 ppm to 5.26 ppm (Figure 52). Major ion analyses (Figure 53) show Madera type water in the Placitas fault zone (group A), increased magnesium in the ground water just north of the Placitas fault zone (group B), high sulfate water further north (group C), and sodium bicarbonate-sulfate type water (group D) from some wells screened in the middle sandstone of the Petrified Forest Formation. Ground water can be divided into

four groups based on stable isotope data (Figure 54): two groups of unfractionated water, a pair of deuterium-enriched waters, and a group of evaporation-altered water. Outliers of mixed-age, evaporation-altered, and unfractionated water are also present. Tritium, CFC, and ^{14}C age dating results show that modern and submodern water is present in this sub-zone (three samples, Table 5, Table 7, and Figure 38).

Springs PS-05 and PS-09 discharge ground water typical of the Madera Formation that, along with the ground water at PS-24, has an unfractionated stable isotope composition. The lack of isotope fractionation, like that observed in the ground water at some locations in Las Huertas Canyon, illustrates that the water discharging from these springs has been recharged by direct infiltration of precipitation. The mean ground-water residence time of 13 years at PS-05 (Figure 7) suggests that ground-water flows relatively unimpeded from the recharge area to this spring. These geochemical data are consistent with the recharge area being on the adjacent north slope of the Sandia Mountains.

The ground-water along the Caballo-Pomecerro fault network is fresher and water levels are consistently higher than in adjacent sub-zones. Artesian wells (PW-006, PW-045, and PW-133), springs (PS-05, PS-09, and PS-024), and abundant wetland vegetation (Figure 52), and high ground-water ridges projecting northward from the Placitas fault zone (Figure 9) are common to this sub-zone. North of the Placitas fault zone, TDS concentrations along the Pomecerro fault are low compared to water from corresponding sedimentary units away from the fault. Ground water from the Petrified Forest Formation near the Pomecerro fault (PW-44, PW-45, PW-046, and PW-122) has a lower sulfate and TDS concentrations than ground water from the same formation away from the fault (PW-006 and PW-007). The concentration of sulfate at PW-133, along the unnamed fault east of the Pomecerro fault, is also lower than at PW-006 and PW-007. Ground water pumped by PW-006 and PW-007 to the east has a distinctively different geochemical composition, with a high TDS concentration, deuterium-enriched stable isotope values, and calcium to calcium-sodium sulfate type water, all characteristic of poorly flushed aquifers. These data suggest that the Petrified Forest formation at PW-006 and PW-007 is isolated from recharge in the Sandias by the Placitas fault zone. Ground water discharging at spring PS-24 suggests that mudstone in the lower Petrified Forest Formation also locally impedes ground-water flow across the Placitas fault zone west of the Pomecerro fault. Significant amounts of ground water cross the Placitas fault zone into the

Mesozoic ramp where permeable Triassic and Permian formations are in fault contact with the Madera Limestone. For example, just east of the Pomecerro Fault, the Placitas fault zone juxtaposes the Madera Formation against the Yeso, Glorieta, San Andres, Moenkopi, and Agua Sarca Formations. The water table map (Figure 9, Johnson 1999) for this area suggests that faulted sandstone and limestone units permit significant interaquifer ground-water flow from the Sandia Mountains. The low temperature and TDS concentration, presence of tritium, and an unfractionated stable isotope composition similar to PS-05 suggests that the ground water in the Agua Sarca Formation at PW-005 is well connected to the Madera Formation, and that recharge to this portion of the Agua Sarca Formation occurs by interaquifer flow. The combined water level and geochemical data from along the Caballo-Pomecerro fault system support the existence of preferential flow paths that facilitate ground-water flow northward across, and away from, the Placitas fault zone.

Ground water with a mixed-age stable isotope composition, low dissolved oxygen concentration, and relatively high temperature is present at isolated locations in this sub-zone. The ground water PW-046 and PW-107, completed in the low permeability mudstones of the upper Petrified Forest Formation, has a mixed-age stable isotope composition and a high chloride concentration that suggest that ground water in the upper Petrified Forest Formation is isolated from recent recharge. The low dissolved oxygen and higher temperature of ground water at PW-145 suggests that ground water in this Morrison aquifer has a longer residence time and is less frequently recharged than the nearby Agua Sarca aquifer at PW-005 and that the Morrison aquifer is not directly connected to the Madera Formation in the Sandia Mountains. Even though the Caballo-Pomecerro fault network appears to provide a preferential flow path for ground water, stratigraphic boundaries still isolate and compartmentalize ground water in this sub-zone.

In the middle sandstone of the Petrified Forest Formation west of the Agua Sarca Fault, the geochemistry of the ground water at PW-073 points to a distinct source of recharge but the source of recharge to PW-030 (also completed in middle sandstone of the Petrified Forest Formation), which has a significantly different stable isotope composition, is less certain. The ground water at PW-073 has a low temperature, low TDS and high dissolved oxygen concentrations, an evaporation-altered stable isotope composition, and contains tritium. These data strongly support infiltration of surface water from Arroyo

Agua Sarca as a main source of recharge for PW-073. The ground water at both PW-030 and PW-073 is sodium-bicarbonate type water possibly caused by cation exchange in the Petrified Forest Formation. The higher temperature and TDS concentration, and lower dissolved oxygen concentration in the ground water at PW-030 suggest that the middle Petrified Forest aquifer is not hydraulically connected between these two locations. The stable isotope composition of the ground water at PW-030 however, is unfractionated and more like the composition of ground water at PW-145. The ground-water at PW-030 appears to be recharged by interaquifer flow from the Madera Formation along the Agua Sarca fault.

In summary, ground water in this sub-zone exists in a complex set of discontinuous sandstone, siltstone, and limestone aquifers that are both isolated and connected by a complex fault network, and isolated by interbedded shale aquitards. Recently recharged ground water from the Madera Formation on the north slope of the Sandia Mountains flows along high permeability sedimentary units and faults, and mixes with older ground water that has been affected by reactive and soluble aquifer materials.

Eastern Mesozoic ramp

The most exploited aquifers in the eastern Mesozoic ramp sub-zone are the Jurassic Morrison and Cretaceous Dakota, Hosta-Dalton, and Point Lookout Formations. Some portions of the Lower Mancos Shale also produce water. Dissolved oxygen concentrations range from 0.99 ppm to 7.19 ppm, temperature ranges from 12.5°C to 21°C, and TDS concentrations range from 360 ppm to 7540 ppm (Figure 55). Ground water in this sub-zone can be divided in to three groups based on major ion concentrations (Figure 56). Ground water from along the Placitas fault zone and Cuchilla Lupe generally is similar to Madera type water (group A). Calcium-sodium sulfate-bicarbonate type water (group B) and water with high sodium and/or sulfate concentrations (group C) are produced by aquifers in the Menefee, Petrified Forest, or Lower Mancos aquifers. One sample, PW-001, appears to be a mixture of water from group A and group B. Ground water in this sub-zone can also be divided into five groups based on the stable isotope compositions (Figure 57). There is a group of mixed age or fossil water (four samples), two groups of evaporation-altered water (seven samples), unfractionated water (five samples), deuterium-enriched water (three samples). The stable isotope and major ion analyses do not necessarily produce the same sample groups. Tritium and ^{14}C

age dating results show that modern, submodern, and fossil water is present in this sub-zone (Table 5, Table 7, and Figure 38).

The steep ground-water gradient and the presence of springs along the Placitas fault zone (PS-06) and in the Abo Formation between the Suela fault and the Placitas fault zone (PS-02, PS-03, and PS-20) suggest that the fault zone locally impedes ground-water flow from the Madera Formation to aquifers to the north. In addition, high-TDS sodium-sulfate type ground water is observed immediately downgradient (northwest) of the fault zone at PW-016, PW-112, and PW-113. A long residence time for the ground water at PW-112 and PW-113 can be inferred from the mixed-age stable isotope composition, low dissolved oxygen and high TDS concentrations.

Closer to the village, Madera type water is found downgradient (west) of the Placitas fault zone. The unfractionated stable isotope composition and major ion concentrations in ground water at PW-002, which is completed in the Dakota Formation on the west side of the Placitas fault zone, are very similar to those of PS-02 and PS-03, which discharge from the Abo Formation between the Suela fault and the Placitas fault zone. The evaporation-altered stable isotope composition of ground water at PW-047, which is screened in the Lower Mancos Shale, is nearly identical to that of PS-01, located along the Suela fault. The higher sodium and sulfate concentrations in the water at PW-047 are likely caused by dissolution of aquifer minerals. The ground water at PW-012 has a low temperature, and the ground water at PS-06 and PW-012 has TDS and major ion concentrations that are similar to Madera type water but have anomalous stable isotope compositions. The very low dissolved oxygen and moderate TDS concentrations, ^{14}C age of 6300 years, mixed-age stable isotope composition, and calcium-sodium-sulfate-bicarbonate type water at PW-039 together indicate that water in the Abo Formation at this depth (490 ft) is unaffected by modern recharge, but the presence of tritium suggests that younger Madera type water is mixing with resident fossil water. These data suggest that interaquifer ground-water flow across the Placitas fault zone is a source of recharge to some aquifers northwest of Cuchilla Lupe, and that ground water crosses the Placitas fault zone only where permeable sandstone units are in fault-contact with the Madera Limestone.

The low temperature and elevated dissolved oxygen in ground water from the Menefee Formation along the Caballo fault at PS-19 and PW-147, and the relatively low TDS concentration (for ground water

from the Lower Mancos Shale) in the ground water at PW-001 suggest that the aquifers at these locations are well connected to local recharge. The evaporation-altered stable isotope compositions of ground water at PW-147 and PW-001 and surface water from Arroyo de Ojo del Orno (PSW-001) are quite similar and indicate that the aquifers at these locations may be locally recharged by infiltration of surface water from the arroyos that carry the overflow from the Placitas springs and converge nearby. The variety of sodium and sulfate concentrations in the ground water at these locations is probably controlled by the aquifer materials. Infiltration of surface water may be enhanced by higher transmissivity where faults or more permeable sandstone units intersect the arroyos. The major ion composition of ground water at PW-001 is consistent with dilution of group B (Figure 56) waters with by infiltrated Madera type water from Arroyo de Ojo del Orno. Although both PW-109 and PW-001 produce moderate TDS, calcium-sodium sulfate-bicarbonate type water, the unfractionated stable isotope composition of the ground water at PW-109 is more like that of the ground water from the Madera Formation of Cuchilla Lupe or on the north slope of the Sandias. In addition, the ground water at PW-109 has a low dissolved oxygen concentration. The aquifer at PW-109 may be recharged by interaquifer ground-water flow along the Caballo fault or more plausibly by interaquifer flow from Cuchilla Lupe along high permeability bedding planes in the Morrison and Dakota Formations

North of Arroyo del Oso, the Menefee and Point Lookout Formations (PW-023, PW-078, PW-103, PW-153, and PW-212) produce very poor quality ground water. The water at these locations has very high TDS and sulfate concentrations, and the water at PW-103 has a very high sodium concentration. Ground water in this area is warmer (19°C to 21°C), has high silica concentrations (up to 110 ppm, Figure 28), and moderately low dissolved oxygen concentrations where measured. The ground water at PW-103 contains no tritium, and has a ^{14}C age of 27400 yrs. All of these data show that the aquifers in this part of the study area are isolated from recent recharge. Potential recharge from Arroyo del Oso, Arroyo de Ojo del Orno, and interaquifer flow from the Madera Formation is restricted by the limited connection between the Hosta-Dalton, Point Lookout, and Harmon Sandstones and these recharge sources. The Hosta-Dalton Formation, Point Lookout Formation, and the Harmon Sandstone appear to be isolated from Arroyo del Oso and the Madera Formation of Cuchilla Lupe by the Lower Mancos Shale and the unnamed west-trending fault near

PW-016. Ground-water flow northwest along the Hosta-Dalton, Point Lookout, and Harmon Sandstones is most likely restricted by the black dike except possibly along faults linking the Point Lookout Formation. Recharge by infiltration of surface water from Arroyo de Ojo del Orno is limited to minor sandstone units in the lower Mancos shale. Ground water would then have to flow across unfaulted bedding planes of layered mudstone and shale in the Mancos Shale and Menefee Formation to reach the Hosta-Dalton, Point Lookout, and Harmon Sandstones. The stratigraphic barriers and the lack of a major surface water source of recharge northeast of Arroyo del Oso combine to produce aquifers that receive very little recharge and produce very poor quality water

In summary, ground-water in this sub-zone occurs in a system of relatively continuous Jurassic and more compartmentalized Cretaceous sandstone aquifers. Cretaceous sandstone aquifers north of Arroyo del Oso are isolated from recharge by interbedded shale and mudstone aquitards. The Dakota and Morrison Formations appear to be well connected to recharge. The well-connected aquifers are recharged by reinfiltration of water discharged by the Placitas springs and by interaquifer flows from the Madera Formation.

North-central basin

The water bearing geologic units of the north-central basin sub-zone are the Lower and Upper Santa Fe Formation basin-fill sediments. The ground water in this sub-zone has TDS concentrations ranging from 230 ppm to 530 ppm, dissolved oxygen concentrations greater than 5.41 ppm, and temperatures between 15°C and 19.2°C (Figure 58). Major ion analyses (Figure 59) fall into two groups: calcium-bicarbonate type water with slightly higher sodium and sulfate concentrations than Madera type water (group A), and calcium-magnesium bicarbonate-sulfate type water (group B). Most ground water is this part of the study area has been affected by evaporation (Figure 60). Tritium and ^{14}C age dating results show that only modern water is present in this sub-zone (Table 5 and Figure 38).

Ground water from the Upper Santa Fe Group aquifer at PW-024, PW-108, PW-152, PW-163, PW-203, and PW-218 is similar to Madera type water (group A in Figure 59), suggesting that water is transmitted directly from the Sandia Mountains to the basin, bypassing the Mesozoic ramp. The high

dissolved oxygen concentrations and evaporation-altered stable isotope composition suggest that the Upper Santa Fe Group aquifer along Las Huertas Creek is recharged by local infiltration of surface water. The high concentration of tritium in the ground water at PW-163 further attests to local recent recharge. The major ion and stable isotope composition of the ground water at PW-024 and PW-108 (which are screened in upper Santa Fe Group piedmont deposits) is very different from the composition of water at PW-023 and PW-078, which are screened in the Menefee Formation just to the south, suggesting that little or no water is moving into the basin-fill aquifer from the Menefee. The major ion and stable isotope composition of the ground water at PW-024 and PW-108 is also very different from the composition of ground water at PW-186, which is screened at a similar elevation in the Lower Santa Fe piedmont deposits east of the Escala fault, suggesting that there is little subsurface flow across the Escala fault. Farther north, the ground water at PW-203 and PW-217 is very different from the fossil ground water from PW-143, also east of the Escala fault (northeast basin). This further supports the notion that ground water flow is limited across the Escala fault. All data point to infiltration of surface water from Las Huertas Creek as the major source of recharge to the Upper Santa Fe Group aquifer immediately west of the Escala Fault and discount interaquifer flow across the Escala and Lomos faults.

The ground water at PW-130 has an evaporation-altered stable isotope composition and high dissolved oxygen concentration that are also consistent with recharge from a nearby surface water source. The high temperature, high TDS concentration, and elevated magnesium concentration are indicative of a long residence time in the Santa Fe Formation. The low sulfate concentration suggests that little or no water from the Mesozoic ramp reaches PW-130. The surface water at PSW-05 is much more enriched than any ground water tested in this sub-zone (and the whole study area) showing that the late season flow in Lower Las Huertas Creek is not a major source of ground-water recharge. These data suggest that infiltration of surface water from Lower Las Huertas Creek is the main source of recharge to the basin-fill aquifer at PW-130 (and presumably downstream of PW-130), but that recharge volumes are low and/or recharge events are infrequent.

The major ion composition of ground water from the Upper Santa Fe Group aquifer at PW-131, PW-169 and PW-202, and from the Lower Santa Fe Group aquifer at PW-184 (Figure 58) is intermediate

between Madera type water and the high sulfate water at PSW-01, PS-019, and PW-147. This suggests that water is entering the basin-fill aquifer at this isolated location from the Mesozoic formations to the south, either by interaquifer flow or as surface water in Arroyo de Ojo del Orno. The high dissolved oxygen concentration and evaporation-altered stable isotope composition of ground water at PW-184 is consistent with a local surface-water source of recharge, most likely Arroyo de Ojo del Orno, and precludes significant interaquifer flow from the south. The unfractionated stable isotope composition of ground water at PW-131 and PW-202 suggests that ground water may enter the basin-fill aquifer via interaquifer flow but the high dissolved oxygen concentration is more consistent with infiltration from surface water. While the major ion composition of ground water at PW-169 trends towards water from the Mesozoic ramp, the evaporation-altered stable isotope composition, low temperature, and high dissolved oxygen concentration are consistent with greater infiltration from Lower Las Huertas Creek, which is only 230 m (≈800 ft) to the south. It appears that water from the Mesozoic ramp contributes recharge to the basin-fill aquifer via infiltration from Arroyo de Ojo del Orno, and possibly by interaquifer flow.

In summary, the Santa Fe Group aquifer in this sub-zone is recharged primarily by infiltration of surface water from Las Huertas Creek. Infiltration of surface water from Arroyo de Ojo del Orno is also a source of recharge to the Upper and Lower Santa Fe basin-fill aquifers. Infiltration of surface water appears to be limited to a short reach immediately down stream of the basin-bounding faults and distal recharge is minor and/or infrequent.

Western Mesozoic ramp

The most exploited aquifers in the western Mesozoic ramp sub-zone are the Jurassic Morrison and Cretaceous Dakota, Hosta-Dalton, and Point lookout Formations. Some portions of the Lower Menefee Formation and Lower Mancos Shale also produce water. These aquifers are northeast dipping and relatively continuous and unfaulted, but are separated by interbedded shale and mudstone aquitards. Ground water in this area has TDS concentrations ranging from 230 ppm to 2250 ppm, temperatures from 16°C to 25°C, and dissolved oxygen concentrations from 0.66 ppm to only 1.9 ppm (Figure 61). Only two samples of Madera type water can be grouped based on major ion analyses (Figure 62). The remaining samples have

consistently high sulfate concentrations, but have variable calcium or sodium concentrations. Stable isotope analyses are also varied and include unfractionated, fossil, and evaporation-altered water (Figure 63). Tritium and ^{14}C dating results show that submodern and fossil water is present in this sub-zone (Table 5 and Figure 38).

The similarity of ground water at PW-008 to unfractionated Madera type water suggests that water is transmitted from the Madera Formation to the Dakota Formation, without interaction with Mesozoic formations that could alter its geochemical composition. The other sample of unfractionated Madera type water is spring season runoff from Arroyo Agua Sarca (PSW-02). The major ion and stable isotope match between PW-008 and PSW-02 suggests that Arroyo Agua Sarca is a significant source of recharge in this sub-zone. The ground water at PW-099, which has a stable isotope composition like PW-008 and a lower TDS concentration than ground water further east, may be partially recharged by infiltration from Arroyo Agua Sarca. Recharge from Arroyo Agua Sarca is infrequent, however, as this arroyo flows into the study area only for a short time after an exceptionally deep snow pack melts.

The ground water at PW-014, PW-041, PW-043, PW-063, and PW-126 has a moderately high temperature, low dissolved oxygen concentration, and a very high TDS concentration that illustrate a lack of ground-water flow through, and long ground-water residence time in, much of this sub-zone. The long residence time is also illustrated by the mixed-age stable isotope composition of ground water at PW-041 and PW-063 which suggests that some fossil ground water is still present, and by the ^{14}C ground-water age of 23,280 years at PW-041. The ^{14}C ground-water age of 31,710 years at PW-149 illustrates the lack of ground water flow through the Upper Menefee Formation near the Ranchos fault, and the absence of tritium shows that infiltration of surface water from Arroyo Agua Sarca is imperceptible at this location. The ground water at PW-149 is probably isolated by steeply dipping bedding planes of layered mudstone and shale units found in upgradient geologic formations. There are no other consistent trends in the major ion or stable isotope composition of ground water at these locations. The geochemical data illustrate the isolation of permeable units in this sub-zone.

Contrasting ridges and troughs in the potentiometric surface (Figure 9) suggest that impediments to ground-water flow and "permeability windows" exist along the Placitas fault zone and Caballo fault. Left

separation along the Caballo fault juxtaposes units of widely varying permeability resulting in limited hydraulic connection between permeable units and, locally, hydraulic connections between permeable units that are adjacent to each other. Ground-water flow across the Caballo fault is shown by a tongue of ground water flowing from the Morrison Formation and Dakota Sandstone near PW-145 northwest across the Caballo Fault into the Point Lookout and Hosta-Dalton Sandstones. Hydraulic connection between the Morrison Formation at PW-145 and the Point Lookout Formation at PW-014 is further supported by the matching stable isotope compositions of ground water from each location. There is no geochemical evidence of ground water from the Petrified Forest Formation crossing the Caballo fault from PW-030 or PW-073. The low TDS calcium-magnesium sulfate type water and unusually high ground-water level at PW-085 suggests that north and northwest trending faults that cut Pennsylvanian, Permian and lower Triassic sandstone and limestone units west of Arroyo Agua Sarca could be high permeability preferential flow paths. These preferential flow paths would minimize the geochemical effect of the Petrified Forest Formation on ground water pumped from PW-085. The evaporation-altered stable isotope composition of the ground water at PW-085 suggests that the recharge to the aquifer at this location has been fractionated by partial evaporation of surface water. Evaporation could occur as precipitation falling on the northwest face of the Sandia Mountains flows over the exposed crystalline basement prior to infiltrating the Madera Limestone just south of the Placitas fault zone or from surface-water flows in Arroyo Agua Sarca. Each of these instances illustrate that juxtaposition of permeable units permits limited recharge by interaquifer flow to formations that have no local source of recharge.

In summary, ground water in this sub-zone exists in a system of northeast dipping and relatively continuous aquifers that are isolated by interbedded shale and mudstone aquitards. Geochemical data suggest that modern recharge to these aquifers occurs only in the immediate vicinity of Arroyo Agua Sarca. Very limited interaquifer flow through "permeability windows" is the main source of recharge to permeable units distant from the arroyo.

West basin

The water bearing geologic units of the west basin sub-zone are the Upper Santa Fe Formation piedmont, transition, and axial facies. Water quality is excellent: TDS concentrations are less than 380 ppm, dissolved oxygen concentrations range from 1.59 ppm to 5.41 ppm, and ground-water temperatures range from 18.5°C to 25.6°C (Figure 64). Major ion analyses fall into two groups (Figure 65): calcium- to intermediate-bicarbonate type water from along and east of the Valley View fault (group A) and calcium-sodium-bicarbonate-chloride type water from west of the Valley View fault (group B). One sample from east of the Valley View fault does not fit in these groups (PW-166). Ground water from east of the Valley View fault generally has an unfractionated or evaporation-altered stable isotope composition while ground water from west of the fault generally has a mixed-age or fossil stable isotope composition (Figure 66). CFC results show that submodern and/or fossil water is present in this sub-zone (Table 7 and Figure 38).

Ground water east of, and along, the Valley View fault (PW-135, PW-137, PW-167, PW-179, PW-191, PW-192, and PW-211 in Figure 64) has consistently lower temperatures; lower TDS, sodium, and chloride concentrations; and higher dissolved oxygen concentrations than ground water farther west which is consistent with the standard basin model for geochemical evolution of ground water. Within this group of samples the ground-water temperature is generally lower and dissolved oxygen concentrations are generally higher to the north (PW-167 and PW-191), which indicates that Las Huertas Creek is the main source of recharge to the basin-fill aquifer in this sub-zone. Recharge from Las Huertas Creek to the basin-fill aquifer near PW-167, PW191, and PW-192 is not completely consistent with the ground-water levels in. The elevated magnesium concentration in the ground water east of the Valley View fault is probably caused by incongruent dissolution of limestone pebbles and cobbles in the Upper Santa Fe Group piedmont deposits. The anomalously high dissolved oxygen concentration in the ground water at PW-137 may be caused by infiltration of surface water from Arroyo Agua Sarca. Infiltration from Arroyo Agua Sarca may also be reflected in the ground-water high along the arroyo west of the Ranchos fault.

The higher sodium and sulfate concentrations, and lower dissolved oxygen concentration in the ground water at PW-166 (compared to other ground water between the Ranchos and Valley View faults) may be caused by mixing of water recharged by Las Huertas Creek with ground water from the Menefee formation

but is more likely caused by dissolution of aquifer materials at depth. Mixing calculations, using the major ion composition of ground water at PW-191 to represent the alluvial end member and PW-149 as the Menefee end member, suggests that about 11% of the ground water pumped by PW-166 has entered the basin-fill aquifer from the Menefee formation. The steep ground-water gradient across the Ranchos fault and seeps in Arroyo Agua Sarca at PS-23 (Figure 8) suggest that little ground water crosses the Rancho fault, which is consistent with the general lack of ground-water flow across basin-bounding faults in the study area. The ground water at PW-166 is pumped from up to 91 m (300 ft) deeper than the ground water at PW-191, opening the possibility that the elevated sodium and sulfate are caused by dissolution of aquifer materials as recently recharged water follows a descending flow path. The low chloride concentration in the ground water at PW-166 suggests that the ground water at PW-166 has not undergone as much geochemical evolution as ground water west of the Valley View fault. In my opinion, the geochemical composition of the ground water at PW-166 is best explained by the standard basin model for the geochemical evolution of ground water. Geochemical evidence for interaquifer flow from the Mesozoic ramp into the basin is limited, and suggests that the Ranchos Fault impedes interaquifer ground-water recharge to the basin-fill aquifer.

The ground water west of the Valley View fault (PW-132, PW-162, PW-173, PW-197, PW-198, PW-204, PW-205, PW-215 in Figure 64) has consistently higher temperatures, higher sodium, chloride, and silica concentrations, and lower dissolved oxygen concentrations than ground water east of Valley View fault, and mixed-age or fossil stable isotope compositions. This, together with a mean residence time greater than 56 years at PW-215, suggests that the ground water in this part of the sub-zone is relatively old, and little recharge is occurring in this part of the sub-zone. The TDS is quite low for central basin ground water suggesting that upward flow of deep basin brines is minimal at these locations. The ground water produced by the high capacity well at PW-205 has an anomalously high dissolved oxygen concentration and evaporation-altered stable isotope composition that suggest this water is cycled through multiple recharge and pumping events. Overflow from PW-205 fills settling ponds within about 10 m (≈30 ft) of the well. Partial evaporation from the ponds prior to infiltration is consistent with the evaporation-altered stable isotope composition. The geochemical data for ground water west of the Valley View fault suggests that this part of the basin is not a recharge area and possibly that residential wells in this part of the basin are the

terminal discharge area of a regional ground-water flow system that extends beyond the study area boundaries.

In summary, ground-water flow in this sub-zone generally follows a standard basin ground-water flow model of recharge at the higher elevation basin margin and discharge in the low elevation parts of the basin, and exhibits a standard basin geochemical evolution of TDS, sodium and chloride concentrations increasing down-gradient. The primary source of recharge to the basin-fill aquifer is infiltration of surface water from Las Huertas Creek and minor recharge is contributed by Arroyo Agua Sarca. Residential and community wells near the southwest border of the study area are probably within the terminal discharge area for this sub-zone, and even discharge ground water flowing from up-gradient basins.

Summary of the regional hydrogeology of the Placitas study area

This section summarizes the most important aspects of the hydrogeology of the study area. Regional ground-water recharge is summarized, then the regional effects of structure and stratigraphy on the occurrence, movement, and quality of ground water within the study area are described. The ground-water supply, recharge potential, and ground-water quality in each sub-zone is listed in Table 8. Recharge areas, geologic controls on ground-water flow, and major ground-water flow paths are illustrated in Figure 67.

Regional Ground-water Recharge

The primary source of water to the study area is precipitation in the Sandia Mountains. Winter precipitation (December through February), which falls almost exclusively at high altitudes, is the largest contribution to recharge because recharge occurs when precipitation exceeds the potential evapotranspiration. Infiltration of surface water from Las Huertas Creek is the single most important source of ground-water recharge within the study area. The creek redistributes water directly from the Sandia Mountains to the Albuquerque Basin and is the primary source of recharge to Santa Fe Group aquifers in the northwestern two-thirds of the study area. Consistent recharge to the basin-fill aquifers appears to be limited to a short reach immediately down stream of the basin-bounding faults and distal recharge is minor and/or infrequent. Infiltration of surface water from Las Huertas Creek also recharges the Madera

Limestone in Upper Las Huertas Canyon and can be discharged as far as 8 miles (13 km) north where the Madera Formation of Cuchilla de San Francisco is truncated by the San Francisco fault. Ground water in the Madera Formation is redistributed to aquifers that are not in direct contact with the Madera Formation by infiltration of spring discharge through arroyo channels. Ground water discharged from springs where the Madera Formation is truncated by the San Francisco fault is redistributed to the Lower Santa Fe Group aquifer west of the San Francisco fault by perennial surface-water flow in Arroyo de San Francisco. Arroyo de Ojo del Orno redistributes ground water discharged by the Placitas springs, El Oso Spring (PS-04) and Tunnel Spring (PS-05). Mesozoic aquifers are locally recharged by infiltration from the arroyo as far as one mile (1.6 km) down stream from the springs in the case of PW-001. Infiltration of surface water from Arroyo de Ojo del Orno is also a minor source of recharge to the Santa Fe Group aquifer where the arroyo crosses the Caballo and Lomos faults. Ephemeral flows in Arroyo Agua Sarca, which redistribute ground water from the Madera Formation high in the Sandia Mountains, are a minor source of recharge to aquifers in the west end of the Mesozoic ramp, and a secondary source of recharge to the ground-water flow systems in the basin west of the Ranchos Fault.

Regional Geologic Controls on the Occurrence and Movement of Ground Water

Faults both impede and facilitate ground water flow throughout the study area. Ground-water flow in the Madera Formation is characterized by localized and discrete flow paths along high-permeability north-trending faults and fractures and also along bedding planes. The San Francisco fault appears to be a hydrologic barrier between the Madera and Santa Fe Group aquifers except at two discrete locations: the highly fractured junction of the San Francisco fault and the Placitas fault zone near Tecolote, and the termination of the Madera Formation north of Cuchilla de San Francisco. In addition, the San Francisco fault appears to facilitate the movement of water through the Madera Formation in a continuous path parallel to the fault. Ground water along the Pomecerro-Caballo fault system exists in a complex set of discontinuous sandstone, siltstone, and limestone aquifers that are in some cases isolated, and in other cases connected, by the complex fault network. The Placitas fault zone generally impedes ground-water flow from the Sandia Mountains to Mesozoic aquifers except where permeable sandstone units are in fault-contact with the Madera Limestone or where major north-south faults such as the Pomecerro fault cross the Placitas

fault zone. Little ground-water flows across the Lomos, Ranchos, and Escala faults which cut through basin-fill alluvium.

The Madera and Abo Formations are the major water transmitting geologic units in the Mountain and Cuchilla de San Francisco hydrogeologic sub-zones. Ground-water flow in the Madera Formation is characterized by localized and discrete flow paths, along high-permeability bedding-plane fractures and faults. The ground-water flow system in the Madera Formation is a large and dynamic system characterized by south to north ground-water pathways and barriers to ground-water flow to the east and west. East of Cuchilla de San Francisco, north striking shale units in the Abo Formation isolate permeable sandstone units from the Madera Formation of Cuchilla de San Francisco.

The basin-fill alluvium of the Santa Fe Group is the most widespread aquifer and produces the highest quality water in the Placitas study area. Ground-water flow in the Santa Fe Group aquifer generally follows a standard basin ground-water flow model of recharge at the higher elevations beyond the basin margin and flow towards the center of the basin. The axial deposits of Santa Fe Group are highly permeable and the piedmont deposits are moderately permeable. Both facies provide large quantities of low TDS calcium bicarbonate type ground water. Ground water from Upper Santa Fe deposits has concentrations of arsenic up to 64 ppb. As a result of it's extent and good ground-water quality, the Santa Fe Formation is the most exploited aquifer in the study area.

Ground water is pumped from more than 20 identifiable geologic units in the Mesozoic ramp that have widely varying production capacities and water quality (Table 9). The Agua Sarca, Morrison, and Dakota Formations can provide a good source of ground water that consistently has TDS concentrations less than 1000 ppm. The Point Lookout and Menefee Formations can provide a good source of ground water that consistently has TDS concentrations more than 1000 ppm. Only the Lower Mancos, Todilto, and Lower Petrified Forest Formations are unlikely to produce a good supply of ground water. The interbedded sandstone, shale, and mudstone units and strike and dip of these formations generally results in limited exposure to surface water recharge and poor interaquifer connections.

Ground-Water Recharge Rates

The principal sources of ground-water recharge in the study area are direct infiltration of precipitation in the Sandia Mountains, and infiltration of surface water from Las Huertas Creek and ephemeral streams. Interaquifer ground-water flow is also a critical component of the ground-water budget. This section presents the theoretically important controls on recharge and attempts to constrain the amount of ground-water recharged to the study area.

The amount of ground-water recharge by direct infiltration of precipitation is affected by the amount and seasonality of precipitation, geology and soil types, and vegetation, (Lerner et al., 1990). The amount of precipitation is important because recharge is likely when precipitation exceeds a threshold value. The seasonality of precipitation is important because infiltration of winter snow-melt is a slow steady process and brief intense summer thunderstorms tent to overwhelm the specific storage of the soil to produce runoff. The seasonality of precipitation is also important because increased evapotranspiration during the spring, summer, and autumn severely limits ground-water recharge. Recharge is greater through thin, high-permeability coarse mineral soils than through a vadose zone of clay-rich soils. Aquifers with high specific storage are able to accept more recharge than aquifers with low specific storage, and the amount of recharge to an aquifer is proportional to the exposed surface area of the aquifer.

Recharge by infiltration of water from streams depends on characteristics of the stream flow, stream channel, vadose zone under the stream, and the aquifer being recharged. Greater infiltration is associated with flows of low discharge and long duration (i.e. winter type flows) as opposed to flashy short lived summer events except in areas where stream flow only occurs during exceptional local storms. The viscosity of water decreases with increasing temperature resulting in greater infiltration. The amount of infiltration is also proportional to the effective channel area (length times wetted width) and to the permeability of the sediments. Suspended sediment causes a lower channel permeability as it is deposited during flow recession. Some volume of alluvium is necessary to temporarily store the infiltrated water. The thickness of the vadose zone also affects the amount of infiltration: a near surface water table will reduce recharge rates, and a very thick vadose zone may prohibit any infiltrated water from reaching the water table as the storage space is so large compared to the infiltrated volume and recharge may be isolated in perched

aquifers. A thorough study of recharge would go to great lengths to quantify the parameters that affect both direct infiltration of precipitation and infiltration from streams (e.g. the USGS Albuquerque Basin Study, Bartolino,1997).

Ground-water recharge amounts were calculated by integrating precipitation amounts over the area recharged, taking into account the amount of precipitation, seasonality of recharge, and the geologic characteristics of the vadose zone and aquifers (Figure 68). The assumptions used in the recharge calculations are based on the foregoing discussion of recharge processes and are generous, resulting in an estimate of the *maximum* amount of ground-water recharge to aquifers in the study area. The following assumptions are explicit in the ground-water recharge calculations:

(1) Recharge by diffuse areal recharge occurs only to the Madera Limestone in the Sandia Mountains and Cuchilla de San Francisco, and runoff from the exposed Precambrian basement infiltrates more permeable formations downhill. Thus all exposed Madera limestone and Precambrian basement is considered to be recharge areas.

(2) Ground-water divides in the Sandia Mountains are assumed to coincide with surface-water drainage divides.

(3) All winter season (December 1 through February 28) precipitation infiltrates the aquifer (i.e. there is no evapotranspiration during the winter and soil-moisture deficits have been corrected by late autumn precipitation).

(4) Winter season precipitation (December 1 through February 28) constitutes 83% of total recharge, and the remaining 17% of recharge is from summer monsoons (calculated from the stable isotope data, page 40).

(5) The median amount of winter season precipitation as measured by this study and the NOAA is assumed to be representative of the long term precipitation. The median precipitation amount was calculated from precipitation amounts measured by this study and at nine NOAA sites near the study area (Table 10, Table 11, and Appendix B) after combining the precipitation amounts measured at PPT-01, PPT-02, and PPT-07 with the amounts measured at Sandia Crest, Placitas nr.,

and Bernalillo 3SW respectively. The amount of precipitation was extrapolated between stations on a 50 m (164 ft) grid using the inverse-distance-weighted method.

(6) Infiltration of surface water is only a redistribution of ground water from the Madera Limestone that was recharged by direct infiltration of precipitation.

Estimated ground-water recharge amounts are presented in Table 12. Annual recharge to the Madera Formation is estimated to range from 39% of the median annual precipitation at PPT-01 and PPT-02 to 12% of the median annual precipitation near PPT-03. The estimated annual ground-water recharge is $5.6x10^6m^3/yr$ (4500 acre-ft/yr), more than 90% of which is recharged in the Las Huertas Canyon area. The Las Huertas Canyon area receives about $5.1x10^6m^3/y$ (4100 acre-ft/yr.) of recharge from the Sandia Mountains. The Cuchilla de San Francisco area receives only $4.3x10^4m^3/y$ (35 acre-ft/yr.) of recharge from precipitation. Aquifers in the central part of the Mesozoic ramp are supplied about $1.3x10^5m^3/y$ (110 acre-ft/yr.) of recharge from the north slope of the Sandia Mountains. Aquifers in the western part of the Mesozoic ramp and the basin west of the Ranchos Fault receive a combined $32.4x10^4m^3/y$ (268 acre-ft/yr.) of recharge from Canyon Agua Sarca and the north slope of Rincon Ridge.

These recharge estimates should be used with caution and considered maximum possible amounts because violations of the underlying assumptions are likely. Large annual variations in the amount of precipitation make the short records used in these calculations unreliable for predicting the amount of recharge. Recharge in semi-arid environments occurs when a precipitation event exceeds a threshold intensity and duration, below which infiltrated water is lost to evapotranspiration or replenishment of the soil moisture deficit. No attempt was made to determine the minimum recharge threshold, and event-specific precipitation measurements were not available. The true seasonality of ground-water recharge is not known. Recharge has been described in terms of summer monsoon and winter frontal system end-members based on the stable isotope composition of the precipitation. Although recharge from monsoon storms is more likely between June and August, and recharge from frontal weather systems is more likely between December and February, recharge from both, or either, of these storms types may occur during the rest of the year. In particular, the median stable isotope composition of ground water is very similar to the stable isotope composition of the precipitation collected during the spring seasons of 1997 and 1998 which opens

the possibility that all recharge may occur between March and May. Inclusion of exposed Precambrian basement and Cuchilla Lupe in the recharge area results in generous estimate of the extent of the area recharged. Ground water recharged in the delineated recharge areas of the Sandia Mountains may not flow to the study area because precise matching of surface-water and ground-water divides is unlikely in the Madera Limestone of the Sandia Mountains, where hydraulic anisotropy and high permeability faults may focus ground-water flow across presumed drainage boundaries. For example, an unknown portion of water infiltrated from Las Huertas Creek between the Suela Fault and PW-100 probably flows eastward towards Tanque Arroyo and is not available within the study area. Recharge from infiltrating surface water has not been evaluated. Infiltration of runoff from summer thunderstorms through arroyo beds may be significant, especially in the basin west of the Ranchos Fault. Much of the surface water discharged by springs is lost to evapotranspiration along arroyos before becoming ground-water recharge. In the Sandia Mountains, transpiration, forest floor evaporation and evaporation of precipitation intercepted by the forest canopy probably all reduce the amount of water available for recharge, even in the winter.

The calculation of recharge to individual aquifers of the Mesozoic ramp, was not attempted by this study because of the complexity of the aquifer system and the uncertainty in the applicable parameters. Infiltration from surface water to distinct aquifers may occur at many locations and the characterization of stream bed and flow properties was prohibited by the number and diversity of recharge locations, and losses to evapotranspiration. An estimate of interaquifer flow was not attempted because the error associated with hydraulic conductivity estimates is greatly magnified by the number of aquifers and preferential ground-water flow pathways.

CONCLUSION

Geochemical techniques can be a valuable tool for characterizing ground-water flow through geologically complex mountain front aquifers. Geologic structures and stratigraphic units that effect the occurrence and movement of ground water were identified throughout the study area. Infiltration of surface water from Las Huertas Creek was identified as the single most important source of recharge and Las Huertas Canyon and the north slope of the Sandia Mountains were identified as locations where direct infiltration of precipitation to the Madera Formation is also a significant source of recharge. Ground-water discharge areas along the Placitas fault zone, the San Francisco fault, and in the basin were identified. Preferential ground-water flow paths along permeable stratigraphic units were identified in the Mesozoic ramp and in the Madera Limestone, and faults in the Madera Limestone were recognized as discrete ground-water flow paths. Barriers to cross-fault ground-water flow and permeability windows were identified along portions of the San Francisco fault, the Placitas fault zone, and intrabasinal faults. The residence time of ground water within this ground-water system was quantified and estimated, leading to a qualitative characterization of ground-water recharge rates. Finally, a rough estimate was made of the amount of ground water recharged to the study area.

The effectiveness of geochemistry as a primary method to characterize ground-water flow, like many other methods, is limited by data requirements. The number of samples required is proportional to the geologic complexity of the study area. This project presented a nearly optimal situation where very complex geology was balanced by a large and cooperative populace that allowed sampling from many springs and ground-water supply wells. Prior knowledge of the geology in the study area was critical to the hydrogeologic investigation. Measurements of the stable isotope and major ion composition, temperature, and dissolved oxygen concentrations were the most useful geochemical parameters measured during this study, and the use of a smaller suite of analyses may have been inadequate. Trace metal analyses were less useful for characterizing the ground-water flow system. The scale of this project precluded a detailed understanding of ground-water flow through typically sized residential properties or a quantitative

evaluation of individual aquifer characteristics, so site-specific conditions will still need to be determined on a case-by-case basis.

REFERENCES

Adams, A.I., F. Goff, and D. Counce (1995) Chemical and Isotopic Variations of Precipitation in the Los Alamos Region, New Mexico: Los Alamos National Laboratory report LA-12895-MS.

Allison, G.B. (1982) The relationship between ^{18}O and deuterium in sand columns undergoing evaporation. *Journal of Hydrology*, **55**, p. 163-169.

Anatonellini, M., and A. Aydin (1995) Effect of Faulting on Fluid Flow in Porous Sandstones: Geometry and Spatial Distribution. AAPG Bulletin, 78, p. 355-377.

Awad, M., N.E. El Aribi and M.S. Hamza (1997) Use of Solute Chemistry and Isotopes to Identify Sources of Ground-Water Recharge in the Nile Aquifer System, Upper Egypt. *Ground Water*, **35**, no. 2, p. 223-228.

Bard, E., B. Hamelin, R.G. Fairbanks, and A. Zindler (1990) Calibration of the ^{14}C timescale over the past 30,000 years using mass spectrometric U-Th ages from Barbados corals. *Nature*, **345**, p. 405-410.

Bartolino, J.R. (ed.) (1997) US Geologic Survey Middle Rio Grande Basin Study-Proceedings of the first annual workshop, Denver, Colorado, November 12-14, 1996: US Geologic Survey Open-File Report 97-116.

Caine, J.S., J.P. Evans, and C.B. Forster (1996) Fault zone architecture and permeability structure. *Geology*. **24**, no. 11, p. 1025-1028.

Cather, S.M. (1996) Toward a hydrogeologic classification of map units in the Santa Fe Group, Rio Grande rift, New Mexico. *New Mexico Geology*. **19**, no. 1, p. 15-21.

Cerling, T.E., D.K. Solomon, J. Quade, and J.R. Bowman (1991) On the isotopic composition of carbon in soil carbon dioxide. *Geochemica et Cosmochima Acta*, **55**, p. 3403-3405.

Chebotarev, I.I. (1955) Metamorphism of natural waters in the crust of weathering. *Geochemica et Cosmochima Acta*, **8**, p. 22-48, 137-170, 198-212.

Claassen, H.C. (1985) Sources and Mechanisms of Recharge for Ground Water in the West-Central Amargosa Desert, Nevada-A Geochemical Interpretation. Hydrology of Nuclear Test Sites. USGS Professional Paper 712-F.

Clark, I.D., and P. Fritz (1997) Environmental Isotopes in Hydrology. CRC Press LLC, New York.

Clayton, R.N., I. Friedman, D.L. Graf, T.K. Mayeda, W.F. Meents, and N.F. Shimp (1966) The Origin of Saline Formation Waters. *Journal of Geophysical Research*, **71**, p. 3869-3882.

Cole, D. R., H. Ohmoto, and A. C. Lasaga (1983) Isotopic exchange in mineral-fluid systems. I. Theoretical evaluation of oxygen isotopic exchange accompanying surface reactions and diffusion. *Geochemica et Cosmochima Acta*, **47**, p. 1681-1693.

Coleman, M.L., T.J. Shepherd, J.J. Durham, J.E. Rouse, and G.R. Moore (1982) Reduction of Water with Zinc for Hydrogen Isotope Analysis. *Analytical Chemistry*, **54**, no. 6, p. 993-995.

Connell, S.D., S.M. Cather, B. Ilg, K.E. Karlstrom, B. Menne, M. Picha, C. Andronicus, A. Reed, and P.W. Bauer (1995) Geology of the Placitas 7.5-Minute Quadrangle, Sandoval County, New Mexico. Open-File Digital Geologic Map OF-DM 2, 1:12000. New Mexico Bureau of Mines and Mineral Resources.

Coplan, T.B (1993) Uses of environmental isotopes. In Alley, W.B. (ed.) Regional ground-water quality. Van Nostrand Reinhold. New York.

Craig, H. (1961) Isotopic variations in meteoric waters. *Science,* **133**, p 1702-1703.

Cunningham, E.E.B., A. Long, C. Eastoe, R.L. Bassett (1998) Migration of recharge waters downgradient from the Santa Catalina Mountains into the Tucson basin aquifer, Arizona, USA. *Hydrogeology Journal*, **6**, no. 1, p. 94-103.

Dansgaard, W. (1964) Stable isotopes in precipitation. *Telus*, **16**, p. 436-468.

Davidson, E.S. (1973) Geohydrology and water resources of the Tucson basin, Arizona. USGS Water Supply Paper 1939-E.

Detmer, D.M. (1995) Permeability, porosity, and grain-size distribution of selected Pliocene and Quaternary sediments in the Albuquerque Basin. *New Mexico Geology*, **17,** no. 4, p. 70-87.

Dorroh Jr., J. H. (1946) Certain Hydrologic and Climatic Characteristics of the Southwest. University of New Mexico Publications in Engineering, no. 1. Albuquerque, New Mexico.

Ekwurzel, B., P. Schlosser, W.M. Smethie Jr., N. Plummer, E. Busenberg, R.L. Michel, R. Weppernig, and M. Stute (1994) Dating of shallow ground water: comparison of the transient tracers $^{3}H/^{3}He$, chlorofluorocarbons and ^{85}Kr. *Water Resources Research.* **30**, p. 1693-1708.

Fogg, G.E., C.D. Noyes and S.F. Carle (1998) Geologically based model of heterogeneous hydraulic conductivity in an alluvial setting. *Hydrogeology Journal.* **6,** no. 1, p. 131-143.

Freeze, R.A., and J.A. Cherry (1979) Groundwater. Prentice Hall, Inc., Englewood Cliffs, New Jersey.

Friedmann, I., G.I. Smith, J.D. Gleason, A. Warden, and J.M. Harris (1992) Stable Isotope Composition of Waters in Southeastern California 1. Modern Precipitation. *Journal of Geophysical Research*, **97**, no. D5, p. 5795-5812.

Godwin, H. (1962) Half-life of radiocarbon. *Nature*. **195**, p. 984.

Gonfiantini, R. (1986) Environmental Isotopes in Lake Studies. In Handbook of Environmental Isotope Geochemistry, Vol. 2, The Terrestrial Environment, **B**, p. 113-168. P. Fritz and J. -Ch. Fontes, eds., Elsevier, Amsterdam.

Groffman, A.R., J. Loomis and F. Pazzaglia (1997) Phase 1 Ground Water Assessment For The Placitas Area. Prepared for the Office of Planning, Sandoval County.

Hawley, J.W., C. S. Haase, and R. Lonzinsky (1995) An Underground View Of The Albuquerque Basin. In: The Water Future of Albuquerque and Middle Rio Grande Basin. Proceedings of the 39th Annual New Mexico Water Conference. New Mexico Water Resources Research Institute Report no. 290.

Hem, J.D. (1967) Equilibrium Chemistry of Iron in Ground Water. In Principles and Applications of Water Chemistry. S.D. Faust and J.V. Hunter, eds., J. Wiley, New York.

Hem, J.D. (1985) Study and Interpretation of the Chemical Characteristics of Natural Water. USGS Water-Supply Paper 2254.

Heynekamp, M.R., L.B. Goodwin, P.S. Mozley, and W.C. Haneberg (1999) Controls on Fault-Zone Architecture in Poorly Lithified Sediments, Rio Grande Rift, New Mexico: Implications for Fault-Zone Permeability and Fluid Flow. In Faults and Subsurface Fluid Flow. Geophysical Monograph Series, AGU special volume (in press). W.C. Haneberg, P.S. Mozley, L.C. Moore, L.B. Goodwin, eds.

Huntoon, P.W., and D.A. Lundy (1979) Fracture-Controlled Ground-Water Circulation and Well Siting in the Vicinity of Laramie, Wyoming. *Ground Water,* **17**, no. 5, p. 463-469.

IAEA/WMO (1998) Global Network for Isotopes in Precipitation. *The GNIP Database.* Release 2 May 1998. URL: http:// iaea.org/programs/ri/gnip/gnip.htm

Johnson, P. (1999) Phase II Water Resources Report for the Placitas Development Area. Unpublished report, by the New Mexico Bureau of Mines and Mineral Resources for Sandoval County.

Johnson, P. (1999) A double porosity model of ground-water flow in the Madera Formation based on spring hydrographs and aquifer test analysis form Placitas, New Mexico: New Mexico Geological Society Guidebook (in press).

Kelly, V.C., and S.A. Northrop (1975) Geology of Sandia Mountains and Vicinity, New Mexico. Memoir 29, New Mexico Bureau of Mines and Mineral Resources.

Kelly, V.C. (1977) Geology of Albuquerque Basin, New Mexico. Memoir 33, New Mexico Bureau of Mines and Mineral Resources.

Korte, N.E., and Q. Fernando (1991) A Review of Arsenic (III) in Groundwater. *Critical Review in Environmental Control,* **21**, no. 1, p. 1-39.

Liu, B., F. Phillips, S. Hoines, A.R. Campbell, and P. Sharma (1995) Water movement in desert soil traced by hydrogen and oxygen isotopes , chloride, and chlorine-36, southern Arizona. *Journal of Hydrology,* **168**, no. 104, p. 91-110.

Lerner, D.N., A.S. Issar, and I. Simmers (1990) Groundwater Recharge: A Guide to Understanding and Estimating Natural Recharge. IAH International Contributions to Hydrogeology, **8**, Verlag Heinz Heise, Hannover.

Levens, R.L., R.E. Williams, Dale R. Ralston (1994) Hydrogeologic role of geologic structures. Part 1: the paradigm. *Journal of Hydrology,* **156,** p. 227-243.

Lopez, T.J., and P. Hoffmann (1997) Geochemical Analyses of Ground-Water Ages, Recharge Rates, and Hydraulic Conductivity of the N Aquifer, Black Mesa Area, Arizona. USGS Water-Resources Investigations Report 96-4190.

Maloszewski, P., W. Rauert, P. Trimborn, A. Herrmann, and R. Rau (1992) Isotope hydrological study of mean transit times in an alpine basin (Wimbachtal, Germany). *Journal of Hydrology*, **140**, p. 343-360.

Mazor, E., F.C. Jaffé, J. Fluck, and J.D. Dubois (1986) Tritium corrected ^{14}C and atmospheric noble gas corrected ^{4}He applied to deduce ages of mixed groundwaters: Examples from the Baden region, Switzerland. *Geochemica et Cosmochima Acta*, **50**, p. 1611-1618.

Menne, B. (1989) Structure of the Placitas area, northern Sandia uplift, Sandoval County, New Mexico [M.S. Thesis]: University of New Mexico, Albuquerque.

Molles, M.C.Jr., C.N. Dahm, and M.T. Crocker (1992) Climatic variability and streams and rivers in semi-arid regions. In Robarts R.D and M.L. Bothwell (eds.) Aquatic Ecosystems in Semi-arid Regions: Implications for Resource Management. N.H.R.I. Symposium Series 7, Environment Canada, Saskatoon.

Mook, W.G., J.C. Bommerson, and W. H. Staverman (1974) Carbon isotope fractionation between dissolved bicarbonate and gaseous carbon dioxide. *Earth and Planetary Science Letters,* **22**, p. 169-176.

NOAA/NCDC (1998) U.S. Monthly Precipitation for Cooperative & NWS Sites. Updated August 12, 1998. URL: http://www.ncdc.noaa.gov/ol/climate/online/coop-precip.html

NOAA/OGP (1998) The El Niño - Southern Oscillation (ENSO) Home Page. URL: http://www.ogp.noaa.gov/enso/

Payne, B.R. (1988) The Status Of Isotope Hydrology Today. *Journal of Hydrology*, **100**, p. 207-237.

Pearson, G.W., J.R. Pilcher, M.G.L. Baillie, D.M. Corbett, and G. Qua (1986) High precision 14C measurement of Irish oaks to show the natural 14C variations from AD 184 to 5210 BC. *Radiocarbon*, **28**, p. 911-934.

Phillips, F.M., L.A. Peeters, M.K. Tansey, and S.N. Davis (1986) Paleoclimatic Inferences from an Isotopic Investigation of Groundwater in the Central San Juan Basin, New Mexico. *Quaternary Research*, **26**, p. 179-193.

Picha, M. (1982) Structure and stratigraphy of the Montezuma salient-Hagan basin area, Sandoval County, New Mexico [M.S. Thesis]: University of New Mexico, Albuquerque.

Pine, R.A. (1995) Modeling Groundwater Flow in the Vicinity of Dip-Slip Faults. M.S. Thesis, New Mexico Institute of Mining and Technology.

Plummer, L.N., W.E. Sanford, E. Busenberg, L.M. Bexfield, S.K. Anderholm, and P. Schlosser (1998) Tracing and Dating Ground Water in the Middle Rio Grande Basin, New Mexico-A Progress Report, *in* U.S. Geological Survey Middle Rio Grande Basin Study-Proceedings of the Second Annual Workshop. Albuquerque, New Mexico, February 10-11, 1998, USGS Open-File Report 97-116, J.R. Bartolino, ed.

Rodhe, A. (1981) Spring Flood, Meltwater or Groundwater? *Nordic Hydrology*, **12**, p. 21-30.

Rozanski, K., L. Araguas-Araguas and R. Gonfiantini (1993) Isotopic patterns in modern global precipitation. *In: Continental Isotope Indicators of Climate,* American Geophysical Union Monograph.

Runnells, D.D. (1998) Investigations of Natural Background Geochemistry-Scientific, Regulatory, and Engineering Issues. *GSA Today,* **8**, no. 3, p. 10-11.

Simpson, E.S., D.B. Thorud and I. Friedman (1972) Distinguishing seasonal recharge to groundwater by deuterium analysis in southern Arizona. In: World water balance. Proc Reading Symp 1970. International Association of Scientific Hydrology-UNESCO-WMO, p. 623-633.

Singh, V.P., and Y.K. Birsoy (1975) Studies on Rainfall Modeling, 1. Estimation of mean Areal Rainfall. WRRI Report 061, New Mexico Water Resources Research Institute.

Smith, L., C. Forster, and J. Evans (1990) Interaction of Fault zones, Fluid Flow, and Heat Transfer at the Basin Scale. In: Hydrogeology of Low Permeability Environments, from a special symposium at the 28th international Geological Congress: Washington, DC., International Association of Hydrogeologists, **2**, p. 41-67. S.P. Neuman and I. Neretnieks Eds., Verlag Heinz Heise, Hannover

Socki, R.A., H.R. Karlsson and E.K. Gibson, Jr (1992) Extraction Technique for the Determination of Oxygen-18 in Water Using Preevacuated Glass Vials. *Analytical Chemistry*, **64**, no. 7, p. 829-831.

Stuvier, M., and H. Polach (1977) Discussion: Reporting of ^{14}C Data. *Radiocarbon.* **19**, no. 3, p. 255-363.

Szabo, Z., D.E. Rice, L.N. Plummer, E. Busenberg, S. Drenkard, and P. Schlosser (1996) Age dating of shallow ground water with chlorofluorocarbons, tritium/helium-3, and flow path analyses, southern New Jersey coastal plain. *Water Resources Research.* **32**, p. 1023-1038.

Titus, Frank B. (1980) Ground Water In The Sandia And Northern Manzano Mountains, New Mexico. Hydrologic Report 5, New Mexico Bureau of Mines & Mineral Resources.

Tuan, Y., C.E. Everard and J.G. Widdison (1969) The Climate of New Mexico. State Planning Office, Santa Fe.

Vogal, J.C. (1993) Variability of carbon isotope fractionation during photosynthesis. In: Stable Isotopes and Plant Carbon - Water Relationships, p. 29-30, J.R. Ehleringer, A.E. Hall, and G.D. Farquhar Eds., Academic Press, San Diego.

Wallick, E.I., and Toth, J. (1976) Methods Of Regional Groundwater Flow Analysis With Suggestion For The Use Of Environmental Isotopes. In Interpretation of Environmental Isotope and Hydrochemical Data in Groundwater Hydrology, IAEA, Vienna.

Williams, J.L., and P.E. McAllister (1979) New Mexico in Maps. Technology Application Center, University of New Mexico, Albuquerque.

Winograd, I.J., A.C. Riggs, and T.B. Coplen (1998) The relative contributions of summer and cool-season precipitation to groundwater recharge, Spring Mountains, Nevada, USA. Hydrogeology Journal, 6, no. 1, p. 77-93.

Woodward, L.A., and B. Menne (1995) Down-plunge structural interpretation of the Placitas area, northwestern part of Sandia uplift, central New Mexico-Implications for tectonic evolution of the Rio Grande rift. Geology of the Santa Fe Region, Guidebook of the 46th NMGS Field Conference.

Woolhiser D.A., T.O. Keefer, and K.T. Redmond (1993) Southern Oscillation Effects on Daily Precipitation in the Southwestern United States. *Water Resources Research*, **29**, no. 4, p. 1287-1295.

ILLUSTRATIONS

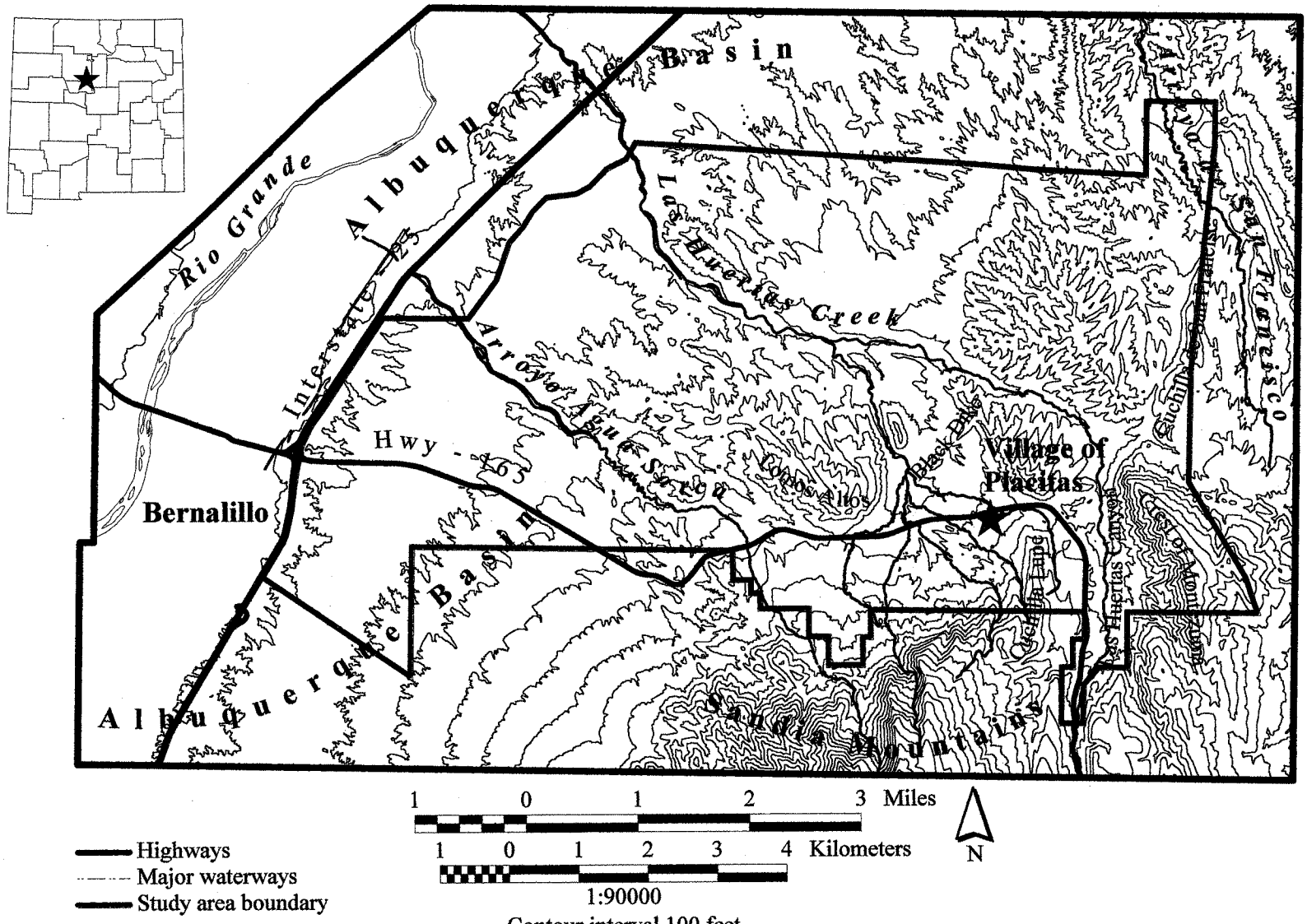

Figure 1. Study area location.

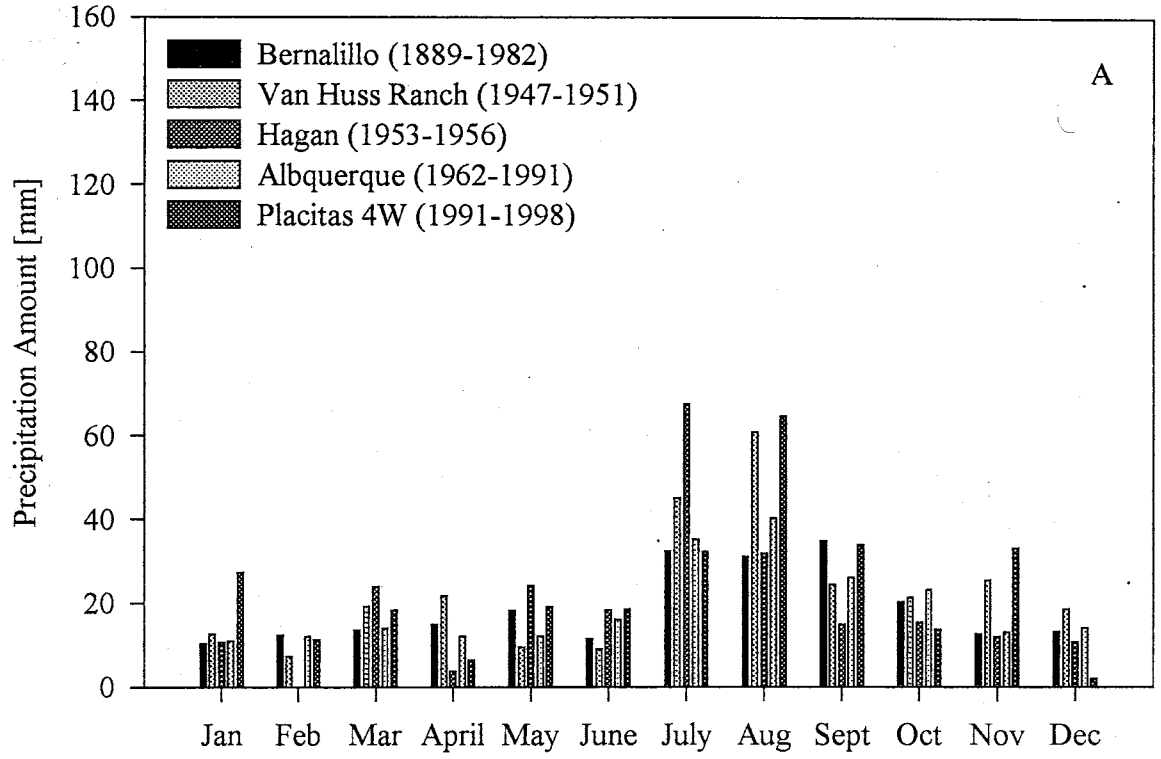

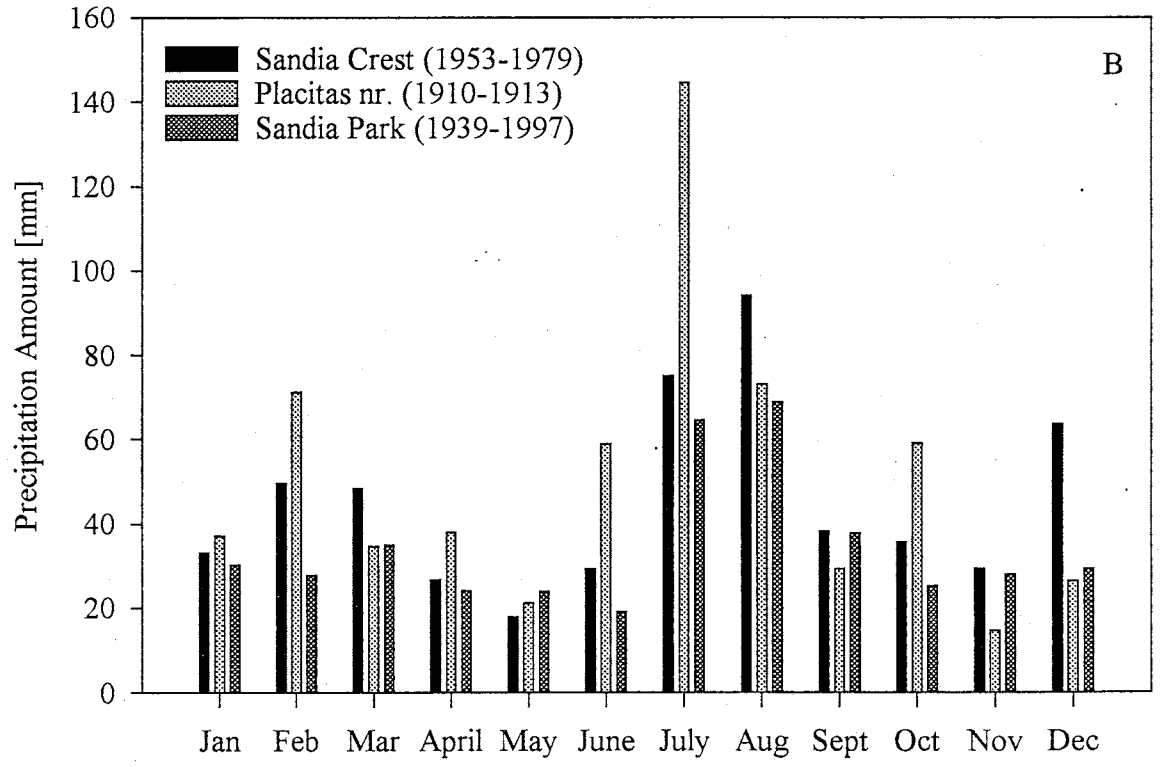

Figure 2. Average monthly precipitation at lowland NOAA stations (A), and NOAA stations in the Sandia Mountains (B) near Placitas (see Figure 11 for locations).

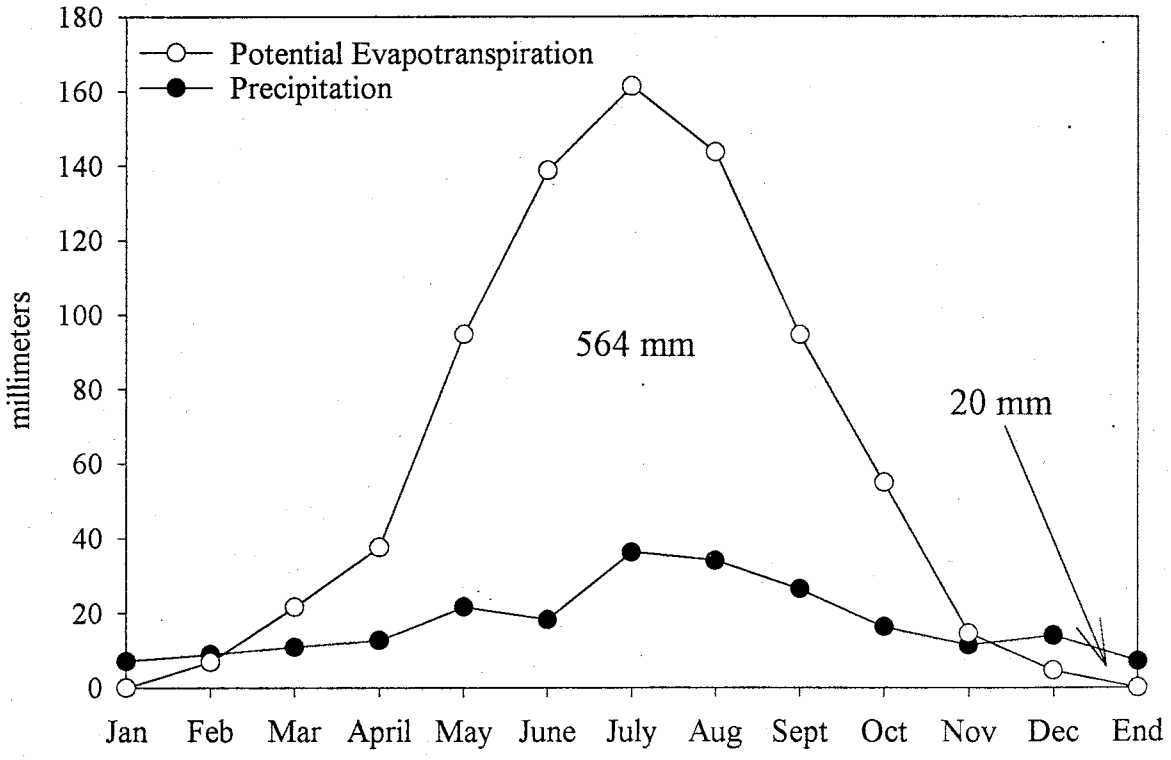

Figure 3. Potential evaporation and precipitation at Albuquerque (from Tuan et al., 1969).

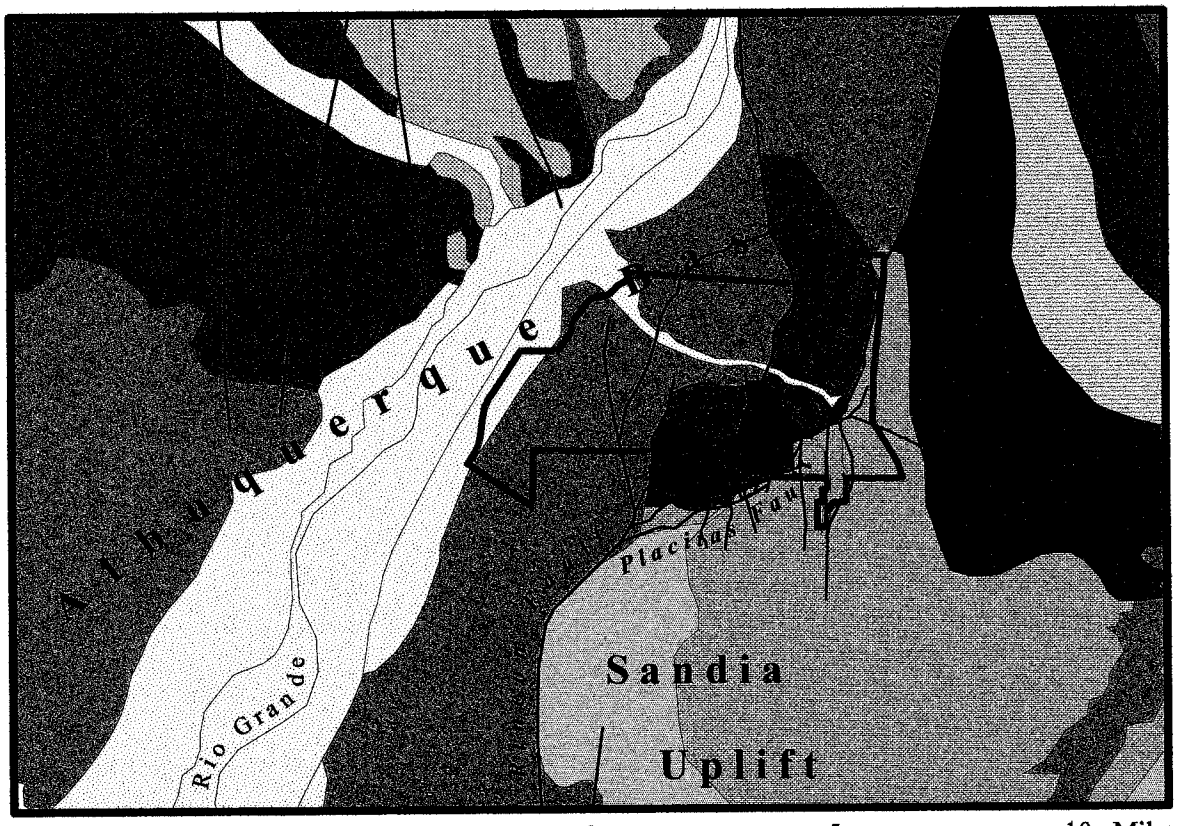

Figure 4. Geologic setting of the study area (after Hawley et al., 1995).

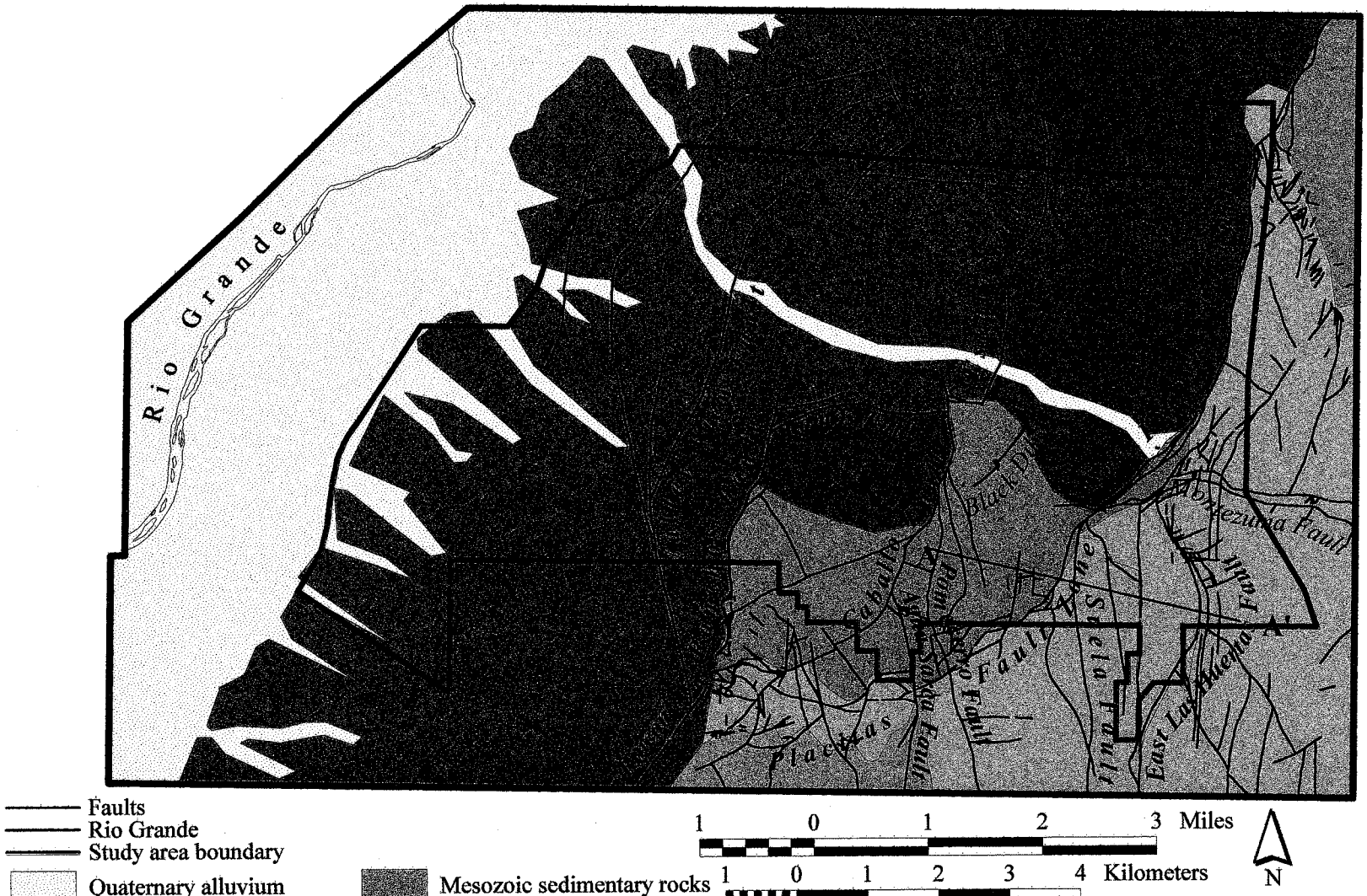

Figure 5. Generallized geology of the study area (Connell et al., 1995).

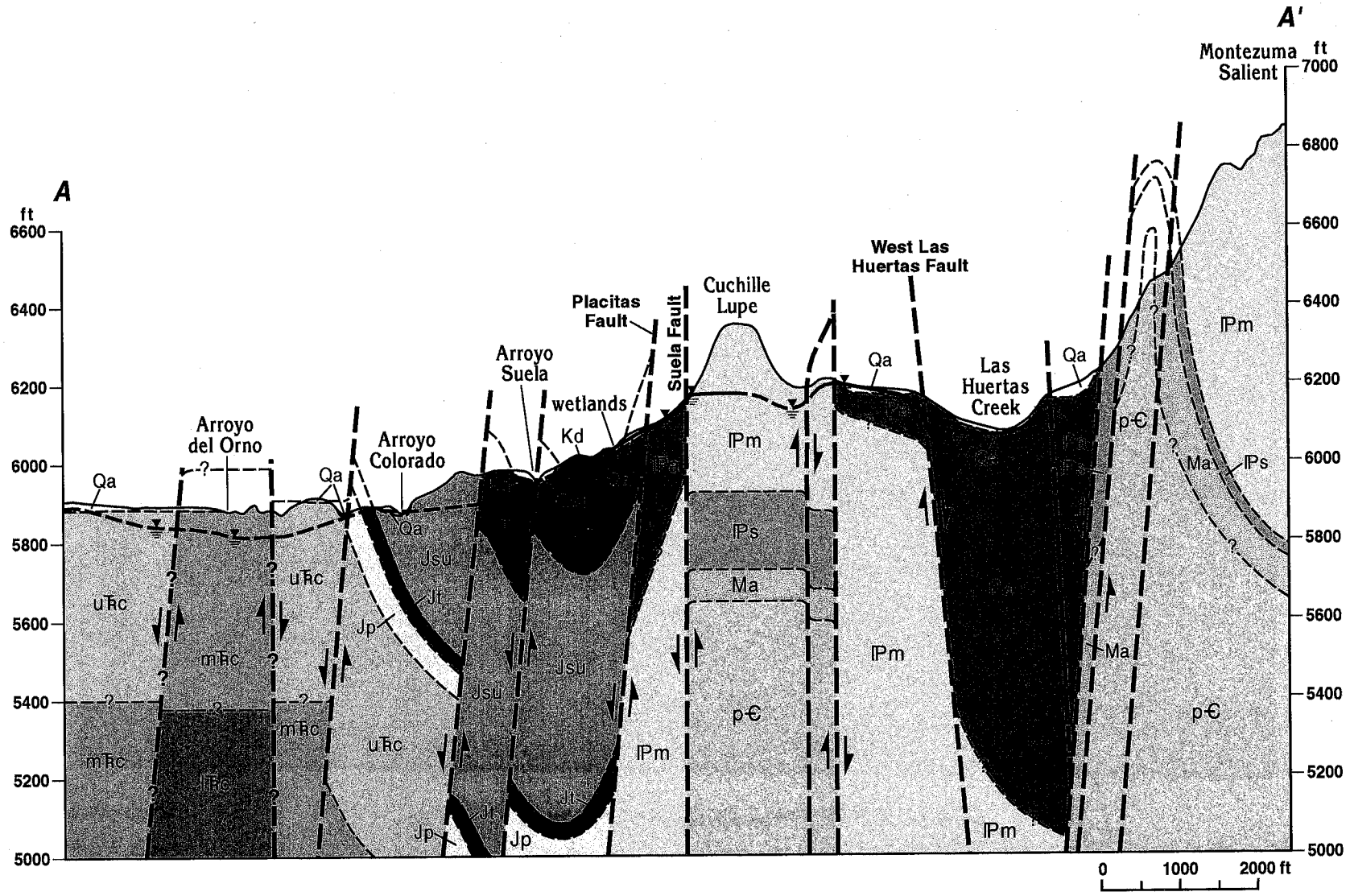

Figure 6. Geologic cross-section (Johnson, 1999)

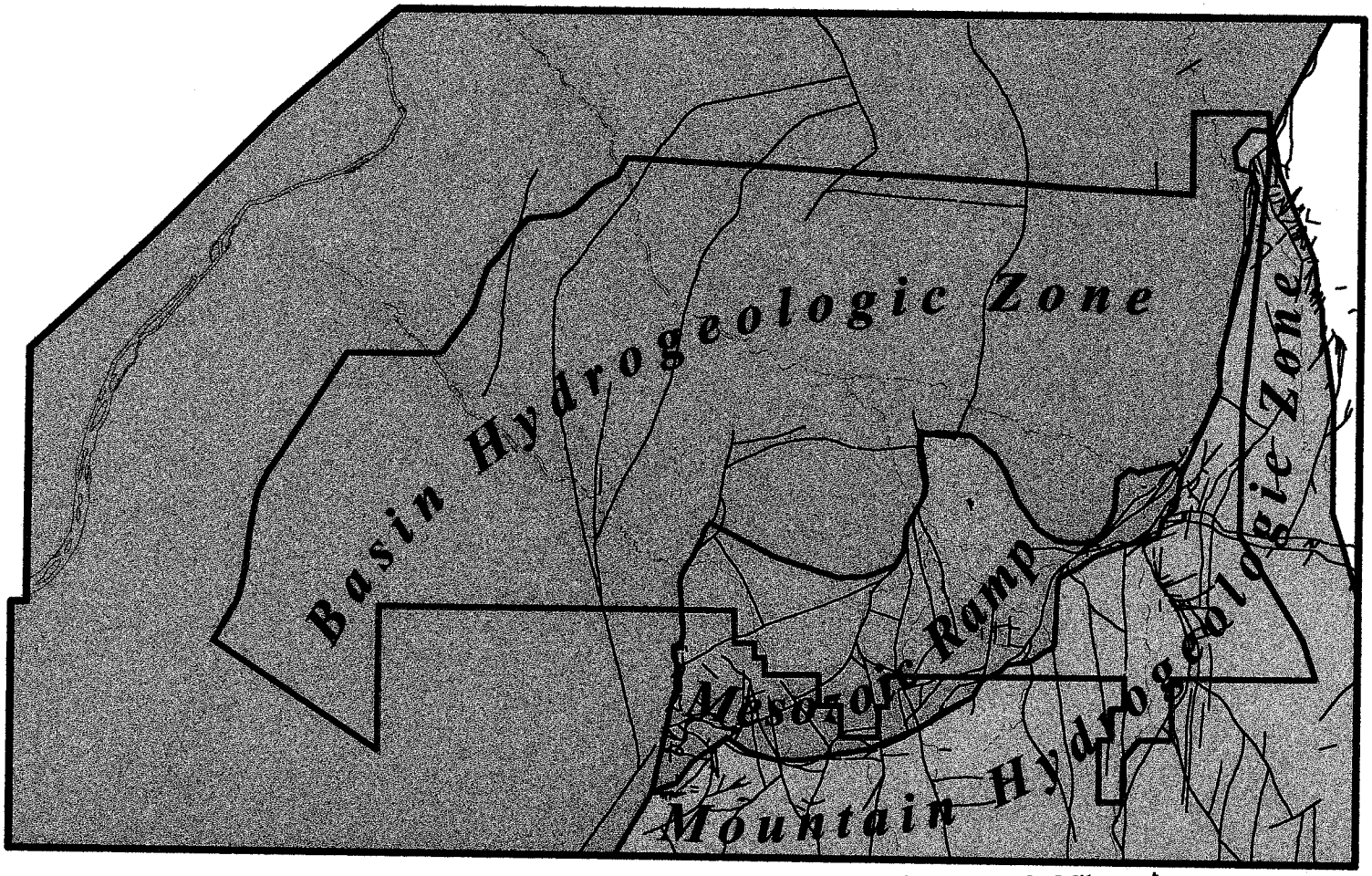

Figure 7. Hydrogeologic zones of the Placitas study area.

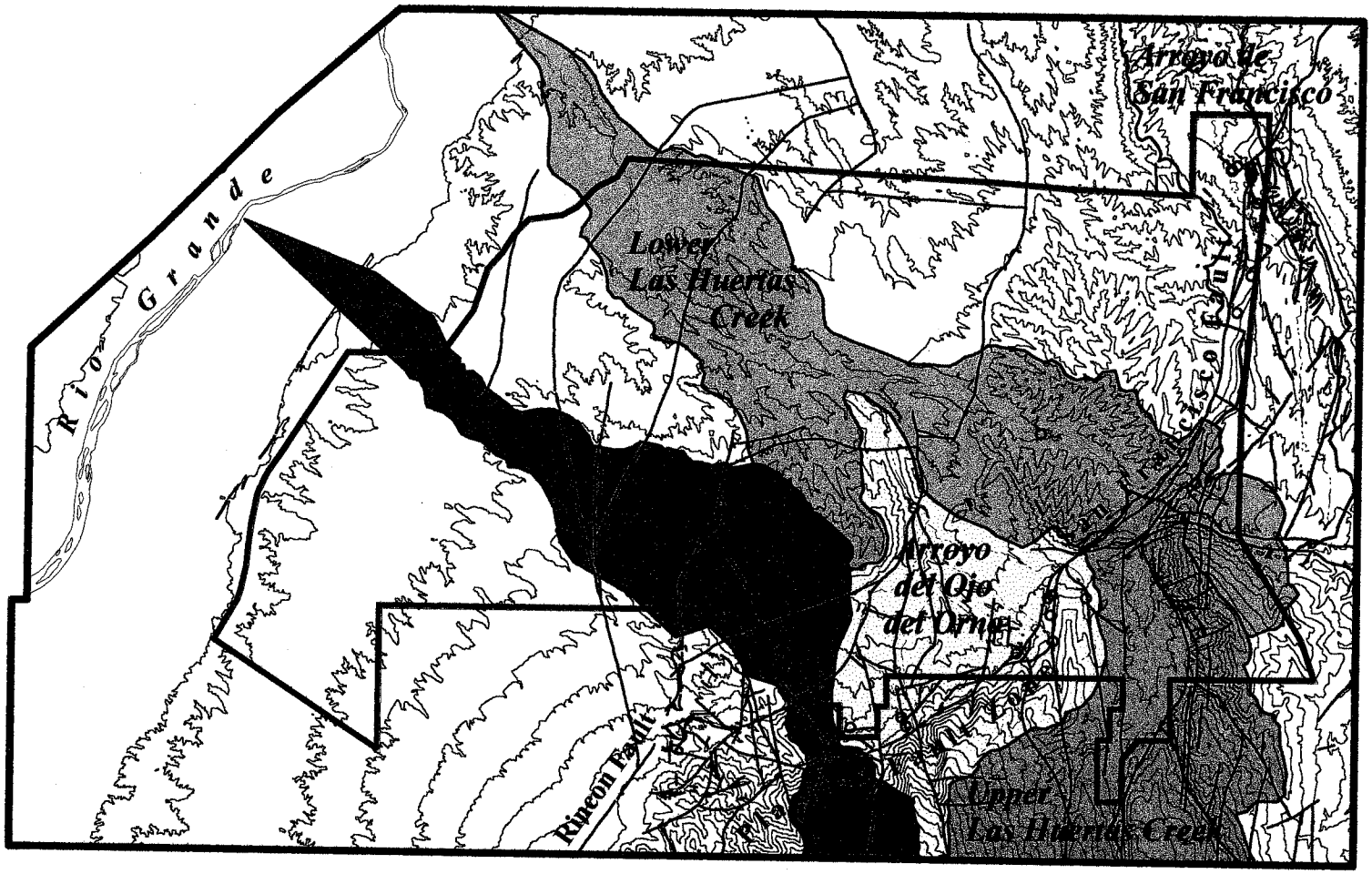

Figure 8. Surface water drainages and springs.

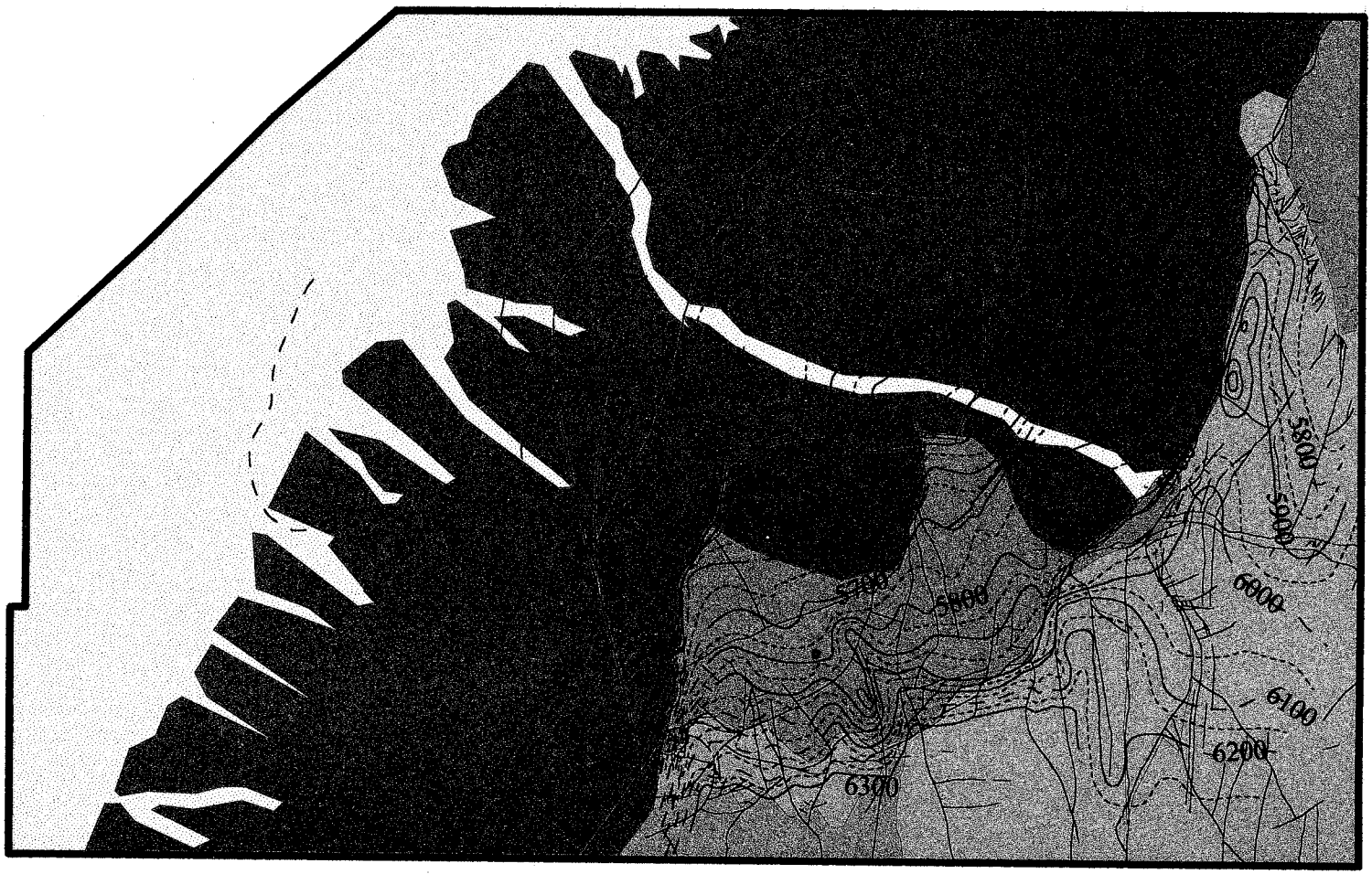

Potentiometric Surface Contours (50 foot interval)

Faults

Geologic units as in figure 5.

1 0 1 2 3 Miles

1 0 1 2 3 4 Kilometers

N

1:90000

Contour interval 100 feet

Figure 9. Potentiometric Surface

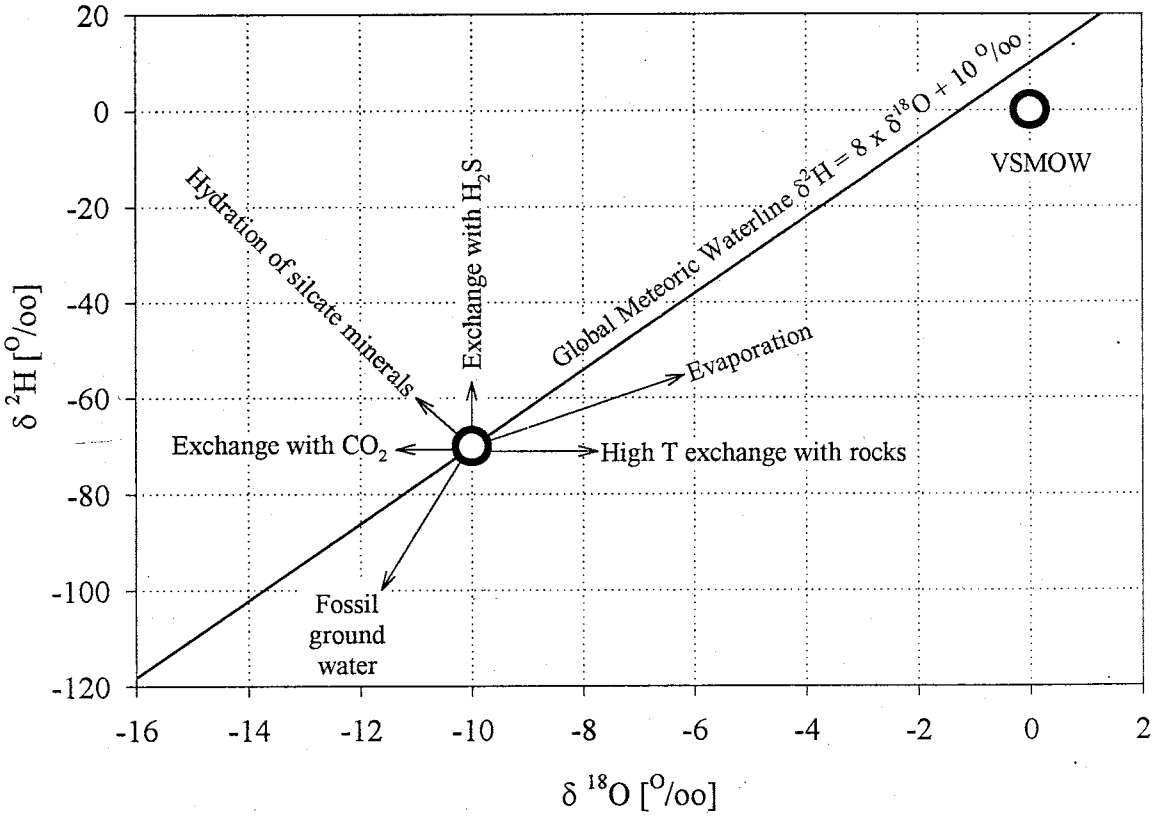

Figure 10. The Global Meteoric Waterline (Craig, 1961), and isotope exchange processes that can modify the isotopic composition of meteoric waters.

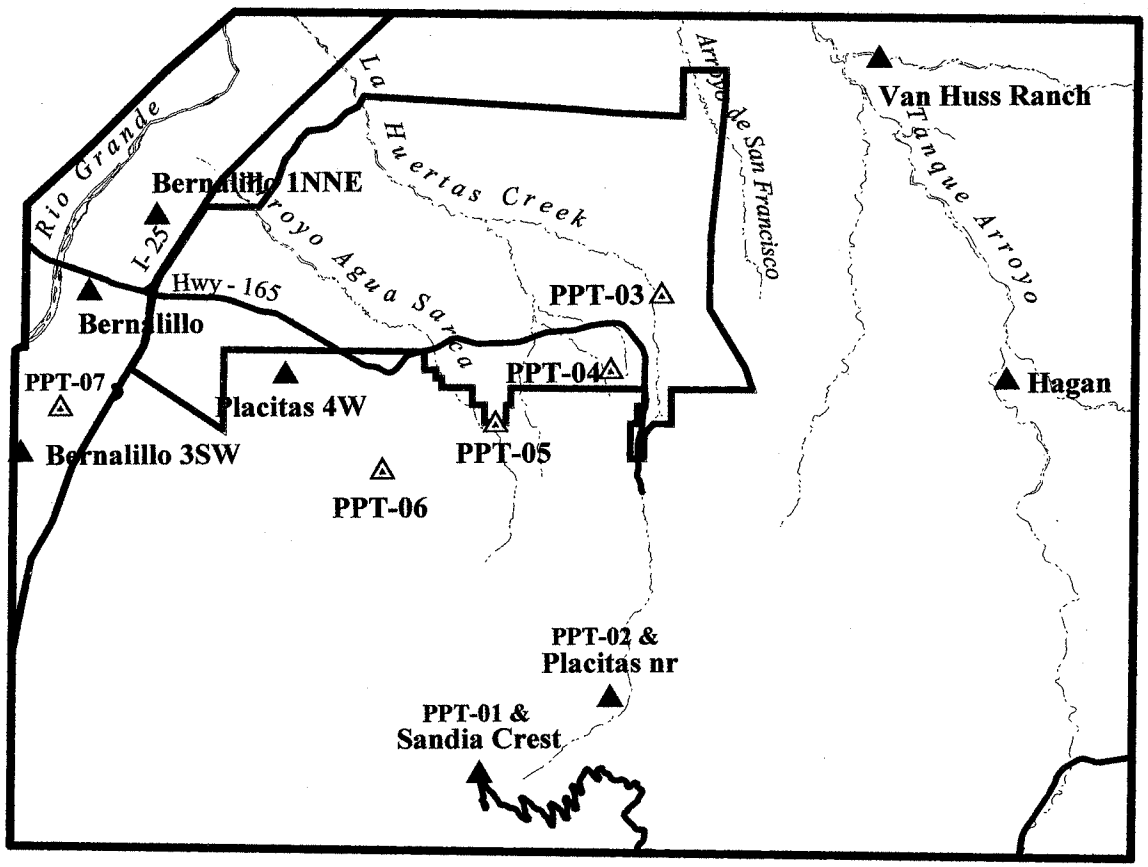

Figure 11. Precipitation collector locations.

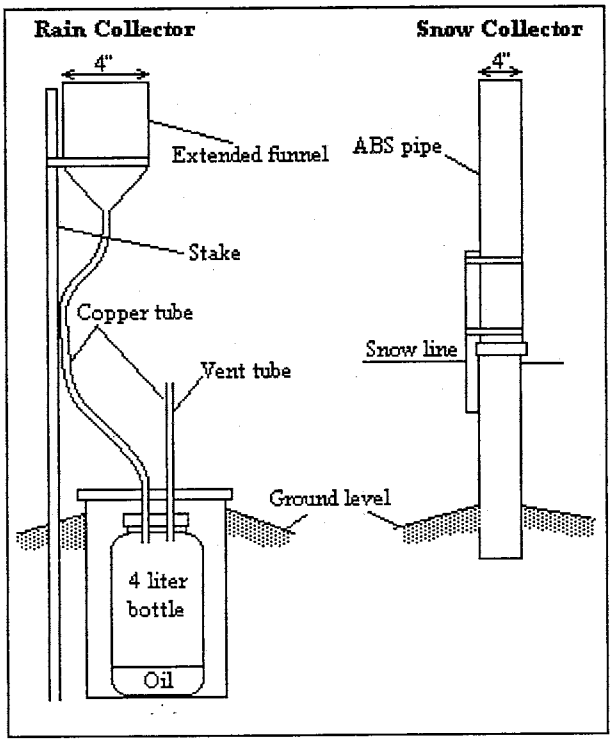

Figure 12. Precipitation collectors for rain and snow.

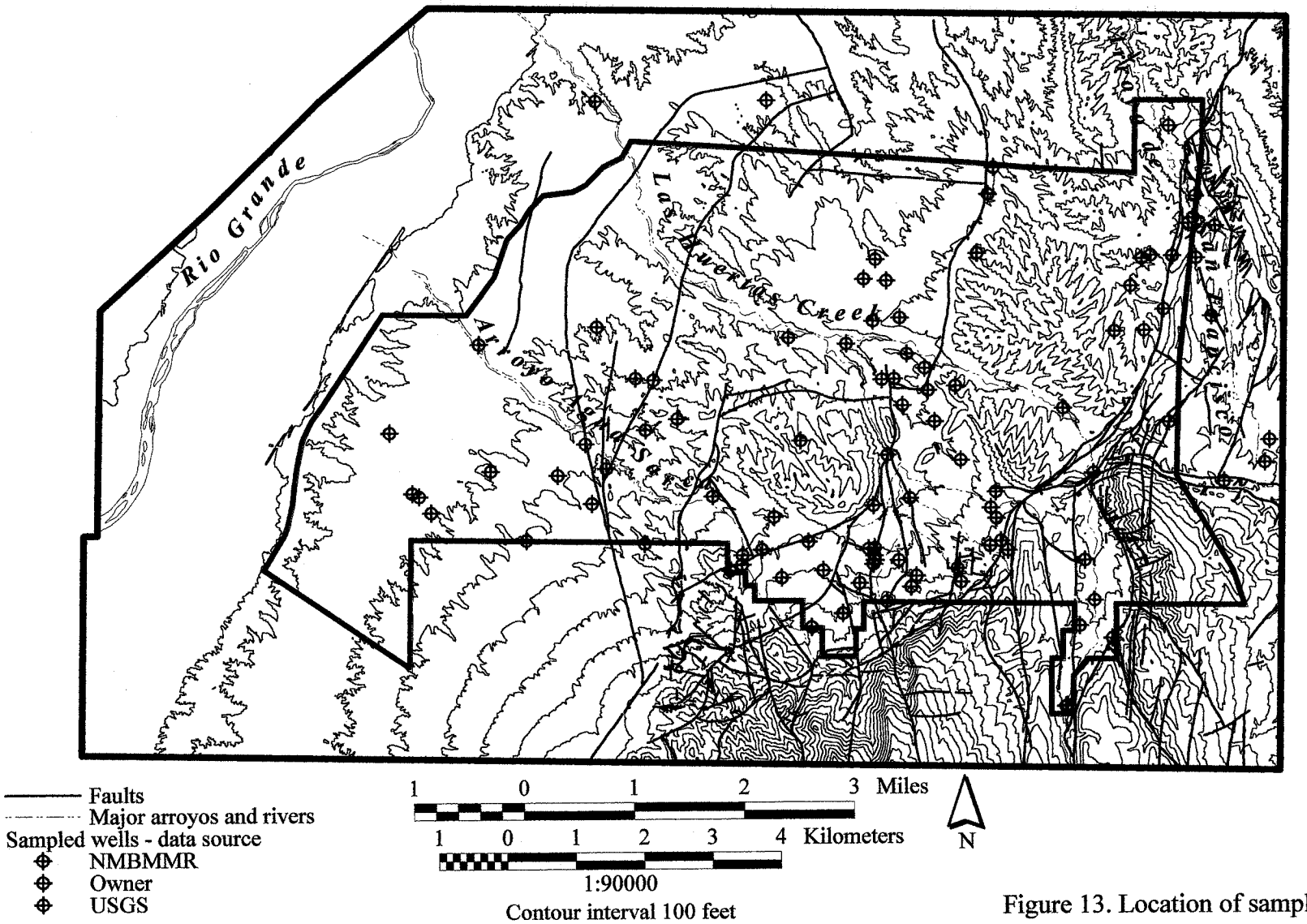

Figure 13. Location of sampled wells.

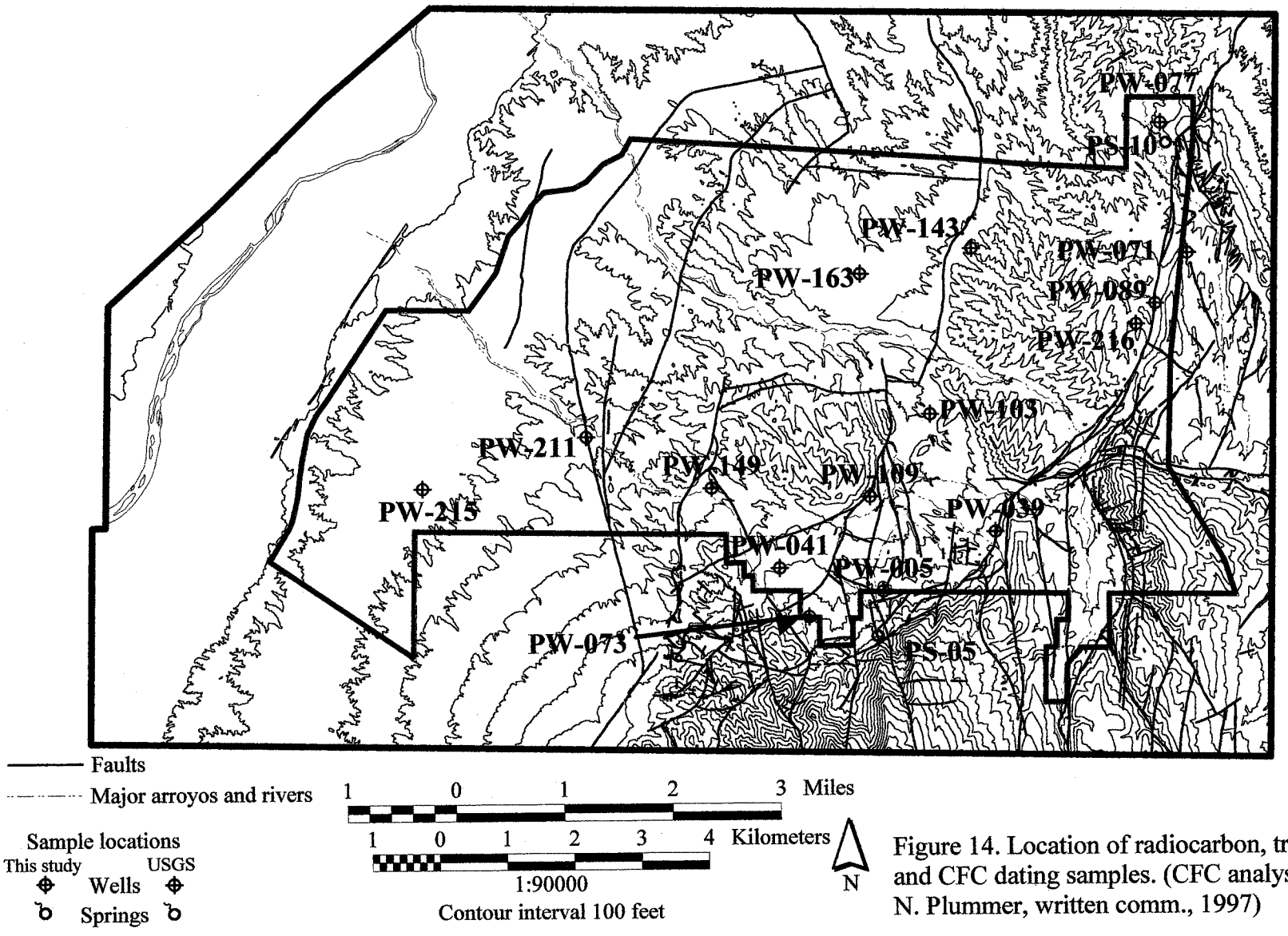

Figure 14. Location of radiocarbon, tritium, and CFC dating samples. (CFC analyses from N. Plummer, written comm., 1997)

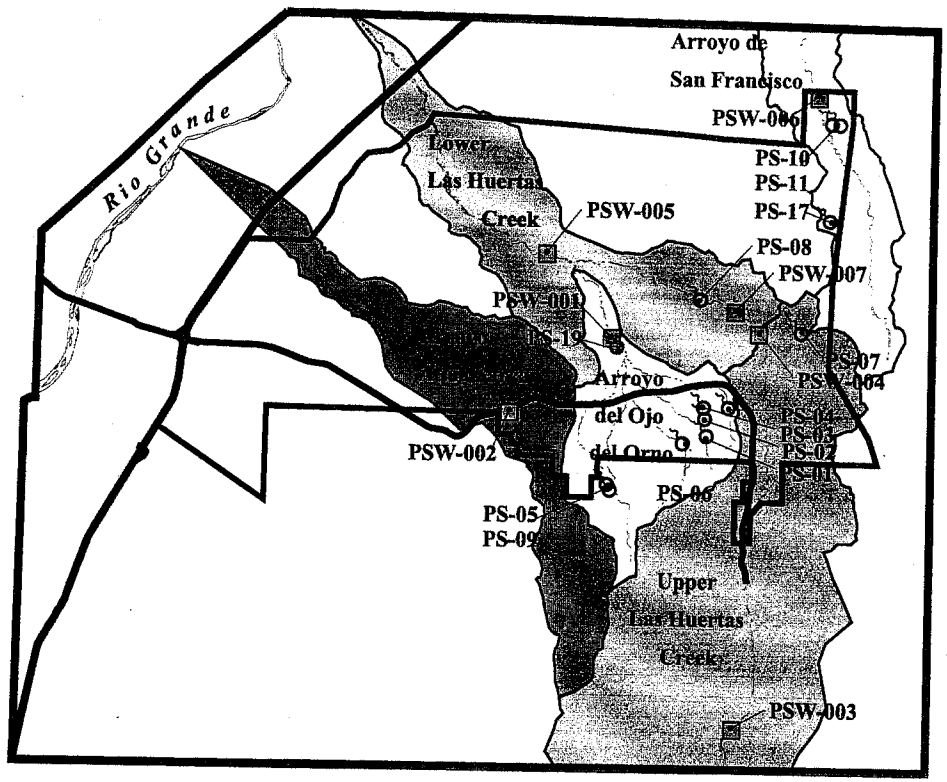

Figure 15. Surface-water and spring sample locations.

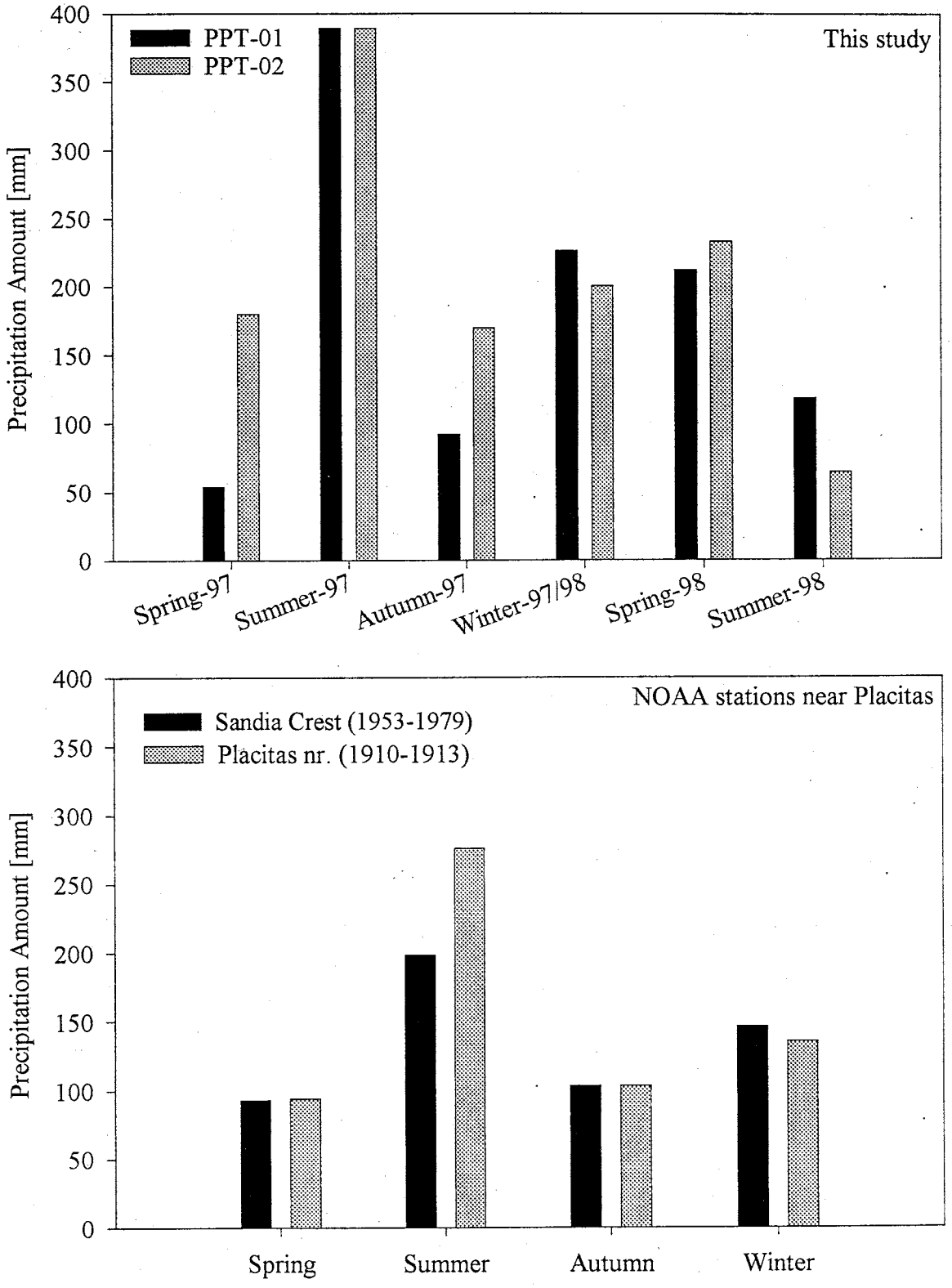

Figure 16. Median quarterly precipitation amounts at mountain stations for spring (March, April, May), summer (June, July, August), autumn (September, October, November), and winter (December, January, February). See Figure 11 for site locations and Table 3 for collection schedule.

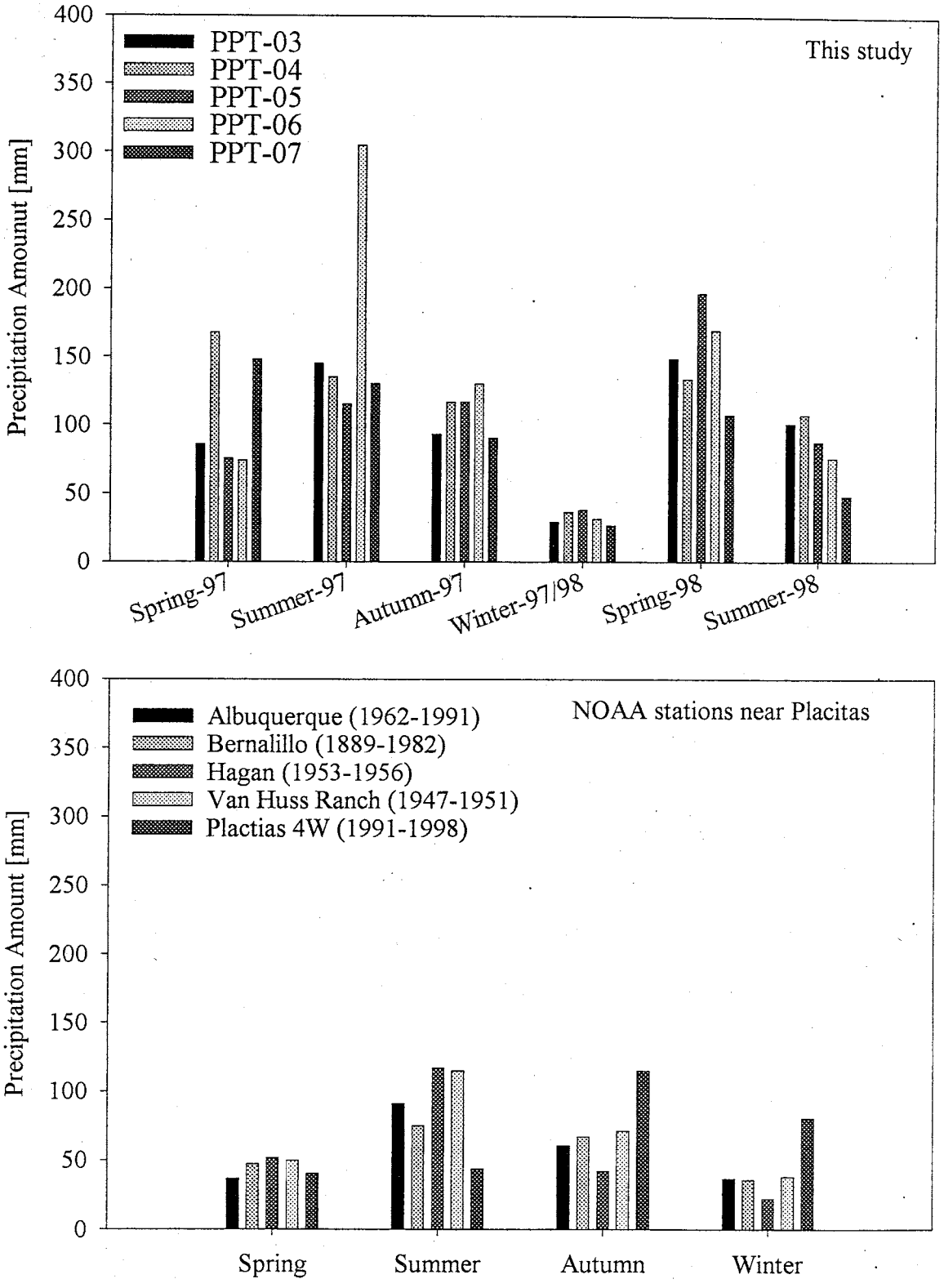

Figure 17. Median quarterly precipitation amounts at lowland stations for spring (March, April, May), summer (June, July, August), autumn (September, October, November), and winter (December, January, February). See Figure 11 for site locations and Table 3 for collection schedule.

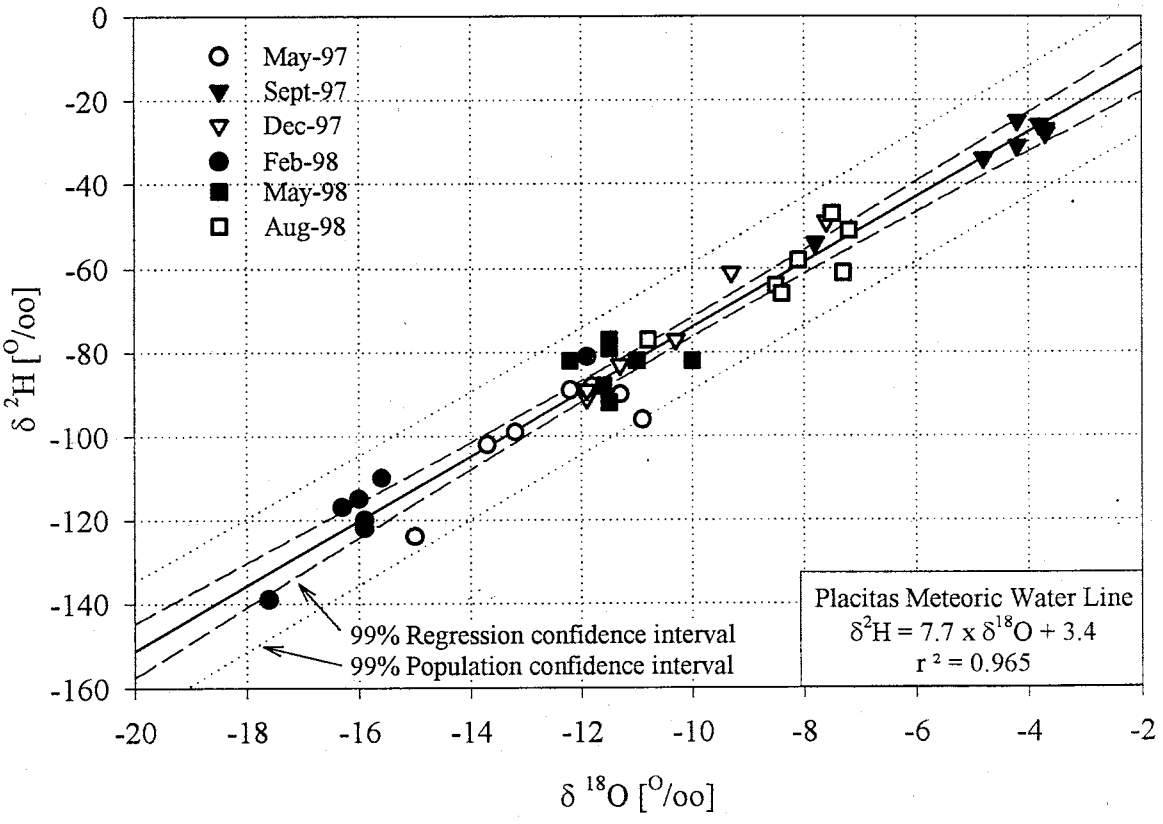

Figure 18. Isotopic composition of precipitation and the Placitas meteoric water line. April 1997 to August 1998.

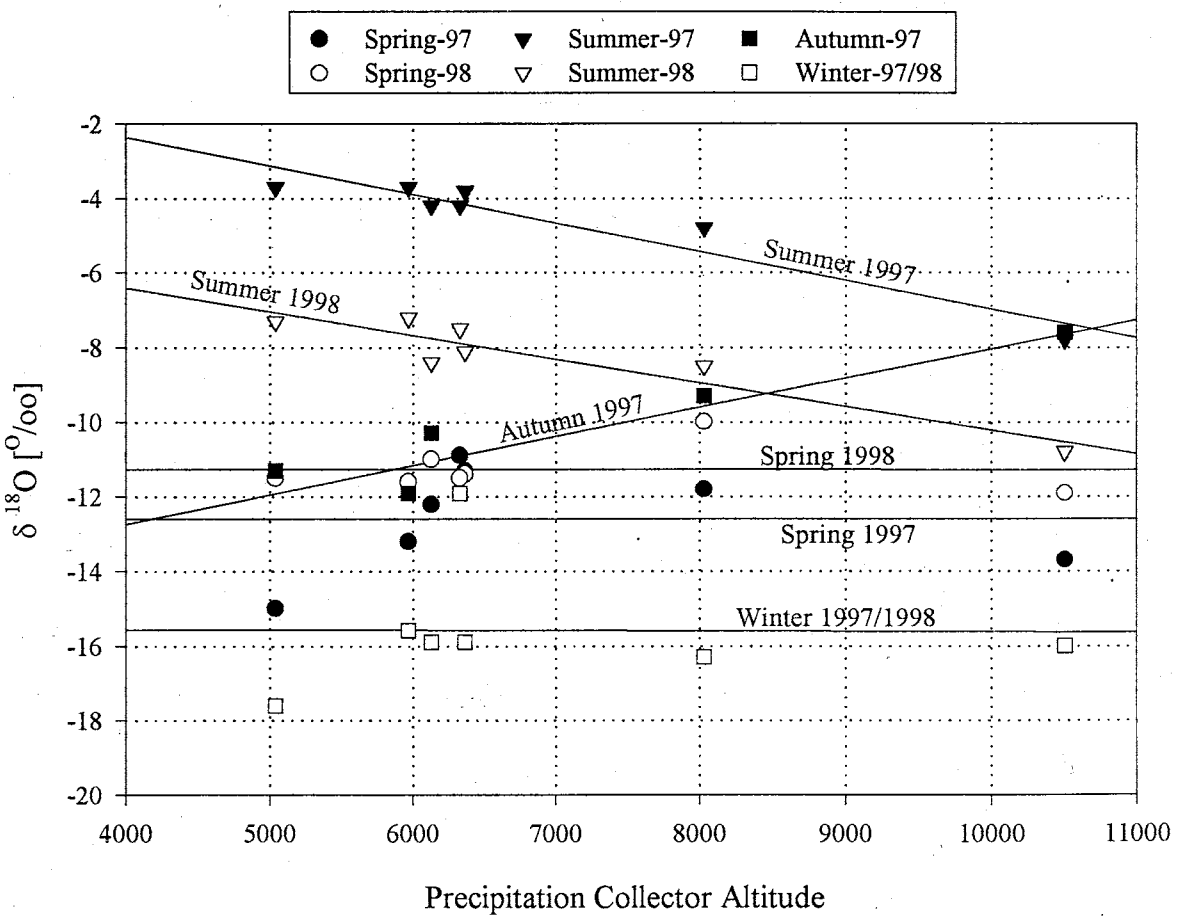

Figure 19. $\delta^{18}O$ composition of precipitation v.s. the altitude of precipitation collector. The best-fit linear regression lines for each seasonal sample set is shown.

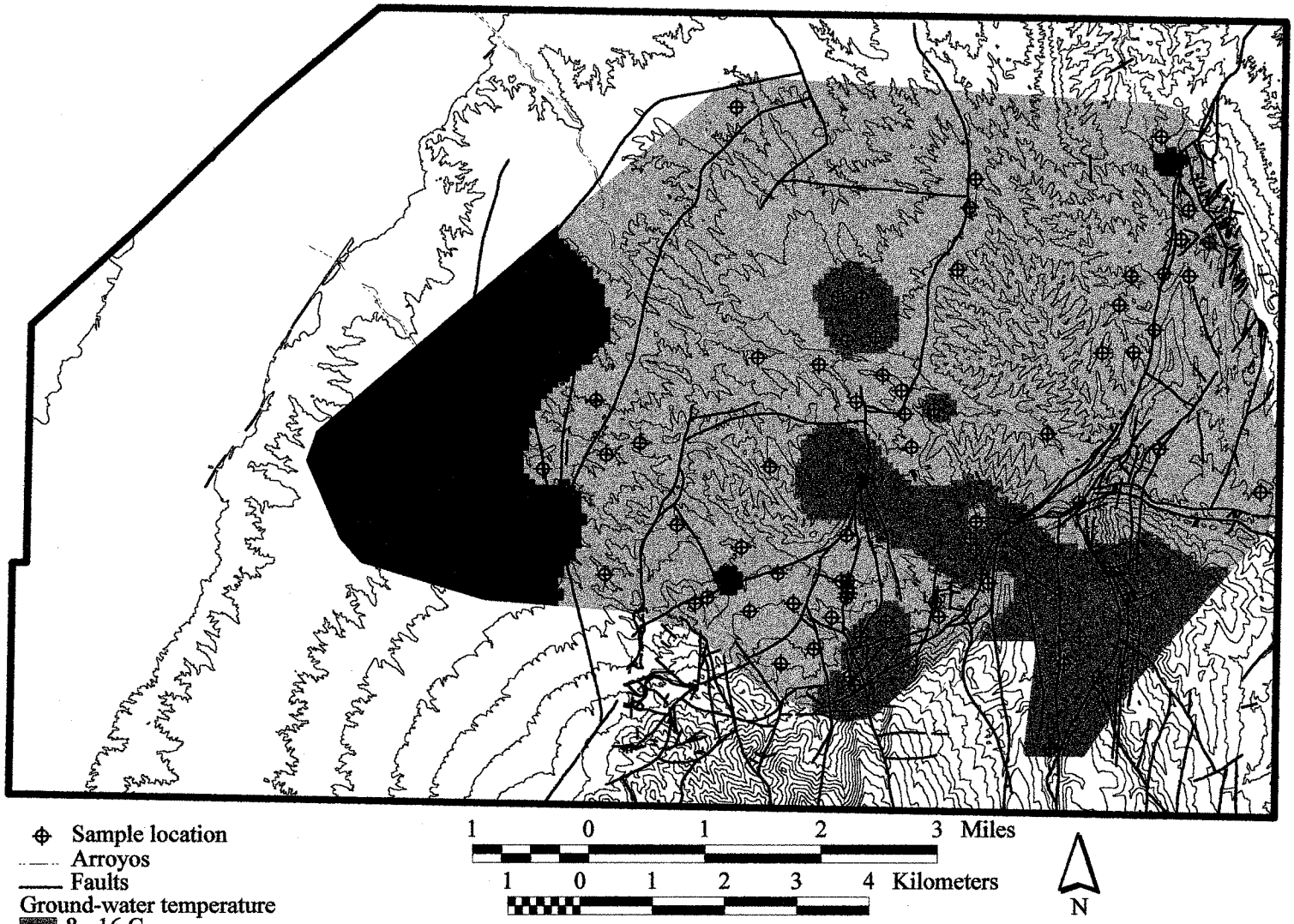

Figure 20. Temperature of ground water.

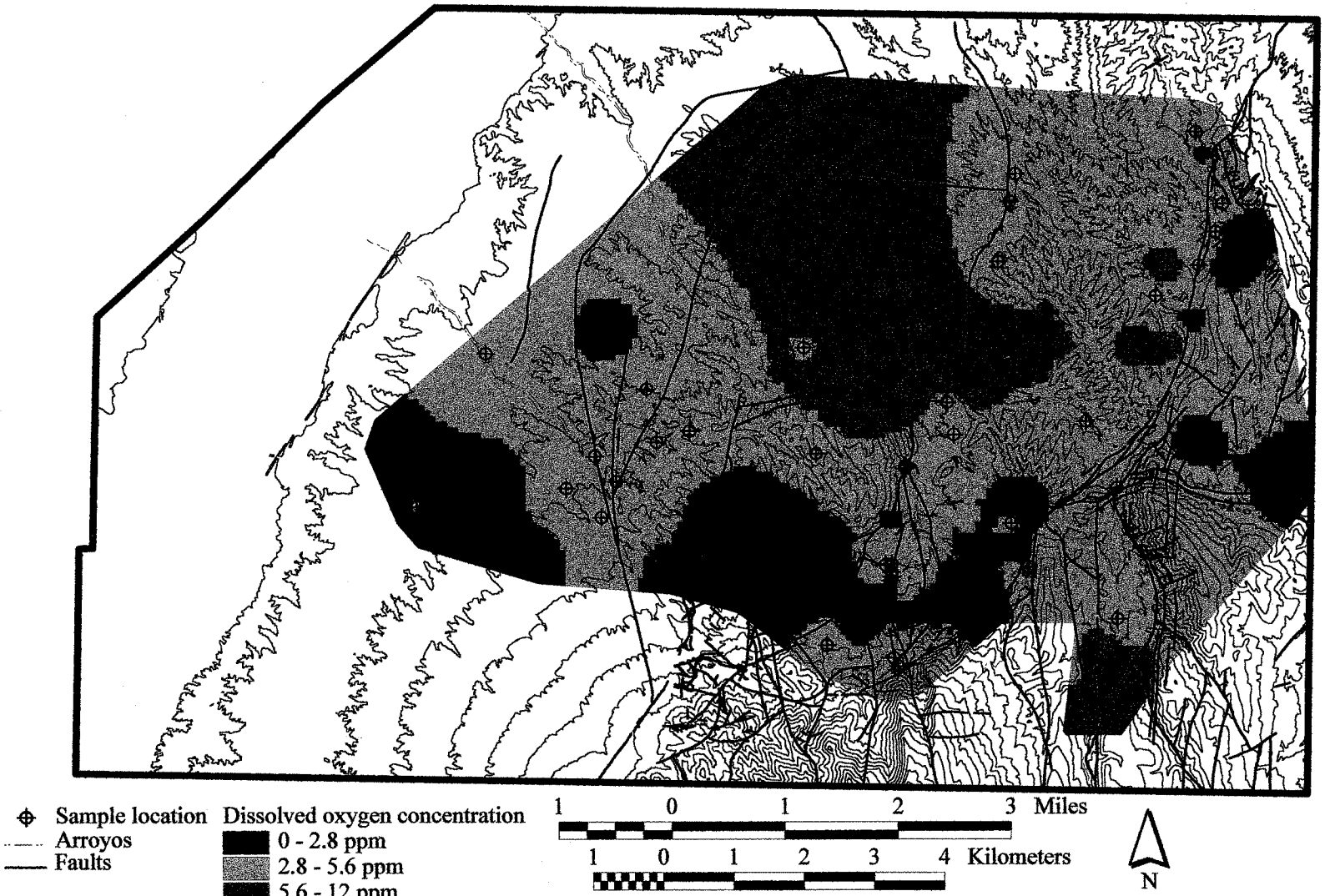

Figure 21. Distribution of dissolved oxygen in ground water.

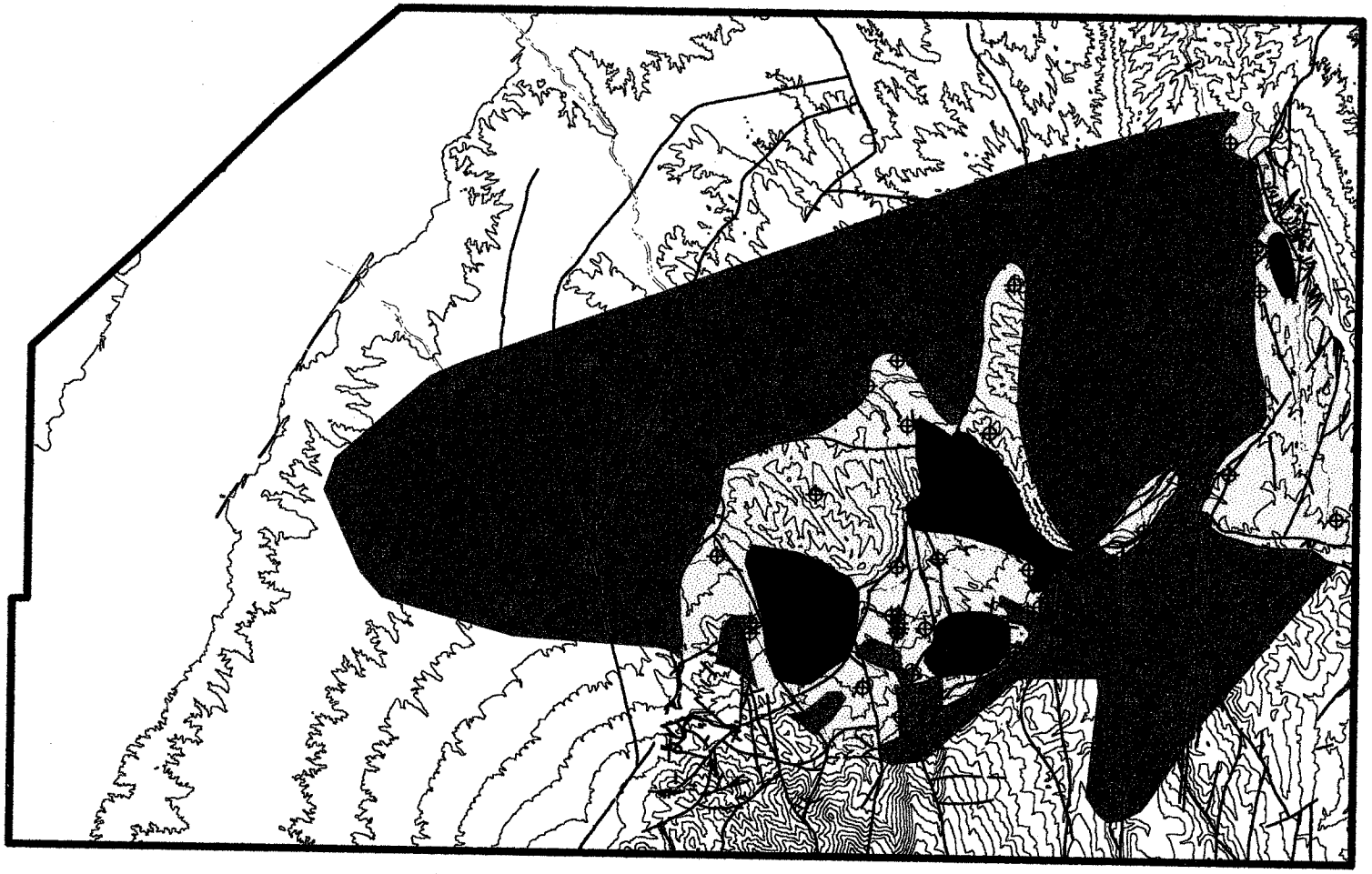

Figure 22. Distribution of TDS in ground water.

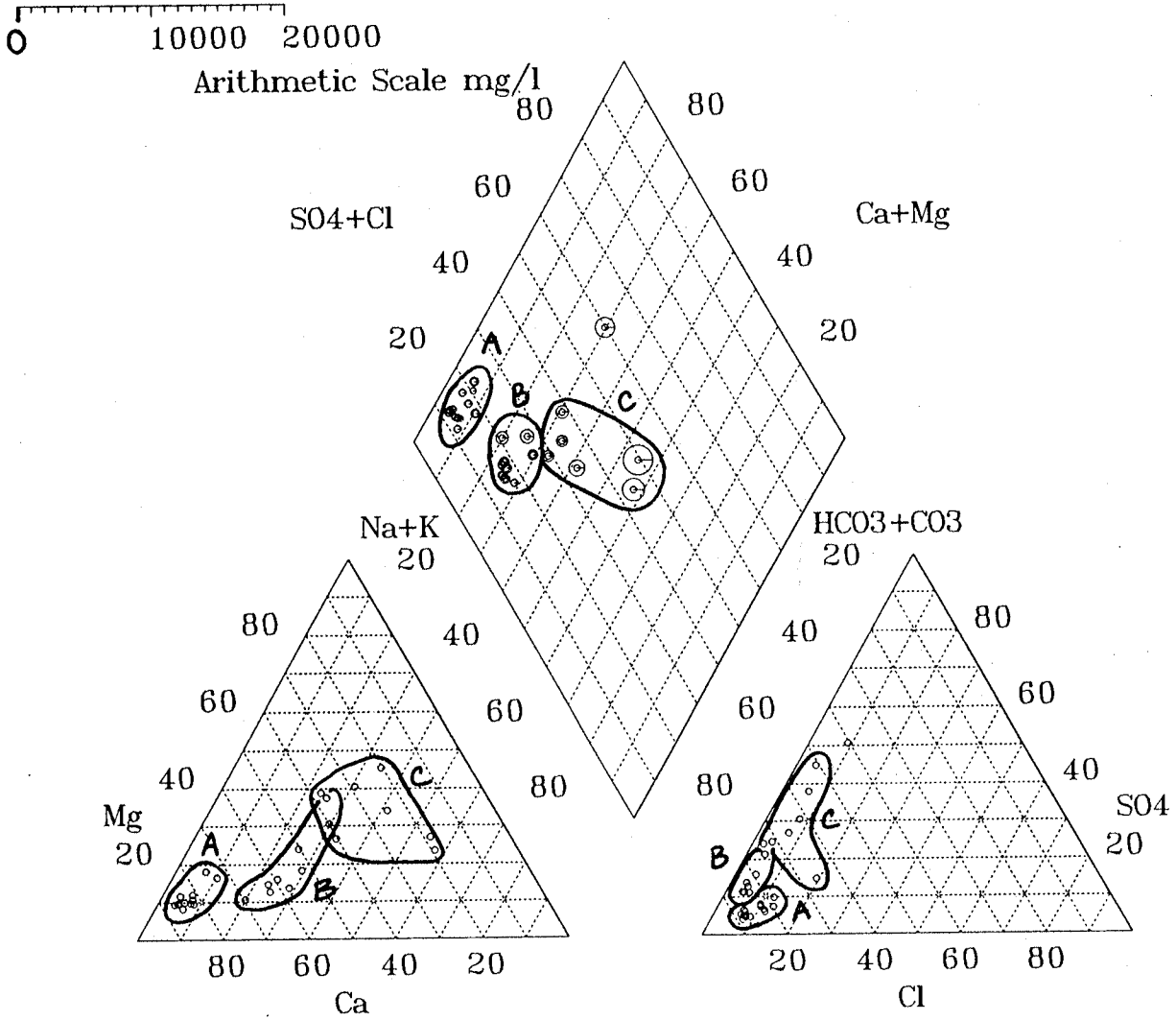

Figure 23. Major ion geochemistry of ground-water samples from the mountain hydrogeologic zone. Labeled groups are from (A) the Madera and Abo Formations along the Chuchilla Lupe and upper Las Huertas Canyon, (B) Madera Formation along Cuchilla de San Francisco, and (C) the Abo Formation east of Cuchilla de San Francisco. Symbol size in central field is arithmetically proportional to the concentration of total dissolved solids.

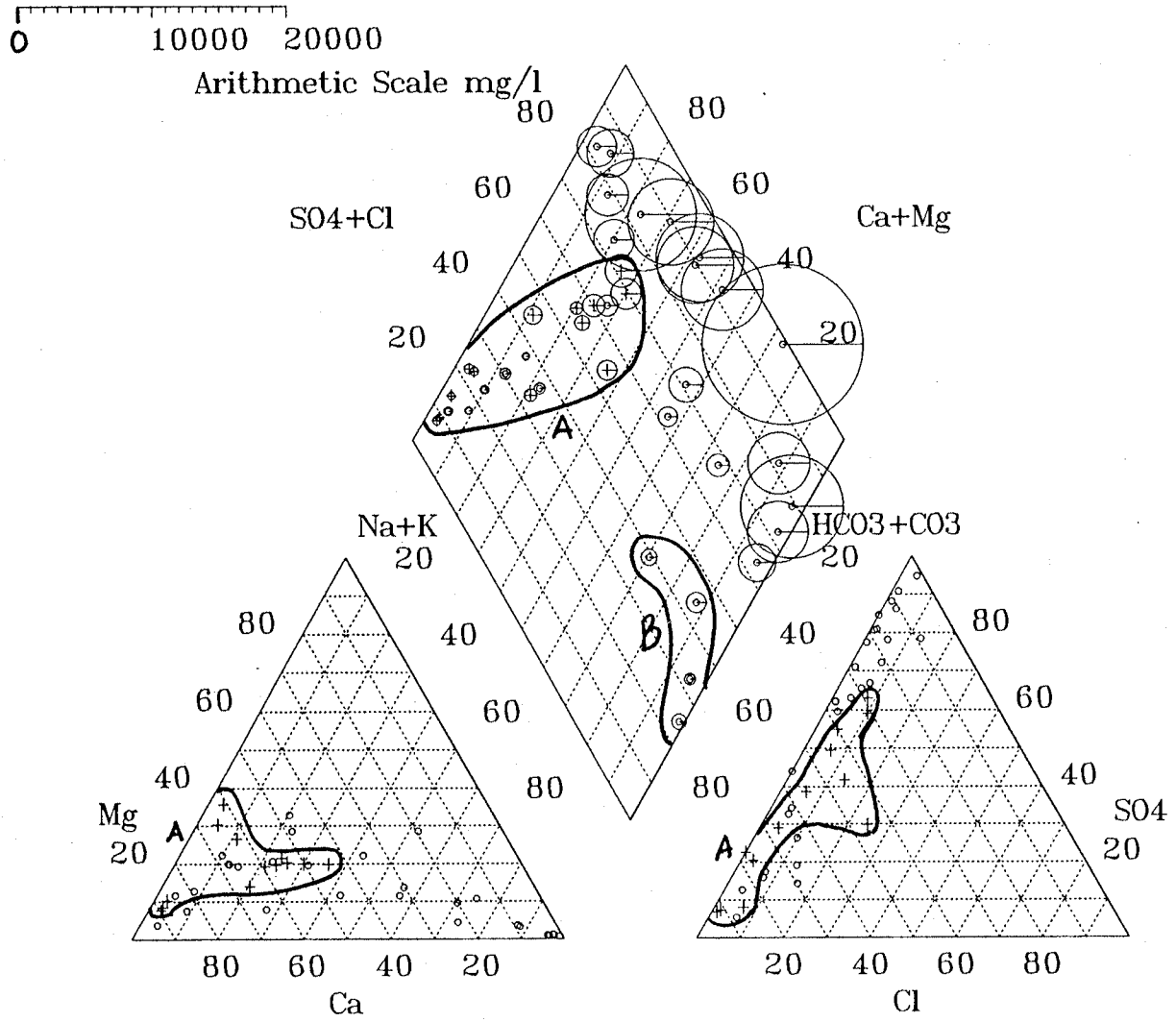

Figure 24. Major ion geochemistry of ground-water samples from the Mesozoic ramp. Labeled samples are from: (+ in circled group A) along the Agua Sarca fault, (B) Middle sandstone of the Petrified Forest Formation. Symbol size in central field is arithmetically proportional to the concentration of total dissolved solids.

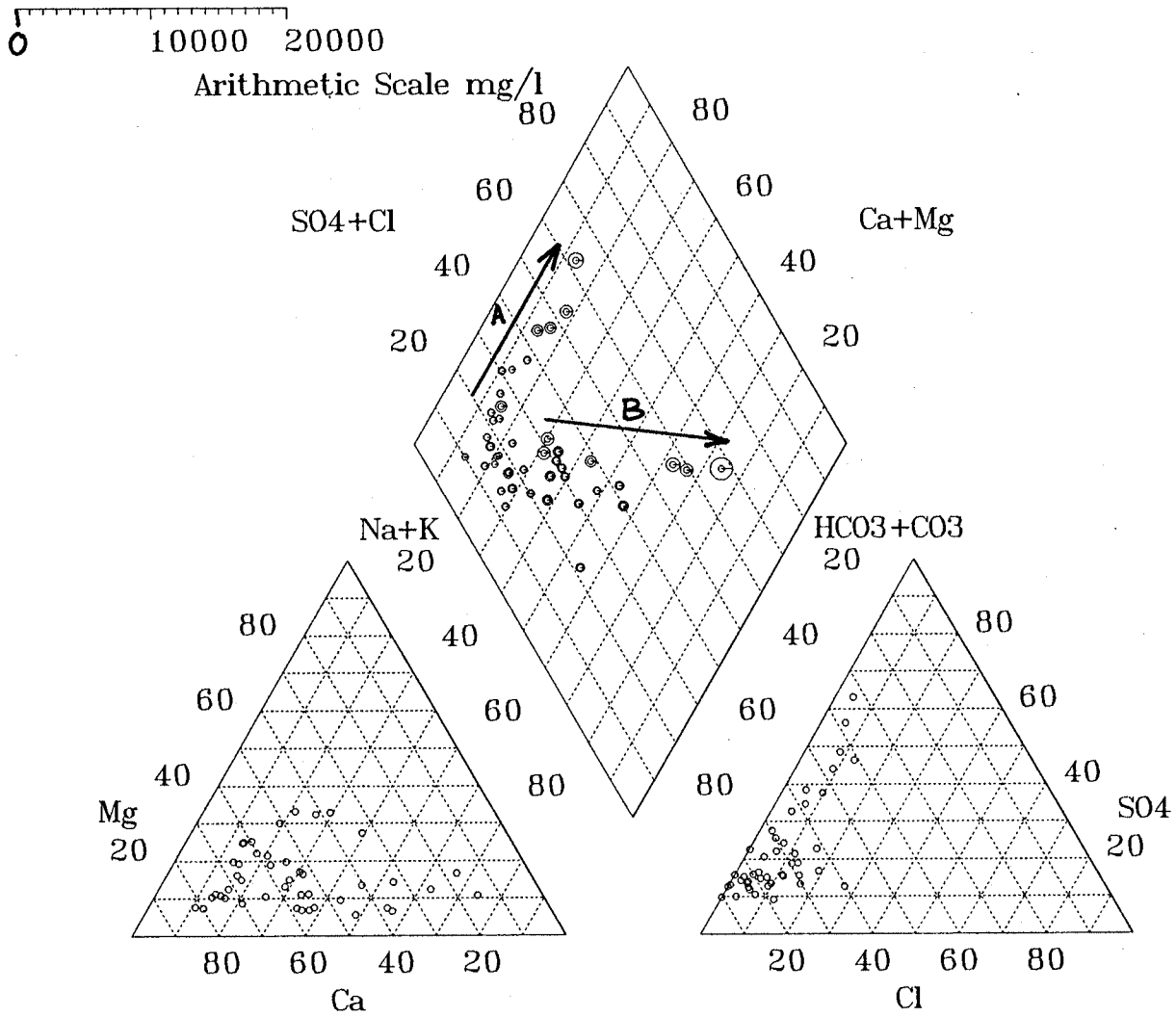

Figure 25. Major ion geochemistry of ground-water samples from the basin hydrogeologic zone. Labeled arrows illustrate (A) mixing trend in samples for north of the Caballo fault, (B) dissolution of aquifer materials in samples from west of the Ranchos faults and north of Las Huertas Creek. Symbol size in central field is arithmetically proportional to the concentration of total dissolved solids.

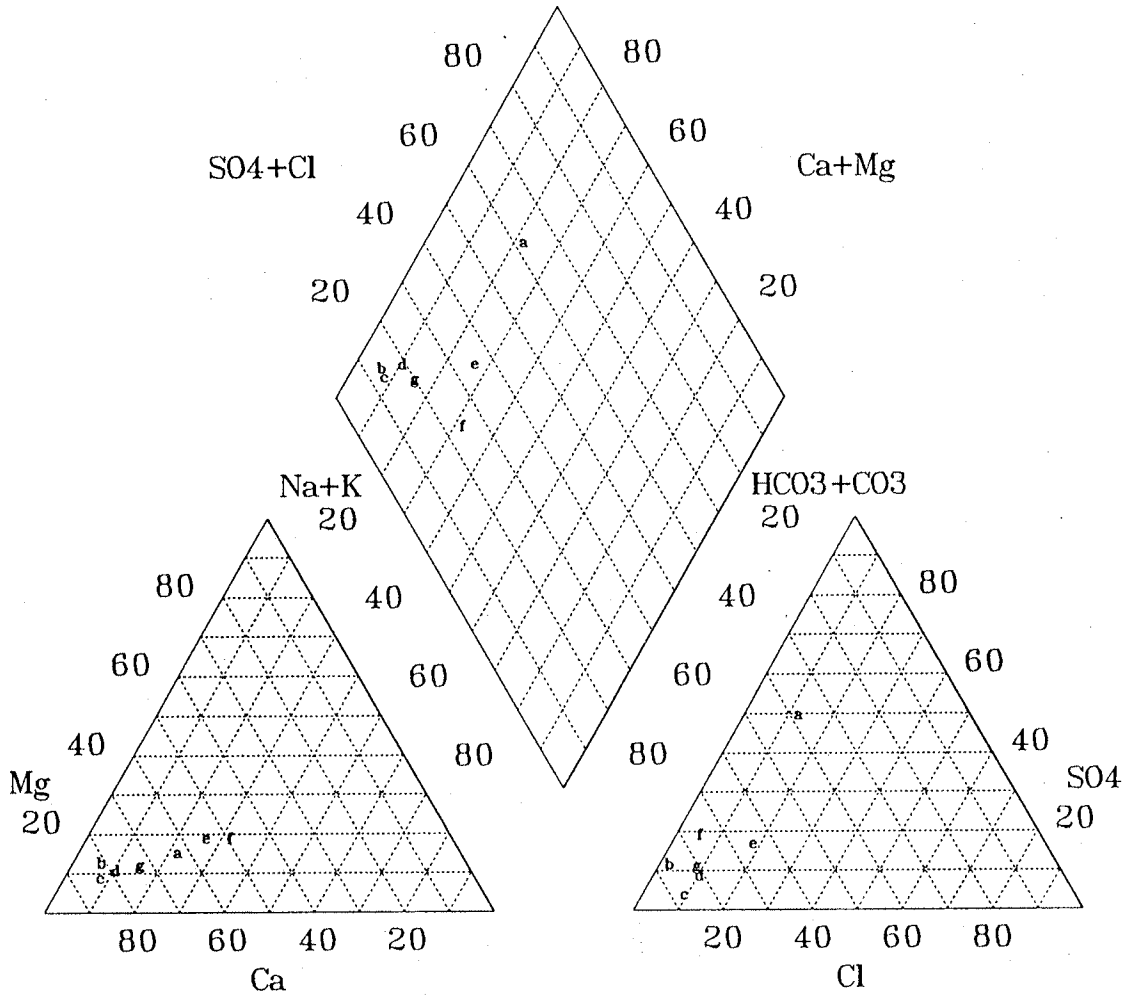

Figure 26. Major ion geochemistry of all surface-water samples from the Placitas study area. Labeled samples are (a) PSW-01, (b) PSW-02, (c) PSW-03, (d) PSW-04, (e) PSW-05, (f) PSW-06, and (g) PSW-07. Sample locations are shown in Figure 15.

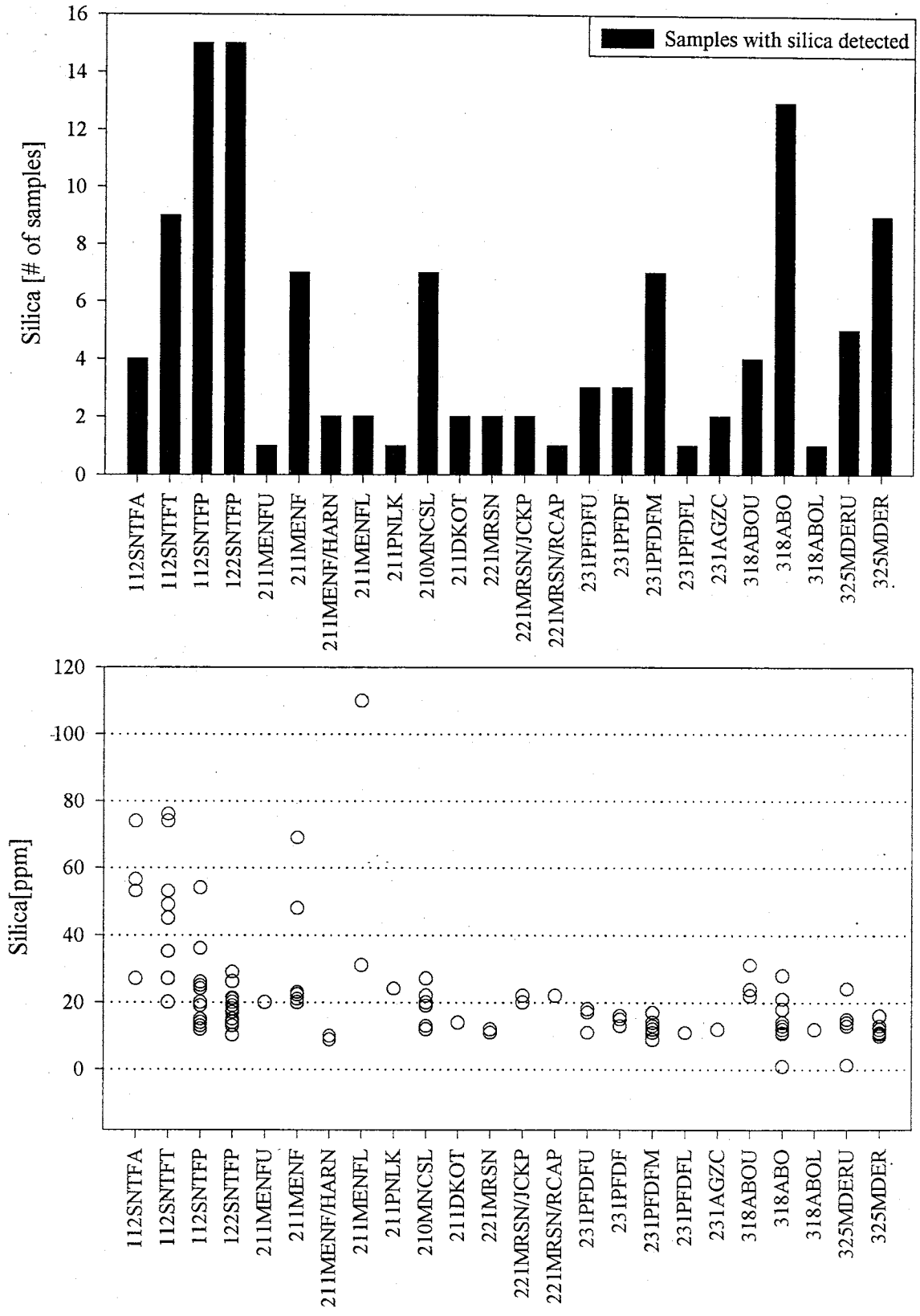

Figure 27. The occurence and concentration of silica in ground water.

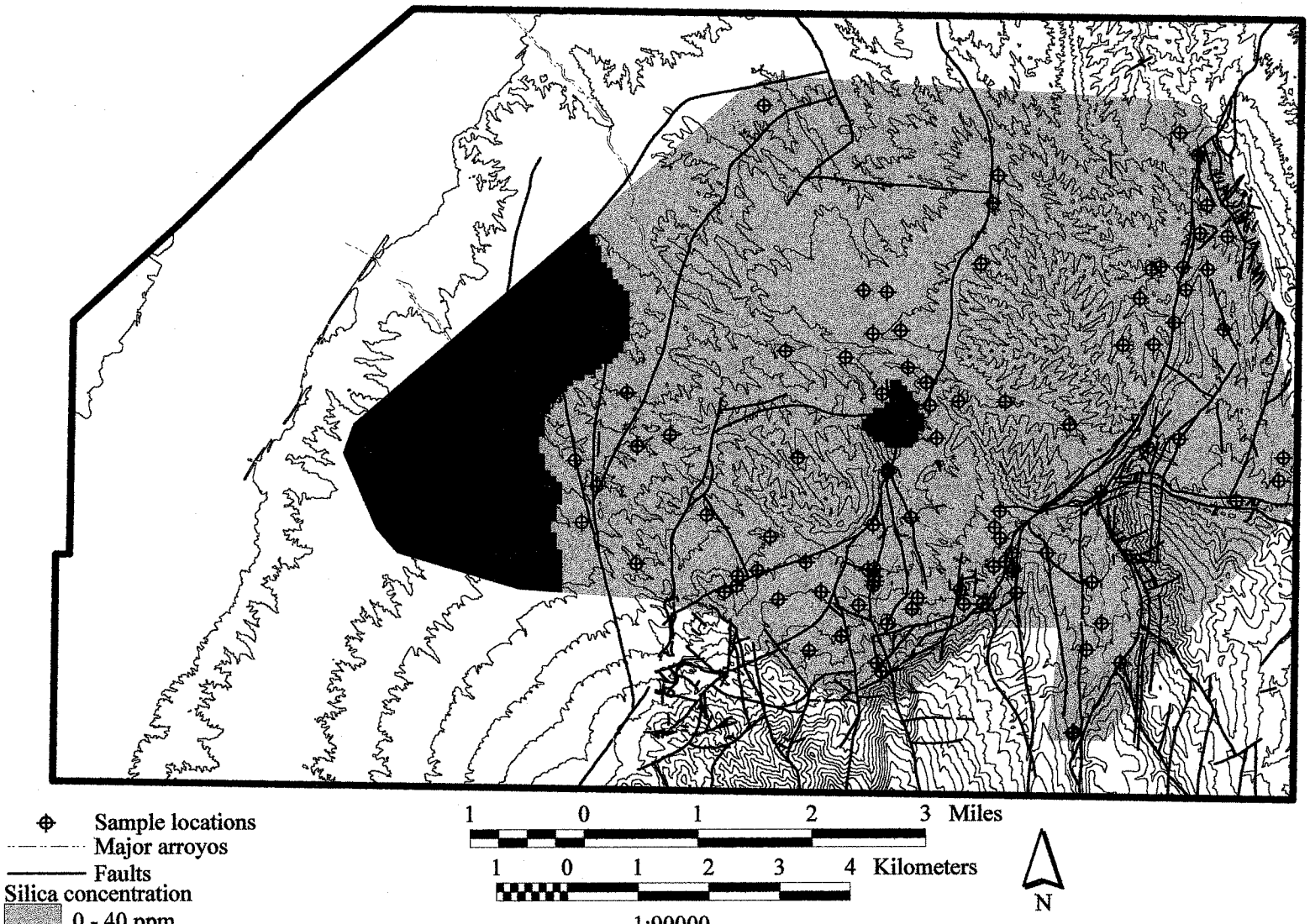

Figure 28. Map of silica in ground water.

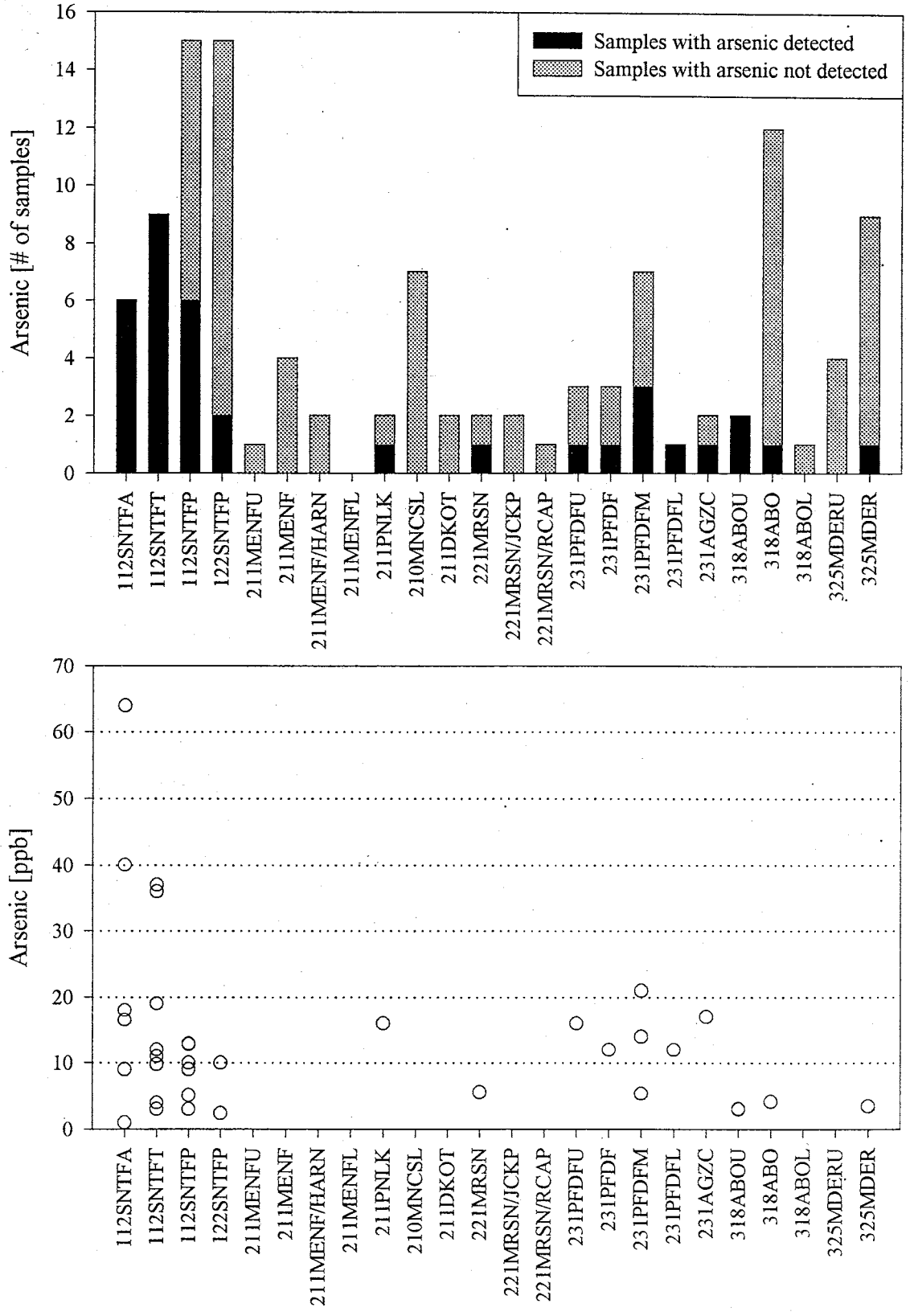

Figure 29. The occurence and concentration of arsenic in ground water.

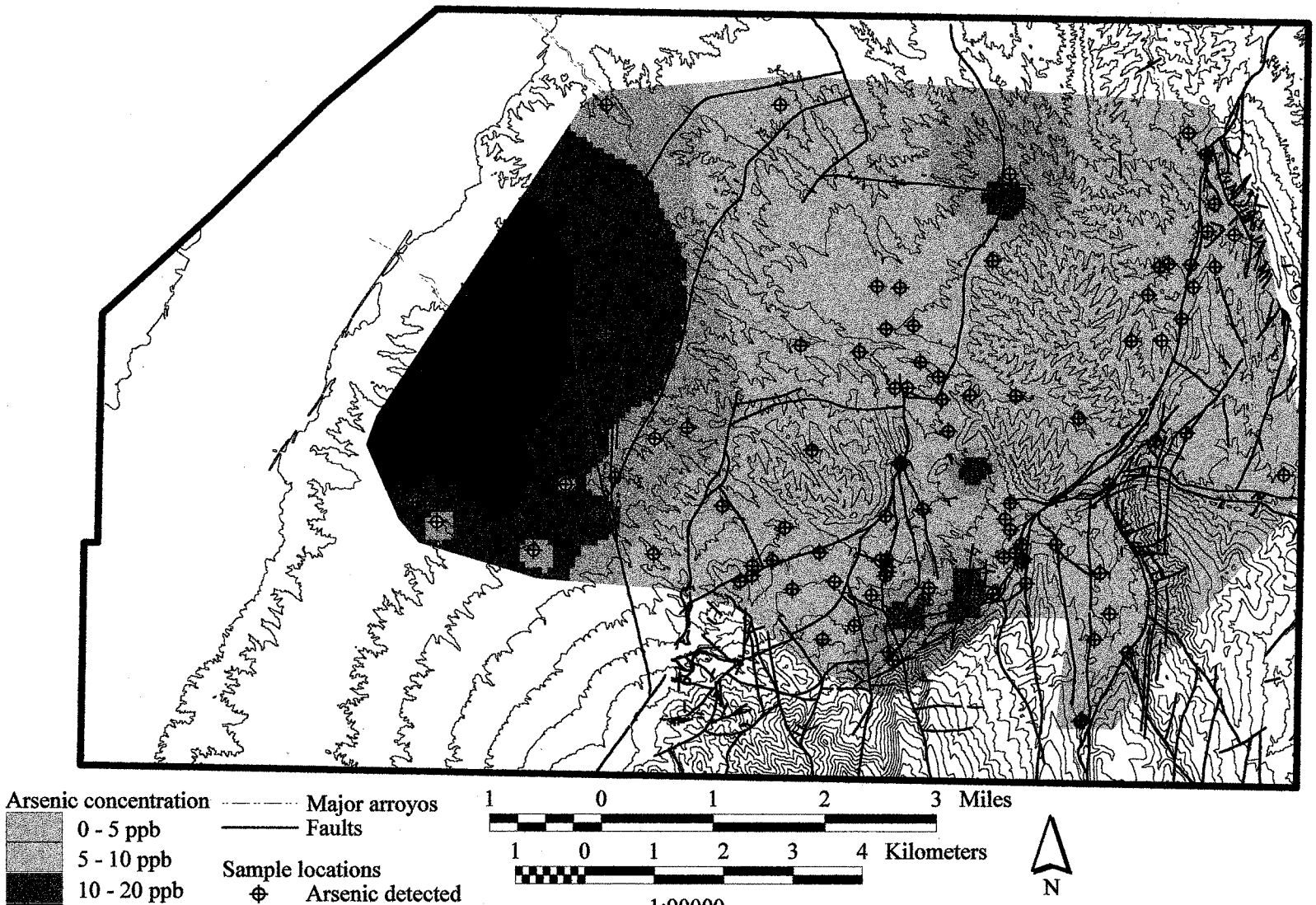

Figure 30. Map of arsenic in ground water.

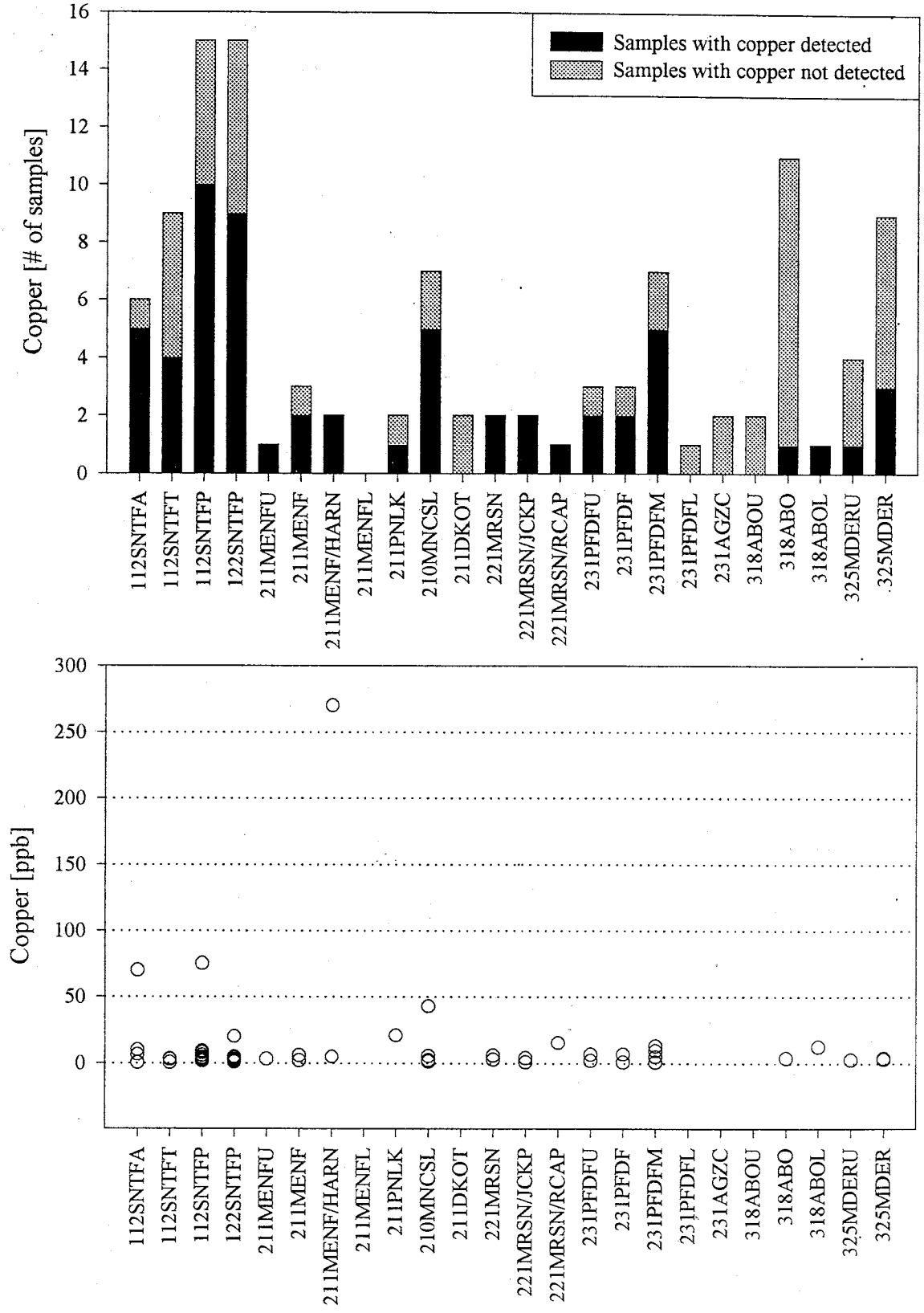

Figure 31. The occurence and concentration of copper in ground water.

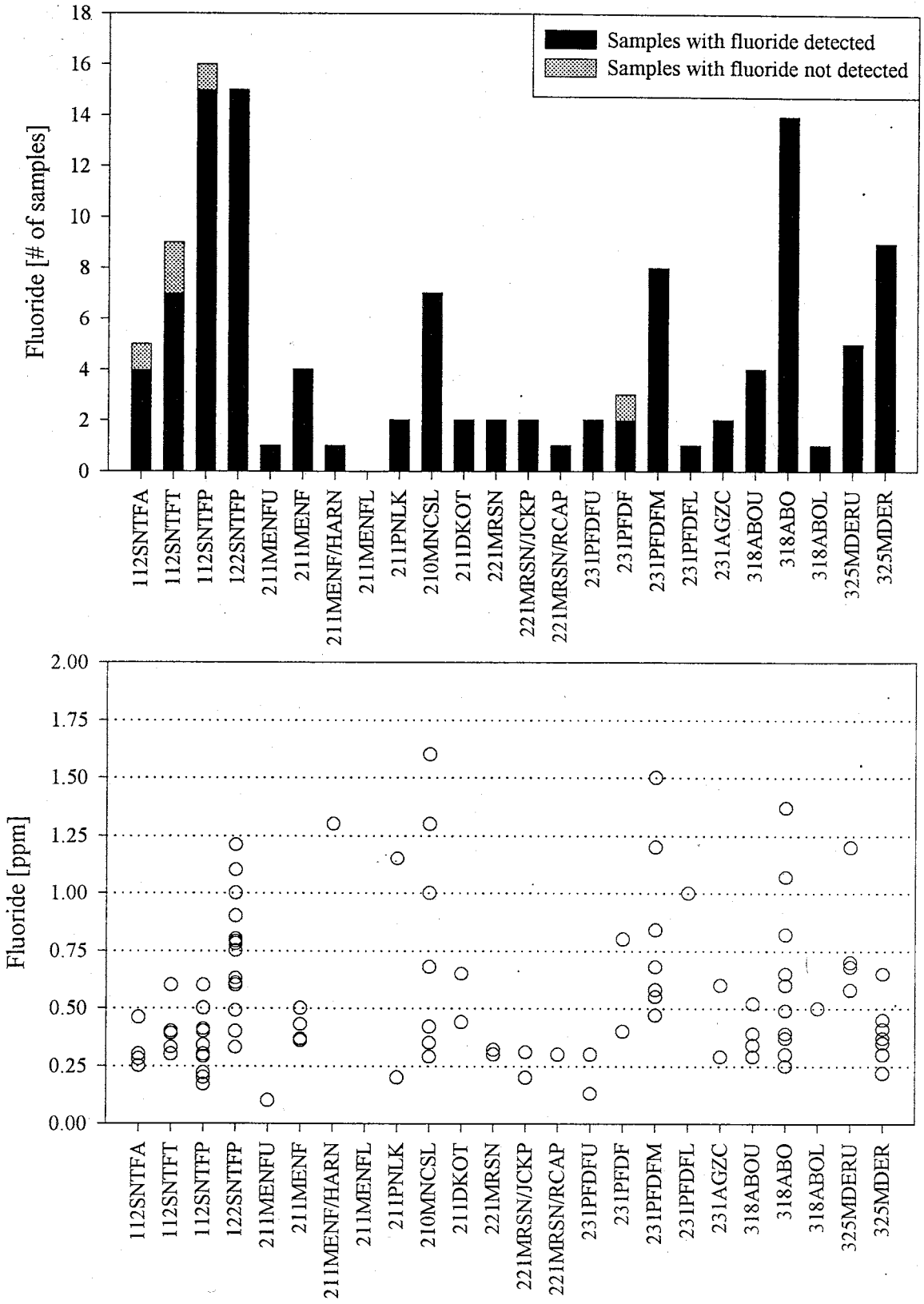

Figure 32. The occurence and concentration of fluoride in ground water.

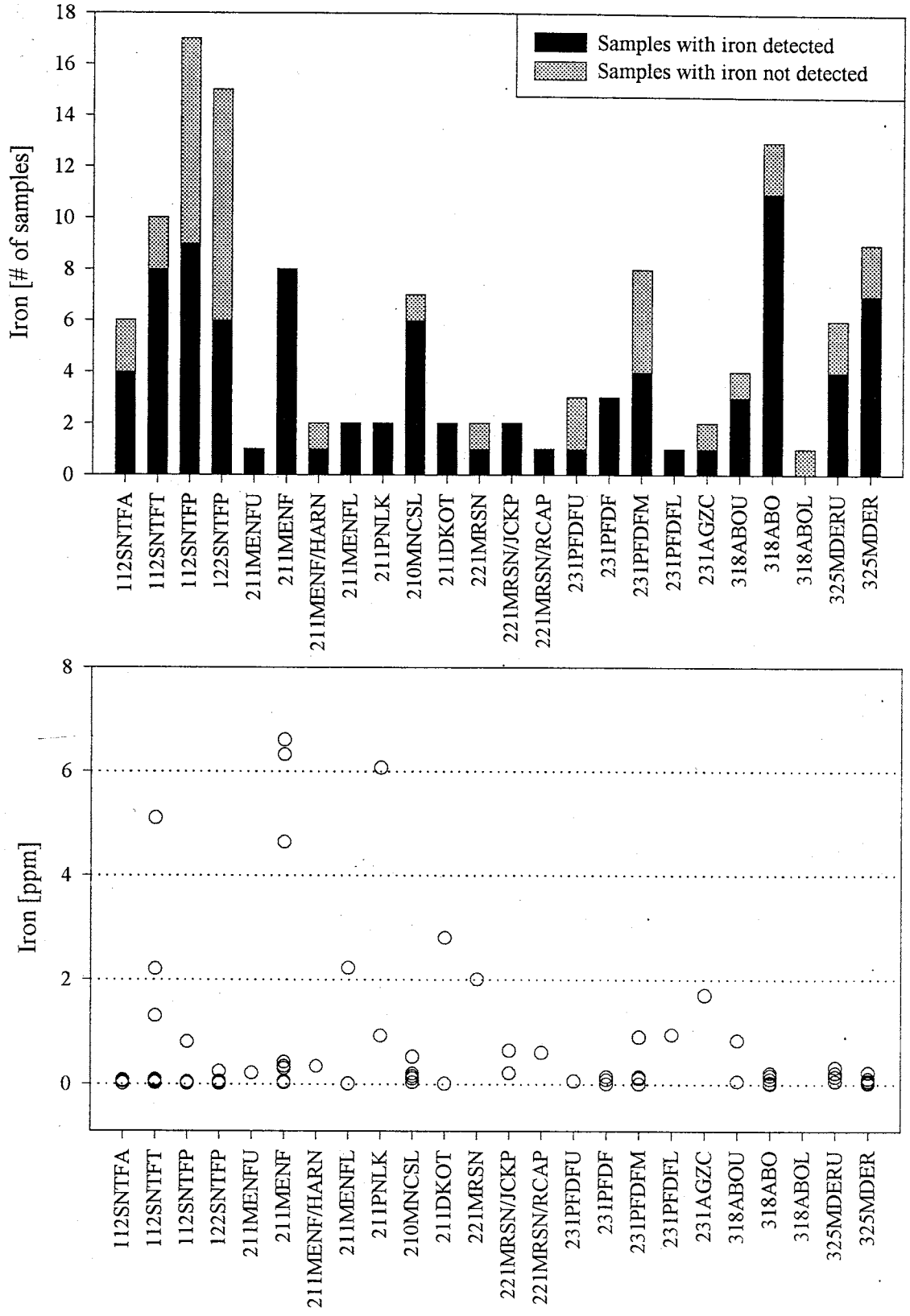

Figure 33. The occurence and concentration of iron in ground water.

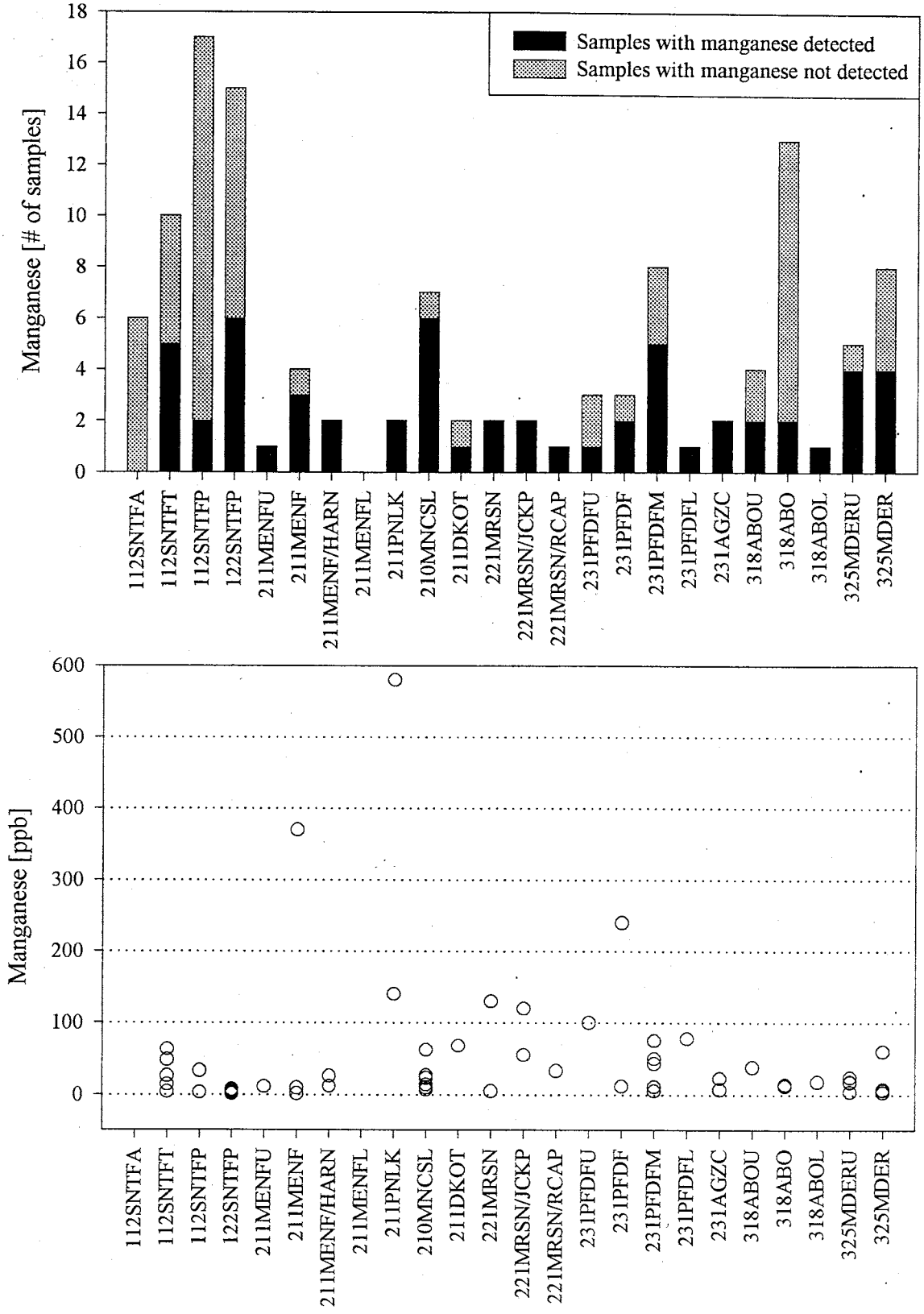

Figure 34. The occurence and concentration of manganese in ground water.

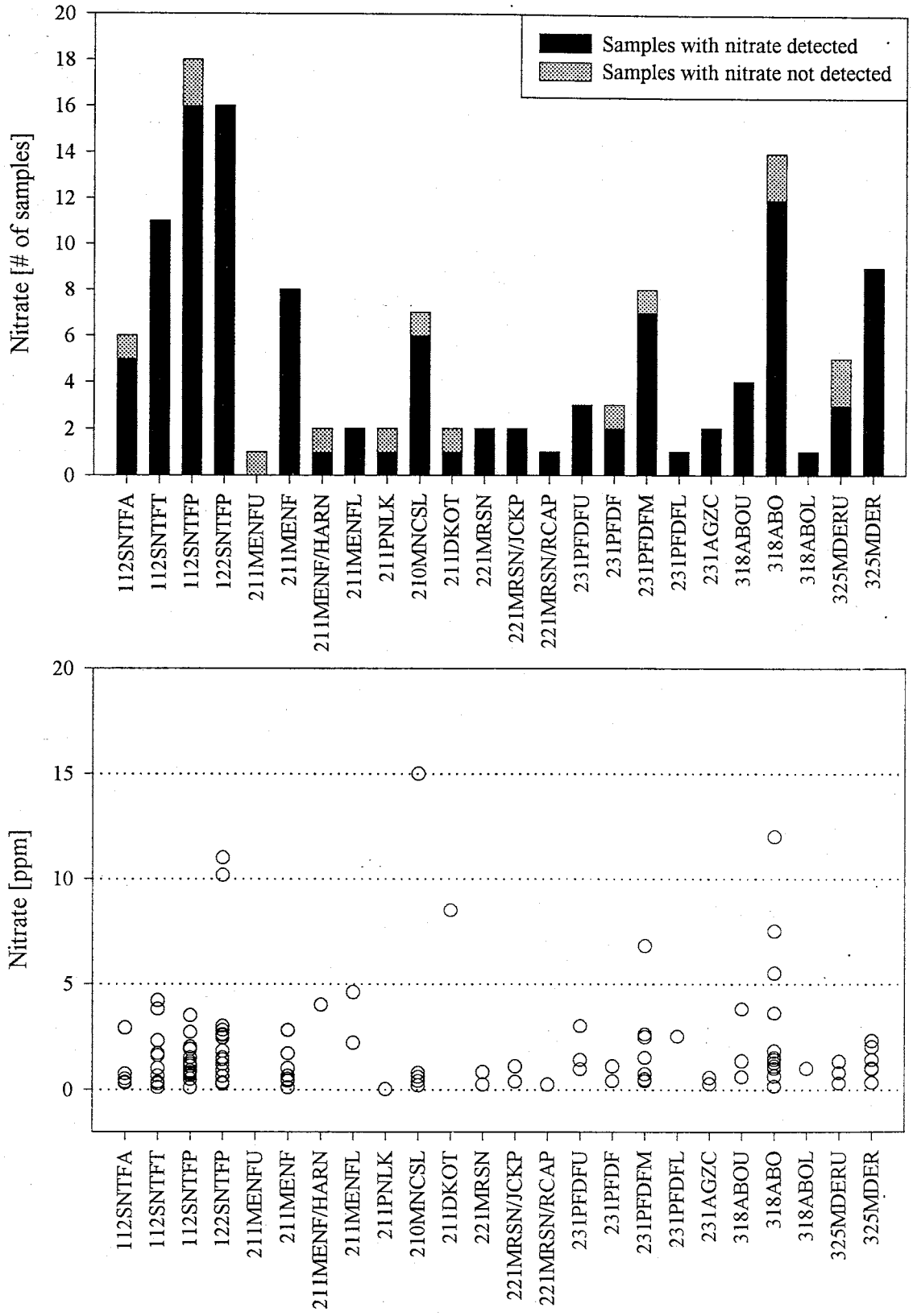

Figure 35. The occurence and concentration of nitrate in ground water.

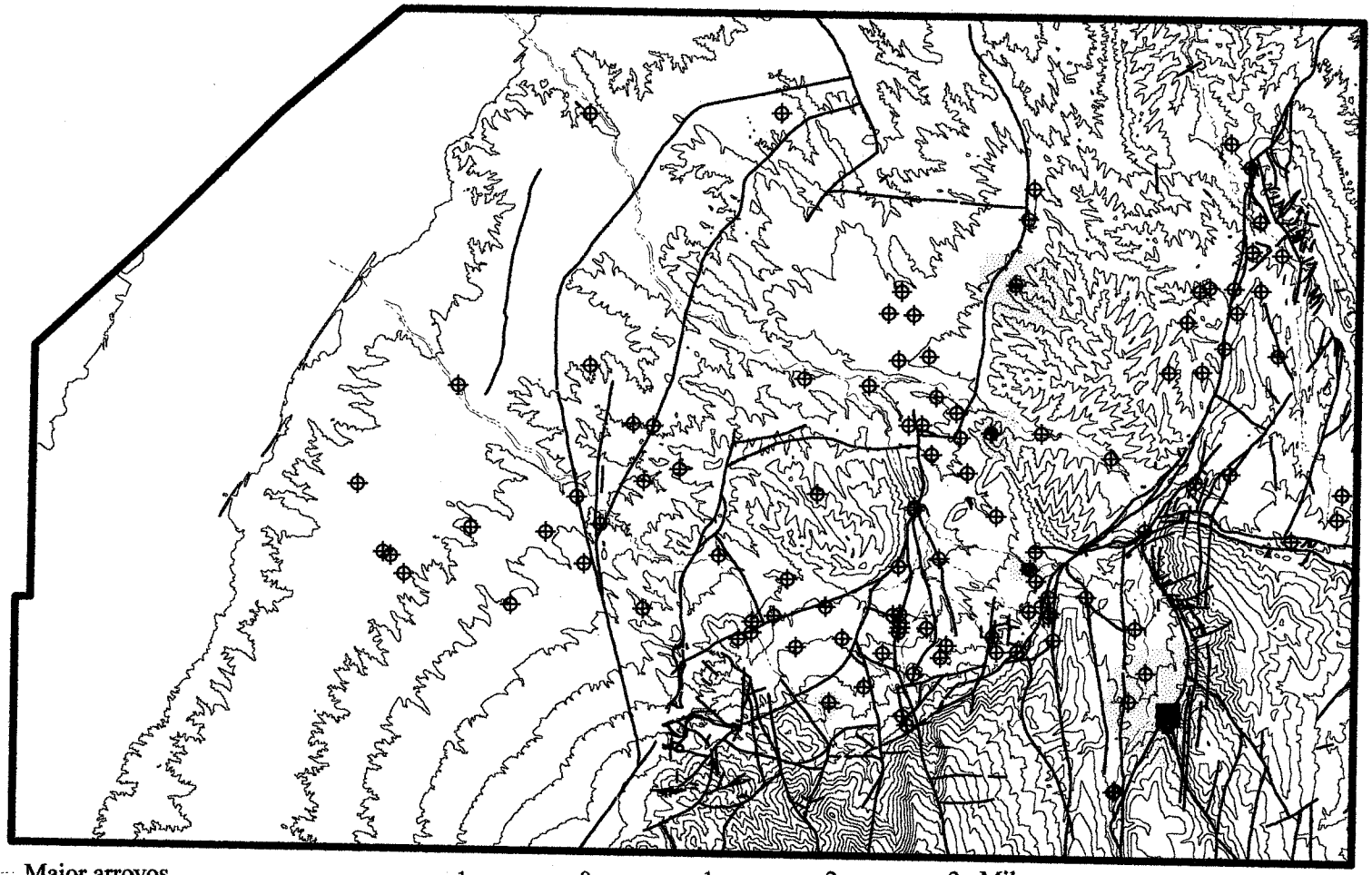

Figure 36. Distribution of nitrate in ground water.

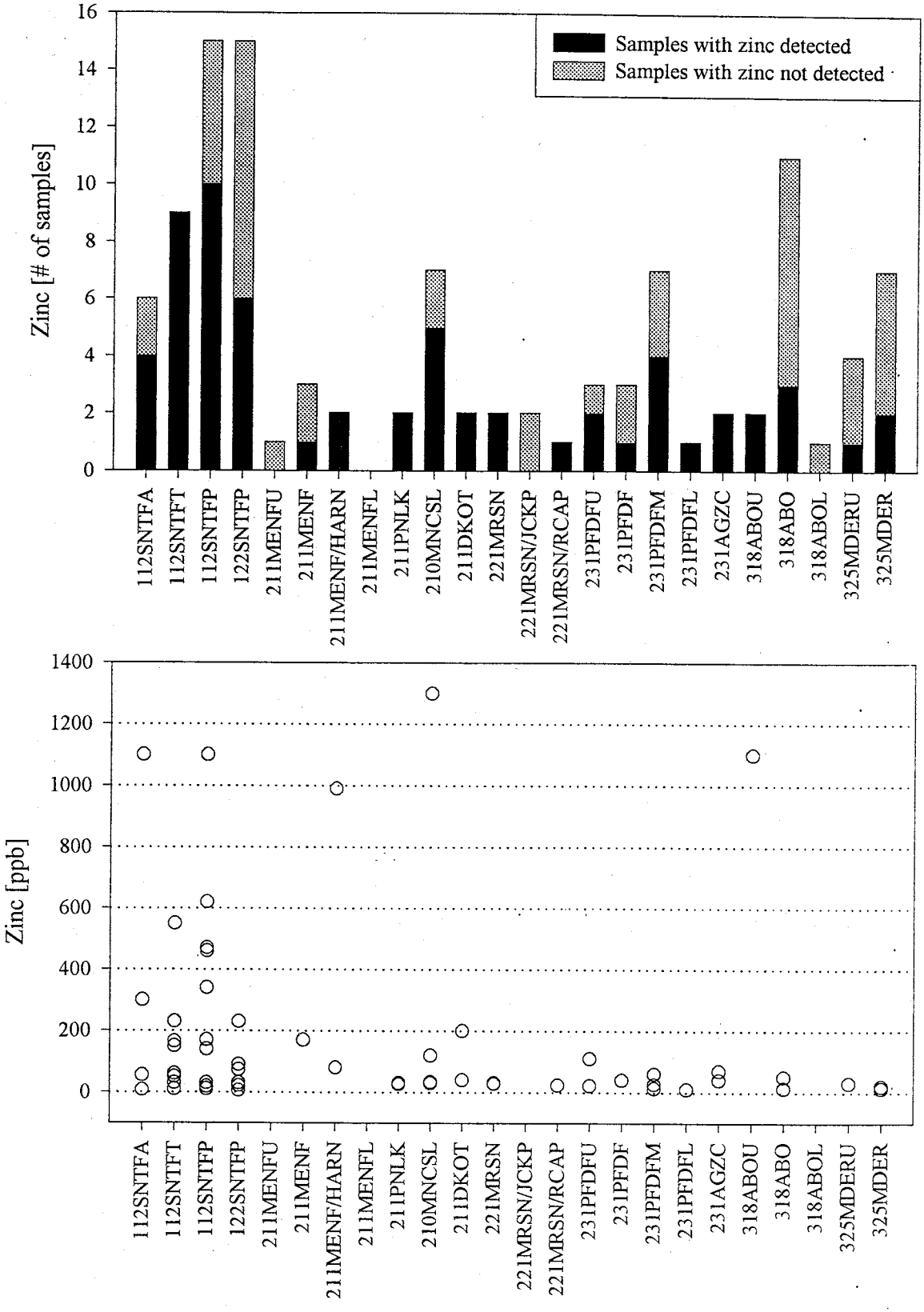

Figure 37. The occurence and concentration of zinc in ground water.

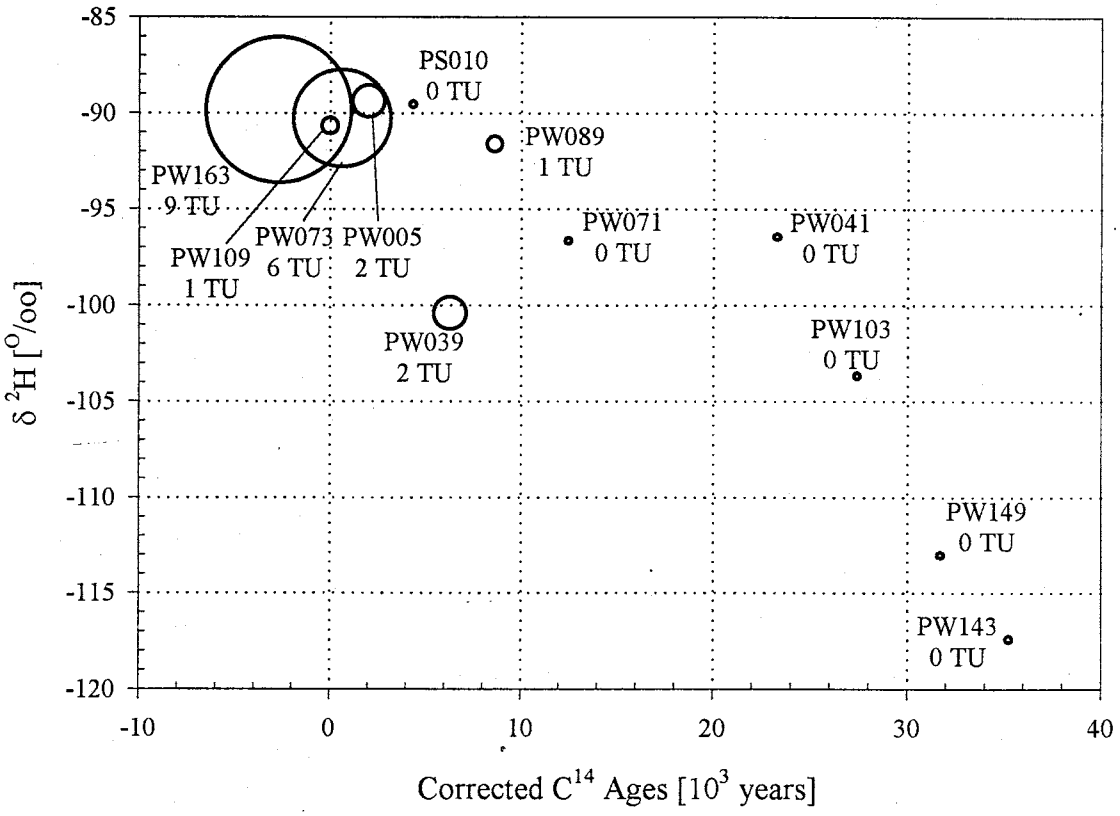

Figure 38. Corrected ^{14}C age and tritium concentration compared to deuterium content in ground-water samples. See text for details about correction of the carbon-14 ages with the $\delta^{13}C$ mixing model. Symbol size is proportional to tritium content.

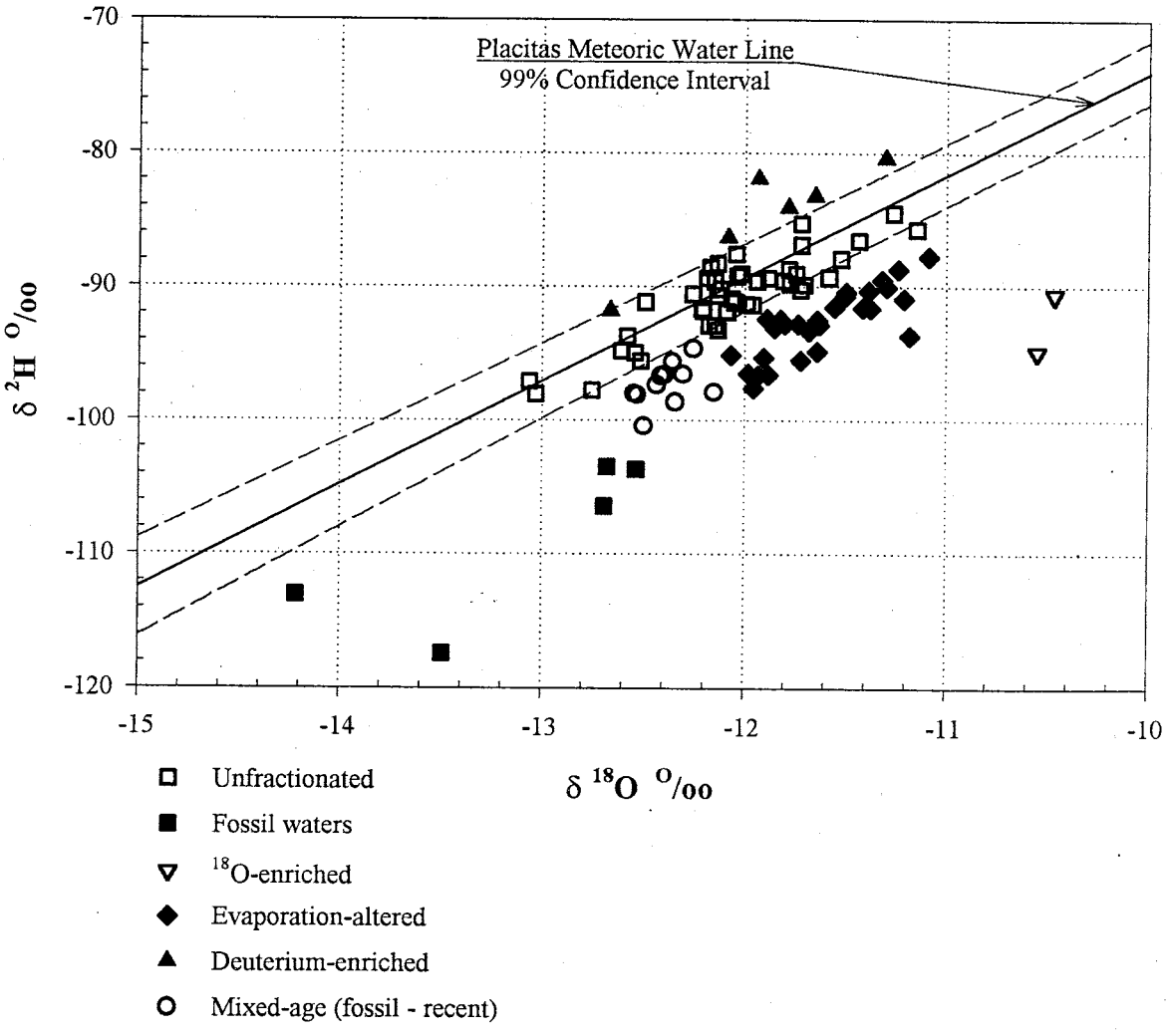

Figure 39. $\delta^{18}O$ and δD composition of ground-water samples grouped by major isotopic process affecting the ground water. Symbol size is ½ standard deviation. Placitas meteoric water line shown for reference. See text for discussion of processes.

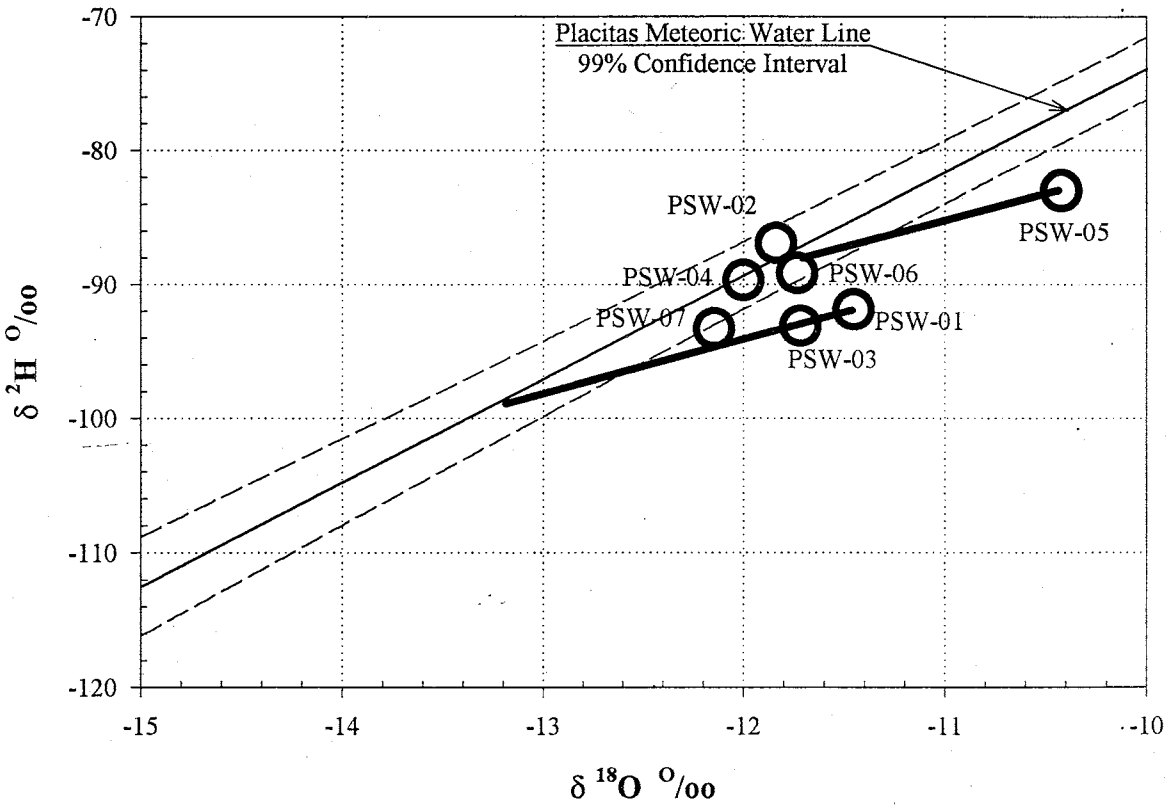

Figure 40. Stable isotope composition of surface-water samples. Heavy solid lines show the effect of evaporation from an open body of water at about 50% relative humidity (slope = 4.4, Gonfiantini, 1986). Symbol size is one standard deviation. Placitas meteoric water line shown for reference. Sample locations shown in Figure 15.

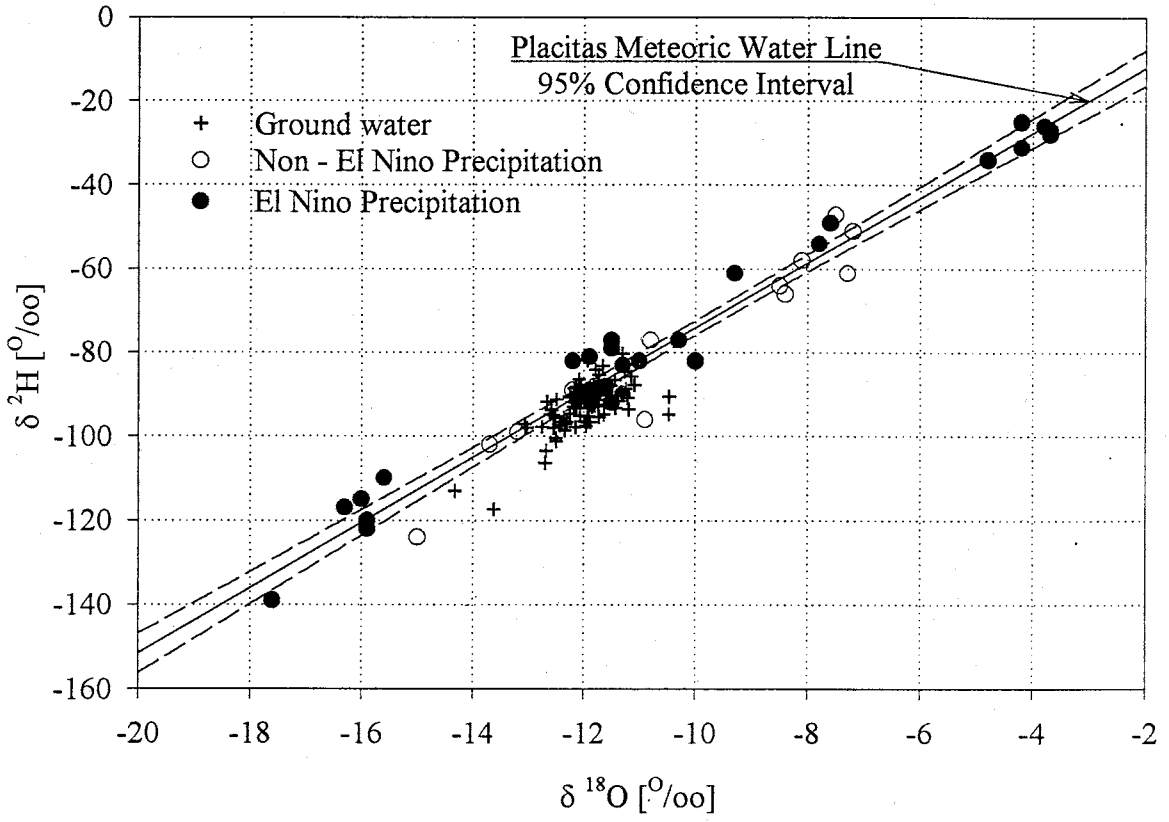

Figure 41. The $\delta^{18}O$ and $\delta^{2}H$ composition of ground- and surface-water compared to the $\delta^{18}O$ and $\delta^{2}H$ composition of precipitation.

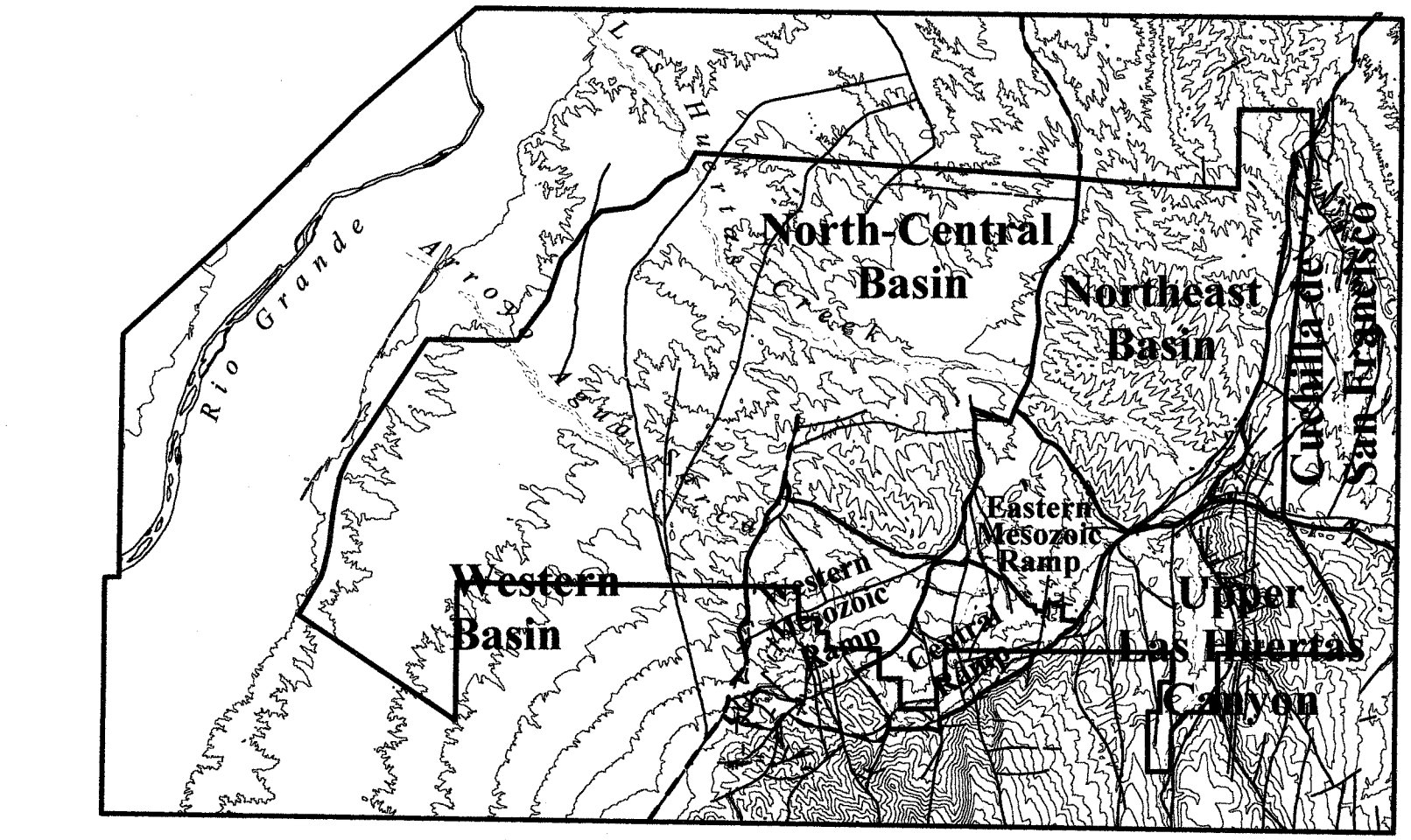

Figure 42. Aquifer Sub Zones

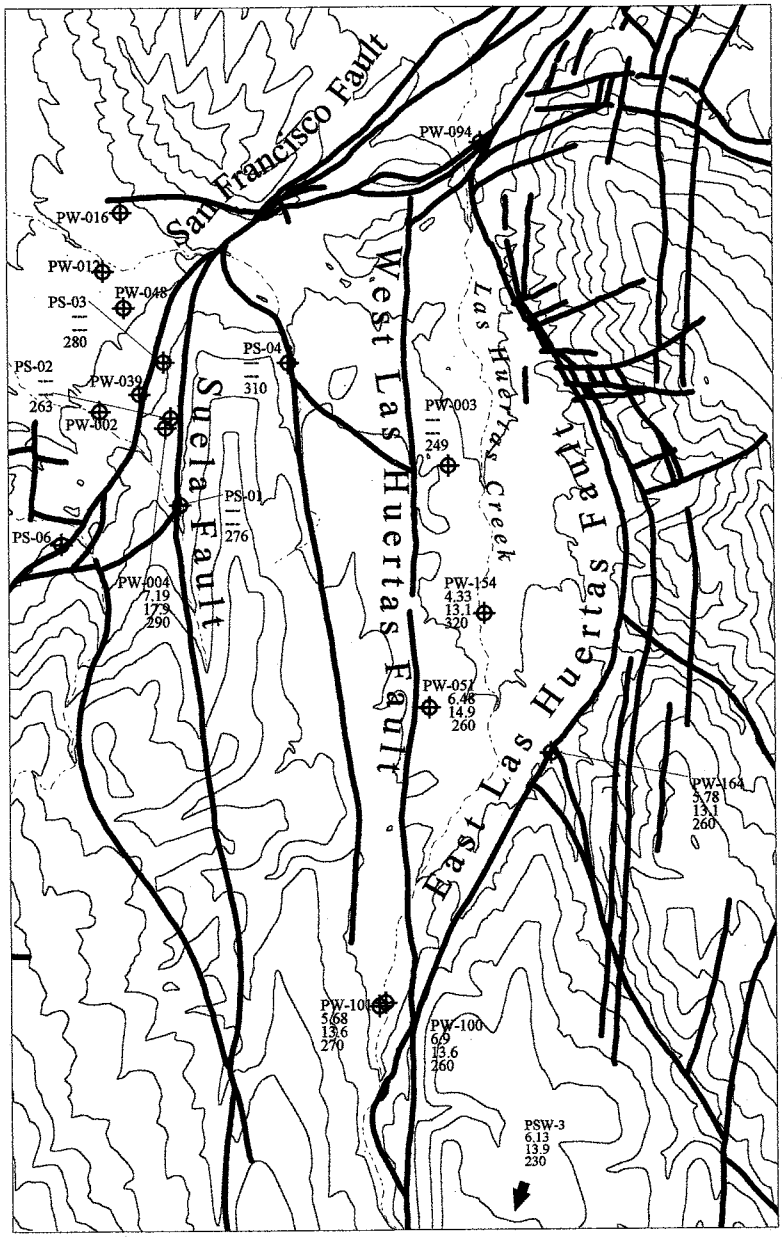

Faults
Arroyos

Sample locations
Spring
Stream
Well
Site ID
PW-385
5.6
17.6
1124
Dissolved Oxygen, ppm
Temperature, C
TDS, ppm

2000 0 2000 4000 Feet
500 0 500 1000 1500 Meters
N
1:30000
Contour interval 100 feet

Figure 43. Location, temperature, dissolved oxygen concentration, and TDS concentration of ground-water samples collected from Cuchilla Lupe and upper Las Huertas Canyon.

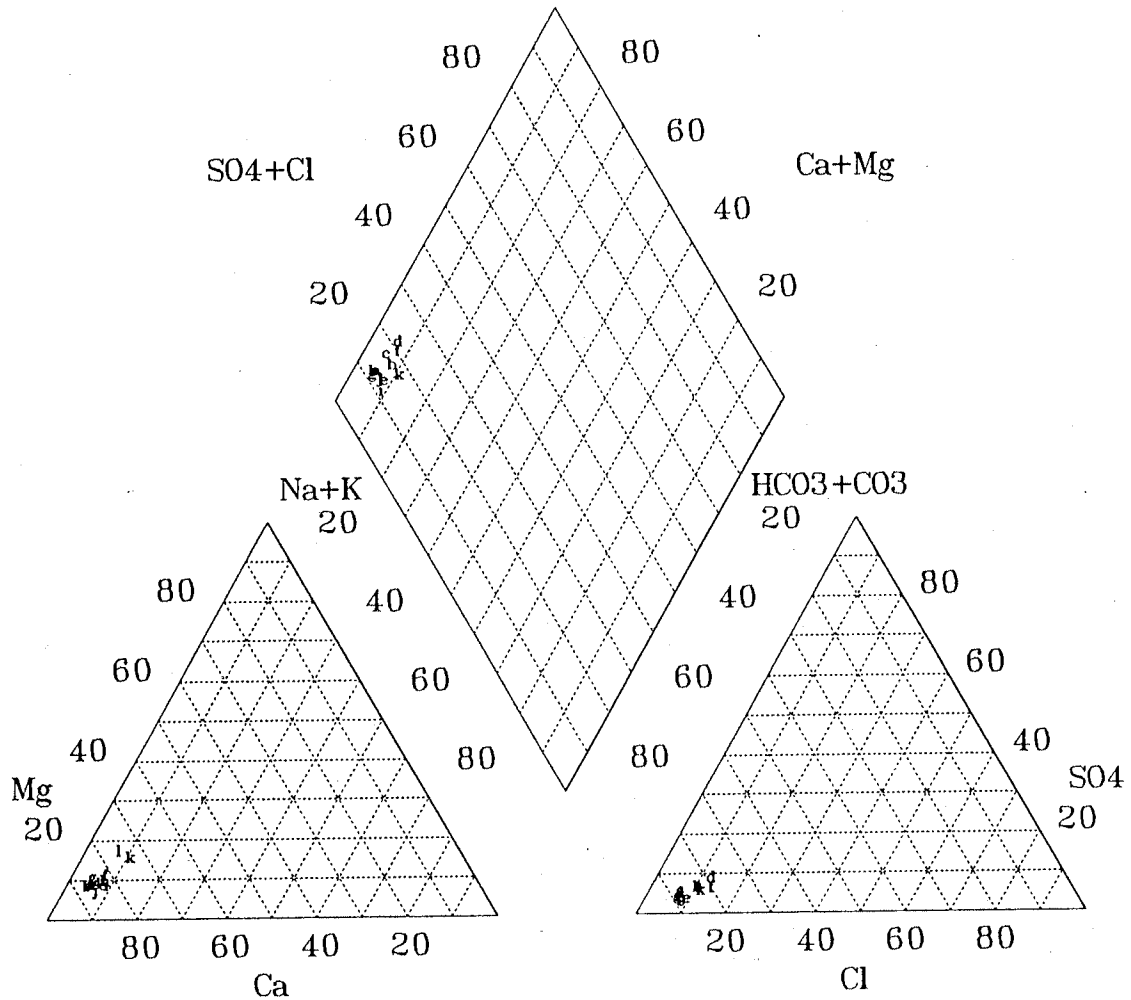

Figure 44. Major ion geochemistry of samples from Cuchilla Lupe and Las Huertas Canyon. Labeled samples are (a) PS-01, (b) PS-02, (c) PS-03, (d) PS-04, (e) PSW-03, (f) PW-003, (g) PW-004, (h) PW-051, (i) PW-100, (j) PW-101, (k) PW-154, and (l) PW-164. Sample locations are shown in Figure 43.

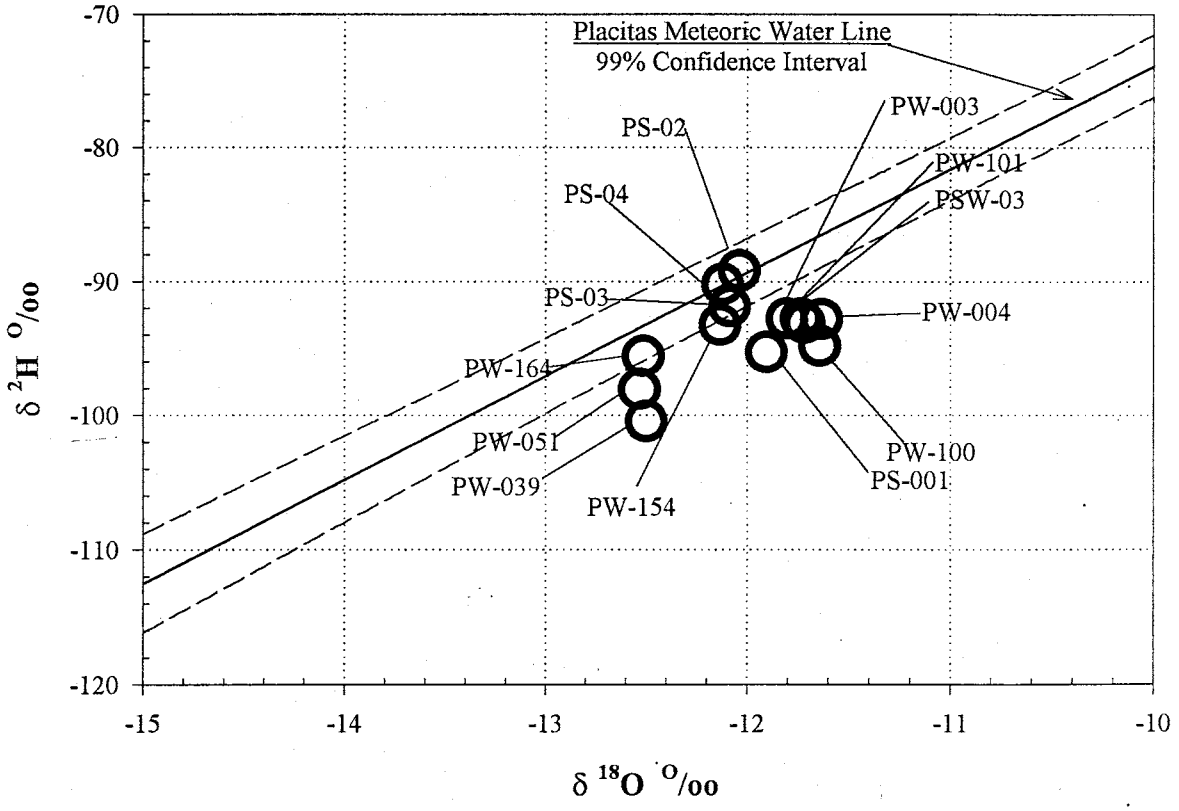

Figure 45. $\delta^{18}O$ and $\delta^{2}H$ composition of ground-water samples collected from Cuchilla Lupe and Las Huertas Canyon. Sample locations are shown in Figure 43. Symbol size is one standard deviation. Placitas meteoric water line shown for reference.

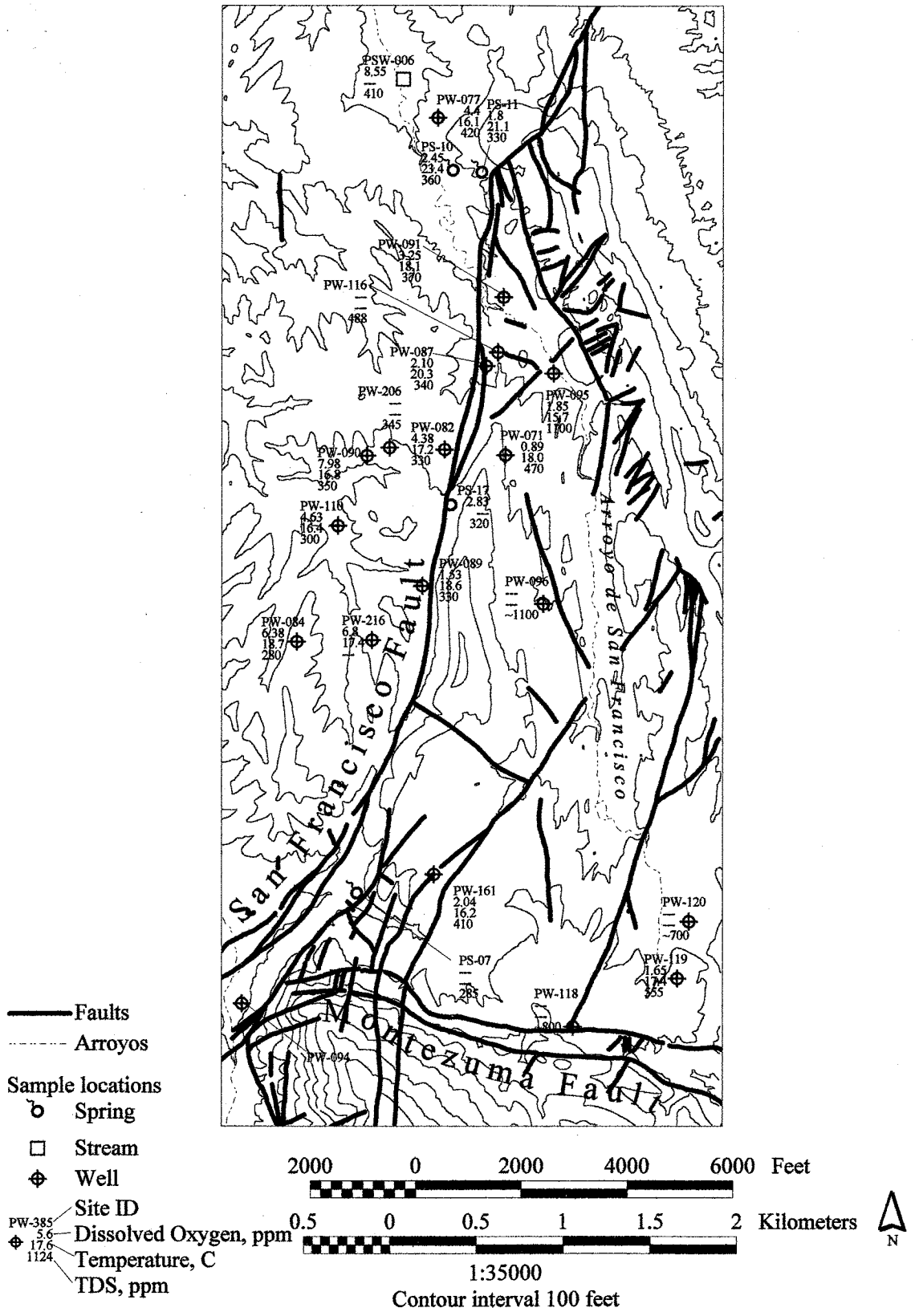

Figure 46. Location, temperature, dissolved oxygen concentration, and TDS concentration of ground-water samples collected from near Cuchilla de San Francisco.

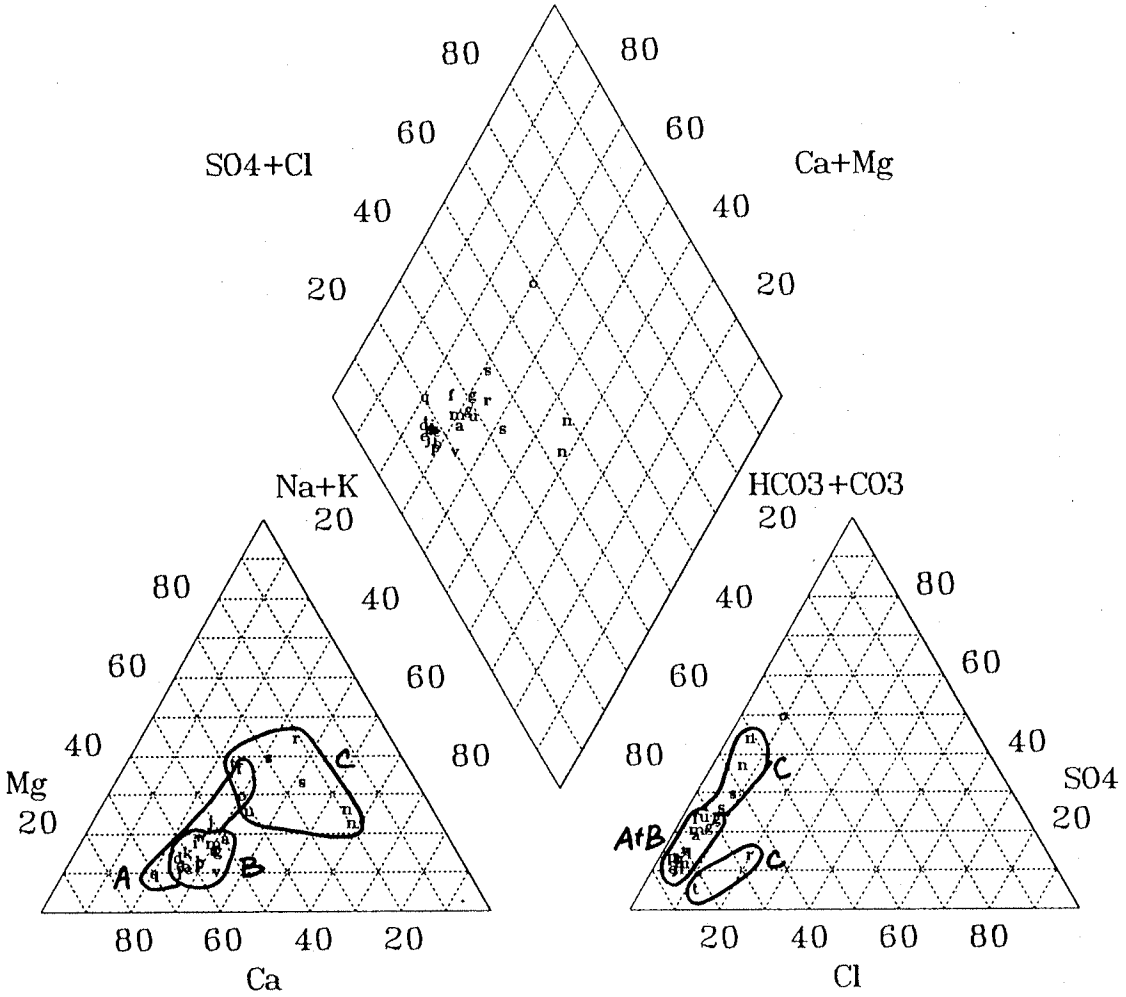

Figure 47. Major ion geochemistry of samples from Cuchilla de San Francisco. Labeled samples are (a) PSW-06, (b) PS-07, (c) PS-10, (d) PS-11, (e) PS-17, (f) PW-071, (g) PW-077, (h) PW-082, (i) PW-084, (j) PW-087, (k) PW-089, (l) PW-090, (m) PW-091, (n) PW-095, (o) PW-096, (p) PW-110, (q) PW-116, (r) PW-118, (s) PW-119, (t) PW-120, (u) PW-161, (v) PW-206, and (w) PW-216. Circled groups are from the (A) Madera, (B) Lower Santa Fe, and (C) Abo Formations. Sample locations are shown in Figure 46.

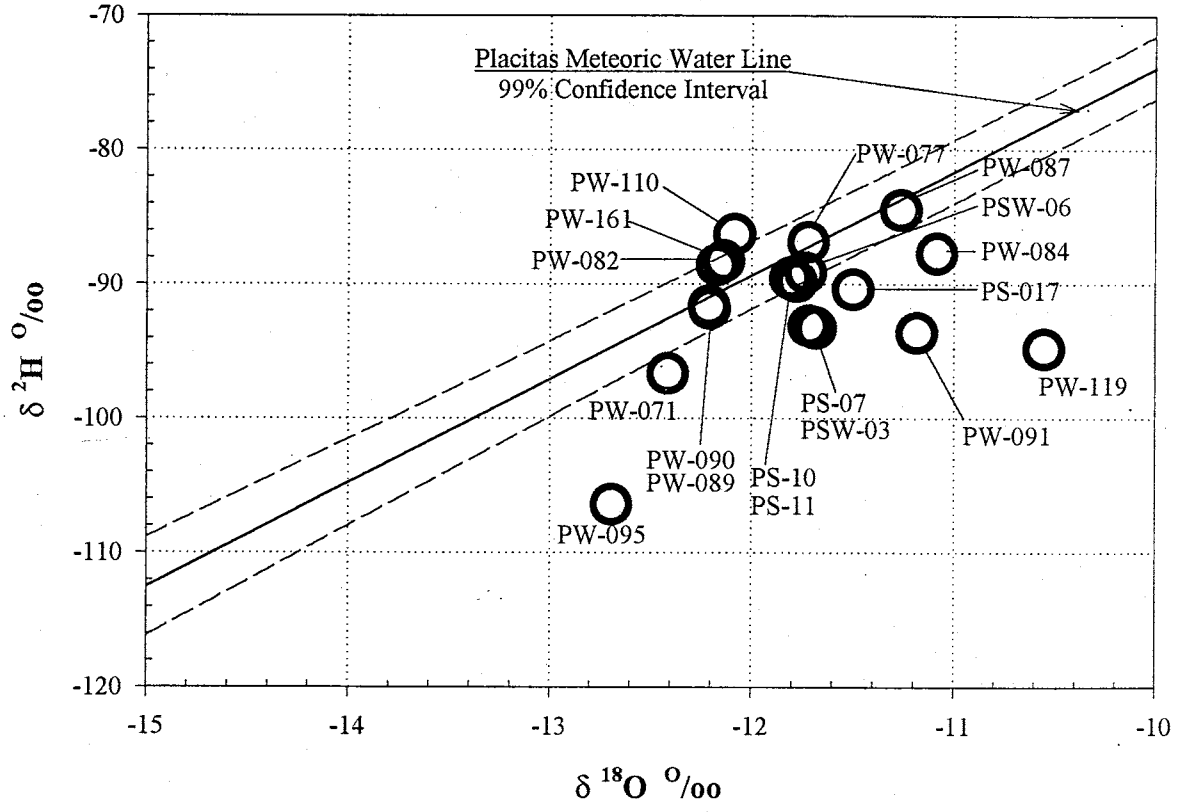

Figure 48. $\delta^{18}O$ and $\delta^{2}H$ composition of ground-water samples collected from near Cuchilla de San Francisco. Sample locations are shown in Figure 46. Symbol size is one standard deviation. Placitas meteoric water line shown for reference.

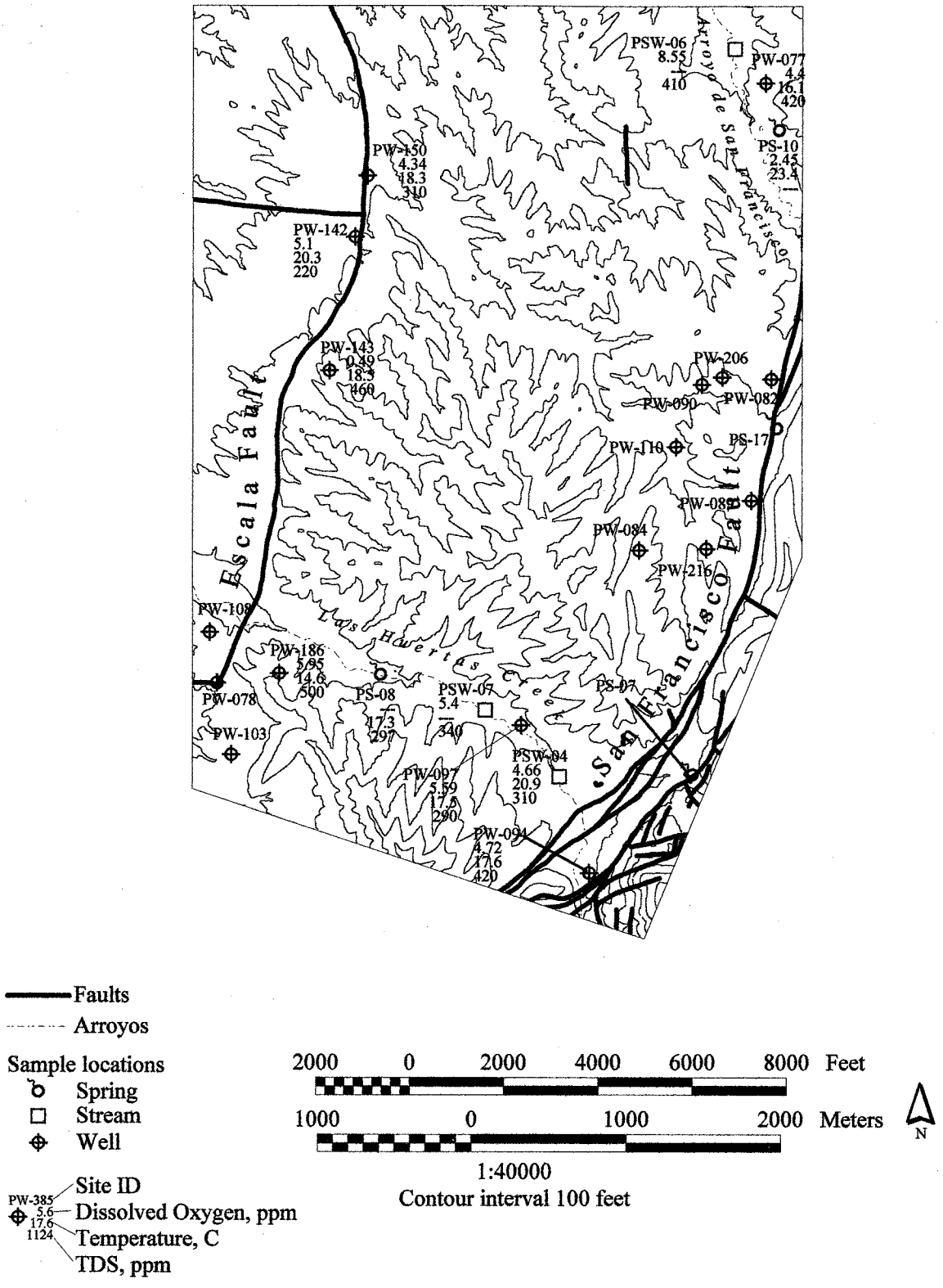

Figure 49. Location, temperature, dissolved oxygen concentration, and TDS concentration of ground-water samples collected from the northeastern part of the basin.

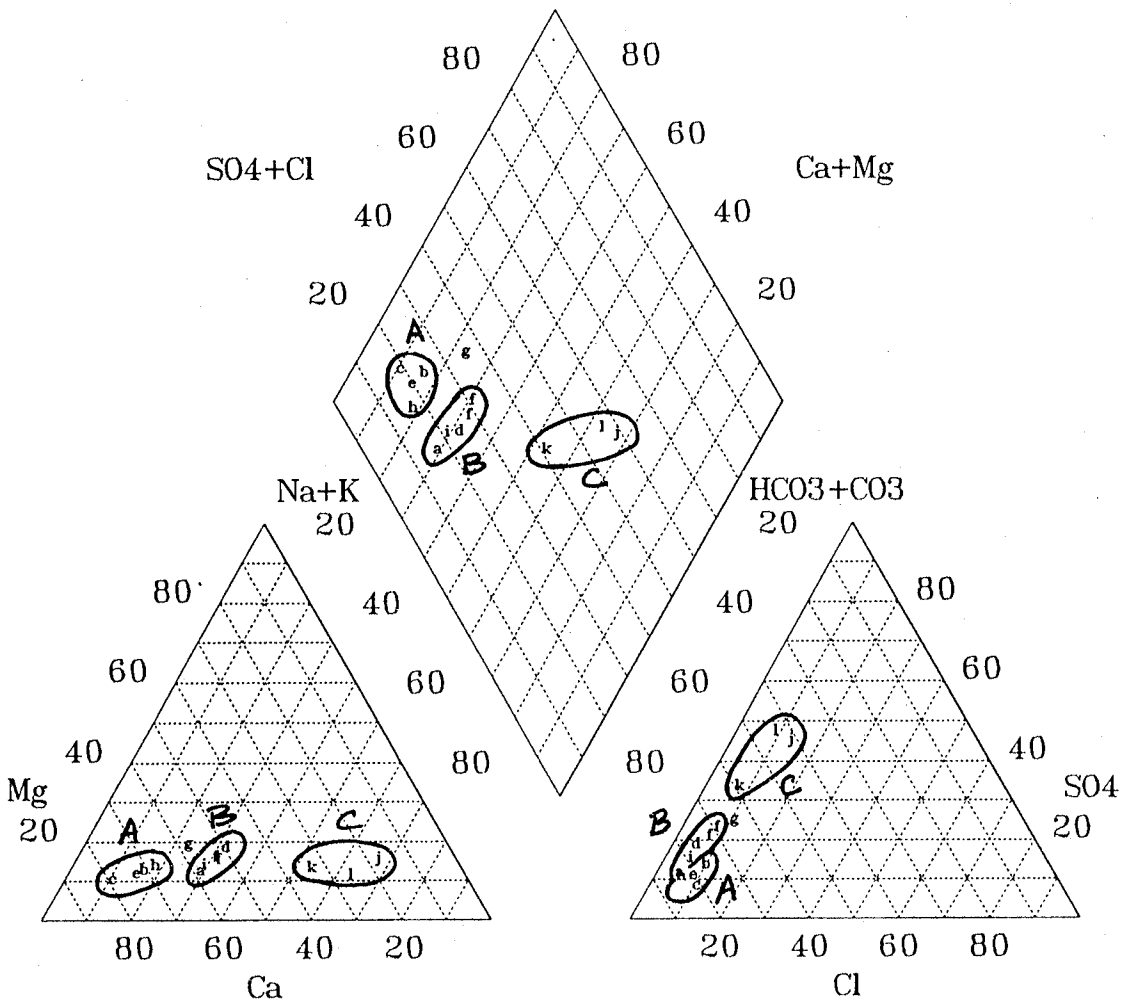

Figure 50. Major ion geochemistry of samples from the northeastern part of the basin. Labeled samples are (a) PS-07, (b) PS-08, (c) PSW-04, (d) PSW-06, (e) PSW-07, (f) PW-077, (g) PW-094, (h) PW-097, (i) PW-142, (j) PW-143, (k) PW-150, and (l) PW-186. Labeled groups are (A) Ground and surface water from along Las Huertas Creek, (B) ground and surface water from the basin NW of Cuchilla de San Francisco, and (C) ground water from along the Escala fault. Sample locations are shown in Figure 49.

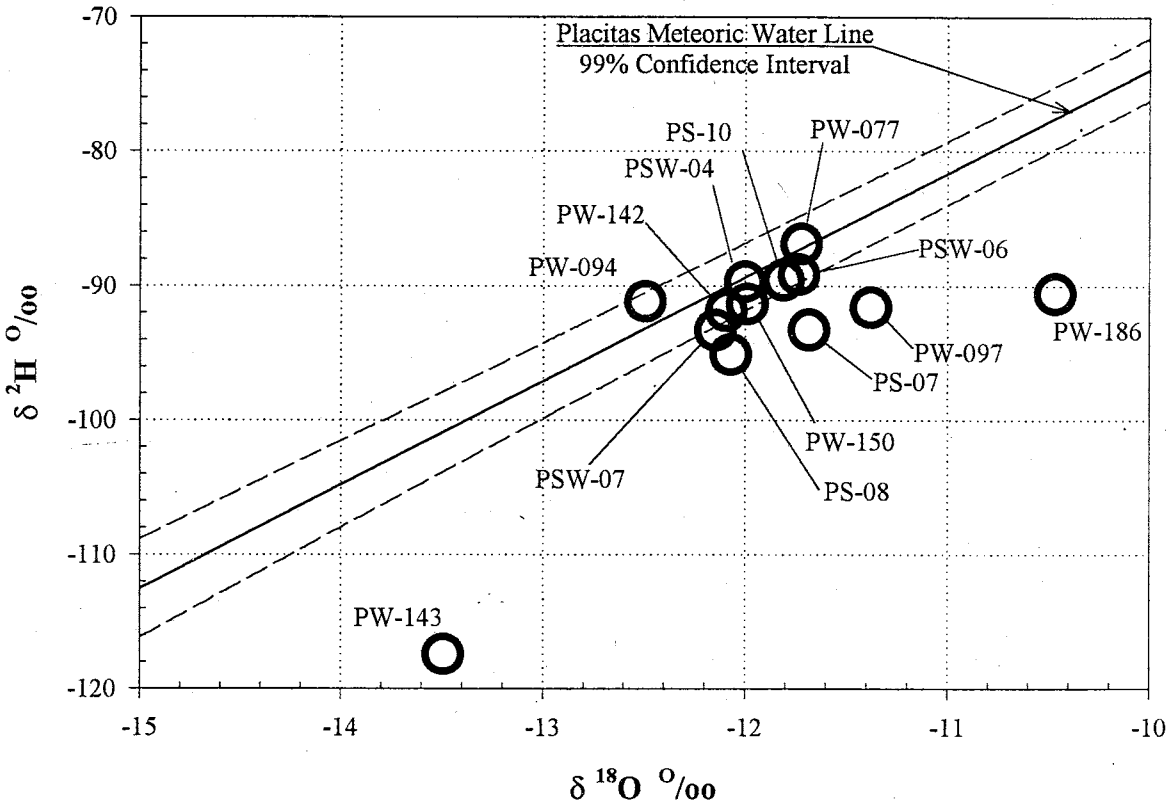

Figure 51. $\delta^{18}O$ and $\delta^{2}H$ composition of ground-water samples collected from the northeastern part of the basin. Sample locations are shown in Figure 49. Symbol size is one standard deviation. Placitas meteoric water line shown for reference.

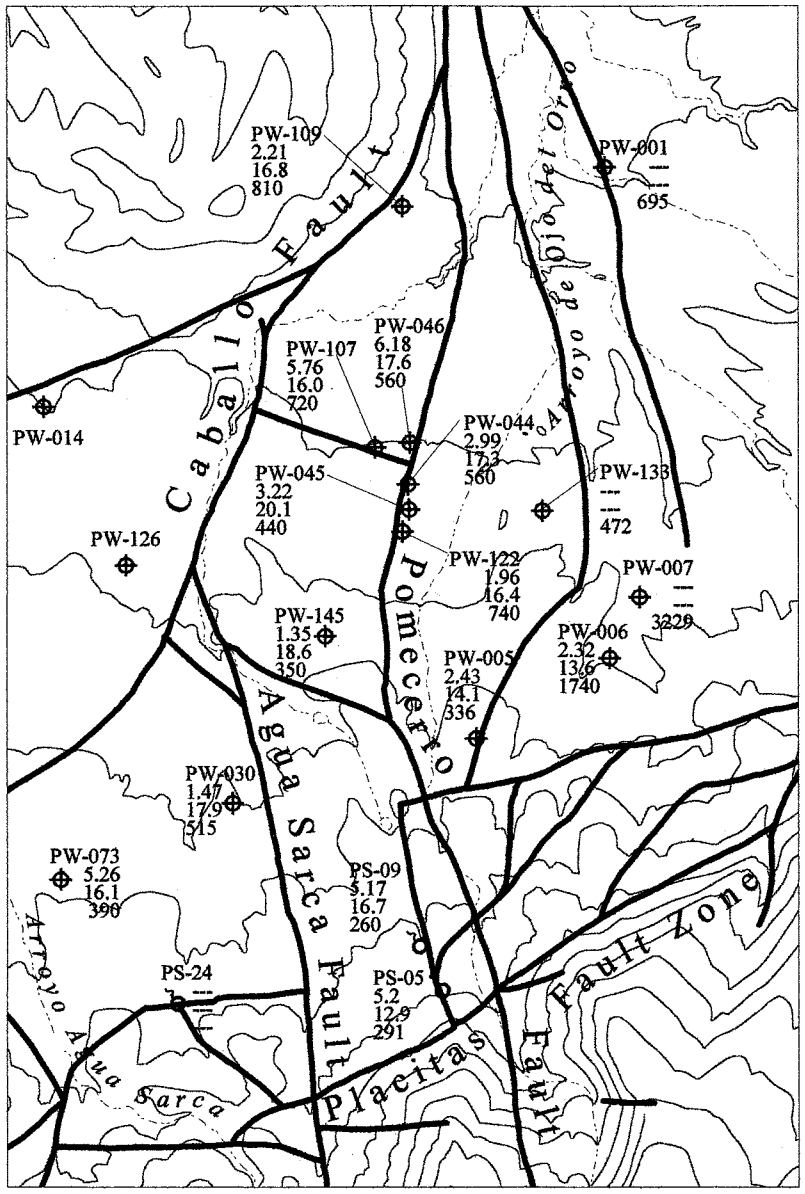

Faults

Arroyos

Sample locations

Spring

Stream

Well

Site ID

PW-385
5.6
17.6
1124

Dissolved Oxygen, ppm

Temperature, C

TDS, ppm

1000 0 1000 2000 3000 4000 Feet

250 0 250 500 750 1000 Meters

1:20000

Contour interval 100 feet

N

Figure 52. Location, temperature, dissolved oxygen concentration, and TDS concentration of ground-water samples collected from the central part of the Mesozoic ramp.

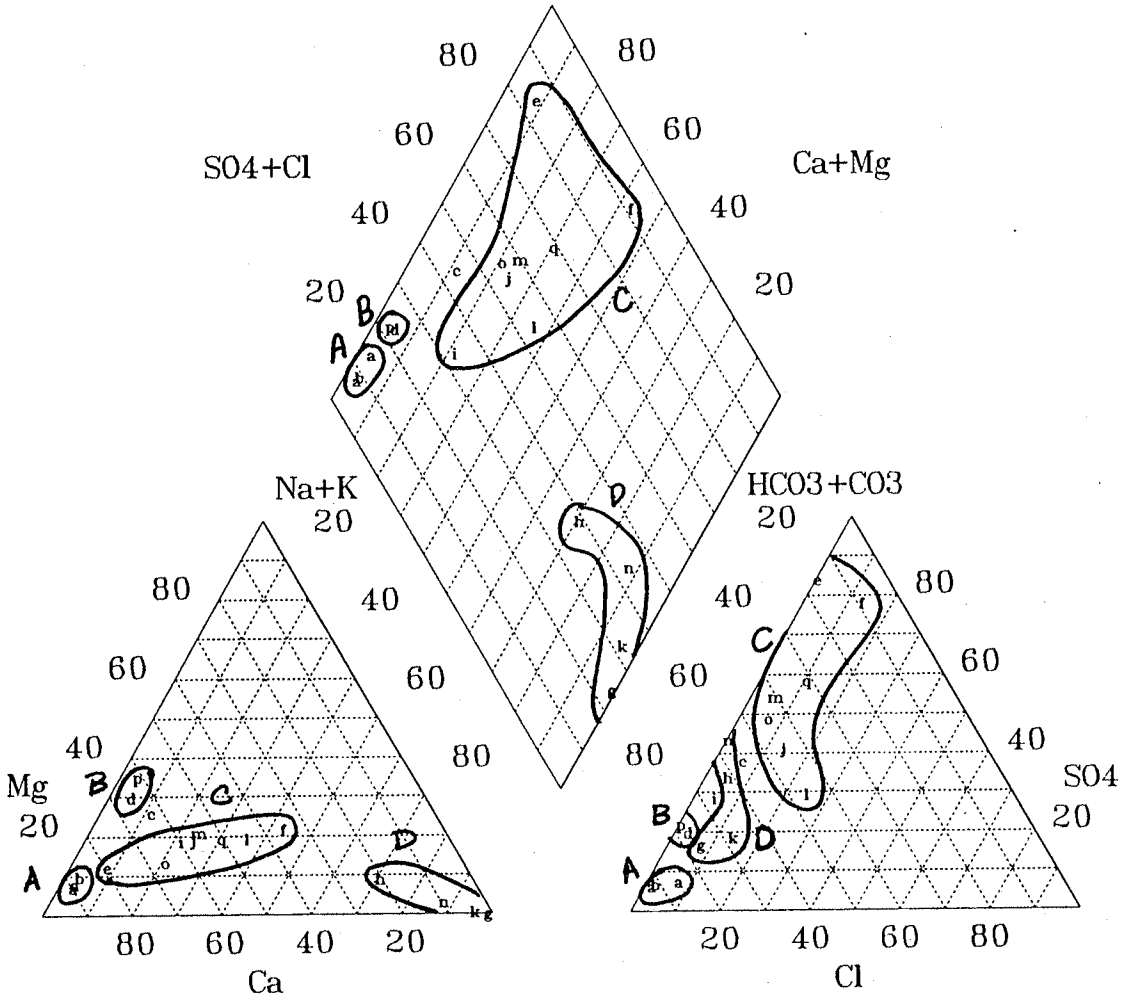

Figure 53. Major ion geochemistry of samples from the central Mesozoic ramp. Labeled samples are (a) PS-05, (b) PS-09, (c) PW-001, (d) PW-005, (e) PW-006, (f) PW-007, (g) PW-030, (h) PW-044, (i) PW-045, (j) PW-046, (k) PW-073, (l) PW-107, (m) PW-109, (n) PW-122, (o) PW-133, (p) PW-145, and (q) PW-147. Labeled groups are from (A) the Placitas fault zone, (B) north edge of the Placitas fault zone, (C) farther north of the Placitas fault zone, and (D) samples from the Petrified Forest Formation affected by cation exchange. Sample locations are shown in Figure 52.

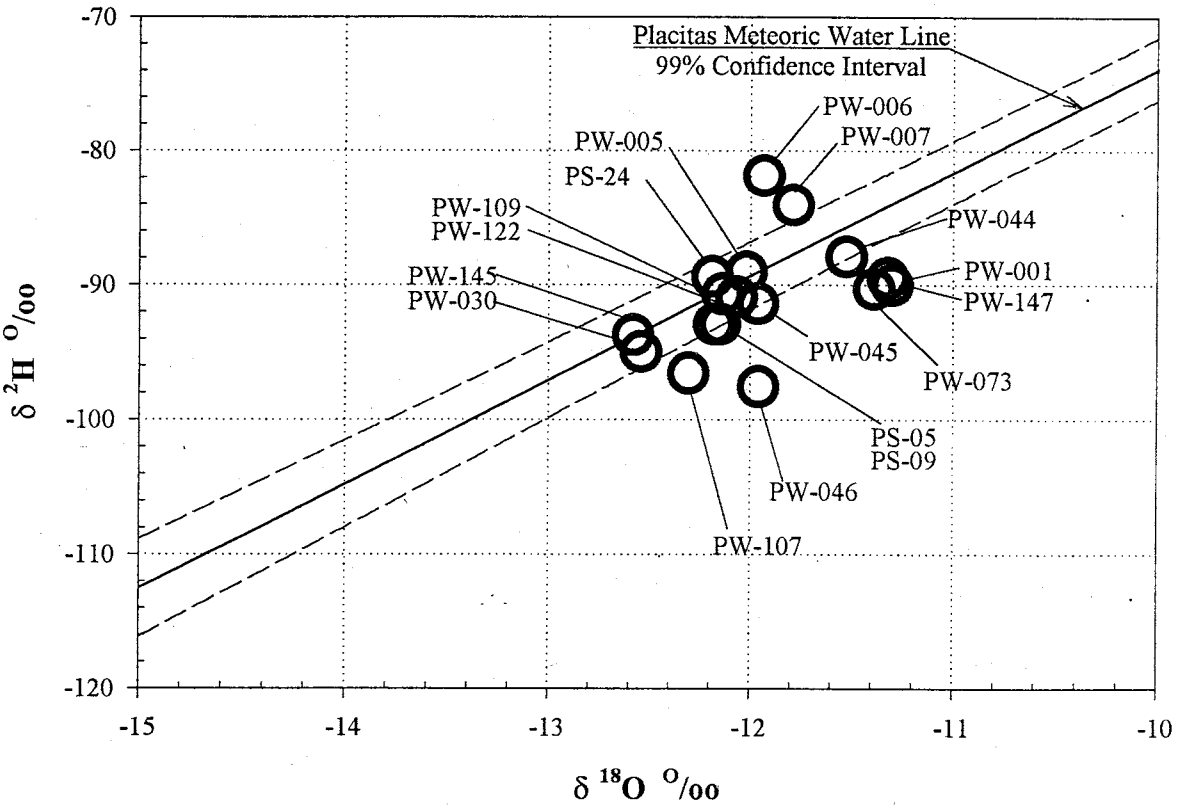

Figure 54. $\delta^{18}O$ and $\delta^{2}H$ composition of ground-water samples collected from the central part of the Mesozoic ramp. Sample locations are shown in Figure 52. Symbol size is one standard deviation. Placitas meteoric water line shown for reference.

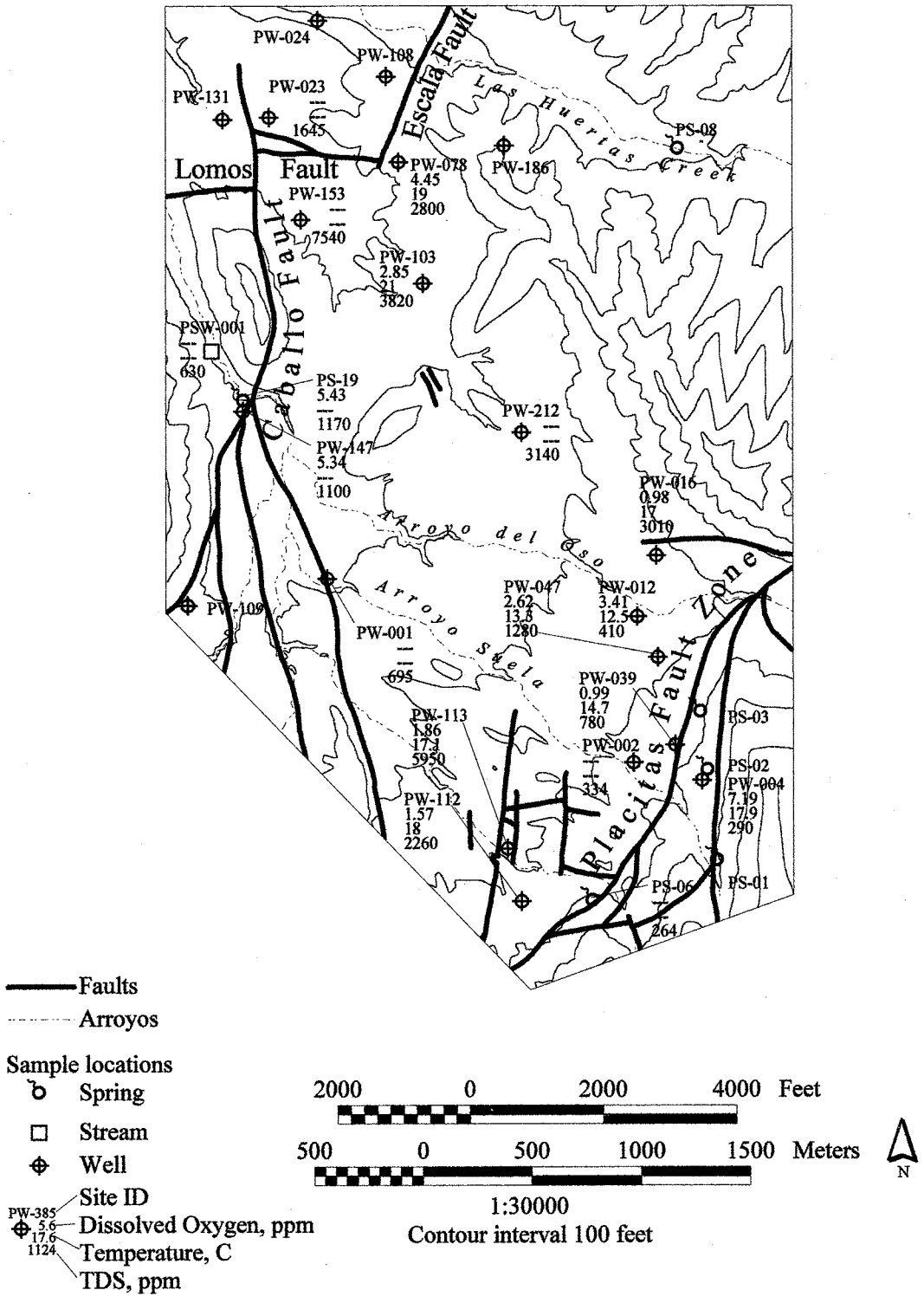

Figure 55. Location, temperature, dissolved oxygen concentration, and TDS concentration of ground-water samples collected from the eastern part of the Mesozoic ramp.

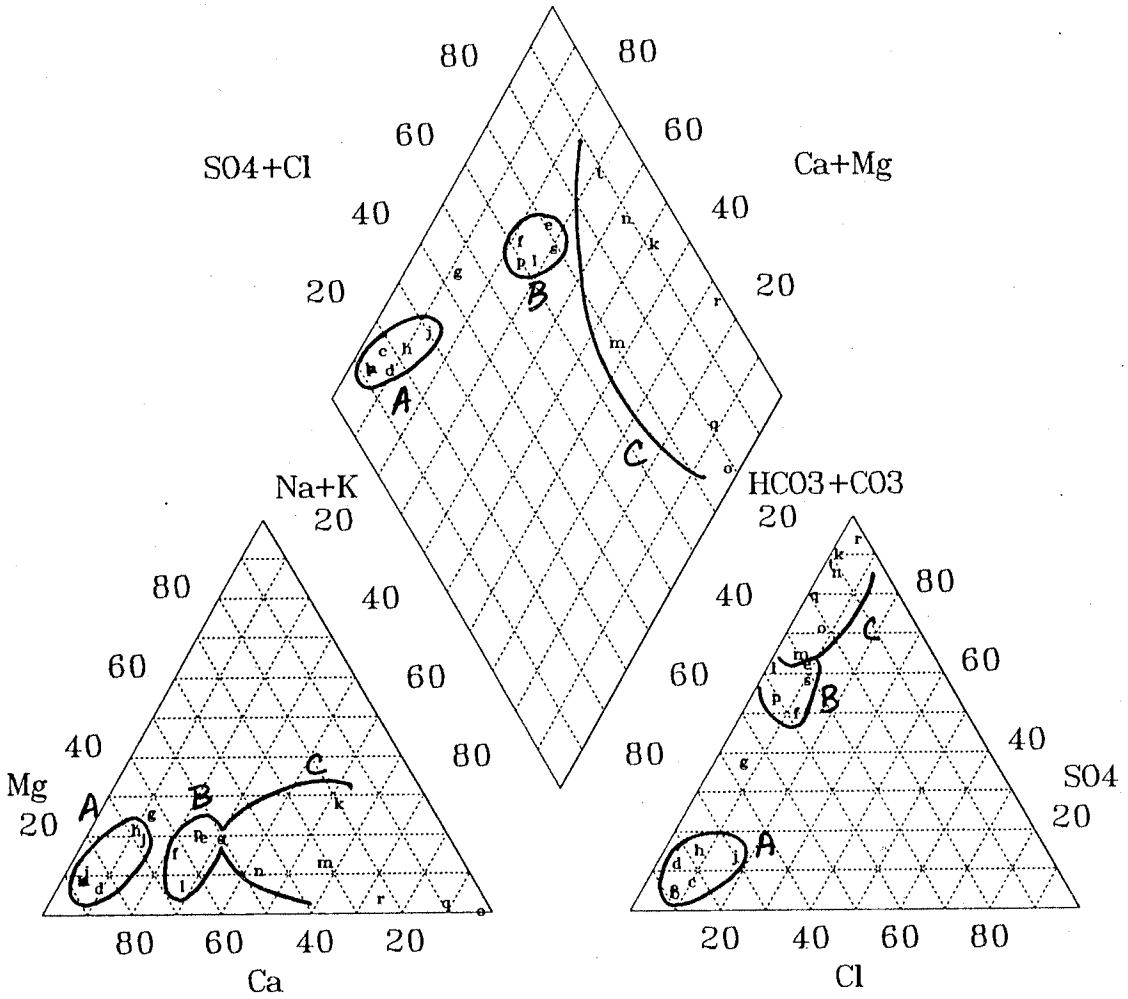

Figure 56. Major ion geochemistry of samples from the east part of the Mesozoic ramp. Sample locations are (a) PS-01, (b) PS-02, (c) PS-03, (d) PS-06, (e) PS-19, (f) PSW-01, (g) PW-001, (h) PW-002, (i) PW-004, (j) PW-012, (k) PW-016, (l) PW-039, (m) PW-047, (n) PW-078, (o) PW-103, (p) PW-109, (q) PW-112, (r) PW-113, (s) PW-147 and (t) PW-212. Labeled groups are from (A) Cuchilla Lupe and along the Placitas fault zone, (B) and (C) Mesozoic formations away from the Placitas fault zone.Sample locations are shown in Figure 55.

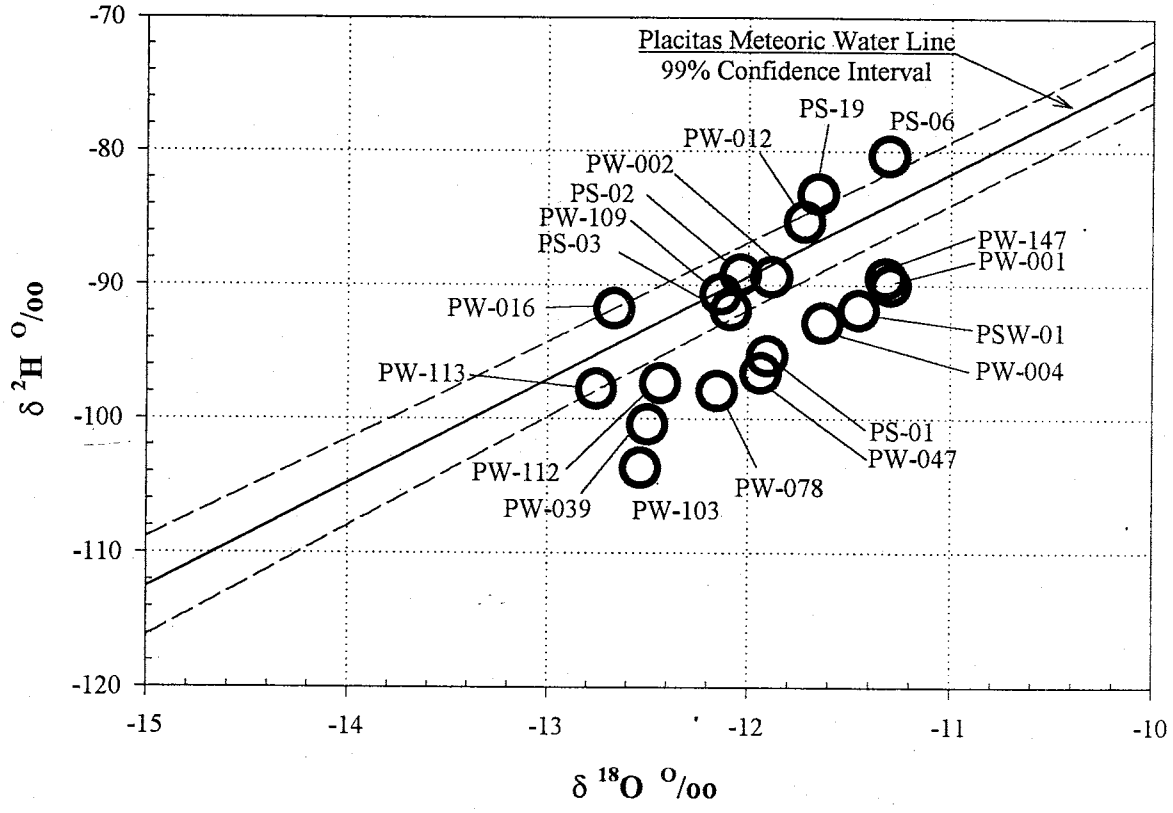

Figure 57. $\delta^{18}O$ and $\delta^{2}H$ composition of ground-water samples collected from the eastern part of the Mesozoic ramp. Sample locations are shown in Figure 55. Symbol size is one standard deviation. Placitas meteoric water line shown for reference.

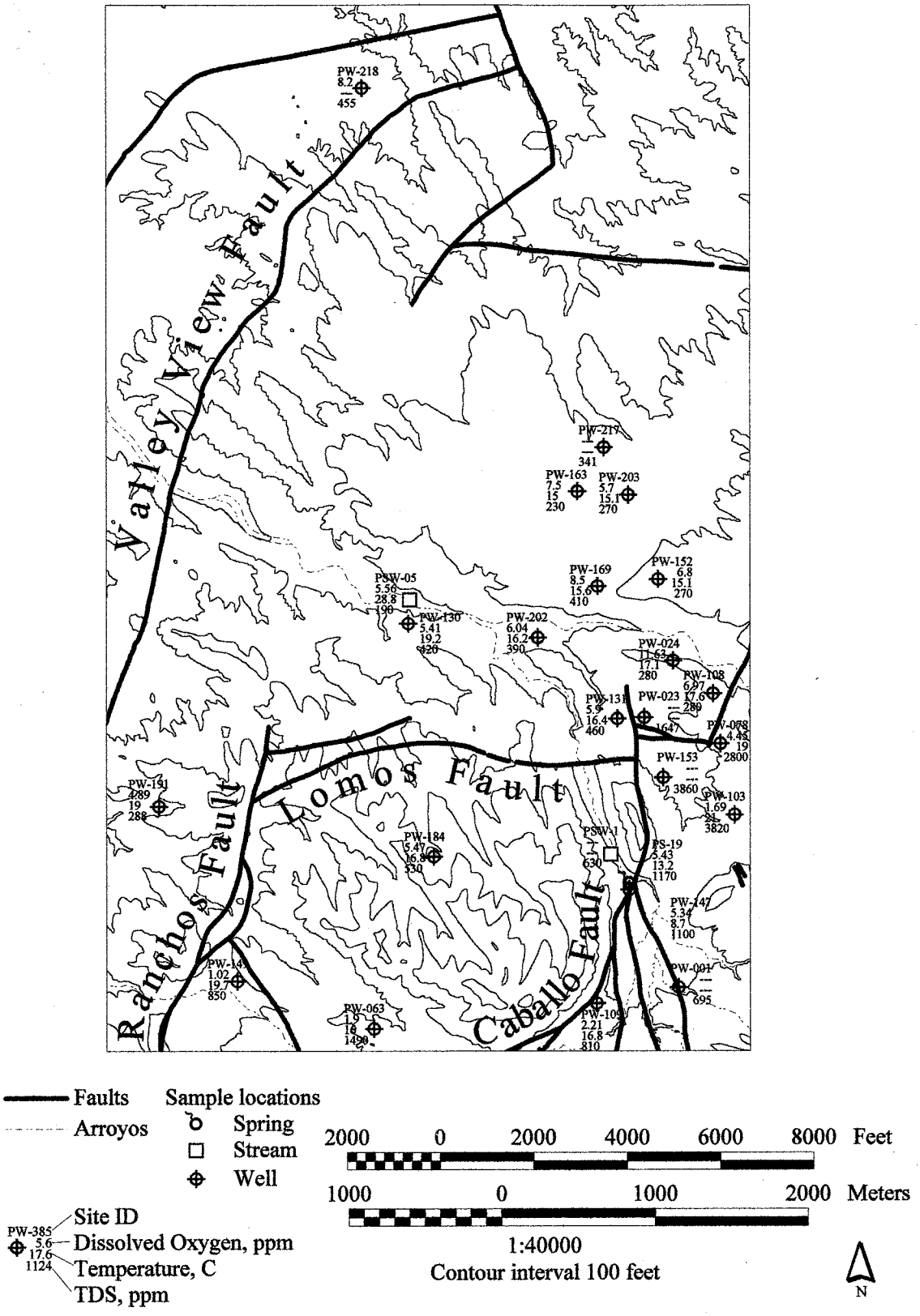

Figure 58. Location, temperature, dissolved oxygen concentration, and TDS concentration of ground-water samples collected from the north-central part of the basin.

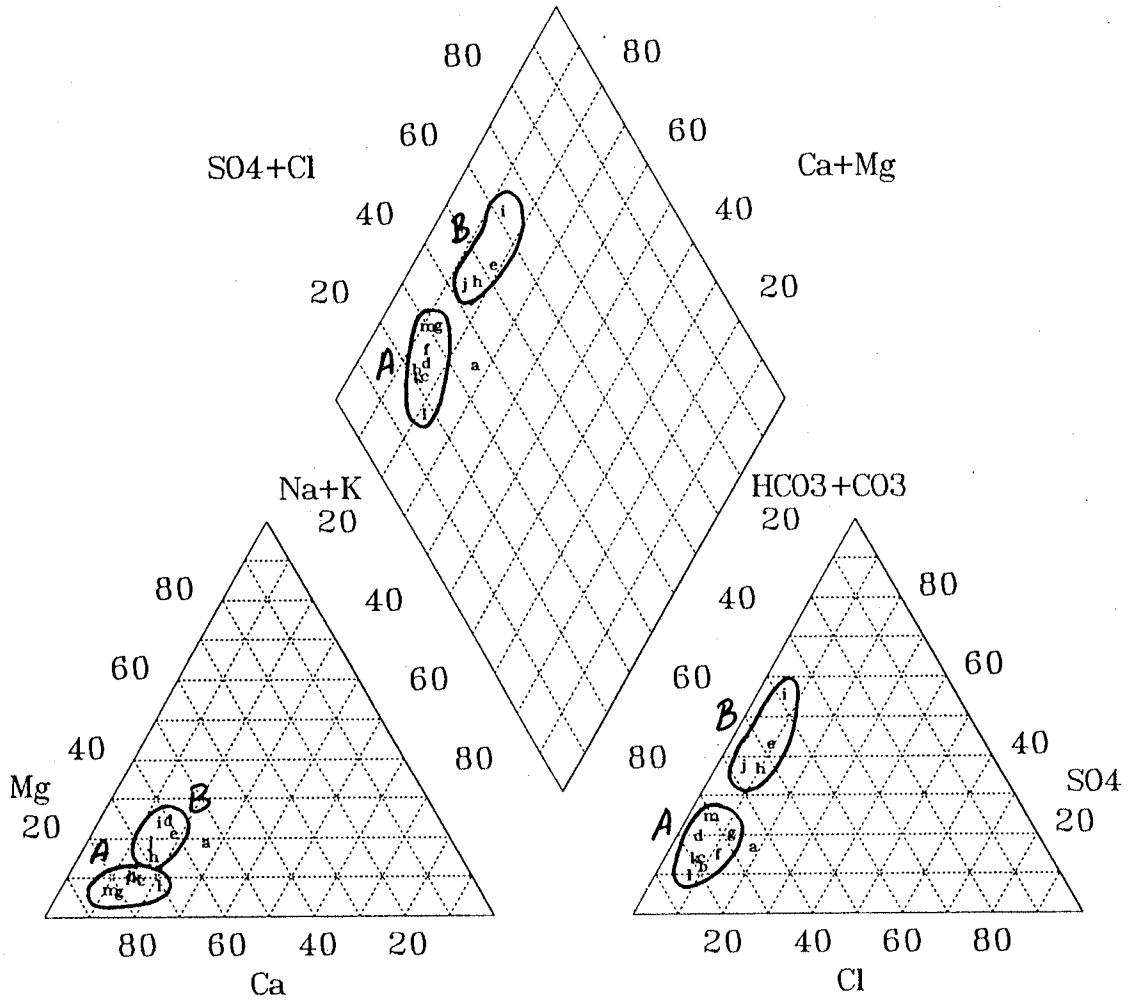

Figure 59. Major ion geochemistry of samples from the north-central part of the basin. Sample locations are (a) PSW-05, (b) PW-024, (c) PW-108, (d) PW-130, (e) PW-131, (f) PW-152, (g) PW-163, (h) PW-169, (i) PW-184,(j) PW-202, (k) PW-203, (l) PW-217, (m) and PW-218. Labeled groups are (A) fresh ground water unaffected by high TDS water from the Mesozoic ramp, and (B) ground water affected by high TDS water from the Mesozoic ramp. Sample locations are shown in Figure 58.

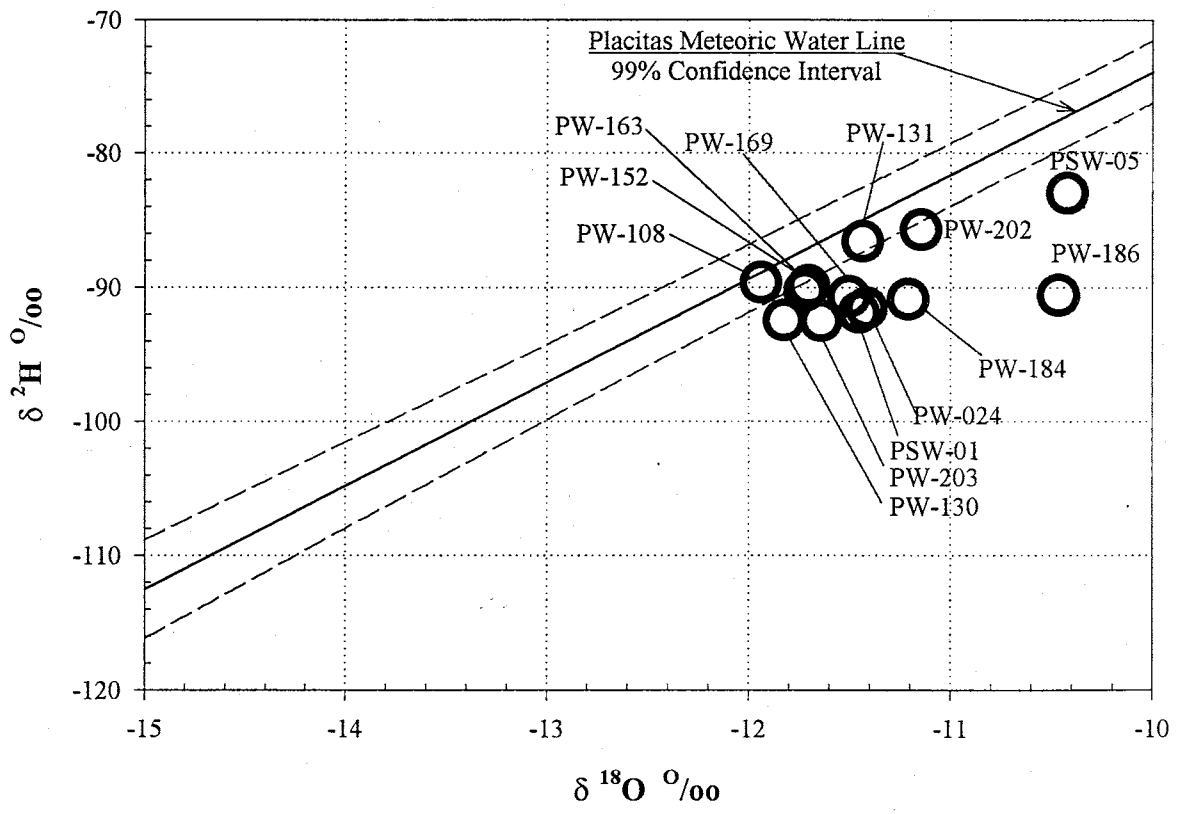

Figure 60. $\delta^{18}O$ and $\delta^{2}H$ composition of ground-water samples collected from the north-central part of the basin. Sample locations are shown in Figure 58. Symbol size is one standard deviation. Placitas meteoric water line shown for reference.

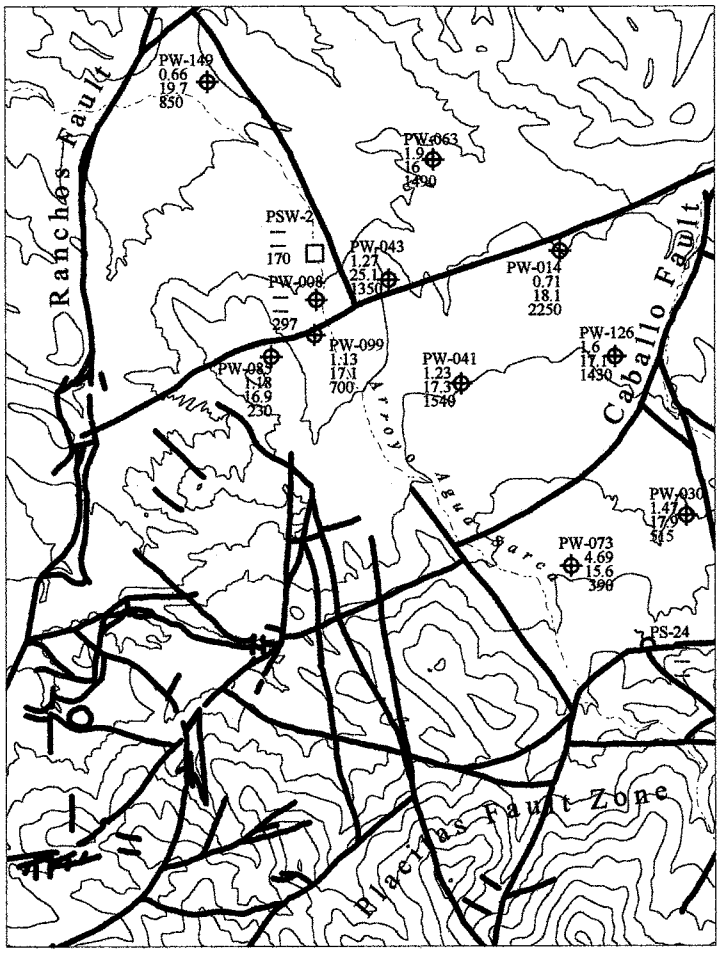

Figure 61. Location, temperature, dissolved oxygen concentration, and TDS concentration of ground-water samples collected from the western part of the Mesozoic ramp.

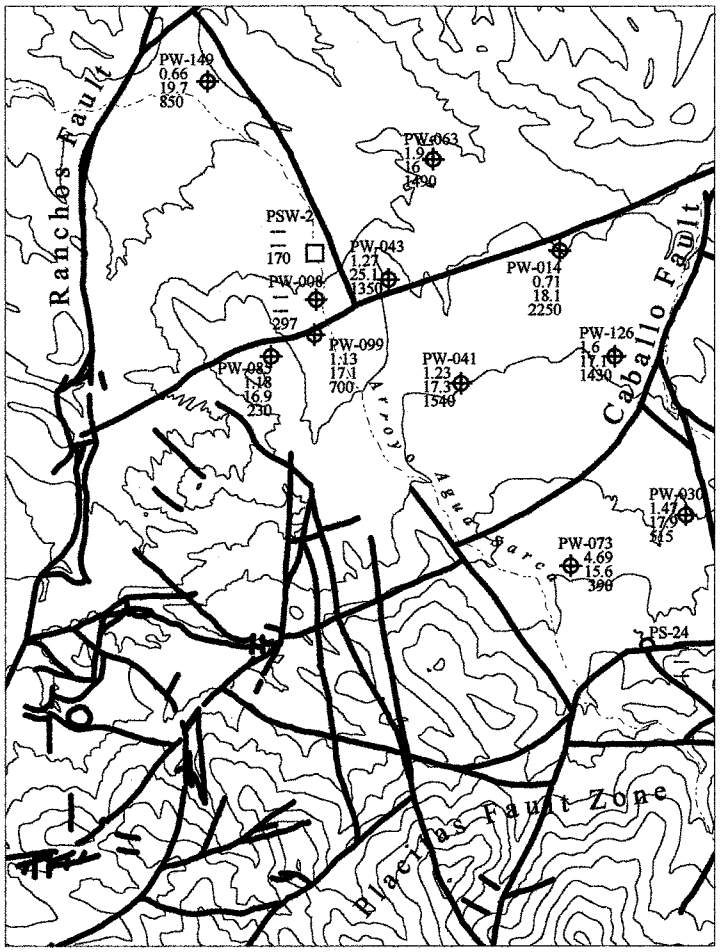

Figure 61. Location, temperature, dissolved oxygen concentration, and TDS concentration of ground-water samples collected from the western part of the Mesozoic ramp.

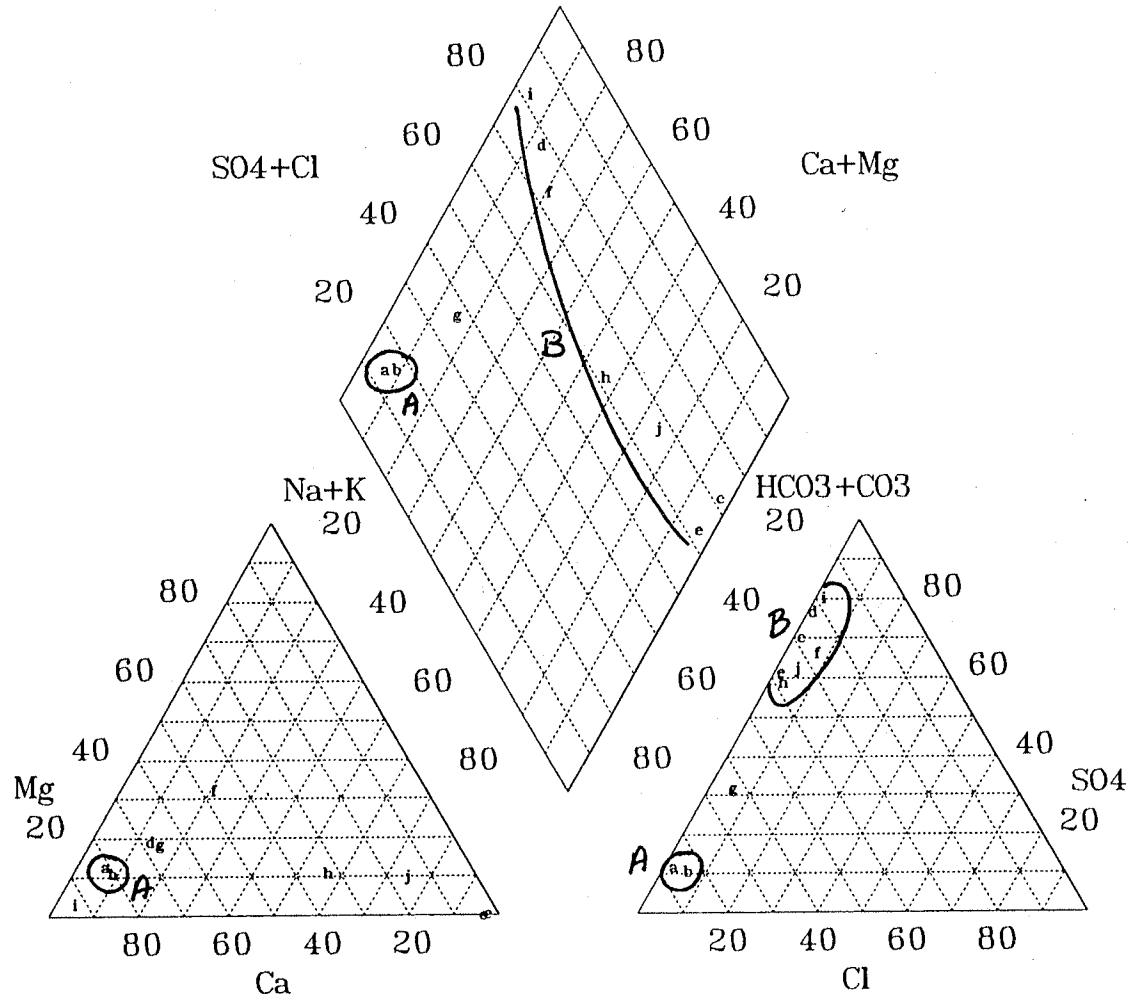

Figure 62. Major ion geochemistry of samples from the western part of the Mesozoic ramp. Sample locations are (a) PSW-02, (b) PW-008, (c) PW-014, (d) PW-041, (e) PW-043, (f) PW-063, (g) PW-085, (h) PW-099, (i) PW-126, and (j) PW-149. Labeled groups are (A) Madera type water from along Arroyo Agua Sarca, (B) high sulfate ground water. Sample locations are shown in Figure 61.

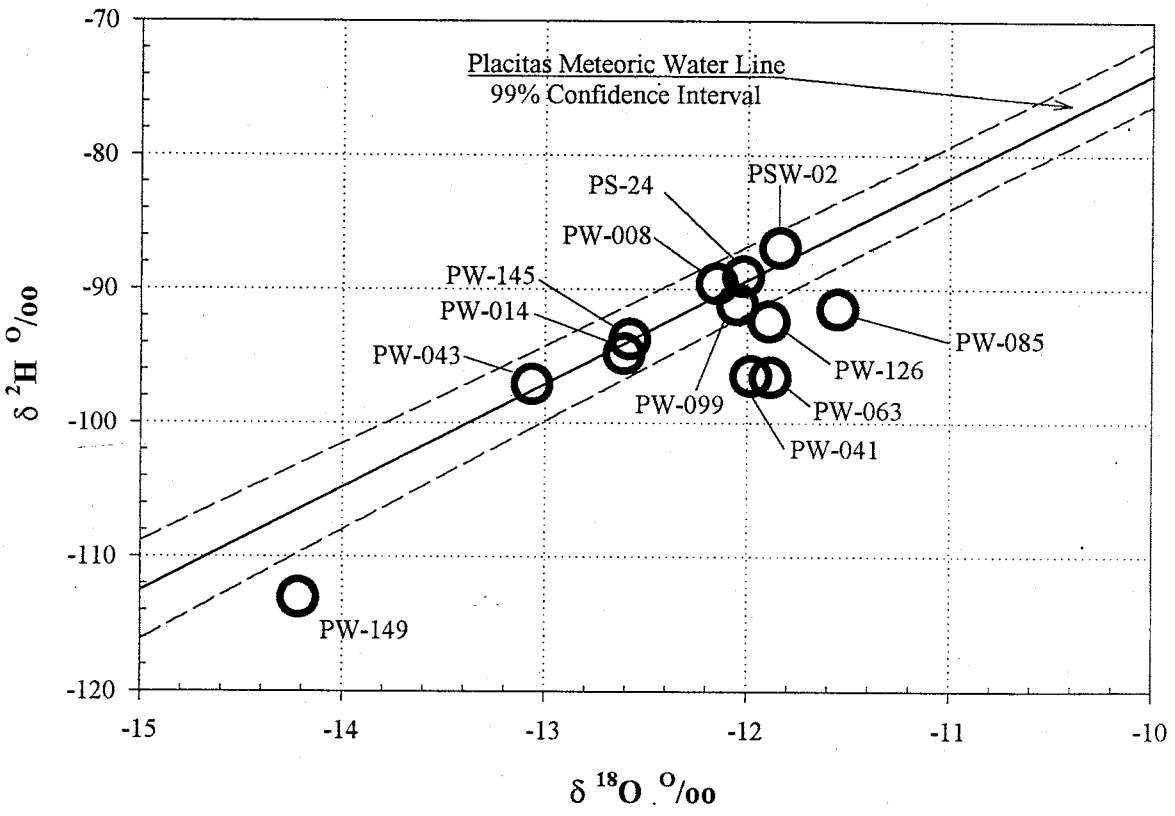

Figure 63. $\delta^{18}O$ and $\delta^{2}H$ composition of ground-water samples collected from the western part of the Mesozoic ramp. Sample locations are shown in Figure 61. Symbol size is one standard deviation. Placitas meteoric water line shown for reference.

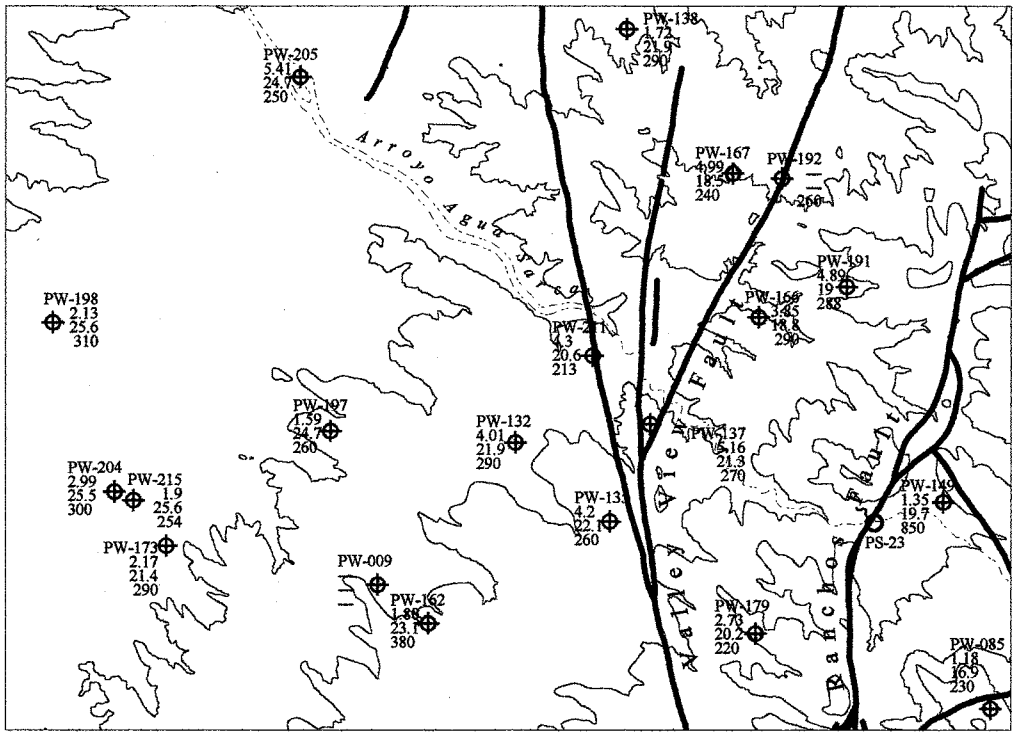

Arroyos

Sample locations

- Spring
- Stream
- Well

PW-385 5.6 17.6 1124

- Site ID
- Dissolved Oxygen, ppm
- Temperature, C
- TDS, ppm

2000 0 2000 4000 6000 8000 Feet

1000 0 1000 2000 Meters

N

1:40000

Contour interval 100 feet

Figure 64. Location, temperature, dissolved oxygen concentration, and TDS concentration of ground-water samples collected from the western part of the basin.

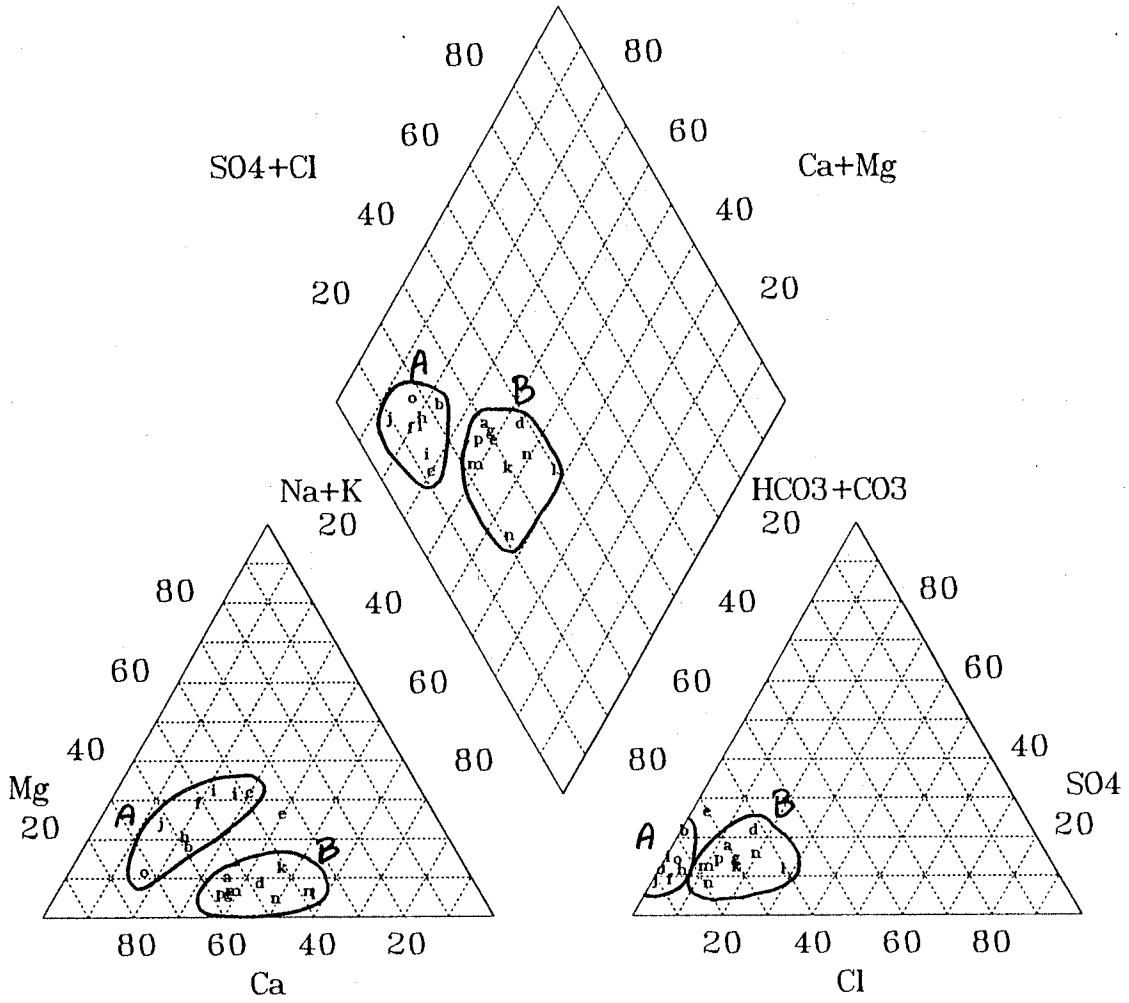

Figure 65. Major ion geochemistry of samples from the western part of the basin. Sample locations are (a) PW-132, (b) PW-135, (c) PW-137, (d) PW-162, (e) PW-166, (f) PW-167, (g) PW-173, (h) PW-179, (i) PW-191, (j) PW-192, (k) PW-197, (l) PW-198, (m) PW-204, (n) PW-205, (o) PW-211, and (p) PW-215. Labeled groups are from (A) along or east of the Valley View fault and (B) west of the Valley View fault. Sample locations are shown in Figure 64.

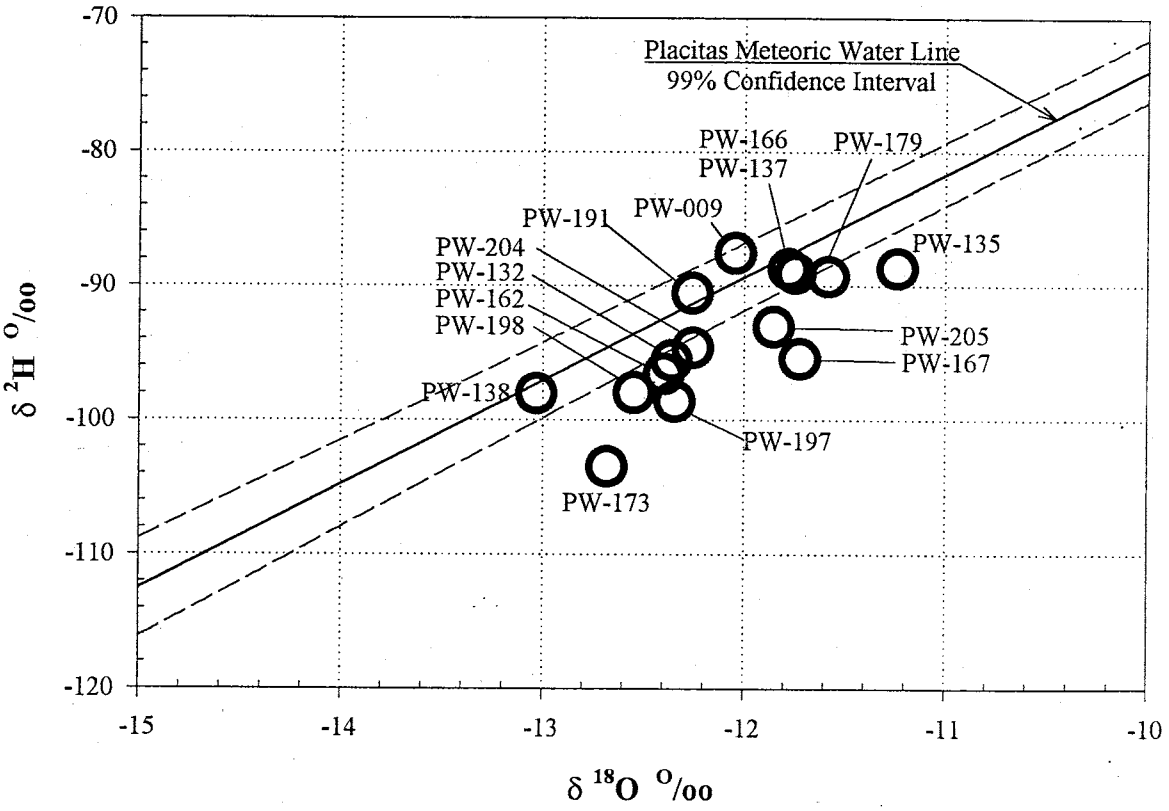

Figure 66. $\delta^{18}O$ and $\delta^{2}H$ composition of ground-water samples collected from the western part of the basin. Sample locations are shown in Figure 64. Symbol size is one standard deviation. Placitas meteoric water line shown for reference.

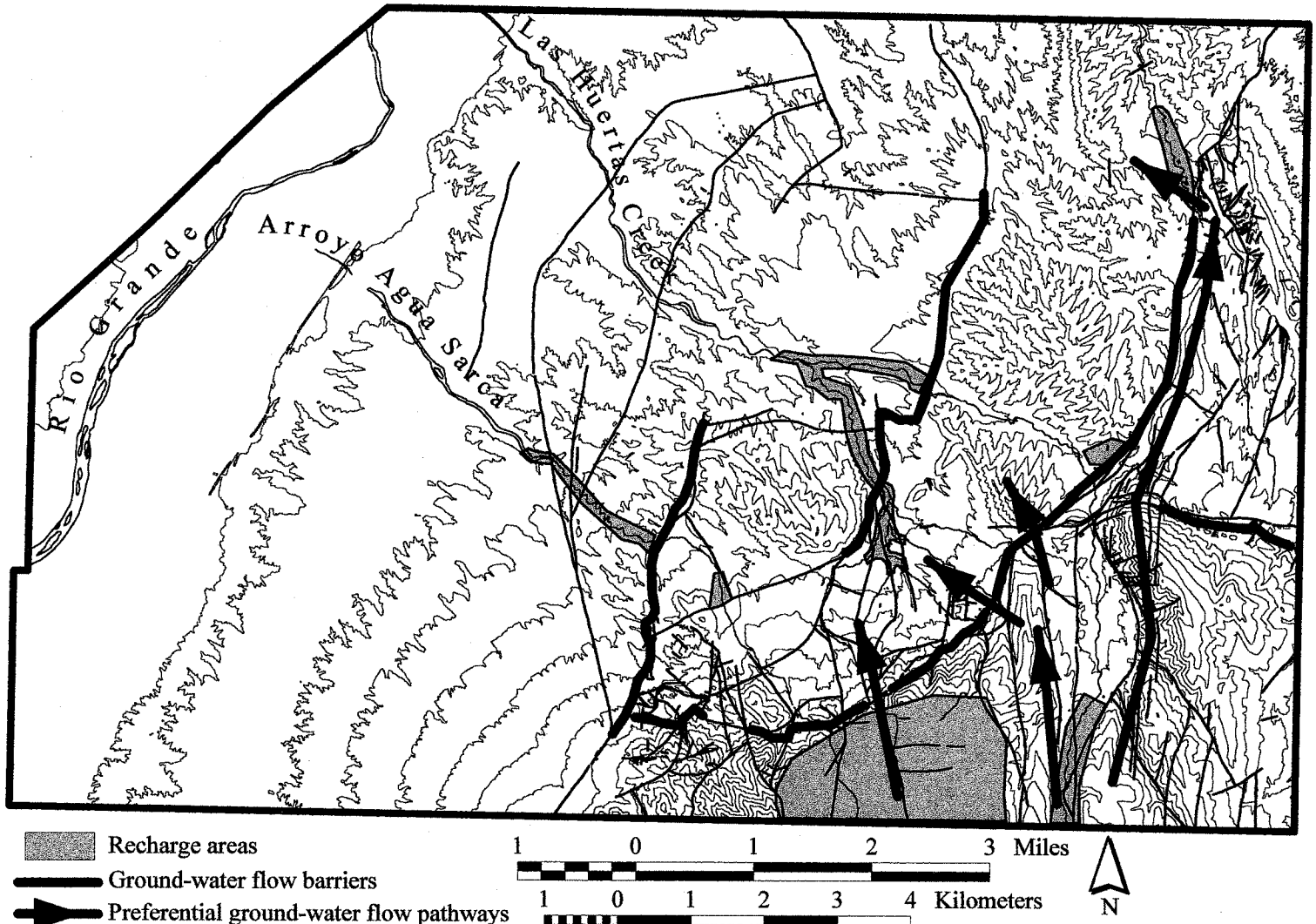

Figure 67. Regional hydrogeology of the Placitas study area.

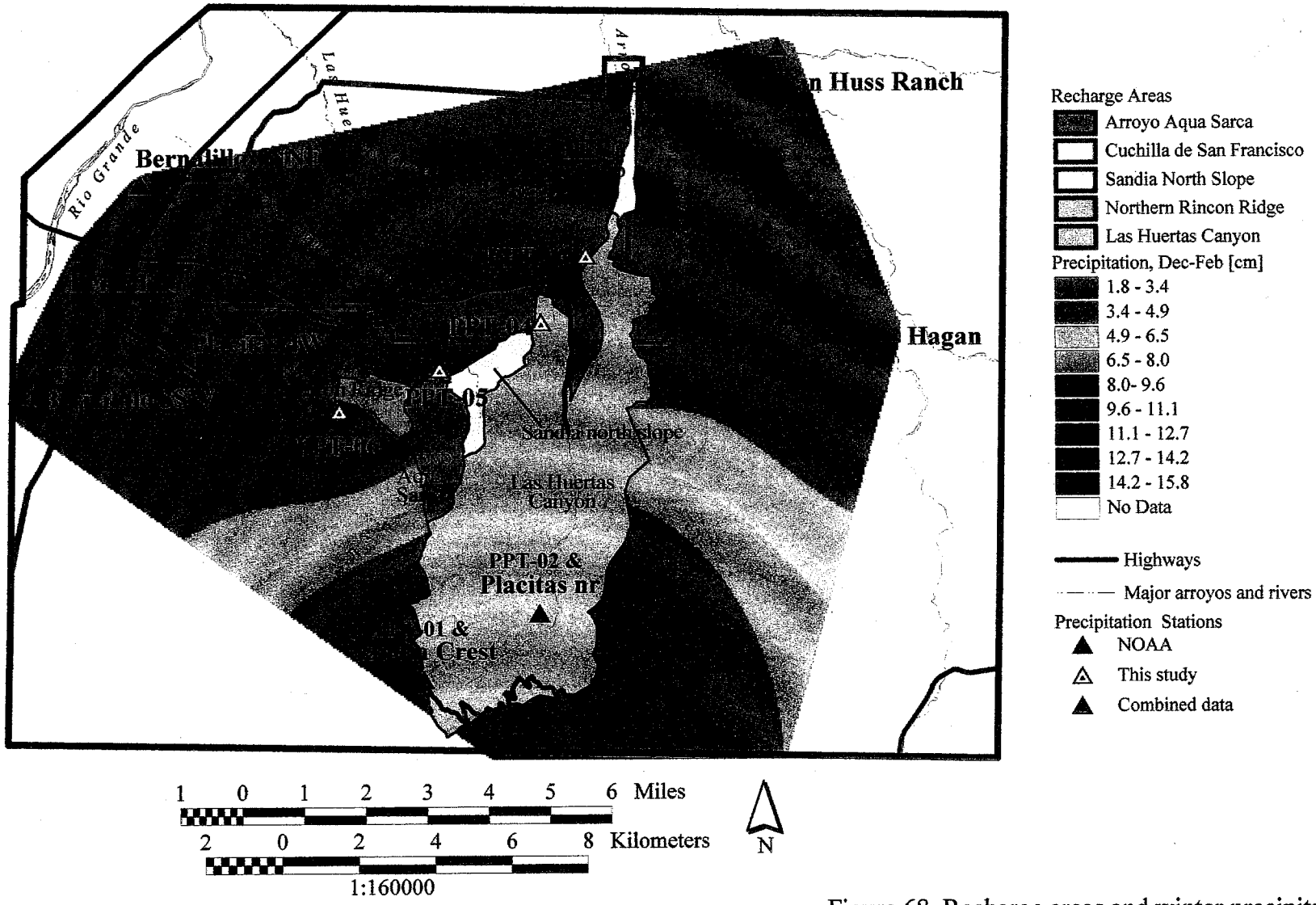

Figure 68. Recharge areas and winter precipitation.

TABLES

Table 1. Stratigraphy of the Placitas study area (Connell et al., 1995).

Erathem	System/Series	Stratigraphic Unit	Thickness	Lithology
Cenozoic	Quaternary	Valley-fill and piedmont alluvium	<20m	Unconsolidated to moderately consolidated, sandy clay loam to poorly stratified sand, gravel and conglomerate.
	Tertiary	Upper Santa Fe Gr.	0-300m	Piedmont deposits of clast supported conglomerate and pebbly sandstone. Axial river deposits of coarse-grained channel sands, rare silt.
		Lower Santa Fe Gr.	0-210m	Well-cemented, clast supported conglomerate.
Mesozoic	Cretaceous	Menefee Fm.	250-560m	Sandstone, siltstone, shale and lignitic coal and ironstone lenses.
		Point Lookout Ss.	75m	Sandstone with limonitic sandstone lenses.
		Mancos Shale	440-490m	Shale with thick weakly cemented sandstone mid-section.
		Dakota Sandstone	22m	Massively bedded, well-cemented sandstone, thin black shale near top.
	Jurassic	Morrison Fm.	260m	Well-cemented friable sandstone, minor mudstone and siltstone.
		Todilto Fm.		Thinly laminated fetid limestone, upper unit of gypsum.
		Entrada Fm.	35m	Massively bedded, well-sorted, fine to medium grained eolian sandstone.
	Triassic	Petrified Forest Fm.	400-500m	Mudstone and very minor sandstone, Sandstone unit near top.
		Agua Zarca Fm.	25-130m	Conglomeratic sandstone, increasing mudstone near top.
		Moenkopi Fm.	20-25m	Micaceous sandstone
Paleozoic	Permian	San Andres Fm.	20-25m	Fine grained limestone.
		Glorieta Fm.	10m	Massively bedded sandstone.
		Yeso Fm.	165-210m	Thick-bedded friable sandstone, minor limestone, siltstone and gypsum near top of formation.
		Abo Fm.	230-330m	Thick red sandstone and mudstone sequences with minor limestone.
	Pennsylvanian	Madera Fm.	380-470m	Thickly bedded limestone with thin black shale. Upper member of limestone, sandstone, thick shale units.
		Sandia Fm.	59m	Thickly bedded, well cemented sandstone and limestone.
	Mississippian	Arroyo Peñasco Fm.	0-23m	Basal sandstone, conglomerate, mudstone, siltstone, and upper quartzite member.
Precambrian		Sandia Granite and Metamorphic rocks	Basement	Crystalline with weathered zone at top and along fractures and faults.

Table 2. Site information about precipitation collectors and surface water samples.

Site ID	Local Identifier	Latitude NAD83	Longitude NAD83	M.P Elev NAVD 88	PPT Collector	Stream Type
PPT-001	11N.5E.6.2113	35.216229	-106.450973	10504	S, R	
PPT-002	12N.5E.33.2313	35.227264	-106.416866	8030	S, R	
PPT-003	13N.5E.34.1124	35.317437	-106.404668	5968	R	
PPT-004	12N.5E.04.2133	35.301535	-106.417426	6327	R	
PPT-005	12N.5E.06.4434	35.290163	-106.446580	6364	R	
PPT-006	12N.4E.12.3233	35.280095	-106.475229	6129	R	
PPT-007	12N.3E.6.4322	35.293368	-106.556398	5040	R	
PSW-01	13N.5E.32.1121	35.318539	-106.440524	5660		E
PSW-02	13N.5E.36.4443	35.304695	-106.462436	5788		E
PSW-03	12N.5E.22.3113	35.249151	-106.411652	7031		P
PSW-04	13N.5E.27.4444	35.319978	-106.408233	5828		E
PSW-05	13N.5E.30.1121	35.333297	-106.455192	5408		E
PSW-06	13N.5E.15.2141	35.362466	-106.396582	5654		P
PSW-07	13N.5E.28.4142	35.323788	-106.413562	5906		P

Local Identifier is Township.Range.Section.¼¼¼¼ sections. Latitude, and longitude in decimal degrees, elevation in feet. Precipitation collectors are (R) rain collecor and (S) snow collector. See text for description of collectors. Stream types are (P) perennial and (E) ephemeral.

Table 3. Precipitation amounts in cm.

Site ID	Installation	Precipitation Collection Date					
	Date	26-May-97	2-Sep-97	4-Dec-97	12-Feb-98	10-May-98	4-Aug-98
PPT-01	10-April-97	5.37	38.96	9.20	22.63*	21.22*	11.78
PPT-02	10-April-97	17.98	38.96	16.95	20.04*	23.31*	6.41
PPT-03	3-March-97	8.58	14.47	9.30	2.89	14.83	10.08
PPT-04	4-April-97	16.77	13.48	11.67	3.62	13.32	10.69
PPT-05	11-April-97	7.56	11.51	11.67	3.78	19.65	8.71
PPT-06	4-April-97	7.40	30.50	12.99	3.12	16.93	7.56
PPT-07	4-April-97	14.80	12.99	9.04	2.63	10.69	4.77

* indicates samples collected in PVC snow collectors.

Table 4. Stable isotope analysis of precipitation.

Site ID	May-97		Sep-97		Dec-97		Feb-98		May-98		Aug-98	
	$\delta^{18}O$	$\delta^{2}H$	$\delta^{18}O$	$\delta^{2}H$	$\delta^{18}O$	$\delta^{2}H$	$\delta^{18}O$	$\delta^{2}H$	$\delta^{18}O$	$\delta^{2}H$	$\delta^{18}O$	$\delta^{2}H$
PPT-01	-13.7	-102	-7.8	-54	-7.6	-49	-16.0*	-115*	-12.2	-82	-10.8	-77
PPT-02	-11.8	-88	-4.8	-34	-9.3	-61	-16.3*	-117*	-10.0	-82	-8.5	-64
PPT-03	-13.2	-99	-3.7	-27	-11.9	-91	-15.6	-110	-11.6	-88	-7.2	-51
PPT-04	-10.9	-96	-4.2	-31	-11.9	-89	-11.9	-81	-11.5	-77	-7.5	-47
PPT-05	-11.3	-90	-3.8	-26	---	---	-15.9	-120	-11.4	-79	-8.1	-58
PPT-06	-12.2	-89	-4.2	-25	-10.3	-77	-15.9	-122	-11.0	-82	-8.4	-66
PPT-07	-15.0	-123	-3.7	-28	-11.3	-83	-17.6	-139	-11.5	-92	-7.3	-61

* indicates samples collected in PVC snow collectors. --- indicates sample destroyed before analysis.

Table 5. Radioisotope and tritium analytical results and ground water residence time interpretations.

Site ID	Uncorrected ^{14}C activity [PMC ± 1σ]	$\delta^{13}C$ [per mil]	Corrected ^{14}C age [Years]	Tritium [TU]	Tritium Age [Years]	$\delta^{2}H$ ‰	Interpretation
PS-10	34.08 ± 0.87	-7.9	4340 ± 230	0 ± 3	>47 yr.	-90	Submodern
PW-005	57.36 ± 0.85	-10.2	2020 ± 130	2 ± 3	Submodern-Modern mix	-89	Submodern - Modern mix
PW-039	31.68 ± 0.93	-9.1	6300 ± 270	2 ± 2	Submodern-Modern mix	-100	Modern - Fossil mix
PW-041	5.05 ± 0.81	-7.7	23280 ± 1340	0 ± 2	>47 yr.	-96	Submodern - Fossil mix
PW-071	12.32 ± 0.68	-6.5	12500 ± 590	0 ± 2	>47 yr.	-97	Submodern - Fossil mix
PW-073	66.12 ± 1.08	-10	630 ± 140	6 ± 2	<5 to 10 yr.	-90	Modern
PW-089	21.34 ± 0.79	-7.8	8610 ± 300	1 ± 2	Submodern Modern mix	-91	Submodern - Modern mix
PW-103	4.60 ± 0.63	-11.3	27400 ± 1090	0 ± 2	>47 yr.	-104	Fossil
PW-109	71.26 ± 0.77	-10	-10 ± 90	1 ± 2	Submodern-Modern mix	-91	Submodern - Modern mix
PW-143	<0.8	-5.2	>35250	0 ± 3	>47 yr.	-117	Fossil
PW-149	2.68 ± 0.80	-11	31710 ± 2190	0 ± 2	>47 yr.	-113	Fossil
PW-163	75.60 ± 1.14	-7.7	-2710 ± 130	9 ± 3	<5 to 10 yr.	-90	Modern

Carbon-14 ages are corrected using a $\delta^{13}C$ mixing model. Qualitative tritium age evaluation based on criteria in Table 6.

Table 6. Qualitative ages based on tritium content (Clark and Fritz, 1997).

Tritium concentration [TU]	Qualitative age
< 0.8 *	Submodern - recharged prior to 1952 (>47 yr.)
0.8 to ~ 4 *	Mixture between submodern and modern recharge
5 to 15 *	Modern (<5 to 10 yr.)
15 to 30	Some "bomb" tritium present
>30	Considerable component of recharge from 1960's or 1970's
>50	Dominantly 1960's recharge (30 to 40 yr.)

* indicates concentration ranges measured in the Placitas study area.

Table 7. CFC dating results (Analyses by N. Plummer, unpubl, 1997).

Site ID	CFC11 [pg/kg]	CFC113 [pg/kg]	CFC12 [pg/kg]	CFC11 Age [Years]	CFC113 Age [Years]	CFC12 Age [Years]	Interpretation
PS005	458	55	227	14	10	14	Modern
PS005	453	61	223	14	10	14	Modern
PW077	5591.1*	29.8	551.1	*	16	3	Modern
PW211	0	0	0	>56	>30	>56	Submodern or Fossil
PW215	0	0	0	>56	>30	>56	Submodern or Fossil
PW216	2	2	10838*	44	>30	*	Submodern

CFC analyses are modeled on atmospheric concentration and water-solubility curves from Szabo et al (1996) and Ekwurzel et al. (1994), contaminated samples indicated by * were not evaluated.

Table 8. Hydrogeologic sub-zones of the Placitas study area.

Sub-zone	Aquifer quality	Recharge potential	Water quality
1. Upper Las Huertas Canyon and Cuchilla Lupe	*good* high permeability aquifer conduit faults	*very good* Las Huertas Creek and direct infiltration of precipitation	*excellent* TDS < 320 ppm Ca/HCO_3
2a. Cuchilla de San Francisco	*good* high permeability aquifer conduit faults	*good* interaquifer flow	*excellent* TDS < 488 ppm $CaNa/HCO_3$
2b. San Francisco basin	*good to poor* permeable sandstone aquifers and mudstone aquitards conduit and barrier faults	*poor* interaquifer flow	*good to fair* TDS < 1100 ppm $NaMgCa/HCO_3SO_4$
3. Northeast basin	*excellent* high permeability sand, gravel, and conglomerate	*fair* interaquifer flow, Las Huertas Creek	*excellent* TDS < 500 ppm Ca/HCO_3 to $NaCa/SO_4HCO_3$
4. Central Mesozoic ramp	*good to poor* discontinuous sandstone and limestone aquifers, aquitards conduit and barrier faults	*good* interaquifer flow	*excellent to fair* TDS < 810 ppm Ca/HCO_3 to $CaMg/SO_4HCO_3$ and Na/HCO_3SO_4
5. East and North Mesozoic ramp	*good to poor* sandstone aquifers and shale and evaporite aquitards barrier faults	*poor* limited interaquifer flow, spring overflow	*excellent to very poor* TDS < 7540 ppm Ca/HCO_3 to $CaNa/SO_4$ to Na/SO_4
6. Central basin	*excellent* high permeability sand, gravel, and conglomerate barrier fault	*good* Las Huertas Creek, interaquifer flow	*excellent* TDS < 530 ppm Ca/HCO_3 to $CaMg/SO_4HCO_3$
7. West Mesozoic ramp	*good to poor* sandstone aquifers and shale aquitards barrier and conduit faults	*poor to good* interaquifer flow	*excellent to poor* TDS < 2250 ppm Ca/HCO_3, Ca/SO_4, Na/SO_4 and Na/HCO_3
8. West basin	*excellent* high permeability sand, gravel, and conglomerate	*good* Arroyo Agua Sarca, Las Huertas Creek	*excellent* TDS < 380 ppm $CaMg/HCO_3$ to $CaNaMg/HCO_3$ and to $CaNa/HCO_3Cl$

Table 9. Aquifer quality in the Mesozoic ramp.

Aquifer	Supply	Quality		# of Wells
		TDS [ppm]	Major Ion	Identified / Tested
210CRCS	Poor - Good	NT		4 / 0
211MENFU	Poor	850	$CaNa\text{-}SO_4HCO_3$	9 / 1
211MENF	Poor - Good	1100 - 2800		7 / 4
		$CaMg\text{- \& }CaNa\text{-}SO_4HCO_3$		
211MENF/HARN	Good	2250 - 3820	$Na\text{-}SO_4HCO_3$	5 / 2
211MENFL	Poor - Good	3860 - 7540	$NaCa\text{-}SO_4HCO_3$	3 / 1
211PNLK	Good	1490 - 3140	$CaMgNa\text{-}SO_4HCO_3$	2 / 2
210MNCSU	Poor - Good	NT		3 / 0
210HOSTD	Good	NT		3 / 0
210MNCSL	Poor - Fair	360 -3010		18 / 6
		$Ca\text{-}HCO_3$ to $NaMgCa\text{- \& }Na\text{-}SO_4HCO_3$		
211DKOT	Poor - Fair	297 - 334	$Ca\text{-}HCO_3$	4 / 2
221MRSN	Poor - Good	350 - 700		6 / 2
		$CaMg\text{-}HCO_3$ & $NaCa\text{-}SO_4HCO_3$		
221MRSN/JCKP	Fair - Good	810 - 1540	$Ca\text{- \& }CaNa\text{-}SO_4HCO_3$	4 / 2
221MRSN/BBSN	Poor - Good	NT		1 / 0
221MRSN/WWCN	Good	NT		2 / 0
221MRSN/RCAP	Poor - Good	230	$Ca\text{-}HCO_3SO_4$	1 / 1
221TDLT	Fair	NT		2 / 0
220ENRD	Good	NT		4 / 0
231PFDFU	Fair - Good	560 - 5950		6 / 3
		$CaNa\text{-}HCO_3SO_4Cl$ to $Na\text{-}SO_4$		
231PFDF	Poor - Good	260 - 560		4 / 3
		$Ca\text{-}HCO_3$ & $NaHCO_3SO_4$		
231PFDFM	Good	390 - 3229		8 / 7
		$Na\text{-}HCO_3$ to $\text{-}SO_4$ & $Ca\text{-}HCO_3SO_4$		
231PFDFL	Poor	1740	$CaSO_4$	3 / 1
231AGZCU	Poor - Good	NT		1 / 0
231AGZC	Poor - Good	336 - 420		3 / 2
		$CaMg\text{-}HCO_3$ & $CaMgNa\text{-}HCO_3SO_4$		
310YESO	Fair - Good	NT		1 / 0

NT - not tested. See page 181 for aquifer codes.

Table 10. National Weather Service Cooperative Weather Stations.

Number	Location	Begin Record	End Record	Latitude	Longitude	Elevation
299342	Van Huss Ranch	1-Jul-47^{+}	30-Jun-51	35.367	-106.350	5404
298011	Sandia Crest	1-Nov-53	30-Apr-79	35.217	-106.450	10686
298015	Sandia Park	1-July-46	Present	35.166	-106.362	7019
296911	Placitas 4W	1-Dec-91	Present	35.300	-106.500	5515
---	Placitas nr	1-Oct-10	31-Mar-13	35.233	-106.417	8000
293781	Hagan	1-Apr-53	31-May-56	35.300	-106.317	5653
290903	Bernalillo*	1-Sep-1889^{+}	1-Jul-46	---	---	---
290903	Bernalillo 3SW	1-Jul-46	10-Nov-53	35.283	-106.567	5043
290903	Bernalillo 1NNE	10-Nov-53	13-Jul-65	35.333	-106.533	5062
290903	Bernalillo	13-Jul-65	31-Aug-82	35.317	-106.550	5052

Number is ID assigned by the NOAA/NCDC, latitude an longitude in decimal degrees (to the nearest minute), elevation in feet (NOAA/NCDC, 1998). The Placitas nr. site is very near (≈100 m) the PPT-02 location based on the elevation and possible locations in the area. Location for the Bernalillo site prior to July 1, 1946 was unavailable. $^{+}$ indicates intermittent record, see Appendix B.

Table 11. Median precipitation depth (December 1 to March 1) Calculated from data in Table 3 and Appendix B.

	Median winter precipitation depth [cm]
Van Huse Ranch	1.83
Sandia Crest	14.30
Sandia Park	9.69
Placitas nr.	15.75
Placitas 4W	3.38
Hagan	2.17
Bernalillo 3SW	2.67
Bernalillo 1NNE	3.20
Bernalillo	2.40
PPT-03	2.89
PPT-04	3.62
PPT-05	3.78
PPT-06	3.12

Depths measured by this study at PPT-01, PPT-02, and PPT-07, were combined with depths measured at Sandia Crest, Placitas nr., and Bernalillo 2SW respectively. Site locations in Table 10.

Table 12. Recharge amounts.

Recharge Area Name	Area [km^2]	Winter Precipitation						Total Recharge	
		Min [cm]	Max [cm]	Range [cm]	Mean [cm]	Stdev [cm]	Total [m^3/yr]	[m^3/yr]	[Acre-ft/yr.]
Northern Rincon Ridge	1.9	3.2	4.2	1.0	3.6	.40	$6.9x10^4$	$8.4x10^4$	68
Canyon Agua Sarca	4.1	3.8	7.9	4.1	4.9	.98	$2.0x10^5$	$2.4x10^5$	200
Cuchilla de San Francisco	1.1	3.2	3.4	0.2	3.3	0.05	$3.6x10^4$	$4.3x10^4$	35
Sandia north slope	2.7	3.6	5.6	2.0	4.1	0.40	$1.1x10^5$	$1.3x10^5$	110
Las Huertas Canyon	45.6	2.9	15.7	12.8	9.2	4.11	$4.2x10^6$	$5.1x10^6$	4100
Totals (rounded)	55.3						$4.6x10^6$	$5.6x10^6$	4500

APPENDIX A. WELL AND SPRING INVENTORY (JOHNSON, 1999)

Appendix A. Site information about springs and wells. Page 1 of 18.

Site ID	Local Identifier	Latitude NAD83	Longitude NAD83	M.P. Elev NAVD 88	Well Depth	Bottom Screen	Top Screen	Bottom Screen Elev	Top Screen Elev	Water Use	Aquifer Code	NMOSE Well File or Data Source
PS-01	12N.5E.4.1243	35.30133	-106.418983	6188						D	325MDER Suela Flt	NMBMMR
PS-02	12N.5E.4.1221	35.304431	-106.419429	6138						I	318ABO Suela Flt	NMBMMR
PS-03	13N.5E.33.3441	35.306419	-106.419767	6088						I	318ABO Suela Flt	NMBMMR
PS-04	13N.5E.33.4324	35.30645	-106.414314	6143						I	325MDER	NMBMMR
PS-05	12N.5E.5.3342	35.291129	-106.439886	6376						I,D,R	325MDER Pomecerro Flt	NMBMMR
PS-06	12N.5E.4.1323	35.299876	-106.424174	6113						U	231PFDF	NMBMMR
PS-07	13N.5E.27.4331	35.320182	-106.398761	6028						I	318ABO Tecolote Flt	NMBMMR
PS-08	13N.5E.28.3211	35.325733	-106.421061	5781						I,D	122SNTFP Las Huertas	NMBMMR
PS-09	12N.5E.5.3323	35.29218	-106.440568	6313						I,R	231PFDF Pomecerro Flt	NMBMMR

Springs have Site ID's beginning with PS- and wells have Site ID's beginning with PW-. Local Identifier is Township.Range.Section.¼¼¼¼ sections. Latitude, and Longitude are in decimal degrees. Elevation, well depth, screen depths, and screen elevations are in feet. Water usage is (D) domestic, (U) undeveloped, (I) irregation, (S) suplimentary, (N) industrial, (P) community production, (A) abandoned. Data sources are (NMBMMR) New Mexico Bureau of Mines for this study, (RG-#####) New Mexico Office of the State Engineer well records, (Owner) testimony of the curent site owner. See page 181 for aquifer codes. Aquifers indicated are the best estimate at time of publication but may change with with additional geologic investigation.

Site ID	Local Identifier	Latitude NAD83	Longitude NAD83	M.P. Elev NAVD 88	Well Depth	Bottom Screen	Top Screen	Bottom Screen Elev	Top Screen Elev	Water Use	Aquifer Code	NMOSE Well File or Data Source
PS-11	13N.5E.15.2424	35.357673	-106.391506	5823						D,I	122SNTFP	NMBMMR
PS-12	13N.5E.15.2431	35.357377	-106.394156	5746						I,S	122SNTFP	NMBMMR
PS-13	13N.5E.15.2430	35.357127	-106.394046	5733						R	122SNTFP	NMBMMR
PS-14	13N.5E.15.2442	35.35689	-106.391424	5800						R	122SNTFP	NMBMMR
PS-15	13N.5E.15.2440	35.356404	-106.3913	5800						R	122SNTFP	NMBMMR
PS-16	13N.5E.14.3131	35.353364	-106.390467	5812						R,C	325MDER SanF Flt	NMBMMR
PS-17	13N.5E.22.4212	35.340378	-106.39314	6027						R	325MDER SanF Flt	NMBMMR
PS-18	13N.5E.14.3313	35.350515	-106.390078	5808						R	325MDER SanF Flt	NMBMMR
PS-19	13N.5E.32.1231	35.316853	-106.439171	5707						R	211MENF Caballo Flt	NMBMMR
PS-20	13N.5E.33.3423	35.30678	-106.419158	6120						I	318ABO Suela	NMBMMR
PS-21	13N.5E.22.2244	35.34477	-106.391158	5948						I,C,R	325MDER SanF Flt	NMBMMR
PS-22	13N.5E.22.2223	35.347048	-106.39241	5878						R	122SNTFP SanF Flt	NMBMMR
PS-23	13N.4E.36.3232	35.309674	-106.472513	5623						U	122SNTFP Ranchos Flt	NMBMMR
PS-24	12N.5E.6.4344	35.289975	-106.448287	6240						I	310YESO	NMBMMR

Site ID	Local Identifier	Latitude NAD83	Longitude NAD83	M.P. Elev NAVD 88	Well Depth	Bottom Screen	Top Screen	Bottom Screen Elev	Top Screen Elev	Water Use	Aquifer Code	NMOSE Well File or Data Source
PW-001	13N.5E.32.3220	35.310792	-106.435524	5774	125	125	103	5649	5671	D,I	210MNCSL	RG-51025
PW-002	13N.5E.33.3344	35.304636	-106.422538	6028	125	125	105	5903	5923	D	211DKOT	Owner
PW-003	12N.5E.3.1114	35.302821	-106.407262	6161	100	90	80	6071	6081	D	318ABO	RG37179
						30	20	6131	6141			
PW-004	12N.5E.4.1221	35.30407	-106.419653	6142	65	65	55	6077	6087	D	318ABO	Owner
PW-005	12N.5E.5.1433	35.297145	-106.439016	5985	322	317	302	5668	5683	D	231AGZC	RG23679X3
PW-006	12N.5E.5.1424	35.2991	-106.435177	5998	162	162	157	5836	5841	I,S	231PFDFL	RG23679X2
PW-007	12N.5E.5.2311	35.300559	-106.434337	5817	115	115	95	5702	5722	A	231PFDFM	RG23679X
PW-008	12N.4E.1.2223	35.303033	-106.46236	5695	92	92	69	5603	5626	D	211DKOT	RG9375
PW-009	13N.4E.34.4324	35.306425	-106.500202	5492	594	591	571	4901	4921	P	112SNTFP	RG11802S
						551	521	4941	4971			
PW-010	12N.5E.6.2431	35.298238	-106.446427	6008.3	475	475	425	5533	5583	D	231PFDFU	RG44507
PW-011	12N.5E.6.2431	35.298651	-106.447055	6023	165	165	145	5858	5878	D	231PFDFU	RG49454
PW-012	13N.5E.33.3142	35.309647	-106.422468	5941.7	60	60	50	5882	5892	D	210MNCSL	RG63893
PW-013	13N.5E.32.2114	35.3178	-106.433321	5755.5	200	200	160	5556	5596	D	210MNCSU	RG55395X
PW-014	13N.5E.31.3444	35.304904	-106.451773	5915	425	425	385	5490	5530	I,S	211PNLK	RG26878
PW-015	13N.5E.31.4333	35.304941	-106.451003	5919	220	220	200	5699	5719	Y,A	211MENFL	RG26878
PW-016	13N.5E.33.1433	35.311752	-106.421714	5971	360	360	320	5611	5651	D	210MNCSL	RG67118

Site ID	Local Identifier	Latitude NAD83	Longitude NAD83	M.P. Elev NAVD 88	Well Depth	Bottom Screen	Top Screen	Bottom Screen Elev	Top Screen Elev	Water Use	Aquifer Code	NMOSE Well File or Data Source
PW-017	13N.5E.32.3411	35.307511	-106.439279	5824.4	90	90	80	5734	5744	U	220ENRD	Owner
PW-018	13N.5E.32.3414	35.306371	-106.437817	5834.3	90	90	80	5744	5754	U	220ENRD	Owner
PW-019	13N.5E.31.3441	35.306295	-106.45293	5889	205	205	195	5684	5694	Y	211MENFL	RG25304
PW-020	13N.5E.31.3440	35.305714	-106.452672	5904	460	460	360	5444	5544	Y,A	211PNLK	Driller
PW-021	13N.5E.31.3442	35.306049	-106.452208	5867.6	190	190	160	5678	5708	D	211MENFL	RG25304
PW-022	13N.5E.29.1134	35.330244	-106.441929	5640	430	430	410	5210	5230	A	112SNTFP	Driller
						230	220	5410	5420			
PW-023	13N.5E.29.1434	35.326598	-106.43825	5645.3	525	525	505	5120	5140	D	211MENFU Lomos Flt	RG43080
PW-024	13N.5E.29.1243	35.329954	-106.436253	5702.3	295	295	275	5407	5427	D	112SNTFP	RG49263
PW-025	13N.5E.32.1221	35.318543	-106.436771	5741.5	430	412	397	5329	5344	D	210HOSTD	RG64481
PW-026	13N.5E.32.1221	35.318797	-106.436389	5735.1	140	140	130	5595	5605	D	210MNCSU	Driller
PW-027	13N.5E.32.2113	35.317693	-106.43415	5745.5	420	420	400	5326	5346	D	210HOSTD	RG62652
PW-028	13N.5E.32.3341	35.305491	-106.441325	5859.2	100	100	80	5759	5779	D	231PFFDFU	Owner
PW-029	13N.5E.29.1434	35.32797	-106.43896	5667.3	345	345	300	5322	5367	D	112SNTFP Caballo Flt	RG38654
PW-030	12N.5E.6.4213	35.295537	-106.446102	6098.5	390	390	370	5709	5729	D	231PFDFM	RG59293

Site ID	Local Identifier	Latitude NAD83	Longitude NAD83	M.P. Elev NAVD 88	Well Depth	Bottom Screen	Top Screen	Bottom Screen Elev	Top Screen Elev	Water Use	Aquifer Code	NMOSE Well File or Data Source
PW-031	12N.5E.6.1234	35.301624	-106.453967	5966.4	315	305	295	5661	5671	D	210MNCSL	RG43244
PW-032	13N.5E.29.4132	35.324125	-106.433338	5719	400	400	360	5319	5359	D	211MENFU	RG41477
PW-033	13N.5E.29.4112	35.325954	-106.43379	5711.2	580	560	545	5151	5166	U	211MENFU Lomos Flt	RG56368
PW-034	13N.5E.29.4114	35.325317	-106.433523	5732	320	320	300	5412	5432	D	211MENFU Lomos Flt	Driller
PW-035	13N.5E.33.4114	35.310077	-106.415587	6064	170	170	160	5894	5904	U	318ABO	Owner
PW-036	13N.5E.33.4114	35.310419	-106.415643	6047	320	320	310	5727	5737	D	318ABO	RG65069X
PW-037	12N.5E.4.2211	35.304177	-106.412057	6188.2	100	100	90	6088	6098	U	325MDER Flt	Owner
PW-038	13N.5E.33.3410	35.30704	-106.420832	6034	420	420	380	5614	5654	I	211DKOT	RG64598
PW-039	13N.5E.33.3430	35.305263	-106.420803	6068	490	490	450	5578	5618	D	318ABOL / 325MDER Suela Flt	RG65764
PW-040	12N.5E.5.1123	35.302962	-106.440406	5915.9	220	220	200	5696	5716	U	231PFDFU	RG65805
PW-041	12N.5E.6.1141	35.30012	-106.455988	5988	330	320	300	5668	5688	D	221MRSN / JCKP	RG55409
PW-042	12N.5E.6.1321	35.300194	-106.458032	5993	420	420	360	5573	5633	D	221MRSN / WWCN	RG64614
PW-043	12N.5E.6.1112	35.30378	-106.459204	5911	535	535	515	5376	5396	D	210MNCSL	RG52896
PW-044	12N.5E.5.1123	35.303182	-106.441103	5915.3	120	120	100	5795	5815	D	231PFDFU	Driller
PW-045	12N.5E.5.1141	35.302576	-106.441059	5950	350	349	342	5601	5608	D	231PFDFM	RG30634

Site ID	Local Identifier	Latitude NAD83	Longitude NAD83	M.P. Elev NAVD 88	Well Depth	Bottom Screen	Top Screen	Bottom Screen Elev	Top Screen Elev	Water Use	Aquifer Code	NMOSE Well File or Data Source
PW-046	12N.5E.5.1121	35.304165	-106.44107	5904	90	90	70	5814	5834	D	231PFDFU	RG64527
PW-046	12N.5E.5.1121	35.304165	-106.44107	5904	90	90	70	5814	5834	D	231PFDFU	RG64527
PW-047	13N.5E.33.3233	35.308262	-106.421581	5982	165	165	155	5817	5827	I	210MNCSL	RG58960
PW-048	13N.5E.33.3233	35.30835	-106.421532	5982	185	180	40	5802	5942	I	210MNCSL	RG58960
PW-049	12N.5E.3.1112	35.303923	-106.407486	6157	100	100	80	6057	6077	D	318ABO	RG36163
PW-050	12N.5E.3.1213	35.303147	-106.403893	6120.7	200	200	180	5921	5941	U	318ABO	RG36218
PW-051	12N.5E.3.3133	35.294189	-106.407989	6260	95	95	85	6165	6175	D	318ABO	Owner
PW-052	12N.5E.3.3122	35.296547	-106.404843	6192	140	140	120	6052	6072	D	318ABO	RG43979
PW-053	12N.4E.1.2424	35.299513	-106.461275	5889	100	100	80	5789	5809	D	221MRSN / RCAP	RG1916
PW-054	12N.4E.1.2423	35.299933	-106.462036	5866						U	221MRSN	
PW-055	12N.4E.1.2244	35.301657	-106.460877	5845.7	95	95	85	5751	5761	U	221MRSN	Owner
PW-056	13N.4E.36.4434	35.304611	-106.462589	5776.2	70	70	58	5706	5718	D	210MNCSL	RG19481X
PW-057	12N.5E.6.1232	35.302334	-106.454148	5958	300	300	280	5658	5678	Y,A	210MNCSL	RG60175
PW-058	12N.5E.6.1232	35.302292	-106.454168	5968	410	410	370	5558	5598	D	210MNCSL	RG60175
PW-059	13N.5E.29.1444	35.326615	-106.435761	5725	505	505	480	5220	5245	D	211MENFU	RG41562
						260	240	5465	5485			
PW-060	13N.5E.32.3413	35.306885	-106.439193	5829	80	80	70	5749	5759	D	220ENRD	Owner
PW-061	12N.5E.4.1212	35.303779	-106.419797	6130	95	95	55	6035	6075	D	318ABO	RG65295

Site ID	Local Identifier	Latitude NAD83	Longitude NAD83	M.P. Elev NAVD 88	Well Depth	Bottom Screen	Top Screen	Bottom Screen Elev	Top Screen Elev	Water Use	Aquifer Code	NMOSE Well File or Data Source
PW-062	13N.5E.34.3114	35.310777	-106.407094	6032	31	31	-	6001	6001	U	318ABO	NMBMMR
PW-063	13N.5E.31.3321	35.3081	-106.457331	5833	220	220	200	5613	5633	D	211PNLK	RG55346
PW-064	12N.5E.3.3323	35.292078	-106.406685	6262	140	140	80	6122	6182	D	318ABO	RG41013
PW-065	13N.5E.22.3420	35.336273	-106.400723	6029	285	285	275	5744	5754	D	122SNTFP	RG57957
PW-066	12N.5E.4.2322	35.300111	-106.413579	6281.6	230	222	202	6060	6080	D	325MDERL	RG51716
PW-067	13N.5E.33.4433	35.305051	-106.412774	6198	85	85	75	6113	6123	D	318ABO Flt	RG61239X
PW-068	12N.5E.9.2241	35.28806	-106.410878	6378	340	340	330	6038	6048	D	325MDER	RG51620
PW-069	12N.5E.9.2442	35.284216	-106.409376	6365	320	280	240	6085	6125	D	325MDER	RG65441
PW-070	12N.5E.9.2442	35.284236	-106.409455	6348.3	300	300	280	6048	6068	U	325MDER	Owner
PW-071	13N.5E.23.1314	35.343024	-106.389747	5974.9	240	240	220	5735	5755	D	325MDERU	RG64808
PW-072	13N.5E.29.1441	35.328051	-106.436409	5685	375	365	355	5320	5330	D	112SNTFP	RG44418
PW-073	12N.5E.6.4133	35.293659	-106.451089	6212	295	295	275	5917	5937	P	231PFDFM	RG18058
PW-074	12N.5E.6.2321	35.300344	-106.448945	6017	176	174	154	5843	5863	P	210MNCSL	RG18058S
PW-075	12N.5E.6.2144	35.300948	-106.448112	5968.6	165	165	155	5804	5814	U	210MNCSL	RG28291
PW-076	13N.5E.34.1210	35.318407	-106.403316	5995.7	105	105	95	5891	5901	D	210CRCS SanF Flt	RG50261
PW-077	13N.5E.15.2231	35.360496	-106.394346	5742	100	100	80	5642	5662	D	122SNTFP	Owner
PW-078	13N.5E.29.4114	35.325123	-106.432765	5727	320	320	300	5407	5427	D	211MENF	Owner

Site ID	Local Identifier	Latitude NAD83	Longitude NAD83	M.P. Elev NAVD 88	Well Depth	Bottom Screen	Top Screen	Bottom Screen Elev	Top Screen Elev	Water Use	Aquifer Code	NMOSE Well File or Data Source
PW-079	12N.5E.6.1132	35.302285	-106.458833	5945	600	580	560	5365	5385	D	221MRSN / JCKP	RG33613
PW-080	13N.5E.29.4114	35.325122	-106.432953	5705.3	300	300	280	5405	5425	U	211MENF	Owner
PW-081	13N.5E.22.3423	35.335682	-106.401868	6115	272	272	250	5843	5865	D	122SNTFP	RG19358
PW-082	13N.5E.22.2414	35.343266	-106.393606	5937	125	125	85	5812	5852	D	122SNTFP SanF Flt	RG35856
PW-083	12N.5E.9.2214	35.288681	-106.411347	6401.6	420	420	330	5982	6072	D	325MDERL	RG52874
PW-084	13N.5E.27.1212	35.333196	-106.402838	6163	440	440	400	5723	5763	D	122SNTFP	RG39416
PW-085	12N.4E.1.2233	35.300983	-106.464299	5983.3	320	320	280	5663	5703	U	221MRSN / RCAP	RG60465
PW-086	12N.4E.1.2243	35.301301	-106.46232	5839.2	100	88	76	5751	5763	U	221MRSN / BBSN	RG24443
PW-087	13N.5E.22.2222	35.347627	-106.391036	5875	365	361	325	5514	5550	D	325MDERU SanF Flt	RG24059
PW-088	13N.5E.27.3331	35.320123	-106.408168	5901.1	100	100	40	5801	5861	U	210CRCS SanF Flt	RG56378X
PW-089	13N.5E.22.4413	35.336181	-106.394902	6023.7	200	200	180	5824	5844	D	325MDERU SanF Flt	RG64529
PW-090	13N.5E.22.2313	35.34289	-106.398542	6027	300	300	280	5727	5747	D	122SNTFP	RG66261
PW-091	13N.5E.14.3311	35.351223	-106.39	5845.6	106	105	95	5741	5751	U	325MDERU	Owner

Site ID	Local Identifier	Latitude NAD83	Longitude NAD83	M.P. Elev NAVD 88	Well Depth	Bottom Screen	Top Screen	Bottom Screen Elev	Top Screen Elev	Water Use	Aquifer Code	NMOSE Well File or Data Source
PW-092	13N.5E.27.3334	35.319225	-106.407204	5915.5	120	120	100	5795	5815	D	210CRCS SanF Flt	RG63974
PW-093	13N.5E.34.1323	35.314435	-106.406012	5971.7	210	210	190	5762	5782	U	230TRSC	Owner
PW-094	13N.5E.34.1323	35.314392	-106.405998	5991	220	220	200	5771	5791	D	230TRSC	Owner
PW-095	13N.5E.23.1124	35.347296	-106.386768	5849.6	114	110	55	5740	5795	U	318ABO	RG60484
PW-096	13N.5E.23.3342	35.335338	-106.387205	5993.8	380	380	320	5614	5674	U	318ABOL / 325MDERU	RG60484
PW-097	13N.5E.28.3211	35.322925	-106.411004	5881	120	112	105	5769	5776	D	122SNTFP	RG56378
PW-098	13N.5E.23.1333	35.341084	-106.389962	6041	300	300	280	5741	5761	D	325MDERU	RG67542
PW-099	12N.4E.1.2240	35.301775	-106.462414	5840	250					D	221MRSN	Owner
PW-100	12N.5E.9.2440	35.283646	-106.409784	6353	100					U	325MDER	Owner
PW-101	12N.5E.9.2443	35.283522	-106.410061	6374	200	190	170	6184	6204	D	325MDER	RG61116
PW-102	13N.5E.23.1131	35.346074	-106.390073	5910	150	150	120	5760	5790	D	325MDERU	RG60857
PW-103	13N.5E.29.4324	35.320968	-106.431665	5744	380	380	340	5364	5404	D	211MENFU	RG59143
PW-104	13N.5E.30.2421	35.329379	-106.444521	5633	360	360	320	5273	5313	D	112SNTFP	RG62363
PW-105	13N.5E.29.3211	35.325892	-106.439184	5639	390	390	360	5249	5279	A	112SNTFP Caballo Flt	Driller
PW-106	13N.5E.29.3211	35.325618	-106.439344	5584	365	365	335	5219	5249	D	112SNTFP Caballo Flt	RG63161
PW-107	12N.5E.5.1112	35.304045	-106.442084	5905	120	120	110	5785	5795	D	231PFDFU	RG52784

Site ID	Local Identifier	Latitude NAD83	Longitude NAD83	M.P. Elev NAVD 88	Well Depth	Bottom Screen	Top Screen	Bottom Screen Elev	Top Screen Elev	Water Use	Aquifer Code	NMOSE Well File or Data Source
PW-108	13N.5E.29.2314	35.328064	-106.433344	5730	360	360	340	5370	5390	D	112SNTFP	Owner
PW-109	13N.5E.32.3141	35.309793	-106.441385	5812	180	180	160	5632	5652	D	221MRSN / JCKP	RG58618
PW-110	13N.5E.22.3224	35.339238	-106.40033	5972	177	177	137	5795	5835	D	122SNTFP	RG27740
PW-111	13N.5E.22.2242	35.345956	-106.390801	5900	180	180	140	5720	5760	D	325MDERU SanF Flt	RG48625
PW-112	12N.5E.5.2420	35.299823	-106.427137	6043.2	425	425	415	5618	5628	U	231PFDFM	RG65067
PW-113	12N.5E.5.2240	35.301616	-106.427759	5965.1	400	400	360	5565	5605	U	231PFDFU	Owner
PW-114	13N.5E.23.1134	35.345432	-106.389536	5941	300	300	280	5641	5661	D	325MDERU	Owner
PW-115	13N.5E.22.2224	35.346905	-106.391432	5899	180	180	173	5719	5726	D	325MDER / 318ABO SF Flt	RG57913
						163	143	5736	5756			
PW-116	13N.5E.14.3333	35.348349	-106.390314	5865	105	105	65	5760	5800	D	325MDERU SanF Flt	RG32494
PW-117	12N.5E.6.2242	35.302226	-106.443427	5928	200	200	160	5728	5768	D	221MRSN / BBSN	RG32612
PW-118	13N.5E.35.1434	35.313417	-106.384939	6264.5	660	660	620	5605	5645	U	318ABO	RG60485
PW-119	13N.5E.35.2144	35.315998	-106.378383	6224	500	496	436	5728	5788	U	318ABOU	RG60066
PW-120	13N.5E.35.2122	35.318966	-106.377683	6183	420	420	360	5763	5823	U	318ABOU	RG60067
PW-121	12N.5E.6.2434	35.298168	-106.445287	6035	221	218	207	5817	5828	D	231PFDFU	RG30686

Site ID	Local Identifier	Latitude NAD83	Longitude NAD83	M.P. Elev NAVD 88	Well Depth	Bottom Screen	Top Screen	Bottom Screen Elev	Top Screen Elev	Water Use	Aquifer Code	NMOSE Well File or Data Source
PW-122	12N.5E.5.1130	35.30205	-106.441251	5956	140	140	120	5816	5836	D	231PFDFM	RG67522
PW-123	12N.5E.6.2122	35.304049	-106.44773	5933	265	265	220	5668	5713	D	211MENFL	RG58788
						200	180	5733	5753			
PW-124	12N.5E.6.2242	35.302689	-106.443032	5918.1	236	234	184	5684	5734	U	221MRSN / BBSN	RG24952
PW-125	12N.5E.6.2242	35.302794	-106.443566	5927	200	200	140	5727	5787	D	221MRSN / JCKP	RG24952
PW-126	12N.5E.6.2413	35.301159	-106.449311	5976	155	155	120	5821	5856	D	210MNCSL	RG43384
PW-127	12N.5E.6.2112	35.303697	-106.450268	5938	100	90	70	5848	5868	D	211PNLK	RB30170
PW-128	12N.5E.6.1413	35.299238	-106.455754	6017	250	250	210	5767	5807	D	221MRSN / BBSN	RG26806
PW-129	12N.5E.6.1412	35.300191	-106.453434	6002.4	198	198	158	5804	5844	U	211DKOT	RG29295
PW-130	13N.5E.30.1232	35.33191	-106.455283	5526	400	400	320	5126	5206	D	112SNTFP	RG62833
PW-131	13N.5E.29.1344	35.3265	-106.440199	5621	200	200	180	5421	5441	D	112SNTFP	RG64459
						120	100	5501	5521			
PW-132	13N.4E.35.1342	35.313302	-106.492184	5484	620	620	580	4864	4904	D	112SNTFT	RG62805
PW-133	12N.5E.5.1232	35.302587	-106.437198	5940	<100					D	231PFDFM	Owner
PW-134	13N.5E.29.4323	35.320969	-106.432068	5744	500			5744		U	211MENFU	Owner
PW-135	13N.4E.35.4131	35.309622	-106.486634	5548	650	650	610	4898	4938	D	112SNTFP	RG63457

Site ID	Local Identifier	Latitude NAD83	Longitude NAD83	M.P. Elev NAVD 88	Well Depth	Bottom Screen	Top Screen	Bottom Screen Elev	Top Screen Elev	Water Use	Aquifer Code	NMOSE Well File or Data Source
PW-136	13N.4E.35.3421	35.307987	-106.488828	5537	660	660	640	4877	4897	D	112SNTFP	RG58639
PW-137	13N.4E.35.2323	35.314284	-106.484379	5543	560	560	540	4983	5003	D	112SNTFP Valley View Flt	RG64580
PW-138	13N.4E.26.2111	35.333073	-106.486103	5404	590	590	550	4814	4854	D,I	112SNTFA	RG63688
PW-139	13N.5E.22.2423	35.343302	-106.391952	5957	220	220	190	5737	5767	D	325MDERU SanF Flt	RG61394
PW-140	12N.5E.5.1411	35.300195	-106.43897	6026	200	200	180	5826	5846	D	231PFDFL	Owner
PW-141	12N.5E.5.1411	35.300147	-106.43803	6041.7	100	100	90	5942	5952	U	231PFDFL	Owner
PW-142	13N.5E.16.3320	35.351195	-106.423397	5691	520	520	500	5171	5191	D	112SNTFP Escala Flt	Owner
PW-143	13N.5E.21.1313	35.343391	-106.425079	5884	725	685	645	5199	5239	D	122SNTFP Escala Flt	RG63468
PW-144	12N.5E.6.1412	35.30034	-106.454824	6007	150	150	110	5857	5897	D	210MNCSL	RG28943
PW-145	12N.5E.6.2420	35.299537	-106.443465	6095	180	180	130	5915	5965	D	221MRSN	RG36306
PW-146	13N.5E.21.1331	35.342122	-106.425276	5860						P	122SNTFP Escala Flt	
PW-147	13N.5E.32.1141	35.31649	-106.439171	5721	32	none	none	5689		U	211MENF Caballo Flt	RG28790
PW-148	12N.5E.6.1412	35.300171	-106.45345	6011	340	340	320	5671	5691	D	221MRSN / JCKP	RG29295

Site ID	Local Identifier	Latitude NAD83	Longitude NAD83	M.P. Elev NAVD 88	Well Depth	Bottom Screen	Top Screen	Bottom Screen Elev	Top Screen Elev	Water Use	Aquifer Code	NMOSE Well File or Data Source
PW-149	13N.4E.36.4114	35.310772	-106.467243	5672	440	420	400	5252	5272	D	211MENFU	RG59899
PW-150	13N.5E.16.3120	35.354764	-106.422575	5667	370	370	340	5297	5327	D	122SNTFP Escala Flt	Owner
PW-151	13N.5E.16.3330	35.349214	-106.423912	5695.4	515	495	515	5200	5180	U	112SNTFP Escala Flt	RG9986
PW-152	13N.5E.20.3432	35.334718	-106.43741	5703	340	340	300	5363	5403	D	112SNTFP	RG59532
PW-153	13N.5E.29.3243	35.323093	-106.43685	5683	800	800		4883		S	211MENFL	Owner
PW-154	12N.5E.3.1343	35.297574	-106.405634	6188						D	318ABO	
PW-155	12N.5E.3.1431	35.298482	-106.404395	6150.6						U	318ABO	
PW-156	12N.5E.3.1431	35.298399	-106.404404	6151.3						U	318ABO	
PW-157	13N.5E.22.4211	35.340968	-106.394618	6023	560	320	80	5703	5943	U	122SNTFP SanF Flt	RG64551EX2
PW-158	13N.5E.32.2233	35.315868	-106.430381	5809.8	115	115	105	5695	5705	U	210MNCSU	Owner
PW-159	13N.5E.32.2233	35.315837	-106.430339	5810	210	205	185	5605	5625	D	210HOSTD	RG56015
PW-160	13N.5E.32.3423	35.306798	-106.437071	5823	175	175	155	5648	5668	D	221TDLT Flt	RG65605
PW-161	13N.5E.27.4414	35.321221	-106.393886	6161	370	370	350	5791	5811	N	318ABO	RG57098
PW-162	13N.4E.34.4443	35.304645	-106.497117	5508	603	603	555	4905	4953	D	112SNTFP	RG44347
PW-163	13N.5E.20.3113	35.339817	-106.443282	5680	280	270	230	5410	5450	D	112SNTFP	RG49597

Site ID	Local Identifier	Latitude NAD83	Longitude NAD83	M.P. Elev NAVD 88	Well Depth	Bottom Screen	Top Screen	Bottom Screen Elev	Top Screen Elev	Water Use	Aquifer Code	NMOSE Well File or Data Source
PW-164	12N.5E.3.3412	35.292614	-106.402678	6236	80	80		6156		D	318ABO / 325MDER Flt	Owner
PW-165	13N.4E.35.2323	35.313944	-106.484004	5540	590	570	565	4970	4975	U	112SNTFP Valley View Flt	RG50111
PW-166	13N.4E.26.4444	35.319448	-106.478163	5528	690	690	380	4838	5148	P	112SNTFT	RG49802
PW-167	13N.4E.26.2443	35.326271	-106.479803	5523	720	708	386	4815	5137	P	112SNTFT	RG49802S
PW-168	13N.4E.23.3343	35.333591	-106.493349	5327	700	520	500	4807	4827	P	112SNTFA	RG49802S2
PW-169	13N.5E.20.3334	35.334257	-106.441745	5695	320	320	300	5375	5395	D	112SNTFP	RG58873
PW-170	13N.4E.35.2323	35.314078	-106.483823	5537	595	595	575	4942	4962	D	112SNTFP Valley View Flt	RG65361
PW-171	12N.5E.6.4133	35.293752	-106.451102	6171	225	215	205	5956	5966	U	231PFDFU	RG19204
						165	155	6006	6016			
						130	120	6041	5892			
PW-172	12N.5E.6.2242	35.302233	-106.443456	5921.7	50	50	30	5872	5892	U	110AVMB / 210MNCSL	RG32612
PW-173	13N.4E.34.3133	35.308141	-106.512487	5365	396	396	-	4969	-	D	112SNTFT	RG29164
PW-174	13N.5E.29.3442	35.320461	-106.435103	5709	220	210	200	5499	5509	D	211MENFL	RG56782
PW-175	13N.5E.22.4323	35.336059	-106.396885	6060	350	350	320	5710	5740	D	122SNTFP	RG68220
						300	280	5760	5780			

Site ID	Local Identifier	Latitude NAD83	Longitude NAD83	M.P. Elev NAVD 88	Well Depth	Bottom Screen	Top Screen	Bottom Screen Elev	Top Screen Elev	Water Use	Aquifer Code	NMOSE Well File or Data Source
PW-176	13N.4E.33.4211	35.311325	-106.517033	5318	420	420	400	4898	4918	D	112SNTFT	RG61931
PW-177	13N.4E.36.3142	35.309937	-106.474402	5591	370	370	290	5221	5301	D	112SNTFP	RG67635
PW-178	12N.4E.2.2210	35.30401	-106.48357	5593	684	674	664	4919	4929	Y,A	112SNTFP	RG54556
						505	500	5088	5093			
PW-179	12N.4E.1.1110	35.304391	-106.478078	5722	830	820	800	4902	4922	P	112SNTFP	RG54556X
PW-180	12N.4E.1.1110	35.30443	-106.478255	5708	800	798	758	4910	4950	P	112SNTFP	RG54556S2
PW-181	13N.5E.32.3133	35.308934	-106.443419	5862	103	103	73	5759	5789	P	211MENFU	RG49957
PW-182	13N.5E.31.4231	35.309689	-106.447311	6090	700	nc	nc	5390	5324	Y,A	211MENF / HARN	RG49940
PW-183	13N.5E.32.3133	35.308536	-106.442901	5869	196	196	186	5673	5683	U	221MRSN / WWCN	RG49957X2
PW-184	13N.5E.31.1221	35.318249	-106.4532	5856	500	500	440	5356	5416	P	122SNTFP	RG52013
PW-185	13N.5E.22.4211	35.340917	-106.39478	6023	230	230	200	5793	5823	U	122SNTFP SanF Flt	RG64551EX
PW-186	13N.5E.29.4221	35.32574	-106.428327	5893	500	500	460	5393	5433	P	122SNTFP	RG61622
PW-187	13N.5E.29.2434	35.326752	-106.428969	5847	530	530	470	5317	5377	P	122SNTFP	RG61624
PW-188	13N.5E.30.1341	35.327593	-106.458119	5684	620	623	580	5061	5104	P	112SNTFP	RG62867
PW-189	13N.5E.30.1433	35.326584	-106.455793	5663	540	540	500	5123	5163	P	112SNTFP	RG62868
PW-190	13N.5E.30.1414	35.329018	-106.455201	5568	420	420	380	5148	5188	P	112SNTFP	RG62869

Site ID	Local Identifier	Latitude NAD83	Longitude NAD83	M.P. Elev NAVD 88	Well Depth	Bottom Screen	Top Screen	Bottom Screen Elev	Top Screen Elev	Water Use	Aquifer Code	NMOSE Well File or Data Source
PW-191	13N.4E.25.3413	35.320965	-106.473053	5575	490	472	272	5103	5303	P	112SNTFP	RG18159
PW-192	13N.4E.25.3112	35.326065	-106.476943	5474	560	520	500	4954	4974	P	112SNTFT Valley View Flt	RG12871CDS
						340	320	5134	5154			
						280	260	5194	5214			
PW-193	13N.4E.36.1131	35.316689	-106.47753	5540	501	500	350	5040	5190	P	112SNTFP	RG10032
PW-194	13N.4E.26.4433	35.319491	-106.481751	5501	670	665	420	4836	5081	P	112SNTFT Valley View Flt	RG10032S
PW-195	13N.4E.36.1111	35.318414	-106.477943	5536	596	596	586	4940	4950	D	112SNTFP	RG59333
						466	416	5070	5120			
PW-196	13N.5E.19.4321	35.336846	-106.449915	5655	340	340	320	5315	5335	P	112SNTFP	RG68743
PW-197	13N.4E.34.2314	35.313726	-106.502994	5406	612					P	112SNTFT	RG42562
PW-198	13N.4E.33.2121	35.318686	-106.5193	5303	580	575	545	4728	4758	P	112SNTFT	RG42562S2
PW-199	13N.4E.35.1124	35.316756	-106.490911	5487	660	655	635	4832	4852	P	112SNTFT	RG53424
PW-200	13N.5E.31.3441	35.306396	-106.453351	5881	345	345	245	5536	5636	P	211PNLK	RG52191S
PW-201	13N.4E.33.2232	35.316649	-106.515779	5311	475	470	460	4841	4851	D	112SNTFT	RG58464
PW-202	13N.5E.30.2232	35.331189	-106.445962	5592	446	446	436	5146	5156	P	112SNTFP	RG48788
PW-203	13N.5E.20.3124	35.339649	-106.439643	5665	405	405	385	5260	5280	D	112SNTFP	Owner
PW-204	13N.4E.33.4200	35.31067	-106.515541	5330	440	440	420	4890	4910	P	112SNTFT	RG59519

Site ID	Local Identifier	Latitude NAD83	Longitude NAD83	M.P. Elev NAVD 88	Well Depth	Bottom Screen	Top Screen	Bottom Screen Elev	Top Screen Elev	Water Use	Aquifer Code	NMOSE Well File or Data Source
PW-205	13N.4E.27.1244	35.330553	-106.505074	5259	521	420	280	4839	4979	N	112SNTFA	RG49516
PW-206	13N.5E.22.2323	35.343326	-106.397111	6056	195	195	155	5861	5901	D	122SNTFP	RG40708
PW-207	13N.5E.27.3334	35.319283	-106.406635	5935	300	300	280	5635	5655	Y,A	210CRCS SanF Flt	Owner
PW-208	12N.5E.4.1424	35.299356	-106.418002	6336.1	270	270	250	6066	6086	U	325MDERL	RG66702EX1
PW-209	12N.5E.4.1424	35.299361	-106.418101	6335.1	273	270	240	6065	6095	U	325MDERL	RG66702EX1
PW-210	13N.4E.33.1114	35.317524	-106.52989	5188						U	112SNTFA	
PW-211	13N.4E.35.1224	35.3175	-106.487778	5462						D	112SNTFT	
PW-212	13N.5E.32.2244	35.315904	-106.427416	5840						P	211PNLK	RG57988
PW-213	13N.4E.11.4333	35.362964	-106.486732	5180						N	112SNTFA	
PW-215	13N.4E.33.4223	35.310278	-106.514444	5340						D	112SNTFA	
PW-216	13N.5E.27.2112	35.333333	-106.398056	6060						D	122SNTFP	
PW-217	13N.5E.20.1332	35.342419	-106.441436	5640						P	112SNTFP	RG31586
PW-218	13N.5E.18.1111	35.363333	-106.4925	5520						S	112SNTFA	
PW-301	13N.4E.28.133	35.327222	106.530278	5097	80							USGS
PW-302	13N.4E.29.222	35.331389	106.531389	5074	55							USGS
PW-303	13N.4E.29.424	35.323611	106.532222	5090	40							USGS
PW-304	13N.4E.21.142	35.3425	106.522222	5085	212							USGS
PW-305	13N.4E.21.324	35.338889	106.523611	5090	450							USGS

Site ID	Local Identifier	Latitude NAD83	Longitude NAD83	M.P. Elev NAVD 88	Well Depth	Bottom Screen	Top Screen	Bottom Screen Elev	Top Screen Elev	Water Use	Aquifer Code	NMOSE Well File or Data Source
PW-306	13N.4E.28.111	35.331944	106.530278	5091	86							USGS
PW-307	13N.4E.28.123	35.331389	106.525278	5110	490							USGS
PW-308	13N.4E.28.123	35.331667	106.524722	5110	91							USGS
PW-309	13N.4E.28.123	35.331944	106.524444	5110	65							USGS
PW-310	13N.4E.28.131	35.33	106.529722	5094	80	75	65	5019	5029		112SNTF	USGS
PW-311	13N.4E.28.421	35.325833	106.515	5210	150							USGS
PW-312	13N.4E.28.421	35.32611	106.515	5211	160						112SNTF	USGS
PW-313	13N.4E.33.212	35.324722	106.532222	5300	451							USGS
PW-314	13N.4E.33.214	35.318056	106.5175	5310	464							USGS
PW-315	13N.4E.34.113	35.316389	106.510556	5350	480							USGS
PW-316	13N.5E.27.2212	35.333889	106.394444	6100	220	220	215	5880	5885	D	325MDER	USGS
PW-317	13N.5E.34.1114	35.317778	106.406667	5941	56	56	26	5885	5915		110PTOD	USGS

Appendix A continued: Aquifer Codes (Johnson, 1999)

Code	Aquifer
112SNTFA	Upper Santa Fe, axial facies
112SNTFT	Upper Santa Fe, transitional facies
112SNTFP	Upper Santa Fe, piedmont facies
122SNTFP	Lower Santa Fe, piedmont facies
211MENFU	Cretaceous Upper Menefee
211MENF	Cretaceous Menefee
211MENF/HARN	Harmon Sandstone Member
211PNLK	Cretaceous Point Lookout
210MNCSU	Cretaceous Upper Mancos
210HOSTD	Cretaceous Hosta Dalton
210MNCSL	Cretaceous Lower Mancos
211DKOT	Cretaceous Dakota
221MRSN	Jurassic Morrison
221MRSN/JCKP	Jackpile Sandstone Member
221MRSN/WWCN	Westwater Canyon Member
221MRSN/BBSN	Brushy Basin Member
221MRSN/RCAP	Recapture Shale Member
221TDLT	Jurassic Todilto
220ENRD	Jurassic Entrada
230TRSC	Triassic undivided
231PFDFU	Triassic Upper Petrified Forest
231PFDF	Triassic Petrified Forest
231PFDFM	Triassic Middle Petrified Forest sandstone
231PFDFL	Triassic Lower Petrified Forest
231AGZCU	Triassic Upper Agua Zarca
231AGZC	Triassic Agua Zarca
318ABOU	Permian Upper Abo
318ABO	Permian Abo
325MDERU	Pennsylvanian Upper Madera
325MDER	Pennsylvanian Madera undivided
325MDERL	Pennsylvanian Lower Madera

APPENDIX B. MONTHLY PRECIPITATION DATA AT NOAA SITES

(NOAA/NCDC, 1998)

Appendix B. Monthly precipitation data at NOAA sites. Page 1 of 7.

Location	Year	Jan	Feb	Mar	Apr	May	Jun	Jul	Aug	Sep	Oct	Nov	Dec	Annual
Bernalillo*	1890	0.13	2.54	3.30	2.54	---	---	2.79	3.05	3.81	1.27	1.52	5.08	---
Bernalillo*	1891	2.54	1.78	4.06	0.00	5.08	0.00	0.05	0.25	7.11	0.00	0.00	1.27	22.61
Bernalillo*	1892	2.54	---	---	---	---	---	---	---	---	---	---	---	---
Bernalillo*	1895	---	---	---	---	---	0.56	6.48	3.91	0.05	2.67	3.05	0.53	---
Bernalillo*	1896	0.03	0.00	0.00	0.00	0.00	1.57	2.03	2.97	3.48	9.42	0.00	0.53	20.04
Bernalillo*	1897	0.71	0.00	1.73	1.40	5.66	1.60	1.75	1.19	10.21	4.50	0.25	0.18	29.18
Bernalillo*	1898	1.32	1.22	0.94	1.45	0.05	1.04	2.29	3.51	0.00	0.30	0.76	1.91	14.78
Bernalillo*	1899	0.38	0.00	0.51	0.25	0.00	1.07	8.15	1.63	4.32	0.00	1.14	0.05	17.50
Bernalillo*	1900	1.40	0.38	0.41	1.14	0.94	0.36	0.00	0.86	4.27	1.47	0.99	0.18	---
Bernalillo*	1901	2.36	0.91	1.02	0.43	1.68	---	---	---	---	---	---	---	---
Bernalillo*	1923	---	---	---	---	1.32	0.05	2.31	5.26	0.91	2.67	3.20	1.04	---
Bernalillo*	1924	0.00	0.56	1.07	3.58	0.33	---	---	---	---	---	---	---	
Bernalillo*	1938	0.38	3.78	0.84	---	---	---	---	---	7.26	2.41	0.00	0.66	---
Bernalillo*	1939	2.77	0.56	3.10	0.69	0.81	0.00	2.11	2.21	3.56	2.03	2.72	0.91	21.46
Bernalillo*	1940	0.64	3.35	1.57	0.41	3.35	2.59	4.80	5.56	3.76	0.74	4.39	4.29	35.46
Bernalillo*	1941	3.51	0.81	3.63	2.90	8.66	0.61	1.88	4.75	7.24	6.83	0.48	1.17	42.47
Bernalillo*	1942	0.08	0.66	0.05	8.03	0.00	0.41	2.79	2.36	4.55	3.28	0.00	2.92	25.12
Bernalillo*	1943	1.17	0.56	0.56	0.00	2.69	1.19	1.42	0.54	1.73	1.04	1.27	2.41	21.59
Bernalillo*	1944	1.47	0.61	2.13	2.64	0.81	0.69	4.37	4.62	5.56	1.91	1.83	1.47	28.12
Bernalillo*	1945	1.37	0.43	1.17	2.79	0.00	0.00	3.12	1.09	1.37	0.76	0.00	0.56	12.67
Bernalillo 3SW	1946	0.66	0.84	0.66	0.64	0.71	0.00	3.89	1.75	0.91	2.13	2.95	0.30	15.44
Bernalillo 3SW	1947	0.38	0.64	0.64	0.00	1.19	0.41	0.25	6.45	1.12	1.14	1.32	4.04	17.58
Bernalillo 3SW	1948	0.69	4.37	0.66	0.81	1.27	---	---	---	---	---	---	---	---
Bernalillo 3SW	1948	---	---	---	---	---	1.45	0.58	1.32	1.52	1.45	0.64	0.36	---
Bernalillo 3SW	1949	1.96	1.30	1.52	3.02	2.72	1.07	4.06	0.53	5.23	0.13	0.00	0.28	21.82
Bernalillo 3SW	1950	0.00	0.64	0.13	0.86	0.00	1.68	7.70	0.94	3.40	0.13	0.00	0.00	15.49
Bernalillo 3SW	1951	1.32	0.66	0.38	0.71	0.51	0.13	1.83	9.73	0.00	0.94	0.25	0.53	16.99
Bernalillo 3SW	1952	0.64	0.18	1.55	2.54	1.27	4.55	3.48	3.58	0.81	0.00	1.52	1.96	22.07
Bernalillo 3SW	1953	0.00	1.32	2.13	0.46	---	3.68	3.63	1.12	0.10	---	---	---	---
Median		0.70	0.66	1.02	0.84	0.94	0.69	2.55	2.67	3.48	1.36	0.88	0.79	21.53

Locations in Table 10. Precipitation depths in centimeters.--- indicates one or more days per month of missing data. Data for Bernalillo* between January 1, 1890 and July 1, 1946 has been attributed to the Bernalillo 3SW location.

Appendix B continued. Page 2 of 7.

Location	Year	Jan	Feb	Mar	Apr	May	Jun	Jul	Aug	Sep	Oct	Nov	Dec	Annual
Bernalillo 1NNE	1953	---	---	---	---	---	---	---	---	---	---	---	0.76	---
Bernalillo 1NNE	1954	1.60	0.15	1.42	0.03	2.74	1.75	5.18	1.22	1.45	1.02	0.30	0.81	17.70
Bernalillo 1NNE	1955	0.84	0.53	0.00	0.36	1.98	0.61	5.03	4.67	0.51	0.03	0.18	0.64	15.37
Bernalillo 1NNE	1956	1.50	1.02	0.00	0.00	0.23	0.25	3.10	3.91	0.00	1.14	0.00	0.00	11.15
Bernalillo 1NNE	1957	1.47	1.75	1.75	1.37	1.37	0.41	3.18	7.52	0.18	6.53	2.79	0.64	28.96
Bernalillo 1NNE	1958	1.07	0.43	4.39	1.42	1.57	0.84	0.33	1.60	3.07	2.62	1.22	2.69	21.26
Bernalillo 1NNE	1959	0.03	0.03	1.85	2.39	0.76	1.65	0.89	8.84	0.10	5.23	0.08	3.86	25.70
Bernalillo 1NNE	1960	1.17	1.12	1.57	0.03	1.70	2.59	3.48	2.29	1.55	8.13	0.43	1.65	25.70
Bernalillo 1NNE	1961	1.40	0.36	1.47	1.55	0.13	0.30	1.73	4.75	0.64	1.75	1.37	2.11	17.55
Bernalillo 1NNE	1962	1.42	0.33	0.23	0.25	0.13	0.71	4.17	0.76	2.46	2.29	3.02	0.94	16.71
Bernalillo 1NNE	1963	0.61	2.57	1.17	0.51	0.13	1.04	2.24	9.27	1.24	1.68	0.81	0.03	21.29
Bernalillo 1NNE	1964	0.05	3.10	0.33	0.76	1.55	0.08	7.21	1.60	0.04	0.20	0.51	1.45	20.57
Bernalillo 1NNE	1965	1.35	2.36	1.85	1.50	1.12	---	---	---	---	---	---	---	---
Median		1.26	0.77	1.45	0.64	1.24	0.71	3.18	3.91	1.24	1.75	0.51	0.88	20.57

Location	Year	Jan	Feb	Mar	Apr	May	Jun	Jul	Aug	Sep	Oct	Nov	Dec	Annual
Bernalillo	1965	---	---	---	---	---	---	---	2.92	3.07	2.95	1.07	---	---
Bernalillo	1966	---	0.71	0.00	0.00	0.66	5.11	1.57	3.02	1.52	0.00	0.05	0.76	---
Bernalillo	1967	0.15	0.69	0.56	0.00	0.05	3.25	4.83	8.46	2.69	0.36	1.19	1.22	23.44
Bernalillo	1968	0.00	2.87	3.68	1.88	2.72	0.18	4.75	5.03	0.15	1.14	1.63	1.52	25.55
Bernalillo	1969	0.13	0.51	1.63	3.00	5.56	0.89	2.36	3.53	3.10	6.96	0.64	1.68	29.97
Bernalillo	1970	0.03	0.71	1.88	0.20	1.63	2.64	8.36	4.47	1.78	1.35	1.24	0.00	24.28
Bernalillo	1971	1.30	1.09	0.28	3.15	1.12	0.13	8.08	3.48	2.77	5.69	1.32	3.28	31.67
Bernalillo	1972	0.86	0.18	0.23	0.00	---	2.51	1.40	5.26	5.16	11.63	2.29	1.88	---
Bernalillo	1973	1.98	1.91	5.84	---	1.73	0.84	5.66	3.76	4.50	0.66	0.25	0.00	---
Bernalillo	1974	3.05	1.22	1.96	0.10	0.99	0.33	6.40	3.28	2.79	7.70	1.04	1.04	29.90
Bernalillo	1975	---	---	3.07	0.48	0.13	0.28	7.67	3.30	6.93	0.00	---	-0.66	---
Bernalillo	1976	0.00	0.56	0.25	2.64	1.70	0.61	4.24	3.68	1.24	0.15	1.27	0.03	16.38
Bernalillo	1977	1.55	0.18	0.89	2.82	0.53	0.46	2.06	5.94	1.85	0.00	2.11	0.46	18.85
Bernalillo	1978	---	---	2.67	0.74	3.15	2.11	2.03	3.05	1.47	3.28	---	2.90	---
Bernalillo	1979	---	1.63	0.91	0.99	6.68	4.47	3.99	6.05	1.32	1.17	3.48	1.75	---
Bernalillo	1980	3.84	2.26	0.84	0.00	1.80	0.00	2.11	0.38	6.17	0.00	0.74	0.94	19.08
Bernalillo	1981	0.15	0.94	1.75	1.14	2.31	1.40	2.24	3.15	1.17	4.65	---	0.03	---
Bernalillo	1982	0.48	---	---	0.00	---	0.00	2.26	3.05	---	---	---	---	---
Median		0.48	0.83	1.27	0.61	1.70	0.84	3.99	3.51	2.69	1.17	1.22	0.99	24.28

Location	Year	Jan	Feb	Mar	Apr	May	Jun	Jul	Aug	Sep	Oct	Nov	Dec	Annual
Hagan	1953	---	---	---	0.76	1.78	1.80	4.90	1.47	0.15	1.57	1.98	1.78	---
Hagan	1954	1.07	0.00	2.39	0.00	3.05	1.88	8.56	4.85	2.79	1.50	0.38	0.33	26.80
Hagan	1955	0.64	0.53	0.00	0.64	1.75	0.41	12.75	7.90	0.71	---	---	---	---
Median		0.85	0.27	1.19	0.64	1.78	1.80	8.56	4.85	0.71	1.54	1.18	1.05	26.80

Appendix B continued. Page 4 of 7.

Location	Year	Jan	Feb	Mar	Apr	May	Jun	Jul	Aug	Sep	Oct	Nov	Dec	Annual
Sandia Crest	1953	---	---	---	---	---	---	---	---	---	---	---	7.04	---
Sandia Crest	1954	5.08	0.91	6.02	0.13	5.56	3.68	7.75	3.76	3.48	2.64	1.45	2.16	42.62
Sandia Crest	1955	4.01	4.09	1.09	0.69	3.35	1.14	15.82	10.74	2.67	0.38	0.30	6.65	50.98
Sandia Crest	1956	6.07	4.57	0.00	0.89	0.46	1.19	11.35	4.98	0.18	3.56	0.33	1.19	34.77
Sandia Crest	1957	5.49	5.79	9.55	7.11	6.38	0.81	7.85	8.89	1.14	11.86	9.25	2.54	76.66
Sandia Crest	1958	5.41	3.00	16.64	8.15	0.97	0.05	1.24	6.78	11.58	7.70	6.81	6.68	75.01
Sandia Crest	1959	2.11	0.76	6.17	5.49	2.03	2.34	4.70	15.70	0.25	7.29	0.64	13.67	61.14
Sandia Crest	1960	8.00	6.17	5.54	1.27	3.10	4.06	2.69	3.71	2.39	12.17	0.89	4.65	54.64
Sandia Crest	1961	5.44	3.71	7.72	3.63	0.99	0.41	5.33	8.71	2.69	1.65	3.51	6.10	49.89
Sandia Crest	1962	4.04	4.78	4.04	0.76	0.13	0.86	9.78	3.61	6.60	3.58	4.83	4.37	47.37
Sandia Crest	1963	3.25	7.26	4.27	1.98	0.30	0.99	3.05	19.41	3.78	2.79	4.01	0.89	51.99
Sandia Crest	1964	1.57	6.71	2.90	3.25	6.40	0.00	13.64	5.46	4.83	0.84	3.81	4.95	54.36
Sandia Crest	1965	2.92	---	6.65	2.67	0.46	8.36	3.73	5.38	9.55	4.62	2.26	13.28	---
Sandia Crest	1966	2.24	3.53	0.64	---	---	9.86	8.56	6.73	3.00	0.13	1.40	1.96	---
Sandia Crest	1967	0.71	4.32	1.40	0.89	0.13	5.13	12.17	16.79	5.64	0.76	3.07	4.85	55.85
Sandia Crest	1968	1.65	7.19	10.77	6.93	3.18	0.61	11.94	14.48	1.80	0.58	6.38	9.25	74.75
Sandia Crest	1969	6.25	6.22	4.17	2.92	5.89	3.15	7.62	---	3.61	10.80	1.91	---	---
Sandia Crest	1970	0.43	3.02	8.81	3.51	0.61	2.79	9.96	9.47	4.80	2.90	1.75	2.95	51.00
Sandia Crest	1971	4.62	3.68	2.24	7.14	0.15	0.00	10.24	8.74	2.84	6.02	7.62	9.17	62.46
Sandia Crest	1972	---	1.02	1.42	0.15	3.02	2.77	4.85	8.53	7.92	14.71	---	6.63	---
Sandia Crest	1973	9.45	4.98	16.18	7.52	3.51	2.84	9.93	4.29	7.06	1.91	6.20	1.73	75.59
Sandia Crest	1974	10.41	3.86	4.09	0.43	0.84	0.15	7.95	9.40	6.48	12.93	1.93	4.52	62.99
Sandia Crest	1975	6.40	12.52	8.43	2.29	1.07	0.00	13.89	4.70	11.73	0.00	5.05	2.13	68.22
Sandia Crest	1976	0.94	3.78	5.82	3.15	---	1.55	8.59	9.35	2.31	---	1.17	0.86	---
Sandia Crest	1977	9.40	4.55	1.96	8.10	0.33	2.18	5.72	11.81	3.91	1.45	3.53	1.93	54.86
Sandia Crest	1978	---	9.98	12.17	1.96	4.88	5.08	4.39	8.97	5.26	---	6.60	5.49	---
Sandia Crest	1979	---	6.22	5.99	3.99	---	---	---	---	---	---	---	---	---
Median		4.62	4.55	5.68	2.92	1.07	1.55	7.95	8.72	3.78	2.90	4.65	54.86	

Appendix B continued. Page 5 of 7.

Location	Year	Jan	Feb	Mar	Apr	May	Jun	Jul	Aug	Sep	Oct	Nov	Dec	Annual
Sandia Park	1939	6.60	2.01	5.87	3.23	0.25	0.61	7.65	7.75	6.25	4.29	3.73	1.24	49.48
Sandia Park	1940	3.28	6.60	5.23	1.85	4.29	1.45	1.22	6.91	4.22	1.83	7.77	6.50	51.16
Sandia Park	1941	6.38	2.72	---	6.35	10.06	2.36	---	3.84	8.36	---	5.54	3.38	83.21
Sandia Park	1942	0.89	---	---	---	0.64	1.37	0.66	---	5.82	7.21	0.00	---	---
Sandia Park	1943	2.06	---	---	---	---	---	---	9.80	1.09	---	---	---	---
Sandia Park	1944	---	---	4.37	3.23	0.76	1.09	8.99	7.80	3.63	3.00	4.11	5.03	---
Sandia Park	1945	4.24	---	---	4.88	0.00	0.76	6.45	8.23	2.67	3.23	0.00	5.61	---
Sandia Park	1946	3.10	0.25	2.08	2.26	1.60	0.84	6.99	---	1.83	6.40	8.56	2.31	52.78
Sandia Park	1947	1.04	0.99	0.94	1.07	2.64	1.14	3.30	9.88	1.52	1.78	3.86	3.78	31.95
Sandia Park	1948	---	---	---	---	---	3.18	3.23	---	---	---	2.79	1.88	---
Sandia Park	1948	2.95	6.81	5.08	1.88	2.08	---	---	---	---	---	---	---	---
Sandia Park	1949	5.33	0.00	4.72	4.62	5.44	2.34	7.77	---	---	0.91	0.38	2.41	---
Sandia Park	1950	4.22	2.46	0.61	0.61	0.46	1.02	---	2.95	7.32	0.10	0.00	0.05	36.12
Sandia Park	1951	3.96	1.12	2.44	1.12	1.22	0.08	7.87	9.32	0.13	1.85	2.01	4.55	35.66
Sandia Park	1952	2.51	2.21	4.14	2.54	4.98	3.35	4.32	---	3.99	0.00	4.98	2.18	46.36
Sandia Park	1953	1.07	2.87	4.32	3.38	2.21	7.72	3.63	4.60	0.00	---	5.44	2.11	---
Sandia Park	1954	3.00	0.18	4.34	0.05	2.59	2.67	---	6.86	3.25	1.78	0.69	1.57	38.35
Sandia Park	1955	1.73	2.59	0.18	0.94	2.95	1.17	9.60	---	6.02	0.36	0.61	4.70	42.16
Sandia Park	1956	2.62	2.29	0.00	0.43	0.99	1.40	7.37	4.62	0.00	4.29	0.69	0.61	25.30
Sandia Park	1957	3.68	4.34	5.64	2.41	4.09	0.28	---	---	0.43	7.14	8.46	0.64	59.41
Sandia Park	1958	2.44	2.82	8.74	7.67	---	0.61	0.51	7.87	---	5.18	4.62	3.51	---
Sandia Park	1959	0.89	---	---	4.17	---	---	5.38	---	---	---	---	---	---
Sandia Park	1960	---	---	---	---	2.92	---	3.20	5.59	1.02	---	1.14	---	---
Sandia Park	1961	---	---	---	---	1.30	1.45	6.40	9.04	3.20	1.02	3.73	3.48	---
Sandia Park	1962	1.98	3.66	1.93	0.28	0.61	2.46	---	2.41	4.83	2.82	4.78	2.90	44.35
Sandia Park	1963	1.60	6.17	5.26	1.40	0.66	2.01	2.67	---	2.87	3.28	1.83	0.76	41.78
Sandia Park	1964	1.75	6.65	1.17	4.09	5.77	0.00	9.25	5.99	4.24	0.79	2.49	3.12	45.31
Sandia Park	1965	3.51	4.37	4.27	2.67	2.06	6.83	9.45	8.08	7.59	3.78	5.44	---	---
Sandia Park	1966	---	0.91	0.13	0.28	2.01	4.72	---	4.47	2.95	1.07	0.53	3.38	---
Sandia Park	1967	---	3.23	2.84	0.86	0.71	5.26	6.68	---	3.76	1.12	1.75	---	---

Continued.

Appendix B continued. Page 6 of 7.

Sandia Park continued	Year	Jan	Feb	Mar	Apr	May	Jun	Jul	Aug	Sep	Oct	Nov	Dec	Annual
Sandia Park	1968	0.20	6.10	---	3.53	2.64	0.28	8.64	---	0.33	0.99	---	3.89	---
Sandia Park	1969	3.02	---	3.28	4.85	8.81	2.54	2.92	9.78	8.69	---	---	5.69	---
Sandia Park	1970	---	0.99	---	---	0.13	2.16	9.98	6.02	3.40	5.26	1.57	---	---
Sandia Park	1971	3.84	---	3.05	2.59	0.15	0.41	---	2.54	4.85	5.49	3.78	7.92	---
Sandia Park	1972	0.81	1.04	0.13	0.00	7.21	1.47	3.73	---	7.19	---	4.34	5.28	56.21
Sandia Park	1973	---	4.57	6.83	3.58	5.36	1.80	9.75	5.21	4.57	1.12	2.44	0.13	---
Sandia Park	1974	6.99	---	2.95	0.76	0.30	0.10	8.08	7.85	4.39	---	2.03	3.48	---
Sandia Park	1975	3.45	5.64	5.13	2.59	2.95	0.00	7.09	6.22	9.73	0.00	---	1.27	---
Sandia Park	1976	0.05	1.78	1.63	0.89	2.29	2.13	8.10	5.11	3.02	0.91	---	0.53	---
Sandia Park	1977	---	1.93	1.27	2.39	1.42	1.09	8.89	8.28	3.68	0.71	3.25	0.41	---
Sandia Park	1978	5.44	4.06	7.14	0.53	7.57	3.84	3.63	6.60	4.47	3.56	---	4.06	---
Sandia Park	1979	5.84	2.90	1.32	---	4.04	4.45	6.25	7.52	1.96	2.21	0.61	2.90	---
Sandia Park	1980	5.54	4.88	---	1.50	1.78	0.28	1.37	3.94	8.28	3.51	2.77	---	---
Sandia Park	1981	---	0.79	---	2.34	4.37	3.48	5.28	---	2.16	3.05	1.63	0.00	---
Sandia Park	1982	---	---	5.49	---	2.49	0.66	4.19	9.47	---	4.17	2.51	3.86	---
Sandia Park	1983	2.74	4.24	---	3.45	0.43	4.88	6.68	5.87	---	---	---	1.09	---
Sandia Park	1984	1.27	0.00	2.62	---	0.00	2.79	0.48	8.81	5.72	---	---	---	---
Sandia Park	1985	---	---	9.17	7.44	4.06	2.39	5.44	3.40	7.70	7.47	2.03	1.60	---
Sandia Park	1986	0.46	---	2.82	3.28	5.72	8.15	---	4.06	6.71	7.42	---	4.90	---
Sandia Park	1987	---	---	1.57	3.91	5.49	4.62	4.17	6.83	0.97	2.13	4.83	6.99	---
Sandia Park	1988	3.58	0.99	2.87	8.26	4.34	6.60	7.21	9.14	9.27	1.63	3.78	2.21	59.89
Sandia Park	1989	4.06	---	3.53	0.30	0.25	0.33	---	3.84	2.54	3.66	0.03	1.70	---
Sandia Park	1990	4.75	6.27	3.66	4.01	1.80	1.35	---	8.86	8.05	1.37	5.61	7.39	65.30
Sandia Park	1991	2.97	3.30	4.37	0.00	3.81	4.72	---	---	6.73	2.18	---	7.21	---
Sandia Park	1992	3.07	2.24	---	0.18	7.44	2.49	8.74	7.04	4.04	4.14	4.52	---	---
Sandia Park	1993	---	---	3.48	0.15	3.10	0.66	7.95	8.69	1.50	5.56	6.17	---	---
Sandia Park	1994	---	---	9.55	3.23	8.00	3.18	7.82	---	3.45	7.62	6.71	2.97	---
Sandia Park	1995	---	2.82	---	3.40	2.18	2.34	4.27	9.30	3.45	0.00	1.37	1.45	---
Sandia Park	1996	---	2.51	1.35	0.00	0.13	---	9.14	8.94	6.78	---	4.83	0.00	---
Sandia Park	1997	---	---	---	---	---	---	---	---	---	---	4.88	7.09	---
Median		3.01	2.77	3.48	2.41	2.39	1.91	6.45	6.88	3.76	2.51	2.78	2.93	45.83

Location	Year	Jan	Feb	Mar	Apr	May	Jun	Jul	Aug	Sep	Oct	Nov	Dec	Annual
Placitas 4W	1992	1.73	1.65	2.59	0.64	5.36	1.12	1.75	5.74	2.97	1.40	4.19	---	---
Placitas 4W	1993	3.71	2.97	1.85	0.00	0.61	0.66	4.32	7.80	1.27	1.32	2.39	0.00	26.90
Placitas 4W	1994	---	0.25	2.87	---	---	3.25	2.29	4.93	3.45	4.47	5.89	2.49	---
Placitas 4W	1995	---	1.96	1.80	1.98	1.91	0.00	1.73	3.40	4.95	0.00	0.00	0.20	---
Placitas 4W	1996	0.08	0.61	0.00	0.00	0.00	5.26	4.14	9.04	4.52	3.61	2.08	0.00	29.34
Placitas 4W	1997	4.24	0.53	0.10	5.44	2.57	2.59	6.07	7.16	3.28	0.99	5.05	2.87	40.89
Median		2.72	1.13	1.83	0.64	1.91	1.85	3.21	6.45	3.37	1.36	3.29	0.20	29.34

Location	Year	Jan	Feb	Mar	Apr	May	Jun	Jul	Aug	Sep	Oct	Nov	Dec	Annual
Placitas nr.	1910	---	---	---	---	---	---	---	---	---	5.44	2.29	1.73	---
Placitas nr.	1911	3.63	10.95	2.57	5.38	2.31	3.68	16.10	2.95	5.54	9.27	1.91	3.84	68.12
Placitas nr.	1912	0.23	4.80	5.44	2.21	1.91	8.08	12.78	11.66	0.30	2.97	0.20	2.36	52.93
Placitas nr.	1913	7.24	5.59	2.39	---	---	---	---	---	---	---	---	---	---
Median		3.63	5.59	2.57	3.80	2.11	5.88	14.44	7.30	2.92	5.44	1.91	2.36	60.53

Location	Year	Jan	Feb	Mar	Apr	May	Jun	Jul	Aug	Sep	Oct	Nov	Dec	Annual
Van Huss Ranch	1944	---	---	---	---	---	---	8.56	7.42	2.74	5.03	1.65	4.42	---
Van Huss Ranch	1945	1.98	0.51	5.51	2.13	0.00	0.18	2.34	8.97	1.30	2.34	0.00	1.85	27.10
Van Huss Ranch	1946	0.00	0.51	1.14	2.18	0.97	0.00	2.18	5.08	1.73	1.91	6.22	0.41	22.33
Van Huss Ranch	1947	0.00	0.89	0.51	0.00	2.79	0.28	1.17	5.26	3.58	0.81	2.24	2.54	20.07
Van Huss Ranch	1948	1.02	---	---	---	---	---	---	---	---	---	---	---	---
Van Huss Ranch	1950	---	---	---	---	0.00	3.18	8.20	3.61	4.09	0.48	0.00	0.00	---
Van Huss Ranch	1951	0.81	1.02	0.58	---	---	---	---	---	---	---	---	---	---
Median		0.81	0.70	0.86	2.13	0.48	0.23	2.34	5.26	2.74	1.91	1.65	1.85	24.71

APPENDIX C. GENERAL CHEMISTRY ANALYSES

Appendix C. General chemistry of ground- and surface-water samples. Page 1 of 6.

Site ID	Sample Date	Ca^{2+} ppm	Mg^{2+} ppm	Na^{+} ppm	K^{+} ppm	HCO_3^{-} ppm	CO_3^{2-} ppm	Cl^{-} ppm	SO_4^{2-} ppm	NO_3^{-} ppm	SiO_2 ppm
PS-01	4/26/96	88	6.1	5	1	270	0	11	16	2	12
PS-02	4/26/96	83	5.5	4	0.85	260	0	13	13	1.4	12
PS-03	4/26/96	88	5.9	5	0.9	260	0	17	19	1.8	11
PS-03	4/26/96	87	5.9	5.1	0.85	260	0	17	21	1.5	11
PS-04	4/26/96	96	7	7.5	0.75	270	0	23	27	2	11
PS-05	5/28/96	96	5.6	3.3	0.77	280	0	12	21	1.4	10
PS-05#	6/18/96	106	5.66	3.5	0.9	326		2.22	19.5	0.33	10.6
PS-05#	6/18/96	108	5.68	3.5	0.9	325		2.22	19.5	0.33	10.7
PS-06	5/29/96	76	8.4	8.6	1.3	242	0	7	29	0	13
PS-07	5/30/96	58	8.4	32	1.8	260	0	7.6	32	1.1	13
PS-08	5/30/96	75	9	19	0.67	246	0	16	38	2.8	13
PS-09	5/15/98	85	6.2	3.1	0.6	278		2.4	18	1.1	15
PS-10	7/17/97	82	9.6	40	2.8	332		14	41	1.2	15
PS-11	7/23/97	77	11	32	2.2	318		12	34	0.9	14
PS-17	9/10/97	73	9	32	1.9	300		7.6	32	0.96	16
PS-19	2/13/98	200	46	110	1.8	340		55	585	1	21
PSW-01	3/11/97	121	28	45	5.1	237		43	252	0	15
PSW-02	5/6/97	53	5.4	4	0.7	175		2	20	0	12
PSW-03	9/ 1/97	70	5	7	0.72	228		13	10	1.2	11
PSW-04	9/13/97	91	8.1	13	0.8	290		21	27	0	14
PSW-05	9/13/97	37	8.2	20	1	137		22	30	0.2	16
PSW-06	1/ 1/98	70	17	50	2.4	335		12	70	0.51	15
PSW-07	1/ 1/98	92	10	21	0.9	315		18	38	0.72	12
PW-001	4/26/96	150	39	30	2	400	0	25	220	0.8	27
PW-002	5/28/96	85	17	12	3.8	280	0	15.5	46	0	14
PW-003	5/28/96	75	6.8	6.8	0.93	220	0	19	16	3.6	10.7

Data sources are (*) analyses conducted at the request of the owner by independent labs, (#) the US Geological Survey (N. Plummer, unpubl., 1997), (+) US dept. Health and Human Services, OEH&E, Indian Health Service, unmarked samples collected by the New Mexico Bureau of Mines and Mineral Resources for this study.

Site ID	Sample Date	Ca^{2+} ppm	Mg^{2+} ppm	Na^{+} ppm	K^{+} ppm	HCO_3^{-} ppm	CO_3^{2-} ppm	Cl^{-} ppm	SO_4^{2-} ppm	NO_3^{-} ppm	SiO_2 ppm
PW-004	7/24/97	95	8	5	1	310		13	15	0.64	14
PW-005	5/30/96	81	23	6.2	1.4	290	0	6.2	61	0.27	12
PW-006	10/29/97	415	41	45	6.2	255		0	1100	2.5	11
PW-007	5/30/96	340	130	470	5.8	270	0	230	1900	0.73	17
PW-008	5/30/96	86	7.6	9.8	0.9	270	0	5.4	29	8.5	14
PW-012	12/19/97	118	18	20	1.2	370		37	53	15	20
PW-012	12/19/97	82	18	21	1.2	275		32	51	15	19
PW-014	7/16/97	12.5	5.1	778	3.3	573		15.5	1152	0	9
PW-016	1/ 3/98	180	160	550	7.1	215		25	1980	0.4	13
PW-023*	3/29/93			461					1490	0.49	
PW-023*	4/ 6/93	740	280						1550	2.8	48
PW-023*	4/23/93	830	270						2125	1.7	48
PW-023*	6/ 1/93	914	352						2100	0.4	69
PW-023*	6/ 9/93	873	297						3550	0.1	22.3
PW-023*	5/ 9/95	392	69.8	290		218	0				
PW-024	8/ 4/97	78	7.1	16	0.64	254		17	33	0.65	12
PW-030	8/11/97	1.2	0.6	200	2.3	405		23	82	2.46	9
PW-030	8/11/97	1.3	0.62	198	2.3	405		23	82	2.6	9
PW-039	8/25/97	160	12	76	2.8	285		5	380	1	12
PW-041	11/18/97	326.5	58	68.5	5.1	325		6.5	910	0.38	22
PW-043	7/18/97	12	2.2	455	3	475		8	635	0.2	12
PW-044	7/18/97	38	11	152	1.8	361		16	160	0.4	16

Data sources are (*) analyses conducted at the request of the owner by independent labs, (#) the US Geological Survey (N. Plummer, unpubl., 1997), (+) US dept. Health and Human Services, OEH&E, Indian Health Service, unmarked samples collected by the New Mexico Bureau of Mines and Mineral Resources for this study.

Appendix C continued. Page 3 of 6.

Site ID	Sample Date	Ca^{2+} ppm	Mg^{2+} ppm	Na^{+} ppm	K^{+} ppm	HCO_3^{-} ppm	CO_3^{2-} ppm	Cl^{-} ppm	SO_4^{2-} ppm	NO_3^{-} ppm	SiO_2 ppm
PW-045	7/18/97	96	19	36	6.1	315		12	108	0	11
PW-046	8/24/97	105	22	50	1.3	260		45	190	3	17
PW-047	11/18/97	123	34	262	4.2	360		38	640	0.6	19
PW-051	7/18/97	82	6.5	8	1.1	246		14	18	5.5	11
PW-063	11/18/97	225	96	110	3.5	400		60	800	0	24
PW-071	7/16/97	65	40	49	4.5	405		8	105	0	24
PW-073	1/15/98	4.6	0.8	155	0.41	250	16	29	63	6.8	14
PW-077#	6/19/97	84.4	16.7	54.2	2.59	332		20.1	92.6	0.33	21.2
PW-077	7/16/97	80	15.4	53.8	2	335		18	82	1.5	21
PW-078	8/ 4/97	395	62	415	16	271		48	1730	0.65	20
PW-082	7/16/97	74	9.1	35	1.7	308		12	38	1.2	17
PW-084	7/18/97	60	12	30	1.5	265		8	36	1.2	29
PW-085	9/ 3/97	56	10	14	1.5	158		7	65	0.25	22
PW-087	7/23/97	66	19	37	3.2	330		10	35	0	13
PW-089	7/16/97	73	12	34	2	318		8	42	0.8	15
PW-090	8/ 3/97	82	8.3	37	1.4	329		7.8	43	2.55	18
PW-091	9/ 4/97	71	15	44	2.6	310		9.4	70	1.32	14
PW-094	7/24/97	86	19	38	1.8	300		27	98	0.56	12
PW-095*	12/20/94	57.5	42.9	192	12.6			30.1	248	0.16	28
PW-095	10/28/97	69	61	230	9.3	588		30	410	0	21
PW-096*	1/ 6/95	98.6	45.8	80	7.15			39.6	300	0.31	1.4
PW-097	7/25/97	74	10	22	1	285		10	32	1.4	19
PW-099	7/25/97	74	16	146	4.1	258		11	321	0.83	12

Data sources are (*) analyses conducted at the request of the owner by independent labs, (#) the US Geological Survey (N. Plummer, unpubl., 1997), (+) US dept. Health and Human Services, OEH&E, Indian Health Service, unmarked samples collected by the New Mexico Bureau of Mines and Mineral Resources for this study.

Appendix C continued. Page 4 of 6.

Site ID	Sample Date	Ca^{2+} ppm	Mg^{2+} ppm	Na^{+} ppm	K^{+} ppm	HCO_3^{-} ppm	CO_3^{2-} ppm	Cl^{-} ppm	SO_4^{2-} ppm	NO_3^{-} ppm	SiO_2 ppm
PW-100	9/ 4/97	81	5.7	9	1	270		12	10	2.3	13
PW-101	9/ 1/97	86	5.1	7	0.82	275		14	12	1	11
PW-103	8/22/97	21	8.5	1273	6.1	741		138	1990	4	10
PW-107	8/12/97	111	30	102	2	353		110	182	1.4	18
PW-108	8/12/97	76	6.4	19	0.64	250		14	39	1.1	14
PW-109	8/12/97	146	35	73	2.3	331		24.3	359	1.1	20
PW-110	8/12/97	65	9	36	1.5	294		3	40	2.44	20
PW-112	9/ 5/97	57	13	665	8.9	380		13	1310	1.5	12
PW-113	9/ 5/97	386	46	1445	6.3	71		118	3910	0.96	11
PW-116*	1/ 1/25	125	11.7	39	3.48	386	0	13.5	61		
PW-118*	11/11/94	35.9	48.9	65	8.33			51.8	55	0.99	0.96
PW-119*	12/ 5/94	42.5	36.1	47.7	6.9			22.5	121	0.59	31.1
PW-119	10/28/97	50	41	94	5.2	410		24	135	3.8	22
PW-119	10/28/97	49	42	91	5.2	414		23	130	3.8	22
PW-120*	1/30/95	56.8	35.5	37.5	5.83			24.6	17.9	1.34	23.8
PW-122	8/30/97	21	5.2	230	6.2	412		0	255	0.4	13
PW-126	9/15/97	403	10	19	1.9	239		12	865	0	22
PW-130	8/23/97	86	22	24	1.7	340		11	74	1.3	26
PW-131	7/21/97	94	21	31	1.6	230		25	170	0.8	20
PW-132	8/21/97	55	7	40	2.6	225		22	48	0.35	45
PW-133*	4/23/87	92.7	12.1	33.2		204	0	16.4	180	0.49	
PW-135	8/31/97	56	11	23	3.2	230		0	53	0.75	36
PW-137	9/10/97	36	19	30	3.7	255		0	29	0	25

Data sources are (*) analyses conducted at the request of the owner by independent labs, (#) the US Geological Survey (N. Plummer, unpubl., 1997), (+) US dept. Health and Human Services, OEH&E, Indian Health Service, unmarked samples collected by the New Mexico Bureau of Mines and Mineral Resources for this study.

Appendix C continued. Page 5 of 6.

Site ID	Sample Date	Ca^{2+} ppm	Mg^{2+} ppm	Na^{+} ppm	K^{+} ppm	HCO_3^{-} ppm	CO_3^{2-} ppm	Cl^{-} ppm	SO_4^{2-} ppm	NO_3^{-} ppm	SiO_2 ppm
PW-138	9/10/97	0.28	0.1	31	274	233		16	199	0	53
PW-142	8/26/97	46	7.5	26	1.8	210		7	25	2	24
PW-143	8/25/97	24	14.4	105	3.4	185		28	165	10.2	15
PW-145	9/ 1/97	79	28	4.5	1.2	314		0	72	0.25	11
PW-147	1/ 8/98	178	43	122	1.8	345		65	520	1.7	23
PW-149	9/13/97	39	17	221	3	260		20	396	0	20
PW-150	9/15/97	35	9.3	64	2.5	190		12	89	2.6	19
PW-152	9/17/97	77	6.4	15	0.65	224		19	38	0.88	13
PW-153*	8/30/95	1100	150						1950	2.2	110
PW-153*	4/13/96								6200	4.6	31
PW-154	12/ 4/97	88	12	13	2.3	310		20	20	7.5	11
PW-161*	1/24/95									0	
PW-161	12/ 3/97	60	24	54	4.6	330		11	90	1.26	18
PW-162	1/ 8/98	63	7.8	64	4.1	255		37	74	1.5	54
PW-163	1/10/98	68	3.8	12	0.8	175		15	44	3.5	12
PW-164	1/17/98	75	11	7.2	1.4	270		6	15	12	13
PW-166	1/24/98	36	18	46	4.8	225	0	4	70	2.3	20
PW-167	1/19/98	45	16	18	3.2	255		4.2	25	0.65	27
PW-167	1/19/98	44	16	17	3.2	240		3.8	20	3.8	27
PW-169	1/19/98	96	14	26	1	230		23	129	2.7	15
PW-173	1/24/98	61	4.6	45	3.4	225	0	28	40	1	49
PW-179	1/24/98	49	11	19	1.6	210	0	6	25	1.9	20
PW-184	1/23/98	111	27	26.5	1.5	210	0	17	245	3	21

Data sources are (*) analyses conducted at the request of the owner by independent labs, (#) the US Geological Survey (N. Plummer, unpubl., 1997), (+) US dept. Health and Human Services, OEH&E, Indian Health Service, unmarked samples collected by the New Mexico Bureau of Mines and Mineral Resources for this study.

Appendix C continued. Page 6 of 6.

Site ID	Sample Date	Ca^{2+} ppm	Mg^{2+} ppm	Na^{+} ppm	K^{+} ppm	HCO_3^{-} ppm	CO_3^{2-} ppm	Cl^{-} ppm	SO_4^{2-} ppm	NO_3^{-} ppm	SiO_2 ppm
PW-186*	8/15/95			137					182	1.8	
PW-186	2/ 4/98	40	12	112	5.3	215		18	190	11	17
PW-191*	4/17/96									0.1	
PW-191*	2/ 5/97	43	19	21	3.4	250	0	0	37	0	
PW-191	2/17/98	38	18	26	3.1	250		0	30	1.2	26
PW-192*	4/17/96									0.1	
PW-192*	2/ 5/97	53	13	12	2.1	243	0	0	21	0.1	
PW-197	1/23/98	38	7.8	43	13	200	0	25	30	4.2	76
PW-198	1/23/98	41	4.5	65	13	198	0	51	33	1.6	74
PW-202	1/23/98	94	17	21	1.5	235	0	12	127	1.9	19
PW-203	2/12/98	70	6.2	16	0.7	235		10	35	2	13
PW-204	2/12/98	58	4.9	45	3.7	260		18	36	1.7	53
PW-205	12/23/96	50.5	3.8	55.9	10	163	0	28	33.9	0.5	
PW-205	2/13/98	33	4	49	11	215		18	20	2.9	74
PW-206*	8/ 5/96	61	7.41	41.7	1.18	246	0	7.27	38.7	0.62	10.2
PW-211#	8/23/96	61.1	6.5	14.7	1.8			3.5	31.3	0.27	35.1
PW-212*	2/1/94	427	103	311		334		23	2180	0.03	
PW-213+	12/23/96	82.8	6.4	52.7	5.8	220	0	24.6	48.4	.3	
PW-215#	8/23/96	65.2	4.79	44.1	4.5			22.8	42.6	0.35	56.5
PW-216#	8/17/96	60.7	13.4	31.6	2			7.53	35.9	0.26	26.1
PW-217*	9/29/89	47.4	3.55	16.4		237	0	12.1	24	0.49	
PW-218#	6/19/97	74.3	4.31	10.4	1.31			7.5	58.4	0.75	27

Data sources are (*) analyses conducted at the request of the owner by independent labs, (#) the US Geological Survey (N. Plummer, unpubl., 1997), (+) US dept. Health and Human Services, OEH&E, Indian Health Service, unmarked samples collected by the New Mexico Bureau of Mines and Mineral Resources for this study.

APPENDIX D. STABLE ISOTOPE AND FIELD PARAMETER ANALYSES

Appendix D. Stable isotope and field parameters. Page 1 of 6.

Site ID	Sample Date	δ^2H °/oo	$\delta^{18}O$ °/oo	Temp °C (field)	DO ppm (field)	pH (field)	Sp. Cond µS/cm @ 25°C (field)	pH (lab)	Cond µS/cm (lab)	TDS ppm	Hardness ppm
PS-01	4/26/96	-95	-11.9					7.3	420	276	245
PS-02	4/26/96	-89	-12.0					7.3	400	263	230
PS-03	4/26/96	-92	-12.1					7.3	430	279	244
PS-03	4/26/96							7.3	420	280	242
PS-04	4/26/96	-90	-12.1					7.5	460	310	269
PS-05	5/28/96	-93	-12.1					7.41	430	291	263
PS-05#	6/18/96			12.9	6.20	7.5	381				
PS-05#	6/18/96			12.9	5.20	7.4	407				
PS-06	5/29/96	-80	-11.3					7.4	400	264	224
PS-07	5/30/96	-93	-11.9					8.26	450	285	179
PS-08	5/30/96	-95	-12.1	17.3		8.1		8.06	500	297	224
PS-09	5/15/98	-93	-12.2	16.7	5.17	7.79	417			260	238
PS-10	5/ 1/98	-90	-11.8	23.4	2.45	7.2	582				
PS-11	7/23/97	-90	-11.8	21.1	1.8	7.2	559		440	330	238
PS-17	9/10/97	-90	-11.5		2.83	7.17	559			320	219
PS-19	2/13/98	-83	-11.7	13.2	5.43	6.92	1740	6.9	1740	1170	689
PSW-01	3/11/97	-92	-11.5					8.0	800	630	417
PSW-02	5/6/97	-87	-11.8					7.9	270	170	155
PSW-03	9/ 1/97	-93	-11.7	13.9	6.13	8.43	419		350	230	195
PSW-04	9/13/97	-90	-12.0	20.9	4.66	7.93	560			310	261
PSW-05	9/13/97	-83	-10.4	28.8	5.56	8.58	352			190	126
PSW-06	1/ 1/98	-89	-11.7	2.6	8.55	8.32	696	7.7	620	410	245
PSW-07	1/ 1/98	-93	-12.1	10.2	5.40	7.35	607	7.3	550	340	271
PW-001	4/26/96	-90	-11.3					7.1	990	695	535
PW-002	5/28/96	-89	-11.9					7.16	550	334	282
PW-003	5/28/96	-93	-11.8					7.34	410	249	215

Data sources are (*) analyses conducted at the request of the owner by independent labs, (#) the US Geological Survey (N. Plummer, unpubl., 1997), (+) US dept. Health and Human Services, OEH&E, Indian Health Service, unmarked samples collected by the New Mexico Bureau of Mines and Mineral Resources for this study.

Appendix D continued. Page 2 of 6.

Site ID	Sample Date	δ^2H °/oo	$\delta^{18}O$ °/oo	Temp °C (field)	DO ppm (field)	pH (field)	Sp. Cond µS/cm @ 25°C (field)	pH (lab)	Cond µS/cm (lab)	TDS ppm	Hardness ppm
PW-004	7/24/97	-93	-11.6	17.9	7.19	7.29	520		420	290	270
PW-005	5/30/96							7.27	500	336	297
PW-005	4/27/98	-89	-12.2	14.1	2.43	7.35	574				
PW-006	10/29/97	-82	-11.9	13.6	2.32	7.02	2180	7.4	1500	1740	1205
PW-007	5/30/96	-84	-11.8					7.24	3250	3229	1384
PW-008	5/30/96	-90	-12.1					7.39	450	297	246
PW-012	12/19/97	-85	-11.7	12.5	3.41	7.3	833	6.9	750	450	369
PW-012	12/19/97							7.1	690	360	279
PW-014	7/16/97	-95	-12.6	18.1	0.71	8.11	3610		3000	2250	52
PW-016	1/ 3/98	-92	-12.7	17.0	0.98	7.34	4210	7.1	3700	3010	1108
PW-023*	4/ 6/93							9		1631	1020
PW-023*	4/23/93							8.2		1641	1100
PW-023*	6/ 1/93							8.6		1637	1266
PW-023*	6/ 9/93							8.2		1645	1170
PW-023*	5/ 9/95							7.4	2800	1680	1265
PW-024	8/ 4/97	-92	-11.4	17.1	11.63	7.68	490		430	280	224
PW-030	8/11/97	-95	-12.5	17.9	1.47	8.95	857		780	510	5
PW-030	8/11/97								760	520	6
PW-039	8/25/97	-100	-12.5	14.9	0.99	7.46	1153			780	449
PW-039	5/ 5/98			14.5	0.60	7.41	1175				
PW-041	11/18/97	-96	-12.0	17.0	2.14	6.88	2000	6.7	1850	1540	1054
PW-041	4/27/98			17.6	0.32	6.77	2010				
PW-043	7/18/97	-97	-13.1	25.1	1.27	8.4	2150		2000	1350	39
PW-044	7/18/97	-88	-11.5	17.3	2.99	7.85	895		850	560	140

Data sources are (*) analyses conducted at the request of the owner by independent labs, (#) the US Geological Survey (N. Plummer, unpubl., 1997), (+) US dept. Health and Human Services, OEH&E, Indian Health Service, unmarked samples collected by the New Mexico Bureau of Mines and Mineral Resources for this study.

Appendix D continued. Page 3 of 6.

Site ID	Sample Date	δ^2H o/oo	$\delta^{18}O$ o/oo	Temp °C (field)	DO ppm (field)	pH (field)	Sp. Cond µS/cm @ 25°C (field)	pH (lab)	Cond µS/cm (lab)	TDS ppm	Hardness ppm
PW-045	7/18/97	-91	-12.0	20.1	3.22	7.29	705		650	440	318
PW-046	8/24/97	-98	-12.0	17.5	6.18	7.58	899			560	353
PW-047	11/18/97	-97	-11.9	13.3	2.62	7.24	2010	7.2	1800	1280	447
PW-051	7/18/97	-98	-12.5	14.9	6.48	7.46	484		440	260	232
PW-063	11/18/97	-97	-11.9	16.0	1.90	6.91	2070	6.8	1900	1490	957
PW-071	7/16/97	-97	-12.3	18.4	1.22	7.41	786		700	470	327
PW-071	4/28/98			17.5	0.55	7.31	801				
PW-073	1/15/98	-90	-11.4	15.1	4.12	8.83	773	8.9	680	390	15
PW-073	4/27/98			16.1	5.26	8.92	774				
PW-077#	6/19/97			16.1	5.80	7.3	714				
PW-077	7/16/97	-87	-11.7	16.2	4.40	7.35	745		600	420	263
PW-078	8/ 4/97	-98	-12.2	19.0	4.45	7.21	3360		2900	2800	1242
PW-082	7/16/97	-89	-12.2	17.2	4.38	7.34	560		460	330	222
PW-084	7/18/97	-88	-11.1	18.7	6.38	7.45	492		460	280	199
PW-085	9/ 3/97	-91	-11.6	16.9	1.18	7.3	578		470	230	181
PW-087	7/23/97	-91	-11.6						470	340	243
PW-089	7/16/97	-91	-12.2						450	330	232
PW-089	4/30/98			18.6	1.53	7.18	558				
PW-090	8/ 3/97	-92	-12.2	16.8	7.98	7.43	562		500	350	239
PW-091	9/ 4/97	-94	-11.2	18.1	3.25	7.36	664			370	239
PW-094	7/24/97	-91	-12.5	17.6	4.72	7.52	647		550	420	293
PW-095*	12/20/94					7.22	2500	7.2	2500		
PW-095	10/28/97	-106	-12.7	15.7	1.85	7.41	1715	7.2	1980	1100	423
PW-096*	1/ 6/95					6.85	1760	6.9	1760		
PW-097	7/25/97	-92	-11.4	17.5	5.59	7.45	542		490	290	226
PW-099	7/25/97	-91	-12.0	17.1	1.13	8.03	1106		900	700	251

Data sources are (*) analyses conducted at the request of the owner by independent labs, (#) the US Geological Survey (N. Plummer, unpubl., 1997), (+) US dept. Health and Human Services, OEH&E, Indian Health Service, unmarked samples collected by the New Mexico Bureau of Mines and Mineral Resources for this study.

Appendix D continued. Page 4 of 6.

Site ID	Sample Date	δ^2H o/oo	$\delta^{18}O$ o/oo	Temp °C (field)	DO ppm (field)	pH (field)	Sp. Cond µS/cm @ 25°C (field)	pH (lab)	Cond µS/cm (lab)	TDS ppm	Hardness ppm
PW-100	9/ 4/97	-95	-11.6	13.6	6.90	7.52	486			260	226
PW-101	9/ 1/97	-93	-11.7	13.9	5.68	7.44	481		400	270	236
PW-103	8/22/97	-104	-12.5	21.0	2.85	7.99	5710			3820	87
PW-103	5/14/98			16.8	1.69	7.99	5700				
PW-107	8/12/97	-97	-12.3	16.0	5.76	7.65	1188			720	401
PW-108	8/12/97	-90	-11.9	17.6	6.97	7.47	524			280	216
PW-109	8/12/97	-91	-12.1	16.9	2.21	7.37	1197			810	509
PW-109	4/28/98			16.7	0.65	7.2	1229				
PW-110	8/12/97	-86	-12.1	16.4	4.63	7.44	551			300	199
PW-112	9/ 5/97	-97	-12.4	18.0	1.57	7.87	3220			2260	196
PW-113	9/ 5/97	-98	-12.8	17.1	1.86	8.1	6860			5950	1153
PW-116*	1/ 1/25							7.3	730	488	360
PW-118*	11/11/94					7.29	1280	7.3	1280		
PW-119*	12/ 5/94					6.94	1140	6.9	1140		
PW-119	10/28/97	-95	-10.5	17.4	1.65	7.3	944	7.1	880	560	294
PW-119	10/28/97							7.1	890	550	295
PW-120*	1/30/95					7.22	1130	7.2	1130		
PW-122	8/30/97	-95	-10.5	16.4	1.96	8.03	1186		1000	740	74
PW-126	9/15/97	-92	-11.9	17.1	1.60	7.05	1794			1430	1048
PW-130	8/23/97	-92	-11.8	19.2	5.41	7.3	689		652	420	305
PW-131	7/21/97	-87	-11.4	16.4	5.90	7.59	775		722	460	321
PW-132	8/21/97	-96	-12.4	21.9	4.01	7.54	507		472	290	166
PW-133*	4/23/87							7.5	790	472	281
PW-135	8/31/97	-89	-11.2	22.1	4.20	7.68	453		380	260	185
PW-137	9/10/97	-89	-11.7	21.3	5.16	7.67	466			270	168

Data sources are (*) analyses conducted at the request of the owner by independent labs, (#) the US Geological Survey (N. Plummer, unpubl., 1997), (+) US dept. Health and Human Services, OEH&E, Indian Health Service, unmarked samples collected by the New Mexico Bureau of Mines and Mineral Resources for this study.

Appendix D continued. Page 6 of 6.

Site ID	Sample Date	δ^2H °/oo	$\delta^{18}O$ °/oo	Temp °C (field)	DO ppm (field)	pH (field)	Sp. Cond µS/cm @ 25°C (field)	pH (lab)	Cond µS/cm (lab)	TDS ppm	Hardness ppm
PW-186	2/ 4/98	-91	-10.5	14.6	5.95	7.77	874	7.8	874	500	149
PW-191*	2/ 5/97							8	470	288	186
PW-191	2/17/98	-91	-12.3	19.0	4.89	7.47	453	7.5	453	240	169
PW-192*	2/ 5/97							8	423	260	186
PW-197	1/23/98	-99	-12.3	24.7	1.59	7.46	516	7.5	516	260	127
PW-198	1/23/98	-93	-12.1	25.6	2.13	7.33	610	7.3	610	310	121
PW-202	1/23/98	-93	-12.1	16.2	6.04	7.3	703	7.3	703	390	305
PW-203	2/12/98	-93	-12.1	15.1	5.70	7.22	474	7.2	474	270	200
PW-204	2/12/98	-93	-12.1	25.5	2.99	7.38	554	7.4	554	300	165
PW-205	12/23/96							7.8	481	234	142
PW-205	2/13/98	-93	-12.1	24.7	5.41	7.4	469	7.4	469	250	99
PW-206*	8/ 5/96							7.4	588	345	183
PW-211#	8/23/96			20.6	4.30	7.5	385				
PW-212*	2/1/94							7	3800	3140	
PW-213+	12/23/96							7.6	586	268	233
PW-215#	8/23/96			25.6	1.90	7.3	543				
PW-216#	8/17/96			17.4	6.80	7.1	490				
PW-217*	9/29/89							8.1	480	240	133
PW-218#	6/19/97			19.1	8.20	7.5	455	7.5	455		

Data sources are (*) analyses conducted at the request of the owner by independent labs, (#) the US Geological Survey (N. Plummer, unpubl., 1997), (+) US dept. Health and Human Services, OEH&E, Indian Health Service, unmarked samples collected by the New Mexico Bureau of Mines and Mineral Resources for this study.

APPENDIX E. TRACE CONSTITUENT ANALYSES

Appendix E. Trace constituents. Page 1 of 6.

Site ID	Sample Date	As ppb	Cu ppb	F ppm	Fe ppm	Mn ppb	Zn ppb	Al ppm	Ba ppb	Be ppb	Cd ppb	Cr ppb	Co ppb	Pb ppb	Mo ppb	Ni ppb	Se ppb	Ag ppb
PS-01	4/26/96	0	0	0.3	0.022	0	0	0	0	0	0	0		0	0	0	0	0
PS-02	4/26/96	0	0	0.3	0.015	0	0	0	0	0	0	0	15	0	0	0	0	0
PS-03	4/26/96	0	0	0.3	0.026	0	0	0	0	0	0	0		0	0	0	0	0
PS-03	4/26/96	0	0	0.3	0.02	0	0	0	0	0	0	0		0	0	0	0	0
PS-04	4/26/96	0	0	0.35	0.023	0	0	0	0	0	0				0	0	0	0
PS-05	5/28/96	0	0	0.45	0	0	0	0			0	0	0	0	0	0	0	0
PS-05#	6/18/96	0	0	0.41	0.051	6		0.004	215			0		1.7	0			
PS-05#	6/18/96	0	4	0.41	0.06	7		0.004	219			0		1.7	0			
PS-06	5/29/96	0	0	0	0.004	0	0	0			0	0	0	0	0	0	0	0
PS-07	5/30/96	0	0	0.82	0.019	0	0	0			0	0	0	0	0	0	0	0
PS-08	5/30/96	0	1	0.33	0.008	0	0	0			0	0	0	0	0	0	0	0
PS-09	5/15/98	12	7	0.4	0.083	240	0											
PS-10	7/17/87	0	1.6	1	0	0	0											
PS-11	7/23/97	0	3	0.8	0	7	90											
PS-17	9/10/97	3.5	0	0.65	0.102		0											
PS-19	2/13/98	0	0	0.36	0.049	9	0											
PSW-01	3/11/97	0	0	0.25	0.066	9.9	0									0		
PSW-02	5/6/97	0	0	0.32	0	0	0							0				
PSW-03	9/ 1/97	0	4.2	0.3	0	9	0											
PSW-04	9/13/97	0	0	0.32	0.018	17	0											
PSW-05	9/13/97	0	3.6	0.38	0.05	3.3	0											
PSW-06	1/ 1/98	0	0	0.9	0.057	62	0											
PSW-07	1/ 1/98	0	0	0.34	0.1	54	0											
PW-001	4/26/96	0	0	1.00	0.029	0	120	0	0	0	0	0		0	0	0	0	0
PW-002	5/28/96	0	0	0.65	2.8	68	200	0			0	0	0	0	0	0	0	0
PW-003	5/28/96	0	0	0.39	0.003	0	0	0			0	0	0	0	0	0	0	0

Data sources are (*) analyses conducted at the request of the owner by independent labs, (#) the US Geological Survey (N. Plummer, unpubl., 1997), (+) US dept. Health and Human Services, OEH&E, Indian Health Service, unmarked samples collected by the New Mexico Bureau of Mines and Mineral Resources for this study.

Appendix E continued. Page 2 of 6.

Site ID	Sample Date	As ppb	Cu ppb	F ppm	Fe ppm	Mn ppb	Zn ppb	Al ppm	Ba ppb	Be ppb	Cd ppb	Cr ppb	Co ppb	Pb ppb	Mo ppb	Ni ppb	Se ppb	Ag ppb
PW-004	7/24/97	0	4	0.3	0.09	14	50											
PW-005	5/30/96	17	0	0.29	1.7	22.5	70	0			0	0	0	0	0	0	0	0
PW-006	10/29/97	12	0	1.00	0.94	78	10											
PW-007	5/30/96	0	0	0.58	0.104	5.2	60	0			0	0	0	0	0	0	0	0
PW-008	5/30/96	0	0	0.44	0.007	0	40	0			0	0	0	0	0	0	0	0
PW-012	12/19/97	0	1.5	0.35	0.200	14	30											
PW-012	12/19/97	0	1.3	0.42	0.150	10	30											
PW-014	7/16/97	0	5	1.3	0.34	26	80											
PW-016	1/ 3/98	0	2.5	1.6	0.52	62	1300											
PW-023*	3/29/93	0		0.37	4.64				0		7	33		0			0	25
PW-023*	4/ 6/93				6.32	1.4												
PW-023*	4/23/93				6.6													
PW-023*	6/ 1/93				0.3													
PW-023*	6/ 9/93				0.34													
PW-024	8/ 4/97	0	8	0.17	0	0	0											
PW-030	8/11/97	5.4	13	0.68	0	0	0											
PW-030	8/11/97	0	13	0.68	0	0	0											
PW-039	8/25/97	0	13	0.5	0	18	0											
PW-041	11/18/97	0	4	0.2	0.64	120	0											
PW-043	7/18/97	0	0	1.3	0	7	0											
PW-044	7/18/97	0	1	0.8	0.14	12	40											

Data sources are (*) analyses conducted at the request of the owner by independent labs, (#) the US Geological Survey (N. Plummer, unpubl., 1997), (+) US dept. Health and Human Services, OEH&E, Indian Health Service, unmarked samples collected by the New Mexico Bureau of Mines and Mineral Resources for this study.

Site ID	Sample Date	As ppb	Cu ppb	F ppm	Fe ppm	Mn ppb	Zn ppb	Al ppm	Ba ppb	Be ppb	Cd ppb	Cr ppb	Co ppb	Pb ppb	Mo ppb	Ni ppb	Se ppb	Ag ppb
PW-045	7/18/97	14	1	1.2	0.9	43	60											
PW-046	8/24/97	0	0	0.3	0	0	22											
PW-047	11/18/97	0	43	0.68	0.106	27	34											
PW-051	7/18/97	0	0	0.3	0.16	0	0											
PW-063	11/18/97	0	21	0.2	0.92	140	26											
PW-071	7/16/97	0	0	0.58	0.21	24	0											
PW-073	1/15/98	0	0	0.47	0.004	11	26											
PW-077#	6/19/97	0	2	1.21	0.237	1	21	0.004	45.2			0		0.3	4.6			
PW-077	7/16/97	0	0	0.79	0.03	6	0											
PW-078	8/ 4/97	0	6	0.5	0.42	370	0											
PW-082	7/16/97	0	0	0.75	0	0	0											
PW-084	7/18/97	0	0	1.0	0	3	0											
PW-085	9/ 3/97	0	16	0.3	0.6	33	24											
PW-087	7/23/97	0	0	1.2	0.32	17	0											
PW-089	7/16/97	0	0	0.68	0.14	18	30											
PW-090	8/ 3/97	0	4	0.61	0	5	0											
PW-091	9/ 4/97	0	3	0.7	0.055	3.8	0											
PW-094	7/24/97	0	0	0.6	0	7	40											
PW-095*	12/20/94			1.37	0	0												
PW-095	10/28/97	4.2	0	0.65	0.21	12	0											
PW-096*	1/ 6/95			0.7	0	0												
PW-097	7/25/97	0	5	0.6	0	5	0											
PW-099	7/25/97	0	6	0.3	2	130	30											

Data sources are (*) analyses conducted at the request of the owner by independent labs, (#) the US Geological Survey (N. Plummer, unpubl., 1997), (+) US dept. Health and Human Services, OEH&E, Indian Health Service, unmarked samples collected by the New Mexico Bureau of Mines and Mineral Resources for this study.

Appendix E continued. Page 4 of 6.

Site ID	Sample Date	As ppb	Cu ppb	F ppm	Fe ppm	Mn ppb	Zn ppb	Al ppm	Ba ppb	Be ppb	Cd ppb	Cr ppb	Co ppb	Pb ppb	Mo ppb	Ni ppb	Se ppb	Ag ppb
PW-100	9/ 4/97	0	3.3	0.22	0.22	60	0											
PW-101	9/ 1/97	0	3.6	0.3	0	3	20											
PW-103	8/22/97	0	270		0	12	990											
PW-107	8/12/97	0	2	0.13	0	0	0											
PW-108	8/12/97	0	4	0.2	0	0	340											
PW-109	8/12/97	0	1	0.31	0.21	55	0											
PW-110	8/12/97	0	0	0.49	0	0	0											
PW-112	9/ 5/97	21	9.4	1.5	0.135	50	14											
PW-113	9/ 5/97	16	6.8		0.058	100	110											
PW-116*	1/ 1/25				0													
PW-118*	11/11/94			1.07	0	0												
PW-119*	12/ 5/94			0.52	0.83	0												
PW-119	10/28/97	3.1	0	0.29	0.05	38	1100											
PW-119	10/28/97	3.0	0	0.34	0.05	38	1100											
PW-120*	1/30/95			0.39	0	0												
PW-122	8/30/97	0	4.9	0.84	0	75	0											
PW-126	9/15/97	0	5.5	0.3	0.2	23	0											
PW-130	8/23/97	0	9	0.4	0	0	1100											
PW-131	7/21/97	0	0	0.5	0	0	19											
PW-132	8/21/97	9.8	3.4	0.3	0	0	550											
PW-133*	4/23/87			0.6	0	0												
PW-135	8/31/97	13	8	0.5	0	0	470											
PW-137	9/10/97	5.1	75	0.4	0.036	3.2	460											

Data sources are (*) analyses conducted at the request of the owner by independent labs, (#) the US Geological Survey (N. Plummer, unpubl., 1997), (+) US dept. Health and Human Services, OEH&E, Indian Health Service, unmarked samples collected by the New Mexico Bureau of Mines and Mineral Resources for this study.

Appendix E continued. Page 5 of 6.

Site ID	Sample Date	As ppb	Cu ppb	F ppm	Fe ppm	Mn ppb	Zn ppb	Al ppm	Ba ppb	Be ppb	Cd ppb	Cr ppb	Co ppb	Pb ppb	Mo ppb	Ni ppb	Se ppb	Ag ppb
PW-138	9/10/97	17	6.6	0.3	0.007	0	0											
PW-142	8/26/97	13	3.2	0.4	0	0	0											
PW-143	8/25/97	0	2.6	0.4	0	0	230							0				
PW-145	9/ 1/97	5.6	2.8	0.3	0	5	28											
PW-147	1/ 8/98	0	2	0.4	0.023	0	170											
PW-149	9/13/97	0	3.2	0.1	0.21	11	0											
PW-150	9/15/97	10	4.2	0.6	0	0	0											
PW-152	9/17/97	0	4.5	0.3	0.006	0	0											
PW-153*	8/30/95				0.01													
PW-153*	4/13/96				2.22													
PW-154	12/ 4/97	0	0	0.3	0.004	0	0											
PW-161*	1/24/95	0		0.6					40		0	0		6			0	0
PW-161	12/ 3/97	0	0	0.5	0.022	0	13											
PW-162	1/ 8/98	9	2.5	0.2	0.006	0	170											
PW-163	1/10/98	0	1.5	0.2	0.011	0	30											
PW-164	1/17/98	0	0	0.4	0.014	0	14											
PW-166	1/24/98	4	0	0.3	0.015	0	30											
PW-167	1/19/98	4	0	0.3	5.1	63	230											
PW-167	1/19/98	11	0	0.3	1.3	26	150											
PW-169	1/19/98	0	6	0.3	0.012	0	0											
PW-173	1/24/98	3	0	0	0.035	0	150											
PW-179	1/24/98	3	0	0.6	0.8	33	620											
PW-184	1/23/98	0	0	0.4	0.052	0	30											

Data sources are (*) analyses conducted at the request of the owner by independent labs, (#) the US Geological Survey (N. Plummer, unpubl., 1997), (+) US dept. Health and Human Services, OEH&E, Indian Health Service, unmarked samples collected by the New Mexico Bureau of Mines and Mineral Resources for this study.

Appendix E continued. Page 6 of 6.

Site ID	Sample Date	As ppb	Cu ppb	F ppm	Fe ppm	Mn ppb	Zn ppb	Al ppm	Ba ppb	Be ppb	Cd ppb	Cr ppb	Co ppb	Pb ppb	Mo ppb	Ni ppb	Se ppb	Ag ppb
PW-186*	8/15/95								20		0	0					0	0
PW-186	2/ 4/98	0	0	1.1	0.007	0	74											
PW-191*	2/ 5/97				0	0												
PW-191	2/17/98	10	0	0.3	0.028	0	140											
PW-192*	2/ 5/97				0	0												
PW-197	1/23/98	36	3.5	0.4	2.2	48	60											
PW-198	1/23/98	37	0	0.6	0.034	14	50											
PW-202	1/23/98	0	0	0.3	0.043	0	10											
PW-203	2/12/98	0	0	0	0.03	0	0											
PW-204	2/12/98	19	3	0	0.08	4	10											
PW-205	12/23/96	40	70		0	0	300		80		0	0		0			0	0
PW-205	2/13/98	64	0	0.5	0.01	0	0											
PW-206*	8/ 5/96	0	20	0.9	0	0	0	0.020	0	0	0	30	0	0	0	0	0	0
PW-211#	8/23/96	12	0.5	0.4	0.063	0	165	0.003	88			0		1.3	2.3			
PW-212*	2/1/94	16	0	1.2	6.07	580	30		0		0	0		0	0	0	0	0
PW-213+	12/23/96	9	10	0	0	0	1100		50		0	0		0			0	0
PW-215#	8/23/96	18	0.3	0.3	0.068	0	8	0.002	107			2		0.2	2.8			
PW-216#	8/17/96	2.4	0.8	0.8	0.045	0	6	0.003	64			0		0	3.1			
PW-217*	9/29/89			0.3	0	0												
PW-218#	6/19/97	1	0.6	0.3	0.043	0	55	0.004	206			1		0.3	1			

Data sources are (*) analyses conducted at the request of the owner by independent labs, (#) the US Geological Survey (N. Plummer, unpubl., 1997), (+) US dept. Health and Human Services, OEH&E, Indian Health Service, unmarked samples collected by the New Mexico Bureau of Mines and Mineral Resources for this study.